Lockheed

MISSILES & SPACE COMPANY, INC.

A SUBSIDIARY OF LOCKHEED AIRCRAFT CORPORATION

SUNNYVALE, CA.

LMSC/D346314
2 July 1973

MULTIBEAM ANTENNA STUDY

PHASE II - FINAL REPORT

JUNE 1973

Prepared For: National Aeronautics and Space Administration
Goddard Space Flight Center

Contract No.: NAS 5-21711

Prepared By: Paul Byrnes
Antenna Systems

Approved By: J. L. Bellamy
Antenna Systems

Approved By: John B. Damonte, Manager
Antenna Systems

PREFACE

The objective of the Multibeam Antenna Study is to develop an antenna concept for point to point communication between any two points within the Continental United States using a synchronous orbit satellite. The study is divided into two parts. Phase I whose objective is to analyze and evaluate several candidate approaches and to select a preferred candidate suitable for the requirements of the study, and Phase II whose objective is to design, fabricate, and test a breadboard model of the preferred concept.

The Phase I effort was completed in November 1972, and the results published in a Phase I Final Report, LMSC/D284597, dated 15 December 1972.

This document is a final report of the Phase II effort. It covers the design and fabrication of a two dimensional artificial dielectric lens contained in a parallel plate waveguide system, and the experimental pattern and VSWR results from tests with four different lenses: (1) a plano-convex natural dielectric (Teflon) lense, (2) a plano-convex artificial dielectric lense, (3) a two-point corrected Teflon lense, and (4) a two-point corrected artificial dielectric lense.

In addition, it includes a computer simulated system design of an operational two lense, 24 beam configuration. The computer design presents overlays of each beam onto the Continental United States from a fixed synchronous orbit satellite with a definition of these areas where beam-to-beam isolation is not sufficient to permit the re-use of frequency.

The experimental results will show first that the patterns from a plano-convex hyperbolic lens as a feed is moved laterally off the lens axis are similar to those from a parabolic reflector. As the feed is moved off-axis, coma lobes form on the side of the beam between the beam boresight and the lens axis, the main beam broadens, and the peak gain decreases. Second, that the measured patterns from a two-point corrected lense, as the feed moves off-axis, are indeed coma corrected. The side lobes remain constant, the main beam shape is unchanged, and the peak gain remains constant. These patterns demonstrate the capability of using a single lense aperture with multiple feeds, to obtain multiple beams with a high level of beam-to-beam isolation, thus permitting the re-use of frequency.

TABLE OF CONTENTS

TABLE OF CONTENTS (continued)

1.0 INTRODUCTION

1.1 Summary

This is the final report of the Phase II effort under Contract Number NAS 5-21711 performed by Lockheed Missiles and Space Company, Incorporated, for the Goddard Space Flight Center of the National Aeronautics and Space Administration.

The purpose of the Multibeam Antenna Study is to develop an appropriate antenna system concept for providing spot beam coverage in the contiguous 48 states. The Phase I analysis, reported in LMSC/D284597, selected a preferred antenna concept for the multibeam application. Phase II, which is described herein, is an experimental evaluation of a breadboard model of the preferred antenna concept selected in the Phase I study.

1.2 Description of the Preferred Candidate

The Phase I analysis concluded that the most suitable candidate for providing the coverage, beam-to-beam isolation, and other desirable characteristics of the multibeam application, is a two antenna, circular aperture artificial dielectric lense.

Each lense would be fed by an arrangement of multiple feeds, half of the beams emanating from one lens with one polarization and the remainder emanating from the other lens with the orthogonal polarization. The lenses would each have a circular aperture of approximately seven feet in diameter with a focal length to diameter ratio of the order of unity.

1.3 Original Phase II Plan

1.3.1 Lense Configuration

The lense to be constructed for the Phase II effort would be seven feet in diameter with a focal length on the order of seven feet. It would be manufactured from an available artificial dielectric material having a relative dielectric constant of 2.0. Eight feeds would be provided which can be arranged in two different configurations to simulate the 16 beams of the two antenna system.

1.3.2 Materials Procurement

A cylindrical block of artificial dielectric material having a dielectric constant of 2.0 would be procured from Emerson and Cuming, Inc., Canton, Massachusetts. The material is a plastic foam loaded with metallic particles. The manufacturer claimed experience in producing this particular model and could provide it on order with a 60 day delivery. The dimensions of the cylindrical lense blank are 100 inches in diameter and 30 inches thick.

1.3.3 Lens Fabrication

An 84 inch diameter plano-convex lense would be fabricated from the lense blank. General Electric (Syracuse, N.Y.) would probably perform the task for LMSC since they have on hand appropriate tooling and have had experience in machining this type of loaded foam.

1.3.4 Feed Design and Fabrication

LMSC would design and fabricate 8 feeds for the lense.

1.3.5 Antenna Tests

LMSC would evaluate the lense performance by making impedance measurements and by recording radiation patterns to simulate the 2 antenna 16 beam configuration.

1.3.6 Final Report

LMSC would prepare and submit a final report on the Phase II effort.

1.3.7 Schedule

To allow sufficient time for the procurement of the lense material and for the machining of the lense by the outside contractor , the end date of the contract must be extended three months from 3 April 1973 to 3 July 1973. No additional funding is required to perform these tasks.

1.3.8 Approval

This plan and schedule for the Phase II effort was approved by the GSFC Technical Monitor in November 1972, and an order was immediately placed with Emerson and Cuming to fabricate the artificial dielectric blank cylinder.

1.4 Phase II Redirection

1.4.1 Artificial Dielectric Material

The manufacturer of the artificial dielectric material had assured LMSC that the fabrication of a 100 inch diameter by 30 inch height cylinder of artificial dielectric material with a dielectric constant of 2.0 was a straightforward operation, and was an extension of a capability that they had developed over the past several years. Their published technical brochures listed this material (known as ECCOFOAM PS-A), as available in diameters up to 100 inches in diameter, with a choice of dielectric constants ranging from 1.1 to 2.0. A technical paper was presented by their Chief Engineer at the Allerton Park Symposium in October 1972, describing their accomplishments in fabricating this artificial dielectric material.

1.4.1 Artificial Dielectric Material (continued)

Emerson and Cuming is a well-known manufacturer of plastics for laboratory and space applications. They have a good reputation as to the quality of their products. However, they were overly optimistic in their own ability to fabricate this artificial dielectric cylinder. They tried for four months to obtain a good sample and finally admitted that they are unable to do so. They made many attempts during this four month period and after each attempt, we would be informed that although that particular attempt was unsuccessful, they now knew what their problem was and the next one would be successful.

As Emerson and Cuming are the only known manufacturer of this type of material, LMSC was compelled to encourage them in their efforts, until they finally admitted that this was a much more difficult task than they had envisioned and, in fact, the successful fabrication would be beyond the present state-of-the-art. They offered a proposal for a developmental program which was not compatible with the funding and/or schedule of this study.

1.4.2 Alternate Phase II Plan

In mid-March 1973, when it was finally apparent that the artificial dielectric cylinder could not be fabricated to our specifications, an alternate plan for the Phase II effort was evolved through several phone conversations between LMSC and the GSFC Technical Monitor. This alternate plan was designed to obtain the maximum information possible within the remaining three month period of the contract.

1.4.2.1 Experimental Effort

Emerson and Cuming had on hand four small cylinders of ECCOFOAM PS-A artificial dielectric that they had fabricated several months previously. These cylinders were 18 inches in diameter and 5 inches in height. The dielectric constants of the samples ranged from 1.80 to 2.10. These cylinders would be made available to LMSC if we could use them.

In the Phase I final report, it was pointed out that analytical tools are not available for predicting pattern performance of lenses with arbitrary contours with the same accuracy that are available for reflectors. Some valuable insight regarding final system performance could be obtained by making a two-dimensional simulation of a lense in a parallel plate region. Pattern measurements with offset feeds would show the coma lobe performance of a selected lense contour and to evaluate the need for coma correction. An interim

1.4.2.1 Experimental Effort (continued)

evaluation program between Phase I and Phase II was proposed as an option to the recommended Phase II effort. Additional funding would be required for this option, as well as an extension of the contract schedule.

Although this option could not be incorporated into this study at that time, a modified version was agreed to for the experimental portion of the alternate Phase II plan.

1.4.2.1.1 Phase II Test Plan

The new Phase II test plan was submitted to GSFC (LMSC/D336755) on 8 April 1973 and approved by the GSFC Technical Monitor. A summary of the test plan is included below.

The breadboard model will consist of a two-dimensional parallel plate artificial dielectric lens. The lens will be 56 inches in diameter with a focal length of 72 inches, a maximum depth of 11.08 inches, and a dielectric constant of 2.0. The separation between parallel plates (the thickness of the lens) will be 0.22 inches, allowing operation up to a frequency of 18 GHz.

Since the artificial dielectric available is a cylinder, 18 inches in diameter and 5 inches in height, the lens must be formed from pieces cut from this cylinder, and as a result, will have seams, or air gaps in the lens. As the effects of these seams on the performance of the lens are unknown, an evaluation of these effects will be made using a solid dielectric lens prior to the artificial dielectric lens tests. A one-piece lens will be machined from a sheet of Teflon and its performance determined by pattern measurements. This one-piece lens will then be cut into several pieces and reassembled to form the same lens except now it will have seams. The performance of this lens will be determined in the same manner as the one piece lens and the results compared to isolate the effects, if any, of the seams.

Two types of lenses will be evaluated. The first, called a one-surface or uncorrected lens is a plano-convex lens with the convex side having a hyperbolic surface. The second, called a two-point or coma-corrected lens, has no plane side (for a dielectric constant of 2.0) and neither of the two sides can be described exactly by a geometrical function.

1.4.2.1.1 Phase II Test Plan (continued)

All of the parallel plate lenses described below have a thickness (or separation between parallel plates) of 0.22 inches.

One Surface Lens

Solid Dielectric - No Seams - The lens used in this test will be made in one piece from a 24 inch x 48 inch x 1/4 inch sheet of Teflon. The lens will have a diameter of 48 inches, a focal length of 61.73 inches (F/D = 1.286) and a maximum depth of 8.9 inches. An H-Plane sectoral horn providing a -10 dB amplitude taper on the lens will be placed on the axis of the lens at the focal plane. As the feed horn is moved axially along the lens axis, the variation in gain and pattern performance will be recorded and the best position determined.

With the feed horn set to the optimum axial position, it will be laterally moved off axis in a plane in one-half inch increments to a maximum offset of six inches. For each offset position, a pattern with gain will be recorded.

The 10 dB feed horn will be removed and a second H-Plane sectoral horn providing a -20 dB amplitude taper on the lens will be positioned in the focal plane. The same sequence of tests will be performed with this feed horn as were performed with the -10 dB horn.

Solid Dielectric - With Seams - The Teflon lens will be removed from the parallel plate section and cut into five pieces such that when reassembled, there are four seams in the lens running parallel to the imaginary line from the focus to the lens surface. This is the same lens as tested previously except for the four seams.

The same tests as described for the one-piece lens will be performed with this five-piece lens. The data from the two series of measurements will be compared and the effects, if any, of the seams determined.

1.4.2.1.1 Phase II Test Plan (continued)

Artificial Dielectric - With Seams - The lens used in these tests will be made from cylinders of Emerson and Cuming, ECCOFOAM PS-A artificial dielectric with a dielectric constant of 2.0. The lens will have a diameter of 56 inches, a focal length of 72 inches (F/D = 1.286) and a maximum depth of 11.08 inches. It will be formed from five pieces of material resulting in four seams. The seams will be located in the same position relative to the lens diameter as were the seams in the Teflon lens. The same measurements will be performed with the lens as those performed with the solid dielectric lens.

Two Surface Lens - The same sequence of tests described for the one surface lens will be followed for the two-surface lens. A Teflon lens will be evaluated with and without seams using both feed horns. Then, the artificial dielectric lens with seams will be evaluated using both feed horns.

2.0 EXPERIMENTAL RESULTS

2.1 Electrical Design

The Phase I analysis had concluded that a lense diameter of approximately seven feet would be used as the breadboard model for the Phase II effort. Because of the unavailability of a large enough sample of artificial dielectric material, the Phase II tests will be performed on a two-dimensional model formed in pieces from a small sample of this material. A Teflon lense would be designed and tested to provide baseline data. Two types of lenses would be tested, a plano-convex, uncorrected lense, and a two-point coma-corrected lense.

2.1.1 Plano-Convex Lense

A sketch of a typical plano-convex lense is shown in Fig. 4-1. In order to provide an in-phase condition of all the rays incident on the convex face of the plane face, it can be shown that the convex face must be a hyperbola. The equation of the convex face is given by:

$$x^2 (n^2 - 1) + 2 F x (n - 1) - y^2 = 0$$

where x and y are the rectangular coordinates

n is the index of refraction of the dielectric material

and F is the focal length measured from the convex face.

The maximum thickness of the lense is given by

$$d_{max} = - \frac{F}{(n+1)} + \sqrt{\left(\frac{F}{n+1}\right)^2 + \frac{R^2}{(n^2-1)}}$$

where F is the lense focal length

n is the lense index of refraction

and R is the radius of the lense.

Using these two equations, a punched paper tape was prepared on the LMSC Tymshare Computer and fed into a Gerber Series 2000 Automatic Drafting Machine. This machine then scribed the desired surfaces onto a metal template from which the dielectric lense was machined.

Since the artificial dielectric lense has to be formed in sections, thus resulting in seams in the lense, the diameter was chosen large enough to be compatible with the size determined from the Phase I analysis and yet of a size which would minimize the number of seams. The artificial dielectric lense is 56 inches in diameter, has a focal length of 72 inches (F/D = 1.286), a maximum depth of 11.08 inches, a dielectric constant of 2.0, with four seams.

2.1.1 Plano-Convex Lense (continued)

The maximum sheet size of Teflon available for use on the study is 24 inches by 48 inches. Thus, the Teflon lense is 47.625 inches in diameter, has a focal length of 61.25 inches (F/D = 1.286, the same as the artificial dielectric lense), a maximum depth of 8.80 inches, and a dielectric constant of 2.09. There are no seams in the Teflon lense.

2.1.2 Two Point Corrected Lenses

Two two-point corrected lenses, one from Teflon, the other from the artificial dielectric, were designed using the computer aided anlaysis described in Section 4.0. The lenses were machined from templates prepared in the same manner as described for the plano-convex lenses. However, to provide a one-to-one comparison, each of these lenses was fabricated to a 47.625 inch diameter with an F/D ratio of 1.286. The surfaces of the two are different because of the different indeces of refraction.

2.1.3 Parallel Plate System

The lenses will be contained in a parallel plate system propagating a TEM wave. The parallel plates will extend from the lense to 2 inches beyond the hyperbolic lense focal point. The separation between plates must be less than one-half wavelength at the highest operating frequency. This separation is 0.22 inches for operation at 18 GHz.

2.1.4 Feed Horns

The feed horns used to illuminate these lenses are H-Plane sectoral horns with an E-Plane dimension equal to 0.22 inches so the horns will just fit inside the parallel plates. Two horns were designed, one to provide 20 dB edge directed illumination, the other to provide 10 dB edge directed illumination at the lense at a frequency of 18 GHz. Sketches of the horn components are shown in Figs. 2-1, 2-2, and 2-3.

2.2 Mechanical Design

Figure 2-4 illustrates the lens and structure assembly. Item 1 (Feed Support) allows the feed horns (Items 12 and 13) to move in and out of the parallel plates for focal length adjustment and may be moved laterally along either set of slots in Item 2 (Support Feed Bracket). The rectangular tubing structure (Item 3) is composed of the tubes, a tie bar and the interface plate. The lens plates (Item 11) are spaced properly by the phenolic separators (Item 8). One Stiffener (Item 9) helps to support the lens plates. Item 7 are flares made adjustable by the turnbuckle and trunnion assembly (Items 4, 5 and 6). The lens is illustrated as Item 10. Item 14 is a waveguide to waveguide transition. Sketches of the details are included and are shown as Figures 2-5 thru 2-15.

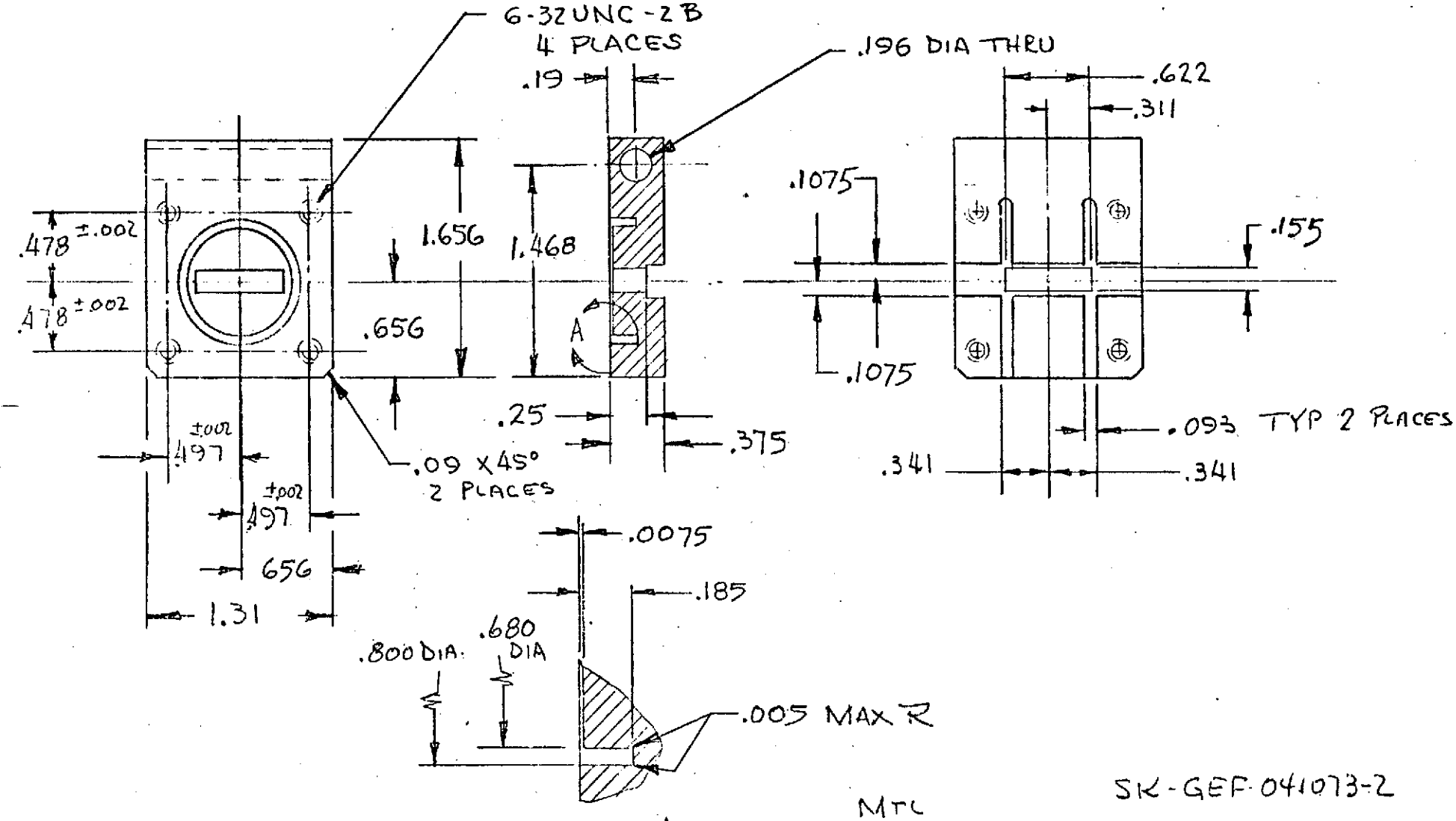

MTL
BRASS
2 REQD

SK-GEF-041073-2

FIGURE 2-1

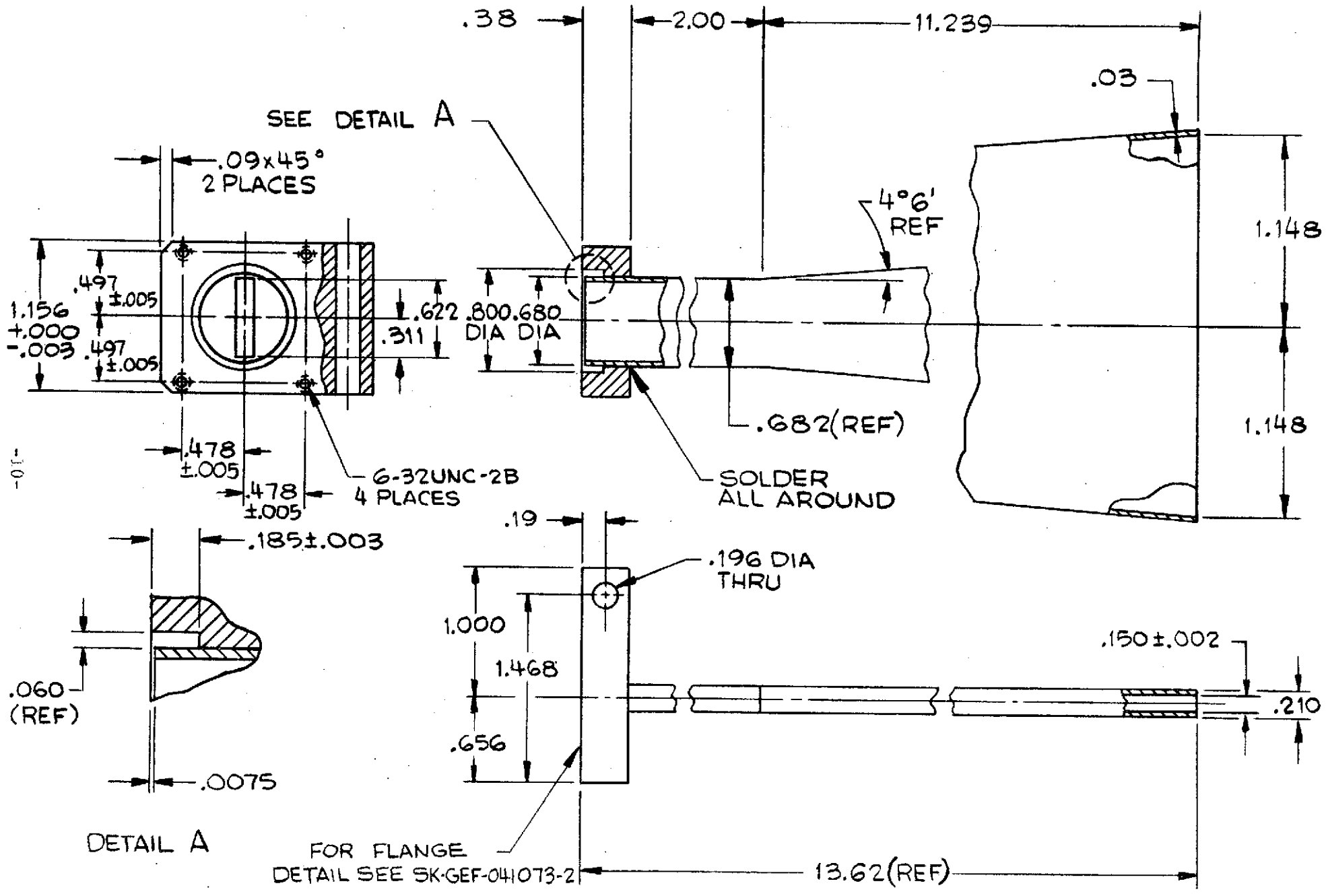

FIGURE 2-2 FEED - LONG SK-GEF-040673-1

MTL: BRASS (ONE REQD)

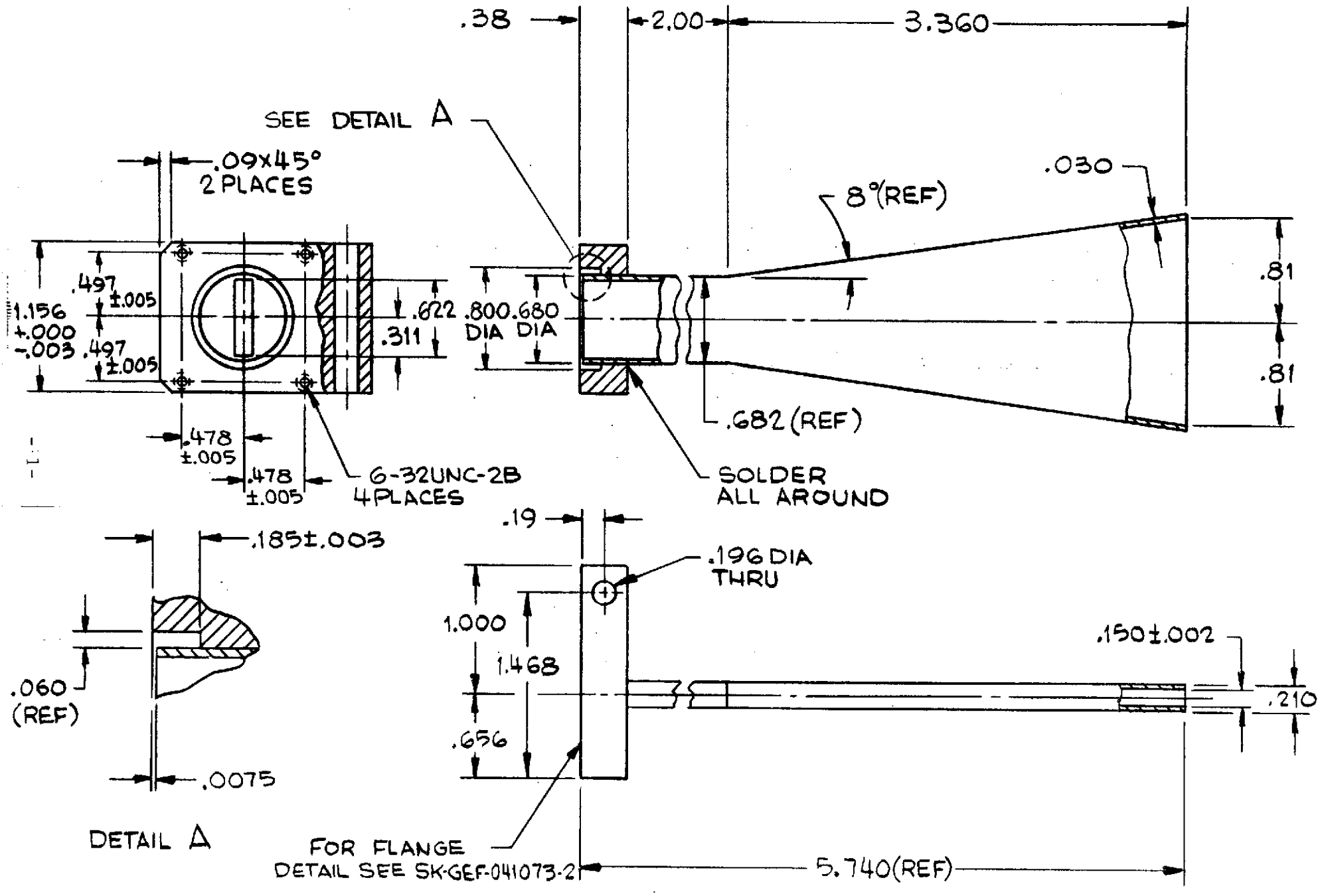

FIGURE 2-3 FEED-SHORT SK-GEF-040673-

MTL: BRASS (ONE REQD)

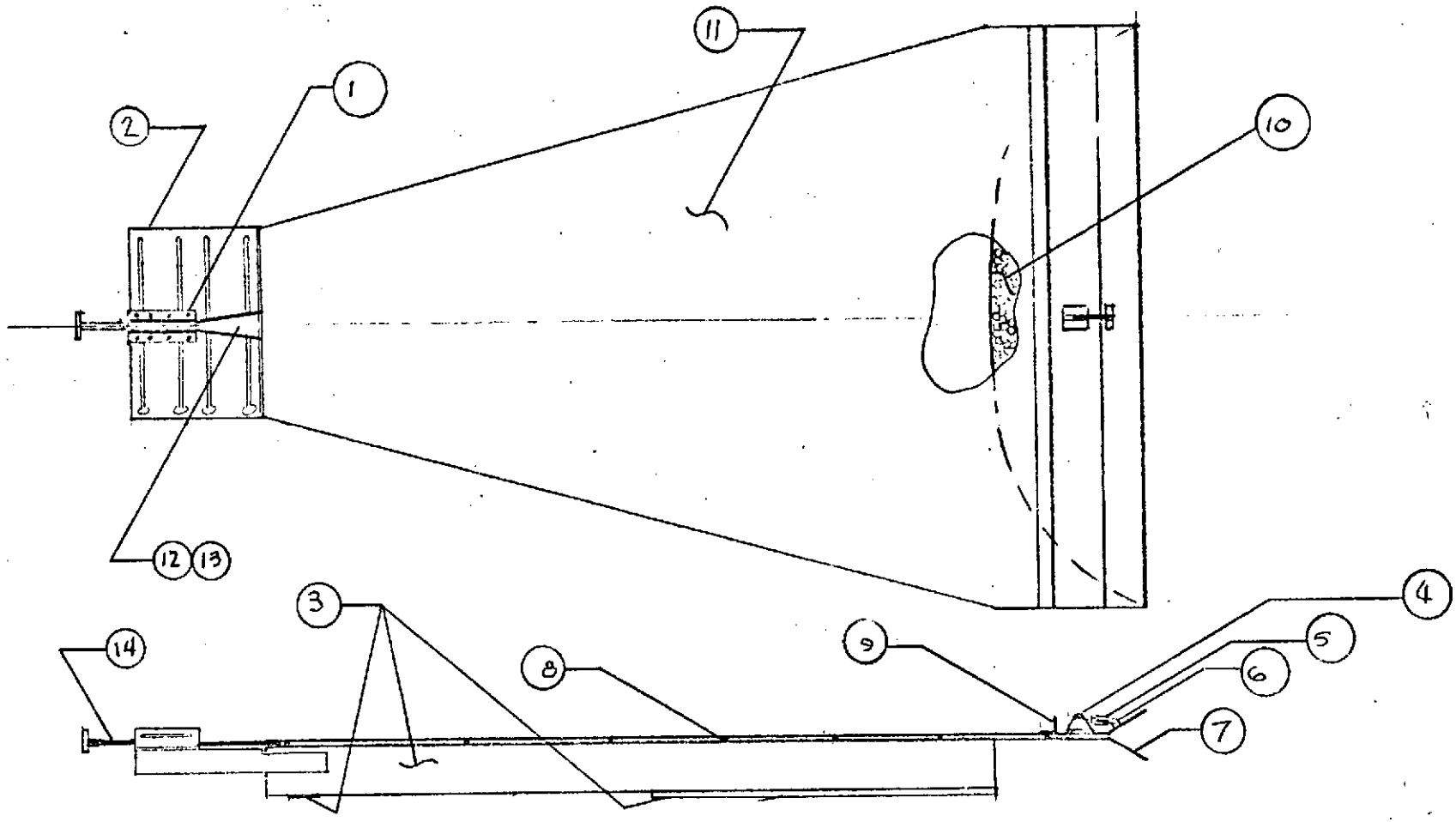

FIGURE 2-4

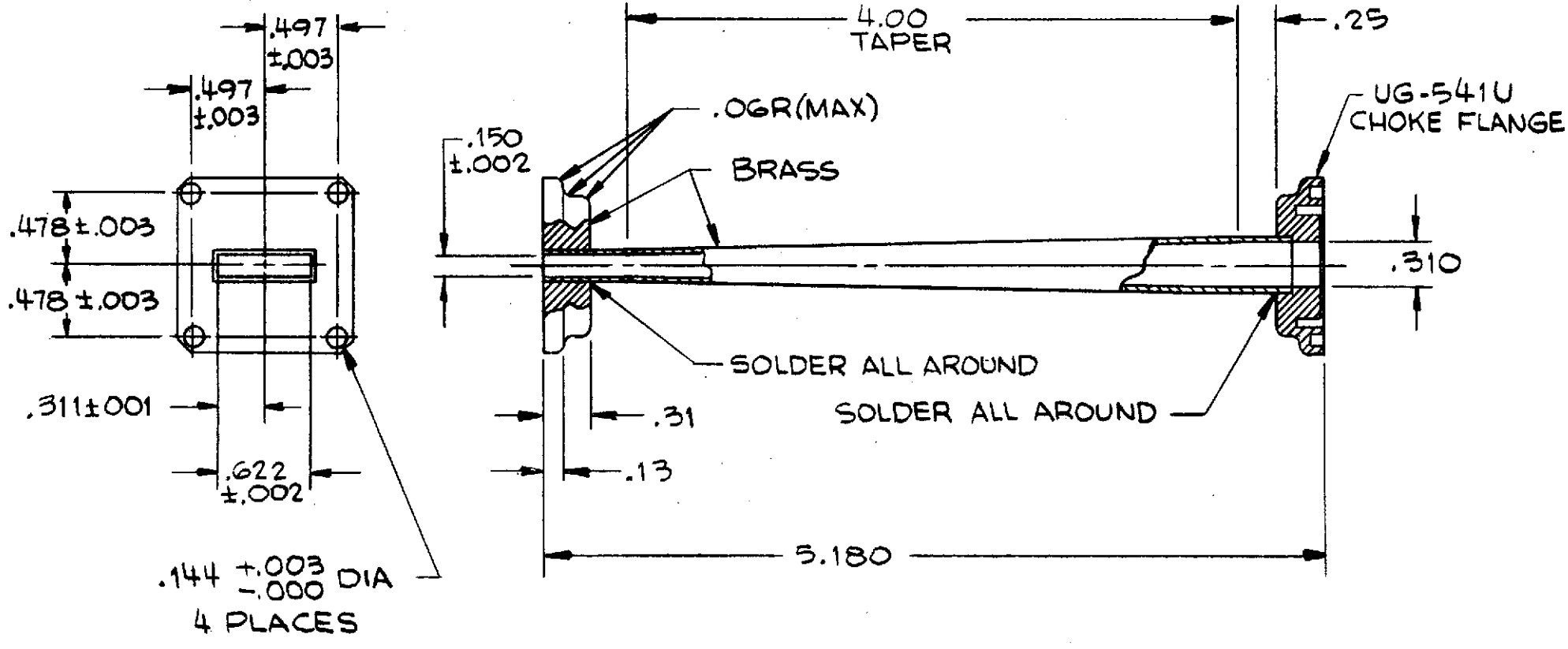

FIGURE 2-5
TRANSITION
2-REQD

SK-GEF-040673-3

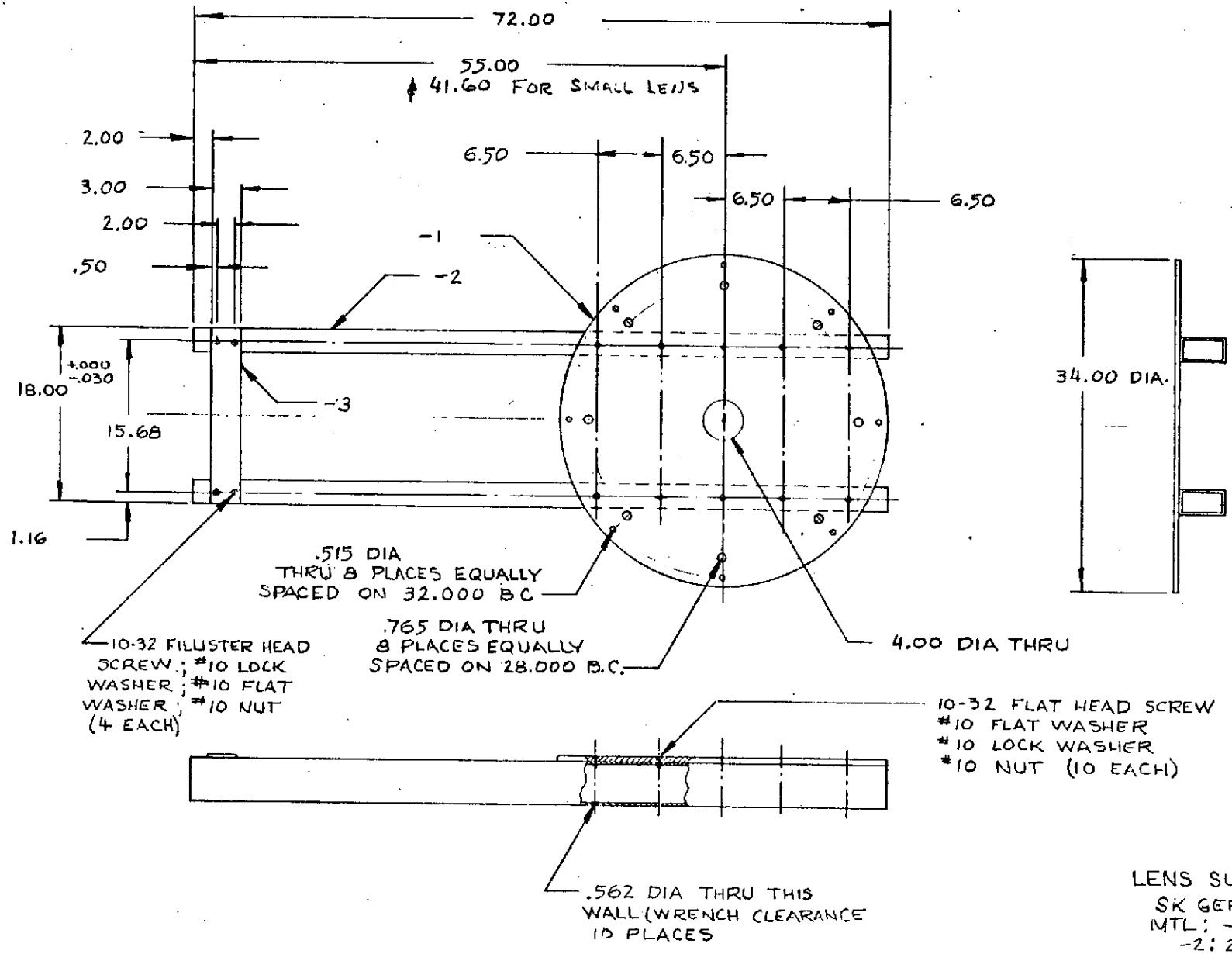

FIGURE 2-6

LENS SUPPORT STRUCTURE
SK GEF 041273A
MTL: -1: .250 THICK ALUM PLATE
-2: $2\frac{5}{16} \times 4\frac{7}{16}$ X.078 W. TUBING
-3: 3X1 3/4 X .12 THICK ALUM SH.

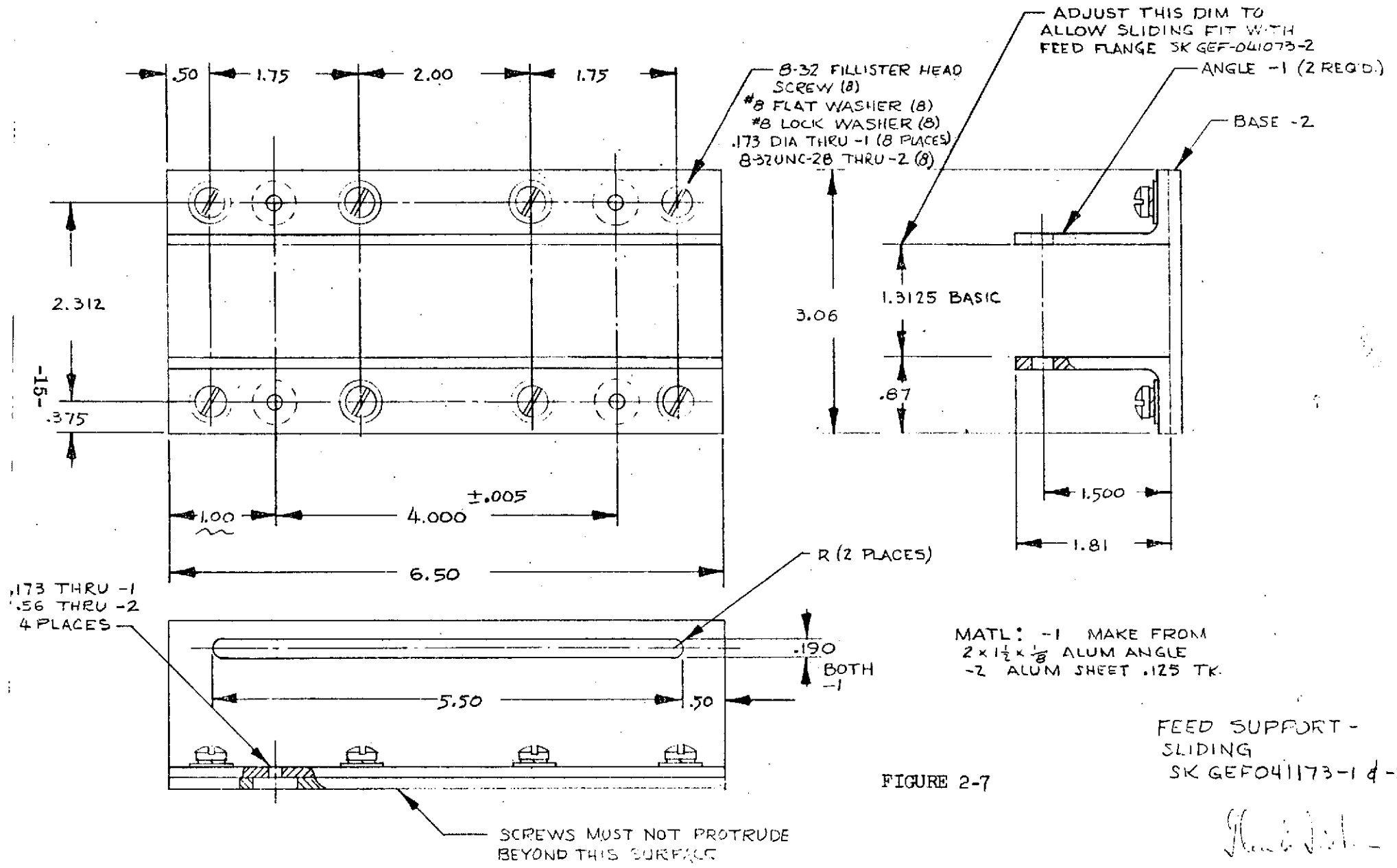

MATL: -1 MAKE FROM $2 \times 1\frac{1}{2} \times \frac{1}{8}$ ALUM ANGLE
-2 ALUM SHEET .125 TK.

FIGURE 2-7

FEED SUPPORT - SLIDING
SK GEF041173-1 & -2

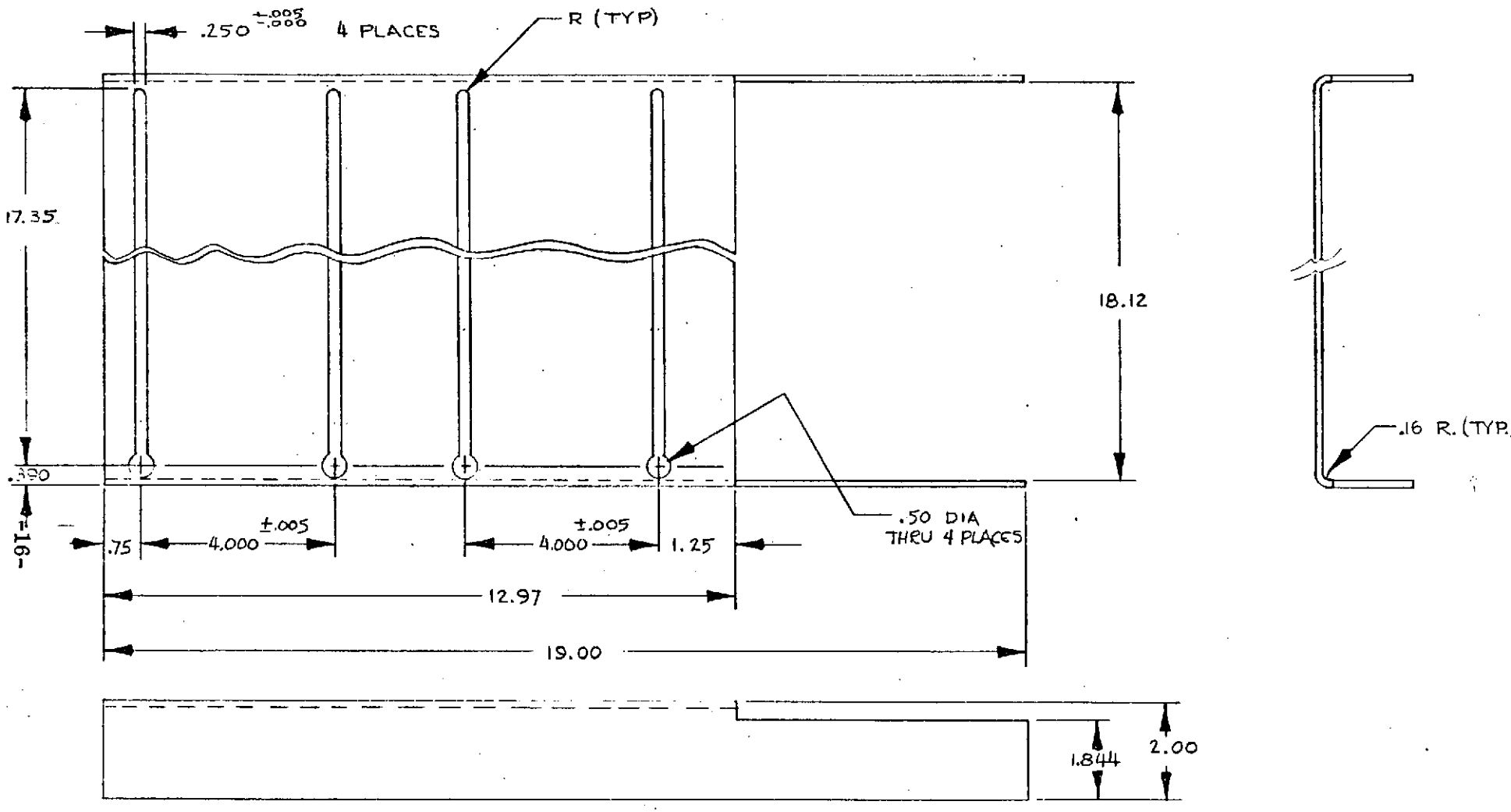

SUPPORT - FEED BRACKET
SK-GEF 041173-1
MTL: 6061 TG ALUM .125 THICK

FIGURE 2-8

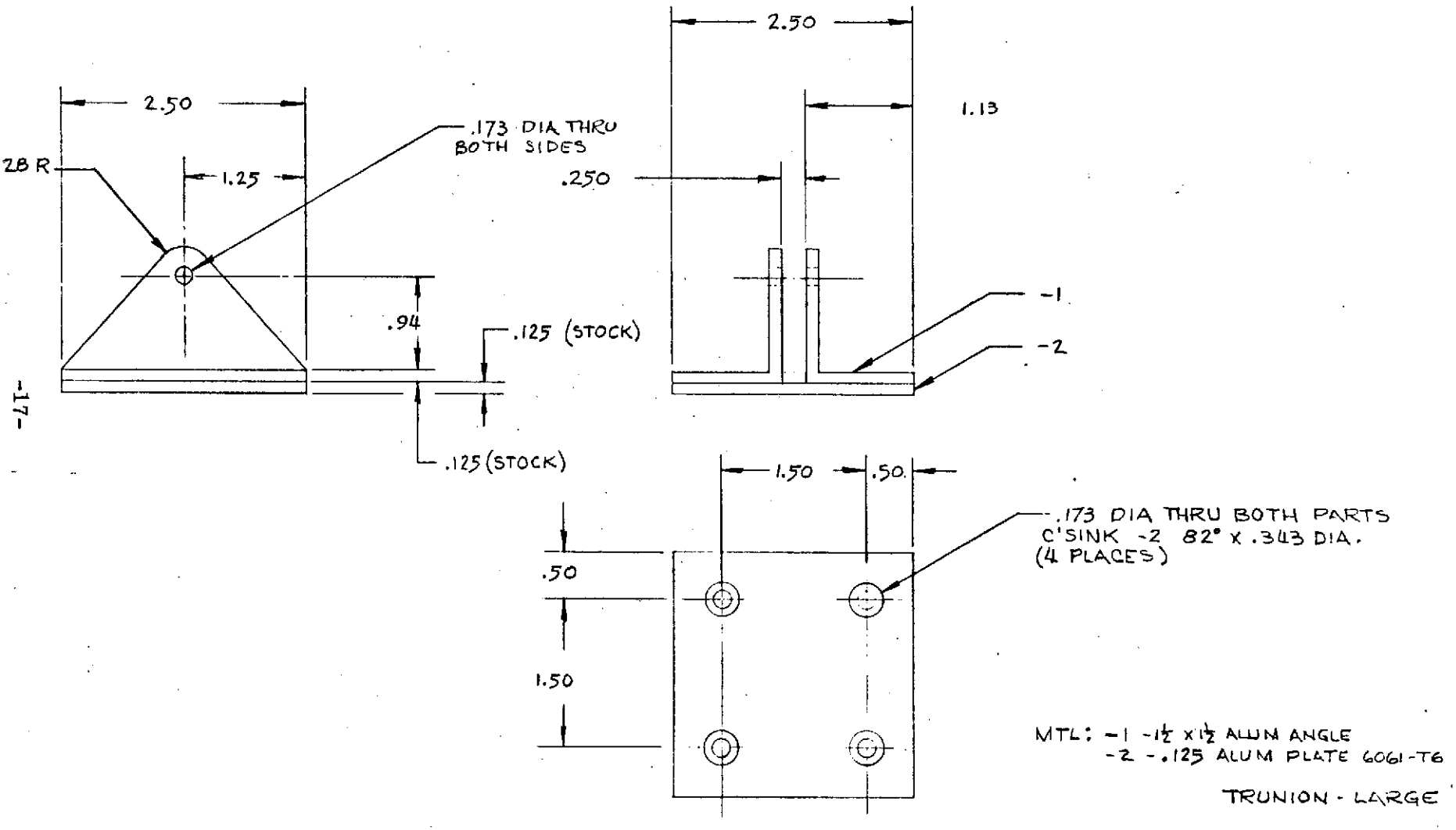

MTL: -1 -1½ x 1½ ALUM ANGLE
-2 -.125 ALUM PLATE 6061-T6

TRUNION - LARGE

SK GEF 041973 A
2 REQD

Glen E. Fisher

FIGURE 2-9

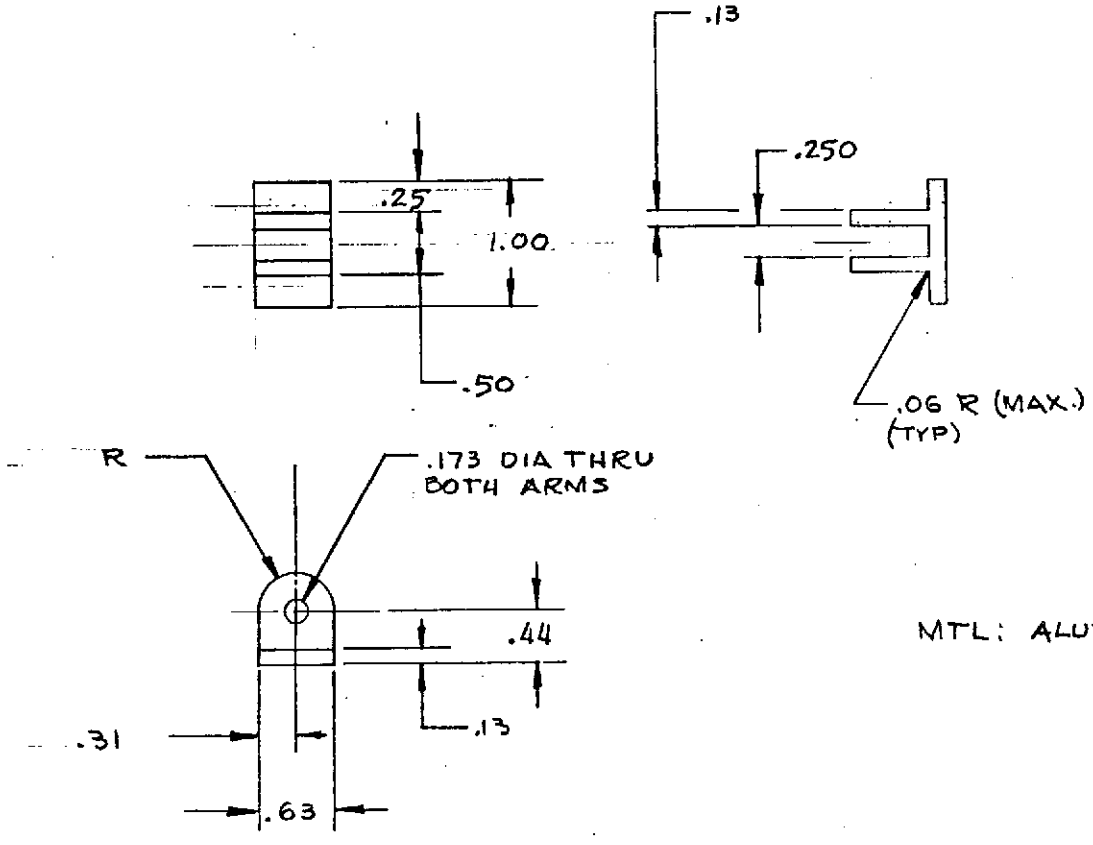

MTL: ALUM BAR 6061

TRUNNION - SMALL
SK GEF 041873 B
2 REQD

FIGURE 2-10

	A $^{+.03}_{-.00}$	B $^{+.03}_{-.00}$	C	D	E	F	G
-1	56.00	18.00	9.00	84.10	11.10	28.00	12° 43'
-2	48.00	16.00	8.00	72.23	9.50	24.00	14° 18'

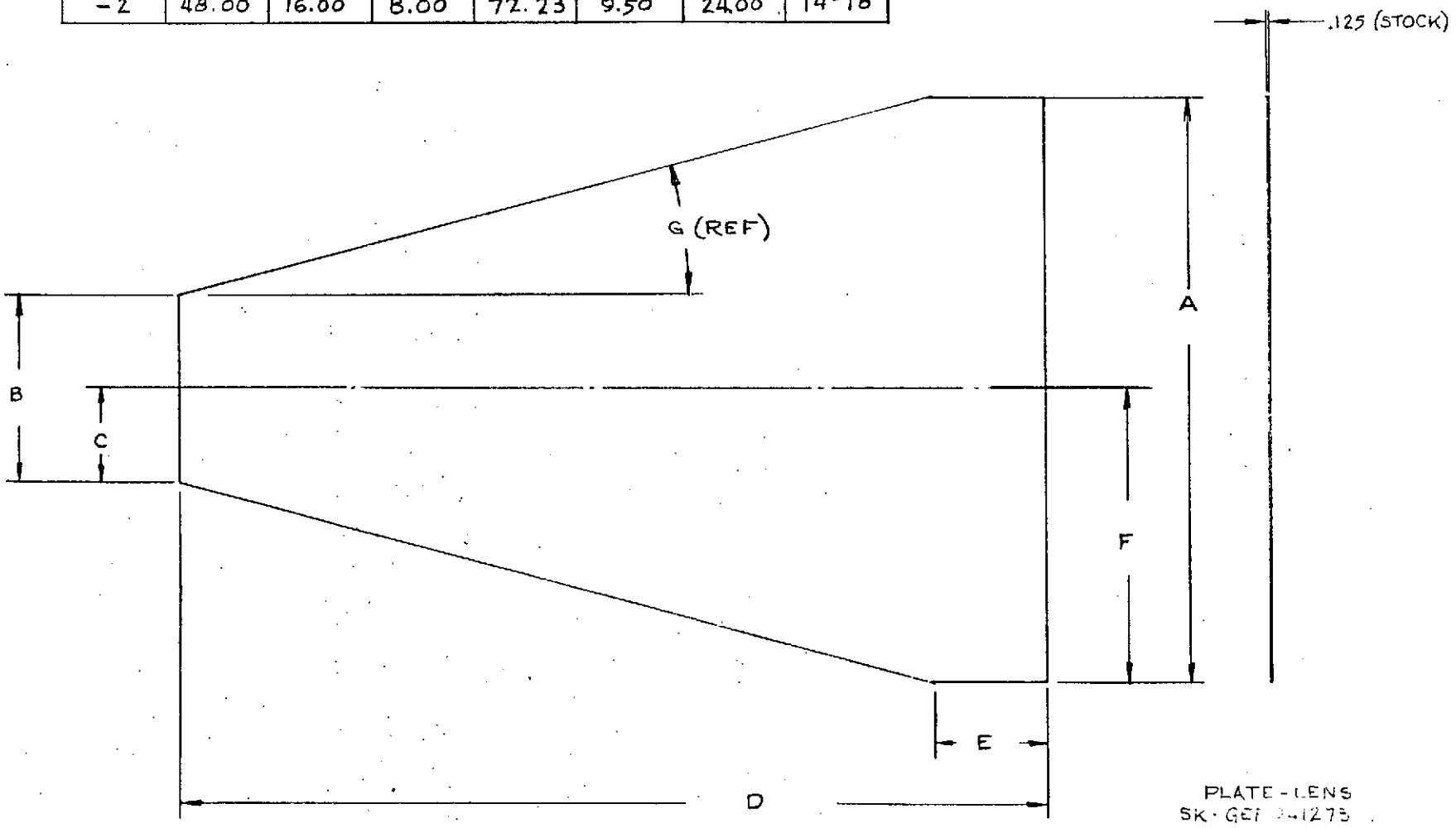

PLATE - LENS
SK - GEI [illegible]
MTL: [illegible] .125 TK.
2 EACH REQD

FIGURE 2-11

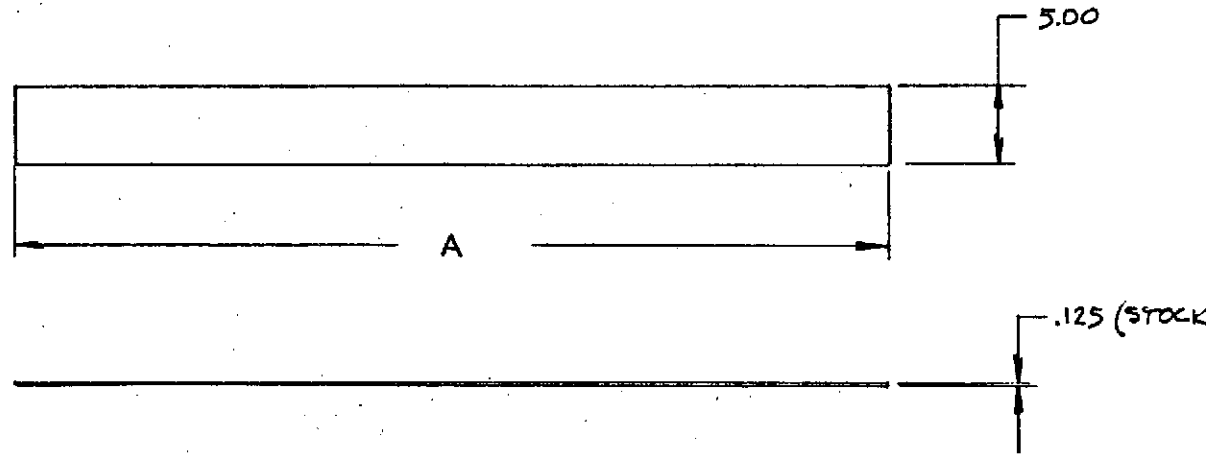

MTL: ALUM SH .125 THICK
6061-T6

	A
-1	56.00
-2	48.00

FIGURE 2-12

FLARE
SK GEF 042073
2 EA REQ D

Glen E. Dick

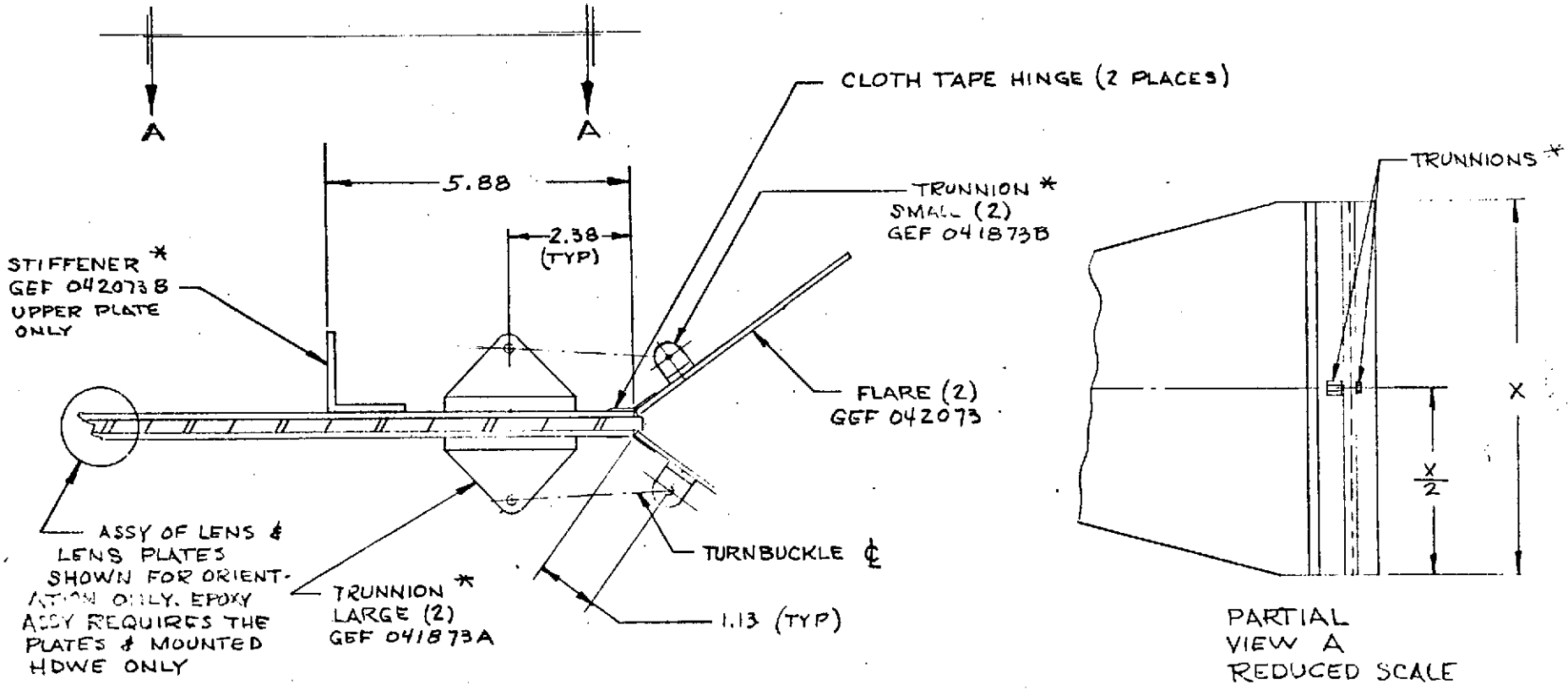

* CEMENT PARTS IN PLACE USING EASTMAN 921 EPOXY CEMENT

FIGURE 2-13

CEMENTED ASSY-LENS
GEF 042573A

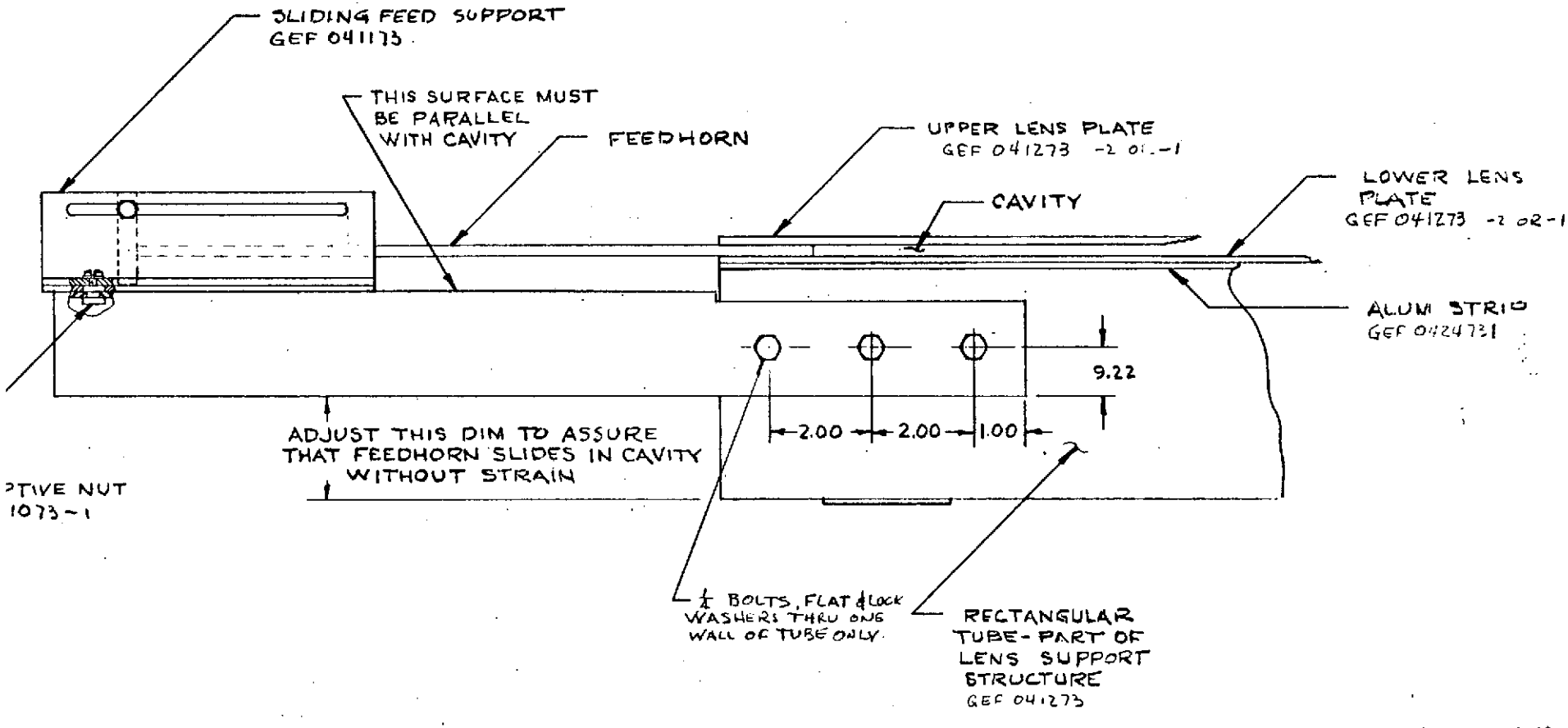

SLIDING FEED SUPPORT ASSY

GEF 0425731

FIGURE 2-14

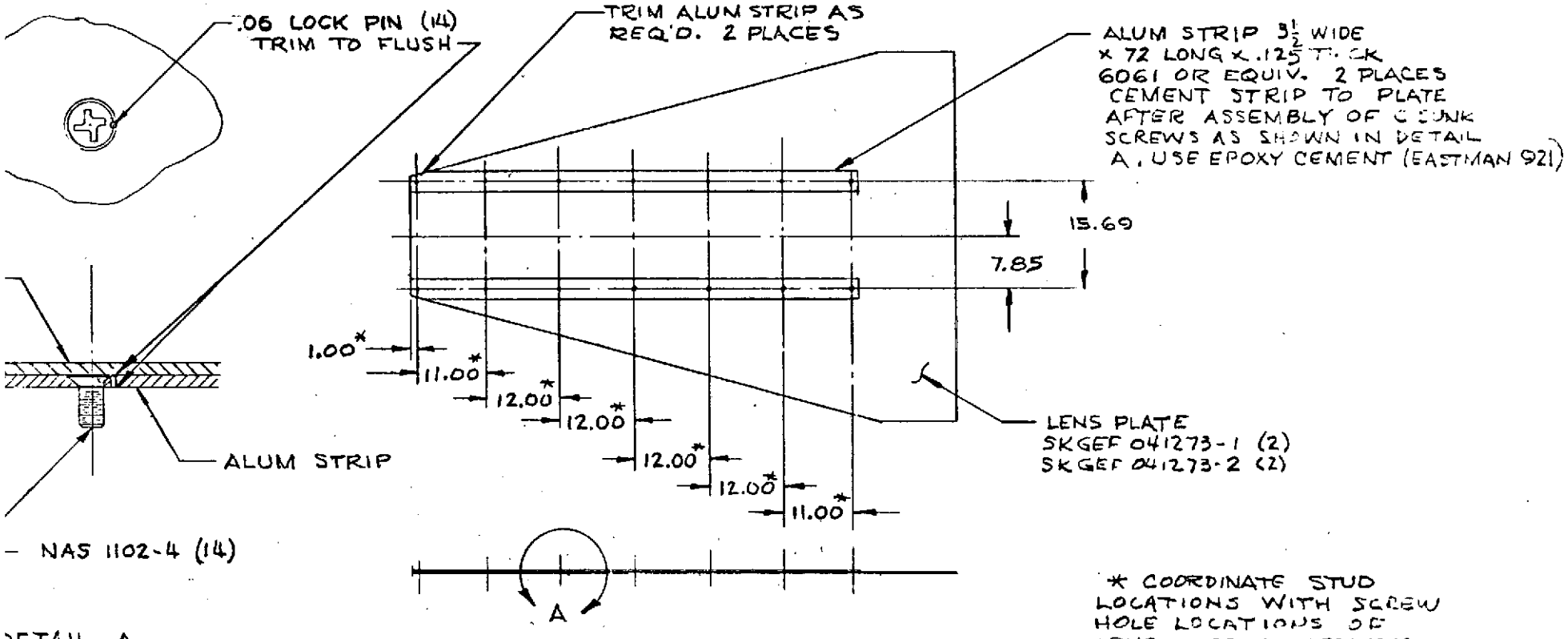

FIGURE 2-15

LENS PLATE-STRIP ASSY.
SK GEF 0424731

Glen E. Sadler

2.2 Mechanical Design (continued)

Solid aluminum plates were utilized for the panels rather than a more rigid, lighter honeycomb structure. The support mechanism for the panels was constructed of large rectangular waveguide tubes which were arranged to accept both lens assemblies. The mounting plate used to interface with the range positioner was attached to the structure so that it could be readily moved to accommodate either lens near its center of gravity. The design of the lens plates avoided holes or seams in the RF transmission area. Studs cemented in these rails were fed thru one wall of the rectangular structure and secured with nuts and washers.

An adjustable feed support bracket was mounted on the support structure so that the feed could be adjusted five inches into the lens and with enough lateral movement to obtain $\pm 5^{o}$ adjustment.

2.3 Test Facility

The pattern tests were performed at the LMSC Large Aperture Test Facility located in the nearby Santa Cruz Mountains adjacent to the Lockheed Santa Cruz Test Base.

Santa Cruz Antenna Test Facilities

The Santa Cruz antenna pattern range facilities are designed primarily for the evaluation of very large aperture antenna systems. A capability is available for the evaluation of antennas having apertures which are as large as 50 feet in diameter.

The site consists of two 3/4 sphere air house radomes -- one 54 ft. in diameter and the other 75 ft. in diameter. Each air house radome includes a stable tower and heavy duty antenna positioner located at its center. A permanent transmitter site, with two antenna towers, Fig. 2-16, is located one mile away from the air houses, providing a pattern range over a natural canyon, having a profile shown in Fig. 2-17.

Also available at the Santa Cruz Test Base site is a 2,000 ft. range to a non-radome enclosed tower (Fig. 2-18) which is often used for smaller antenna evaluation. In addition, a range capability of 3.5 to 5.0 miles is available, using a mobile transmitter in conjunction with one of the receiving site, as shown in Figs. 2-19 and 2-20, respectively.

All these Santa Cruz ranges are equipped with Scientific-Atlanta receivers, pattern recording equipment, and heavy duty 3-axis positioners capable of supporting not only a large spacecraft antenna, but also the associated gravity compensating support fixture and, in some cases, the spacecraft itself. For these tests, the Bldg. 6930 Tower was used for the transmitting site, with the test antenna located in the smaller air house.

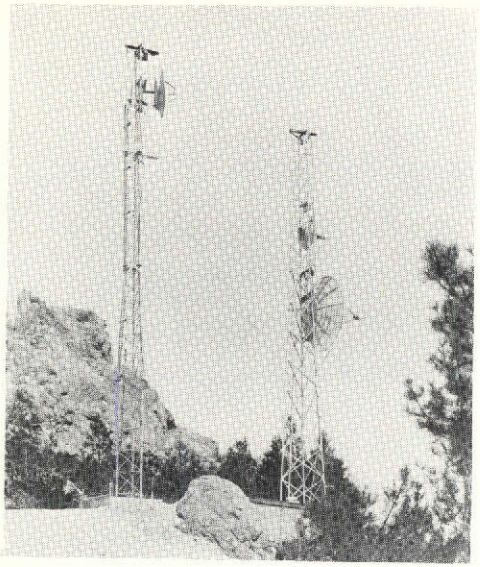

Fig. 2-16 Transmitting Site

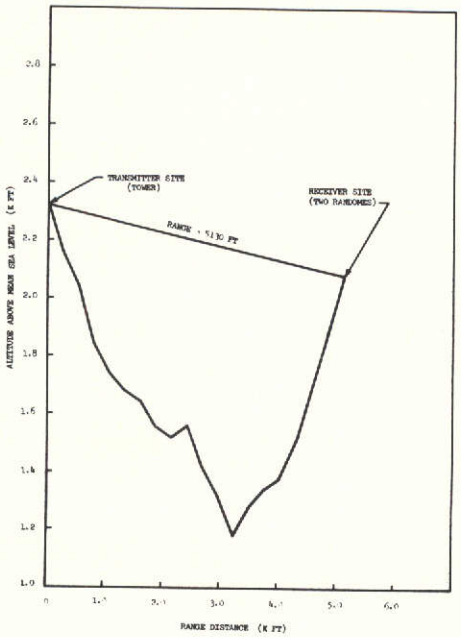

Fig. 2-17 Pattern Range Profile

Fig. 2-18 Transmitting or Receiving Site – Bldg. 6930

Fig. 2-19 Mobile Transmitting Van

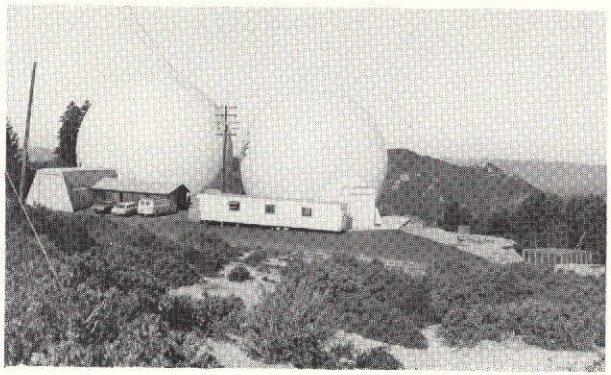

Fig. 2-20 Receiving Site

2.4 Lense Installation

The parallel plate lense was installed on the Scientific/Atlanta 3-axis pedestal as shown in Fig. 2-21 .

Fig. 2-22 is a view looking from the feed toward the lense. The feed horn can be seen extending into the parallel plate region. Back of the feed horn is a transition from the reduced height waveguide of the horn to standard Ku band guide, then a 10 dB fixed attenuator and a tunable waveguide crystal mixer. The feed positioning plate is seen which allows the feed to be moved both axially and laterally from the design axis of the parallel plate section. Also shown are the staples of the antenna business, C-clamps and masking tape.

Fig. 2-23 is a side view showing the entire external parallel plate configuration. Fig. 2-24 is a front view looking from the lense back to the feed. This figure shows the lense inside the parallel plates and an external clamping arrangement made from angle irons and wood, added after the tests were under way. The necessity for this clamp is explained in Section 2.5.

2.5 Diagnostic Measurements

Before discussing the measurement data, it is worthwhile to describe some of the problems encountered in obtaining this data in that it may eliminate future frustrations for anyone making similar measurements.

The Teflon plane-convex lense was tested first. The parallel plate system was installed in the small air house and testing initiated at 18 GHz. An example of the first patterns obtained is shown in Fig. 2-26. The beamwidth is approximately twice what was expected for this aperture size at this frequency. The first side lobes were only down 5 dB from the beam peak yet the nulls in the pattern were 30 dB deep. After checking out all the instrumentation, the source of the trouble was determined to be an insufficient contact between the parallel plates and the lense. It was recognized early in the design stage that it is necessary to have good plate to lense contact and the parallel plate system was designed to insure good contact. However, there still existed several small air gaps when the antenna was assembled for test.

The Teflon lense was removed from the parallel plates and was completely covered with conducting tape on the two sides making contact with the plates. The pattern with the lense taped is shown in Fig. 2-27. Although not perfect, the measured 3 dB beamwidth was now what had been predicted, and the high side lobes had disappeared. This pattern

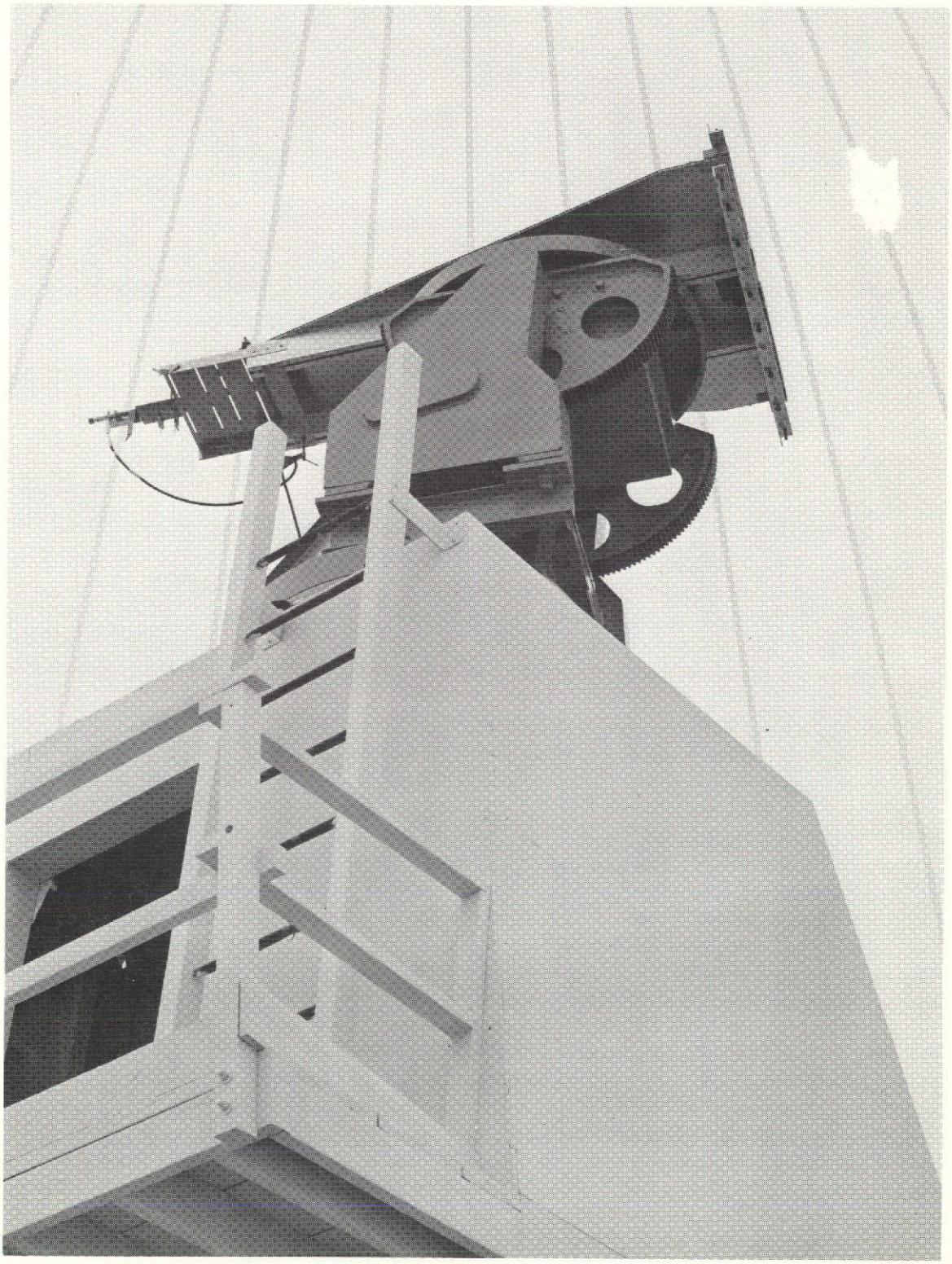

Fig. 2-21 Parallel Plate Lens Installed On-Site

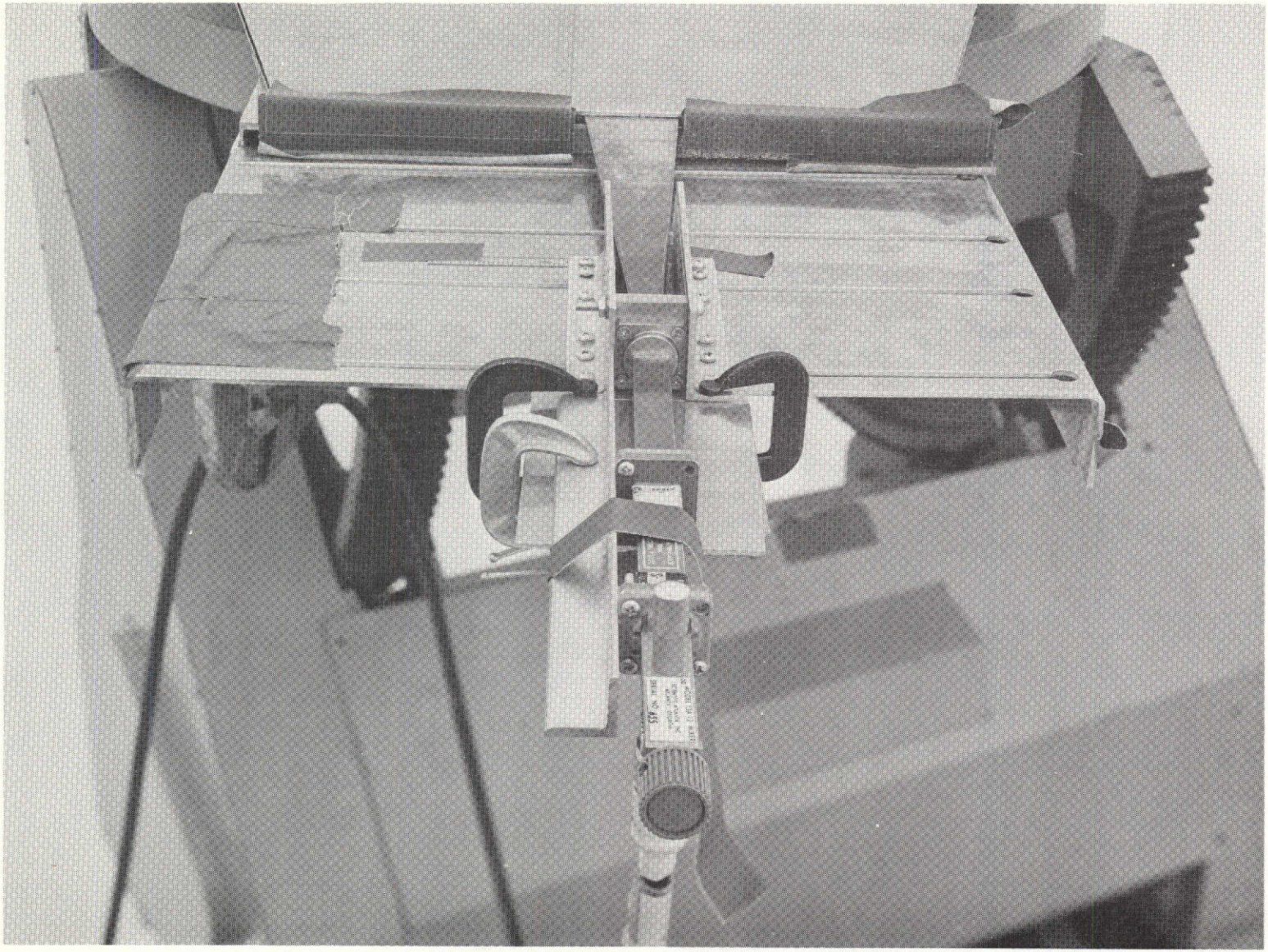

Fig. 2-22 Parallel Plate System Viewed From Feed End

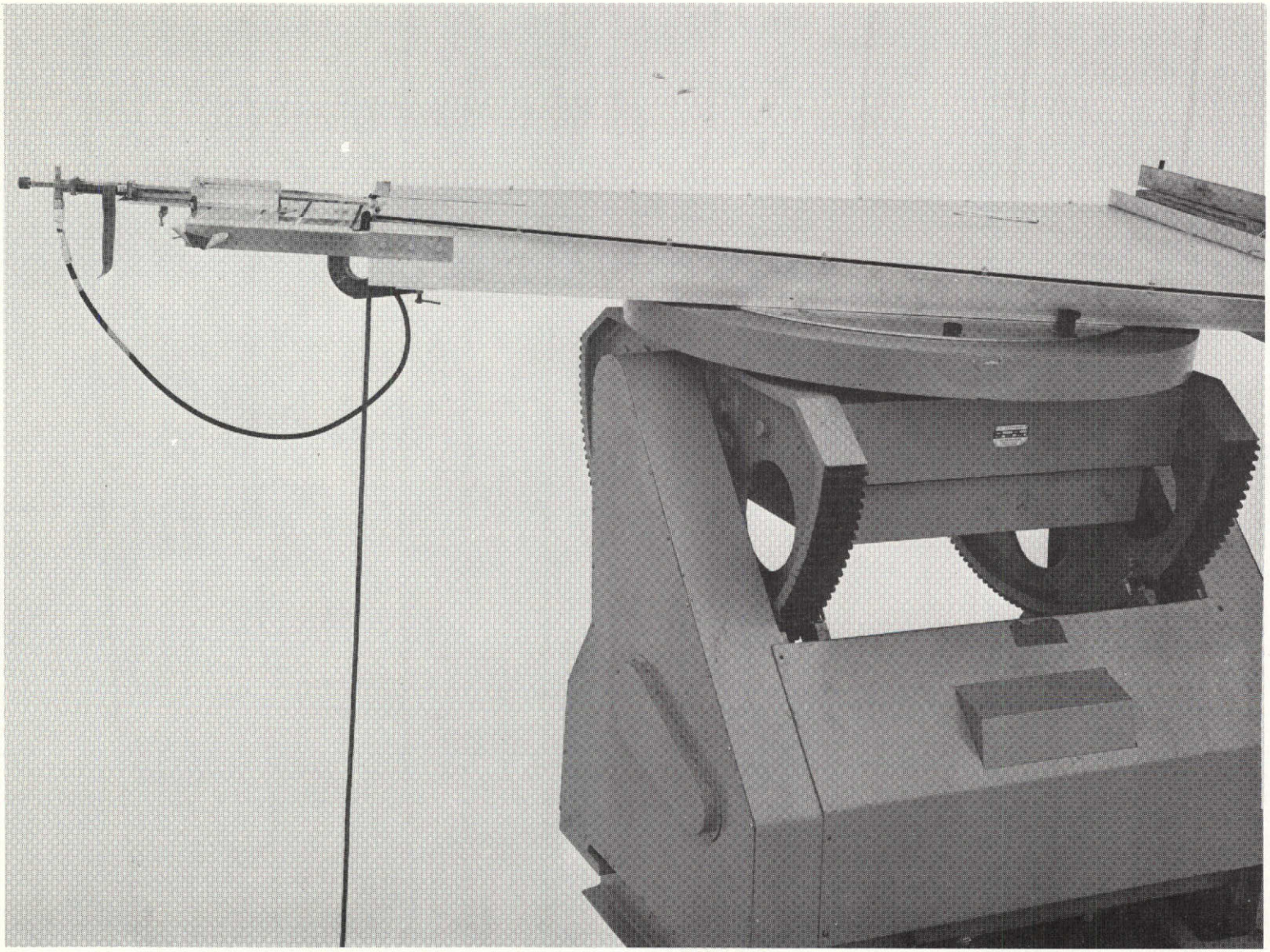

Fig. 2-23 Parallel Plate System, Side View

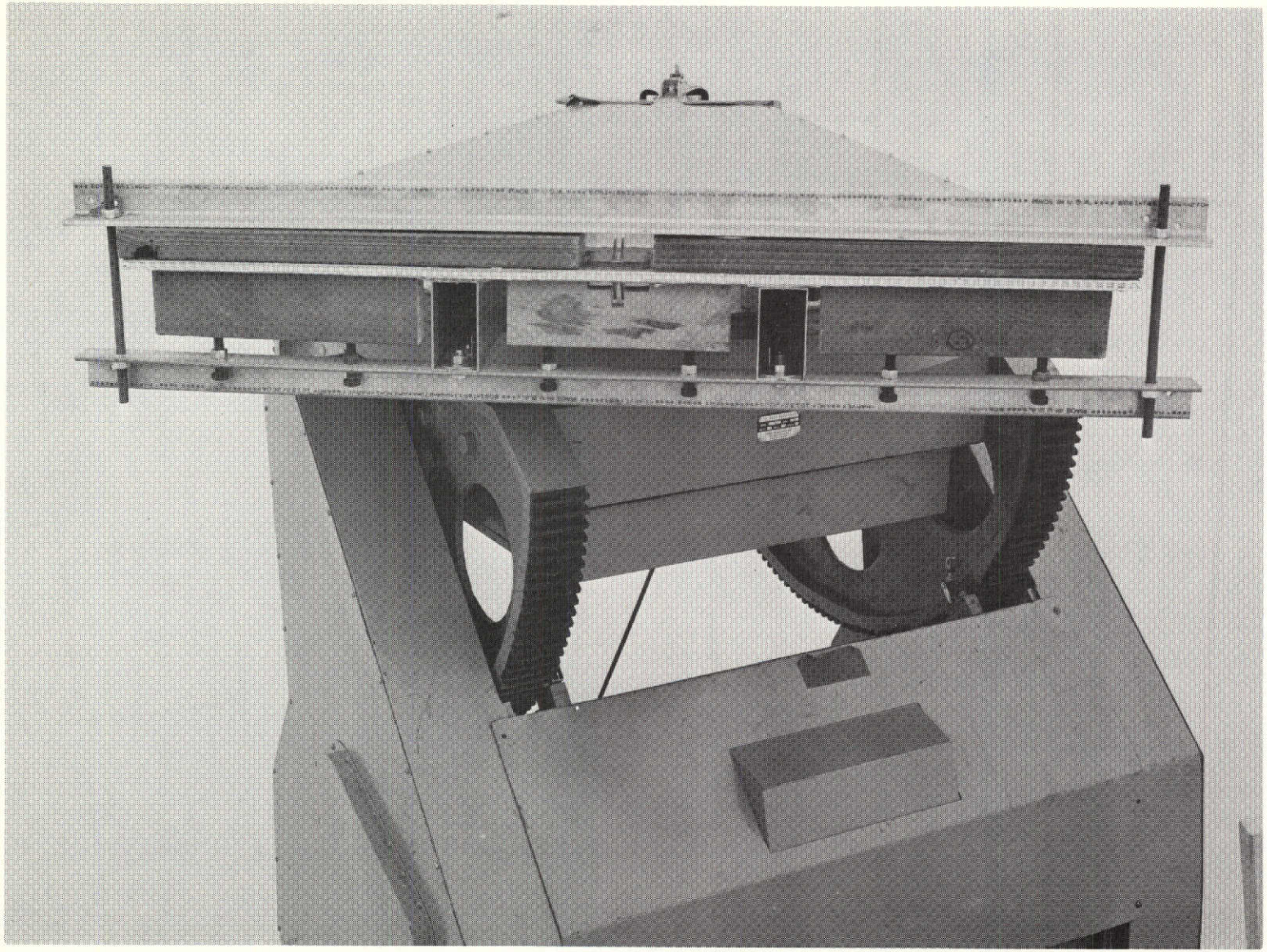

Fig. 2-24 Parallel Plate System, Front View

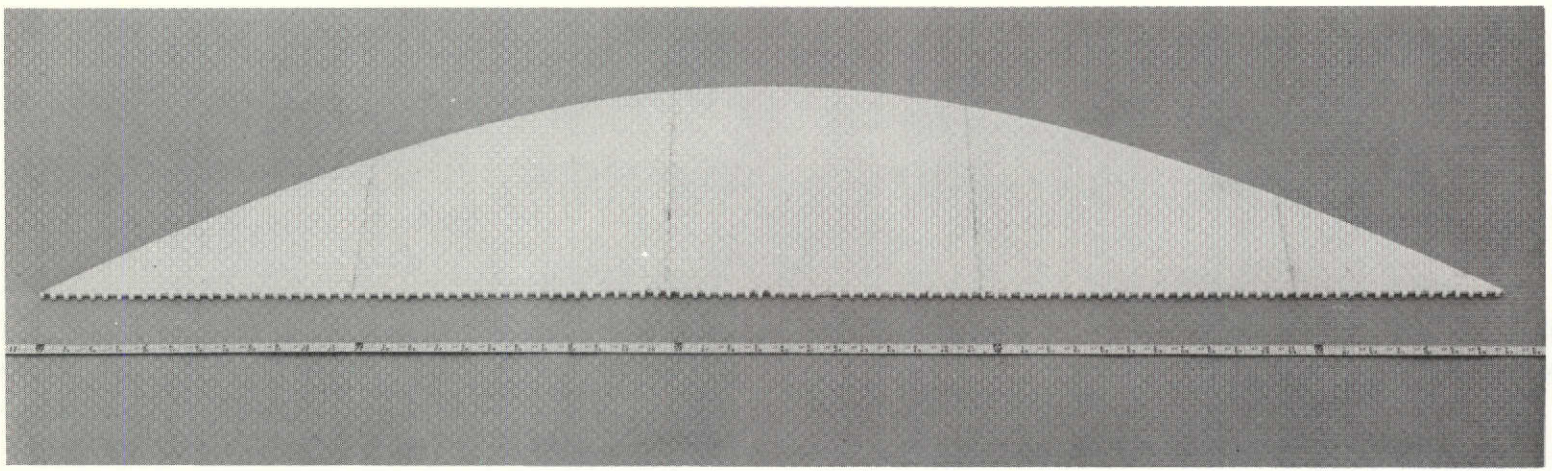

Fig. 2-25 Plano-Convex Artificial Dielectric Lens

2.5 Diagnostic Measurements (continued)

at least began to look like an antenna pattern. To completely eliminate the air gaps, a clamping arrangement was devised on site, and positioned on the parallel plate over the lense. This clamping fixture was mentioned in Section 2-4 and shown in Fig. 2-24. A pattern after installing this clamp is shown in Fig. 2-31. The improvement in overall pattern structure is evident.

After ensuring good lense to plate contact, a new problem was encountered; patterns could not be repeated. A pattern would be recorded and then immediately recorded again (a time delay of approximately 30 seconds). The main lobe was identical but the side lobe structure was different. Some minor lobes were higher, some lower; some nulls were deeper, some shallower. The same pattern was repeated for a third time and, again, the main lobe was the same but the side lobe structure different from either of the first two recordings. The antenna was rotated back to a first side lobe maximum. With the antenna not moving, the amplitude at this side lobe varied 3 dB. After a check of all instrumentation showed no probable source of this variation, it was decided to check out the air house itself. It was not feasible to move the antenna outside of the air house, so with the antenna sitting on a side lobe maximum, the air house was vibrated vigorously by pushing on it. The amplitude level varied 10 dB and then slowly damped out.

Since the small air house had been found to be a major source of pattern instability, the test antenna was moved to the large air house. After re-boresighting the transmit antenna, the same series of measurements were performed at 18GHz as had been performed in the small air house. The patterns were repeatible and the maximum variation in amplitude of a side lobe maximum when the air house was vibrated was 1 dB which damped out to 0 in a very short time. The rest of the measurements were performed with the test antenna in the large air house.

A final comment here on the plane in which the patterns are taken. It was originally intended that patterns would be taken using horizontal linear polarization with the parallel plates oriented perpendicular to the ground. The pattern cuts would be in the elevation plane thus reducing ground reflections by having the narrow beamwidth in this plane. However, after many attempts, a good pattern could not be obtained with the lense in this orientation. When the antenna was rotated ninety degrees so the plates were parallel to the ground, and the transmit polarization changed to vertical, good patterns were obtained, even though there is now a larger possible source of error from ground reflections. When the parallel plates were perpendicular to the ground, air gaps developed between

2.5 Diagnostic Measurements (continued)

the plate and the lense, whereas when the plates were parallel to the ground, the force of gravity plus the clamps kept good contact between them. Therefore, all patterns were taken in the azimuth plane with the parallel plates parallel to the ground using vertical linear polarization.

2.6 Lense Measurements

2.6.1 Plano-Convex Teflon Lens - No Seams

The plano-convex Teflon lense was installed in the parallel plates and the clamping fixture attached and set. The large feed horn, which provides 15 db edge directed illumination to the lense, was installed in the feed positioning structure aligned along the lense axis. With the frequency set to 18 GHz, the feed was moved axially (along the lens axis) starting with the feed aperture two wavelengths from the lense focal point on the opposite side of tne focal point from the lense and ending with the feed aperture five wavelengths from the lense focal point on the same side of the focal point as the lense. The variation in signal response as a function of feed axial position is shown in Fig. 2-28. Successive maxima and minima are approximately one half wavelength apart. The adjacent maximum to minimum variations are nominally 3 dB and the maximum response changes 3 dB over the range of feed movement. The measured peak gain at maximum response is 22.8 dBi.

The VSWR of the feed horn was measured with the horn positioned at each of these same positions. The VSWR of the horn as a function of axial position is shown in Fig. 2-29. The VSWR of the feed horn outside of the parallel plates is 1.65:1. The lens was removed from the parallel plates and the VSWR of the feed horn inside the plates for several axial positions is shown in Fig. 2-30.

With the feed horn set to the maximum response position, a series of patterns were taken at 18 GHz as the feed was moved laterally off axis in 0.5 inch steps. These patterns are shown in Figs. 2-31 thru 2-43. These same patterns were repeated at 14 GHz and are shown in Figs. 2-44 thru 2-56.

These patterns are what were expected from an uncorrected plano-convex lense. As the feed is moved laterally off axis, the main beam broadens and multiple coma lobes

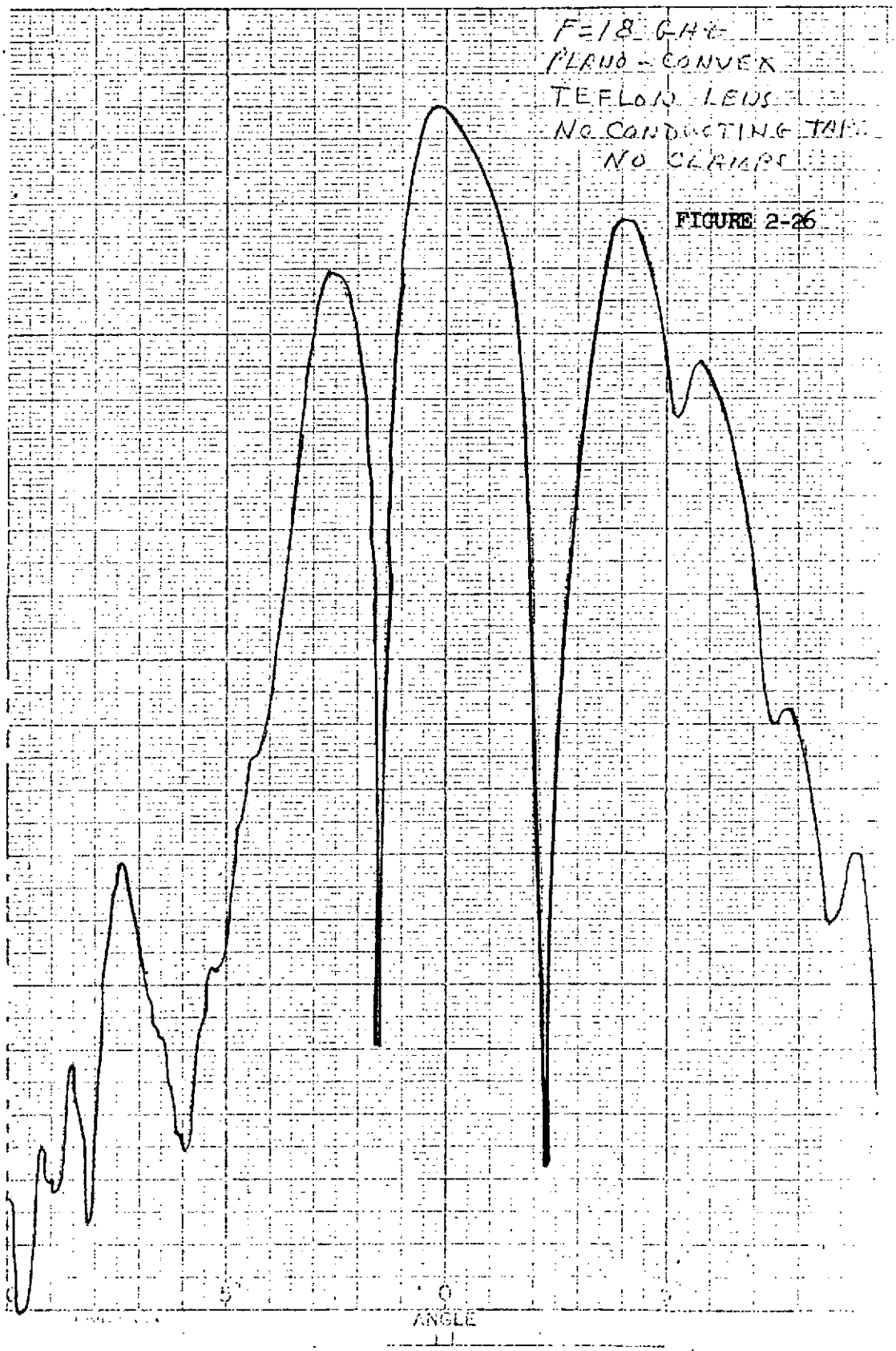
F=18 GHz
PLANO-CONVEX
TEFLON LENS
NO CONDUCTING TAPE
NO CLAMPS
ANGLE

FIGURE 2-26

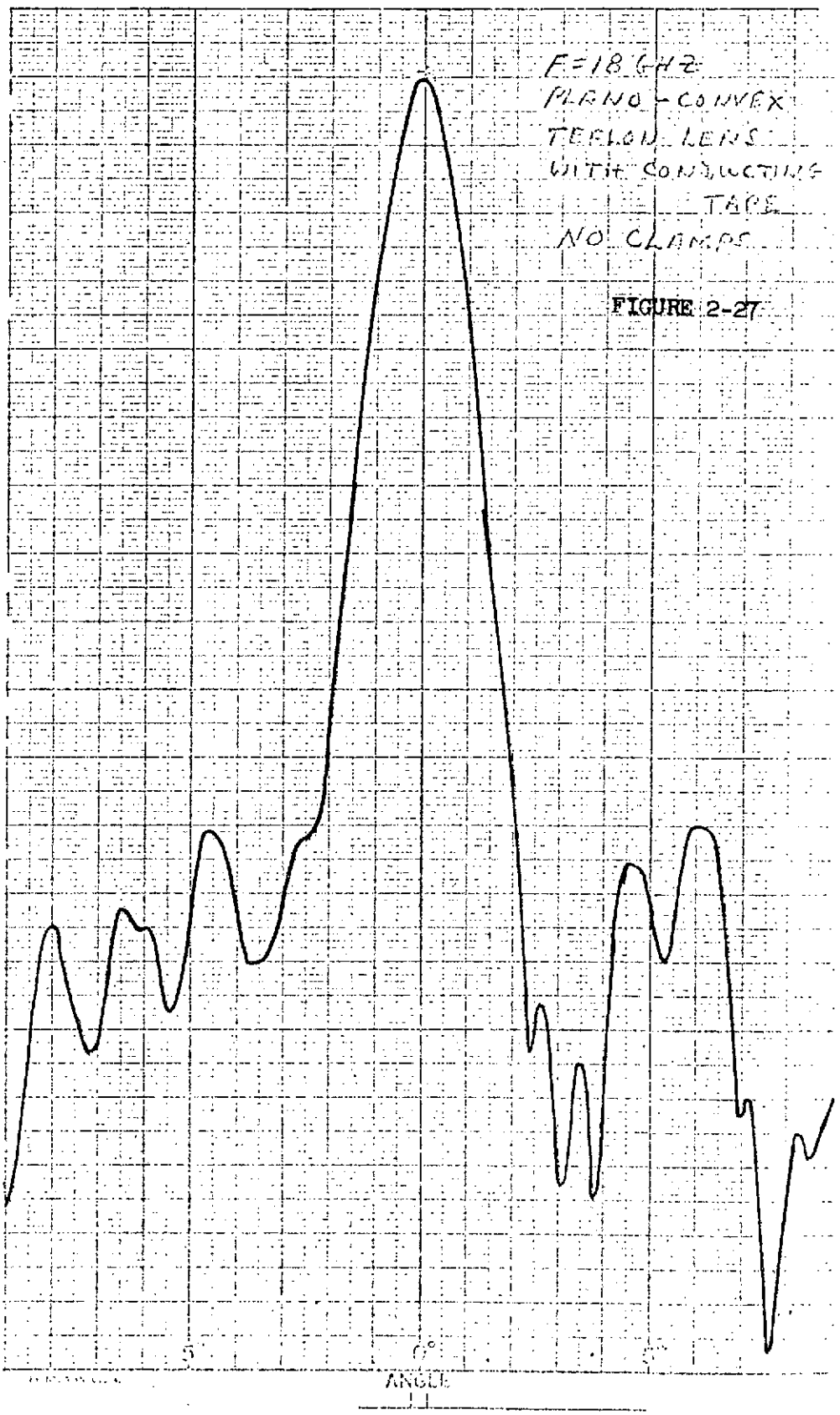
F=18 GHZ
PLANO-CONVEX
TEFLON LENS
WITH CONDUCTIVE
TAPE
NO CLAMPS
5°
0°
5°
ANGLE

FIGURE 2-27

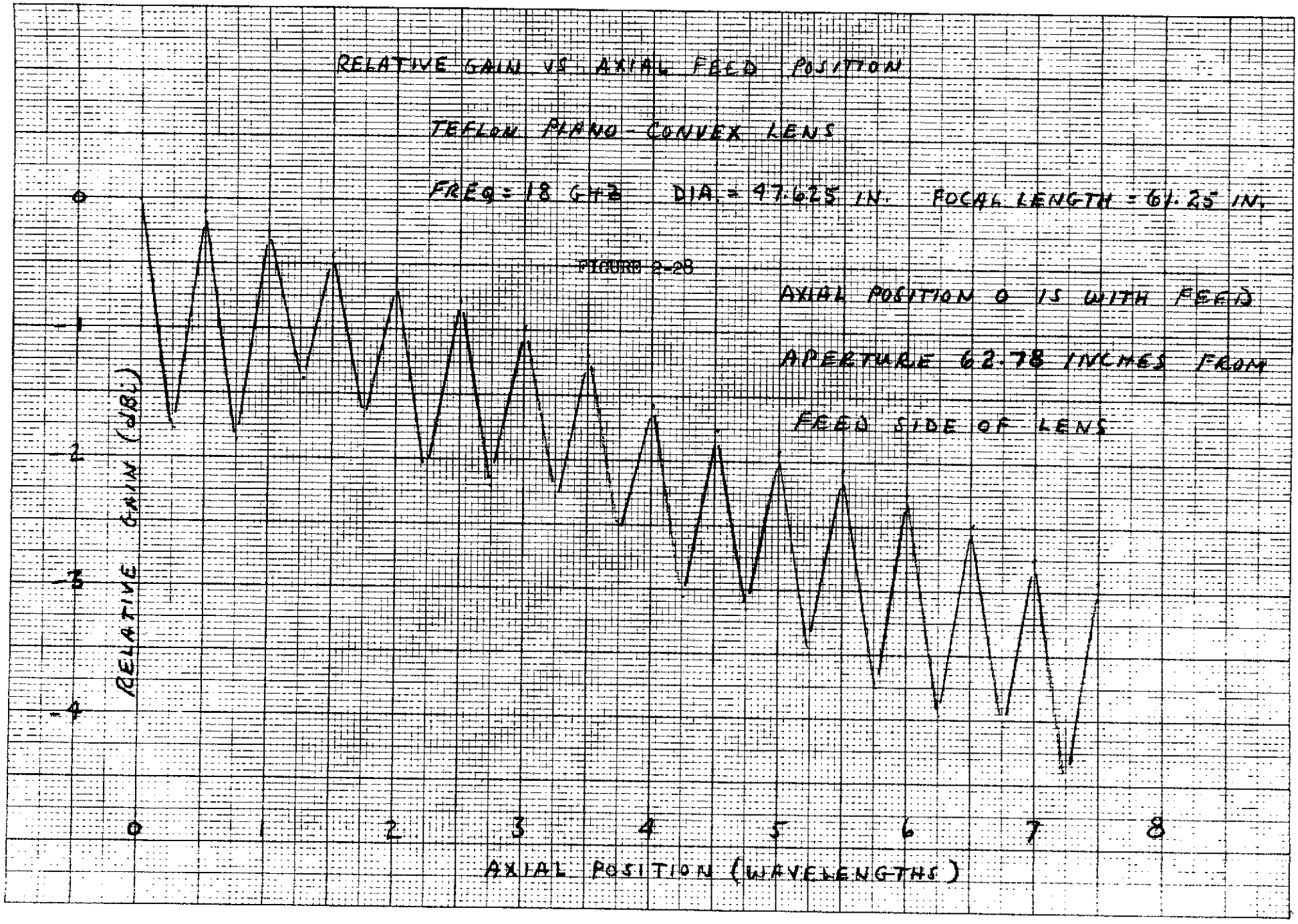

FIGURE 2-28

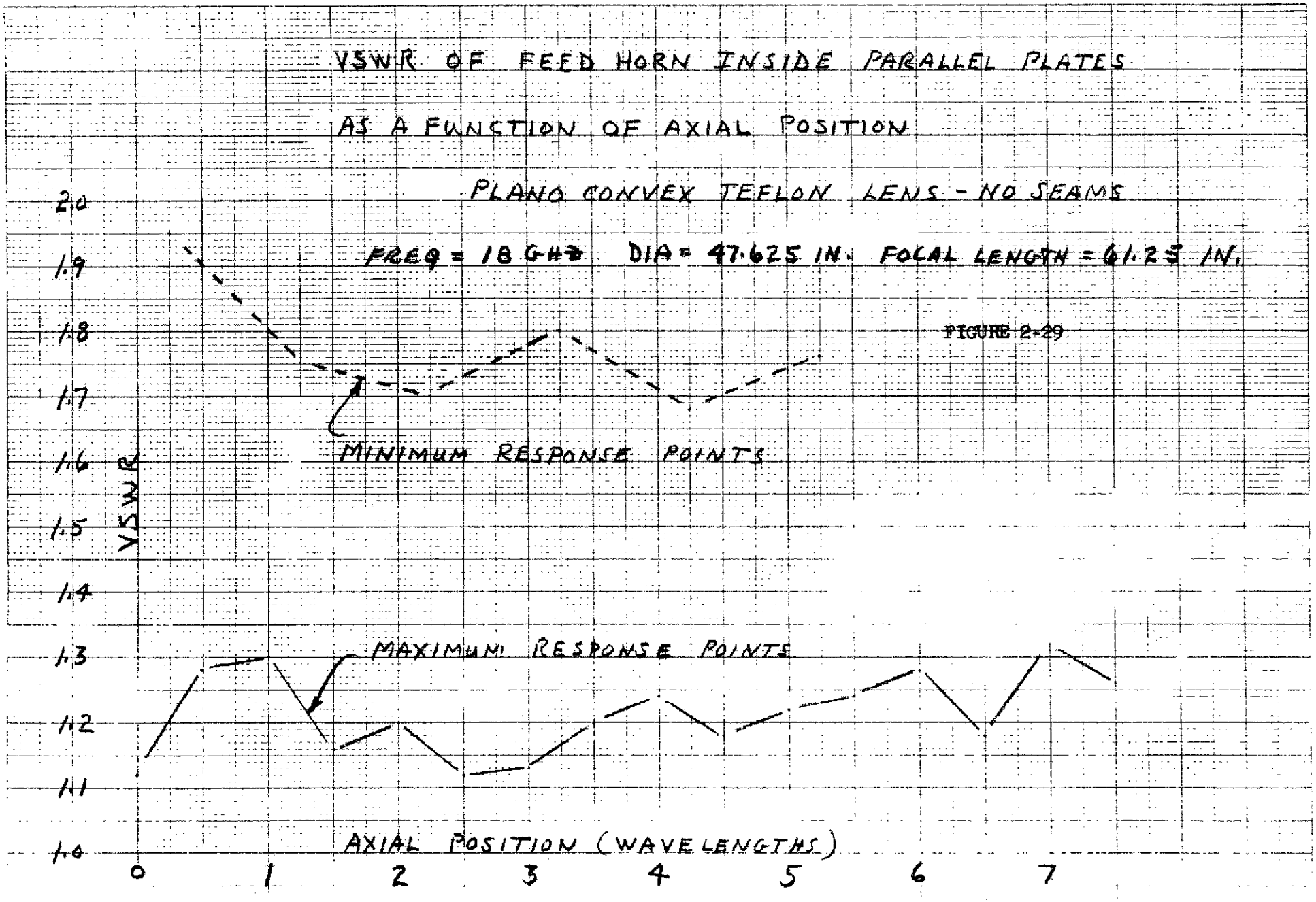
VSWR OF FEED HORN INSIDE PARALLEL PLATES
AS A FUNCTION OF AXIAL POSITION
PLANO CONVEX TEFLON LENS - NO SEAMS
FREQ = 18 GHz DIA = 47.625 IN. FOCAL LENGTH = 61.25 IN.
FIGURE 2-29
MINIMUM RESPONSE POINTS
MAXIMUM RESPONSE POINTS
VSWR
2.0
1.9
1.8
1.7
1.6
1.5
1.4
1.3
1.2
1.1
1.0
0
1
2
3
4
5
6
7
AXIAL POSITION (WAVELENGTHS)

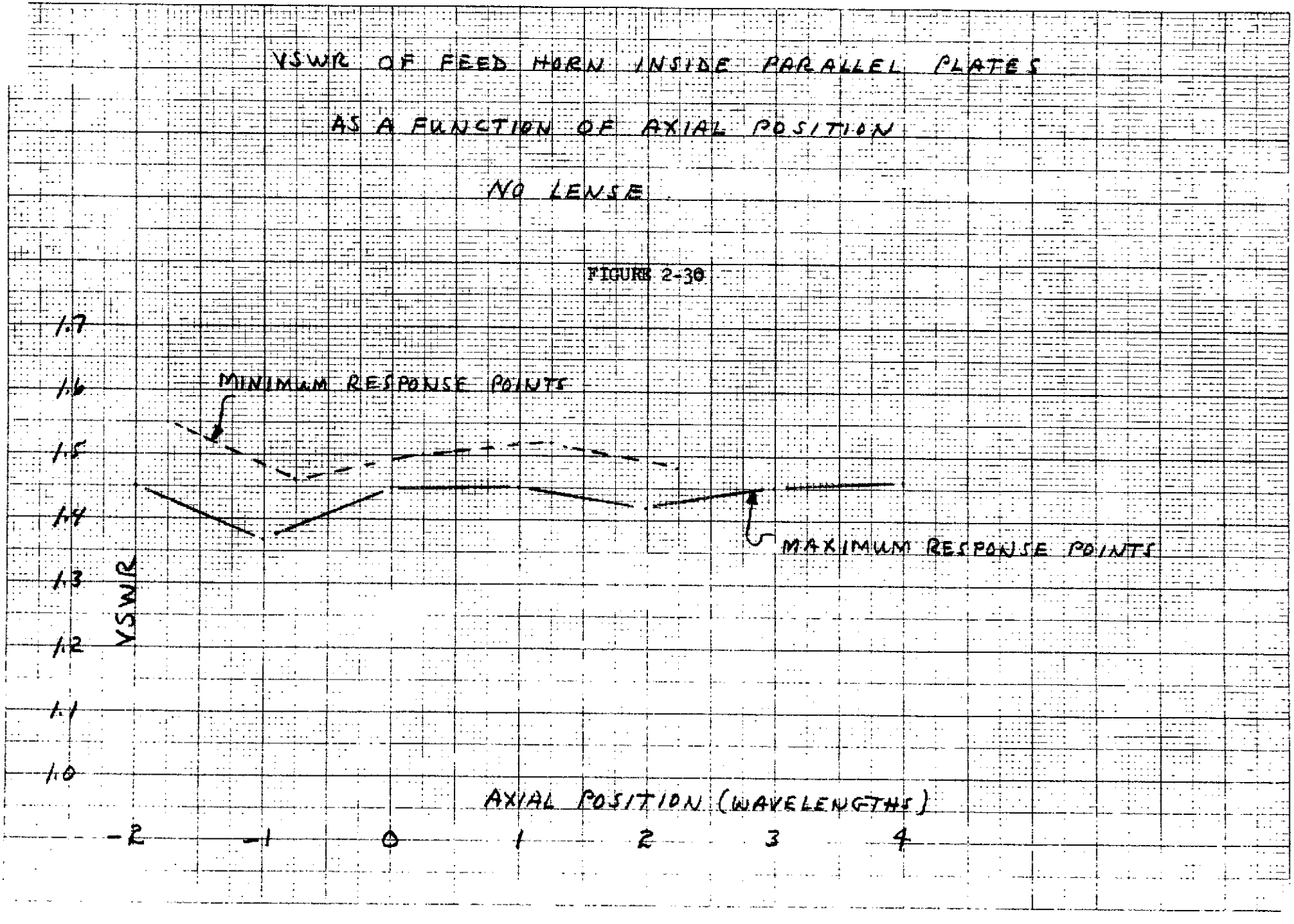
VSWR OF FEED HORN INSIDE PARALLEL PLATES
AS A FUNCTION OF AXIAL POSITION
NO LENSE
MINIMUM RESPONSE POINTS
MAXIMUM RESPONSE POINTS
VSWR
1.7
1.6
1.5
1.4
1.3
1.2
1.1
1.0
AXIAL POSITION (WAVELENGTHS)
-2
-1
0
1
2
3
4

FIGURE 2-30

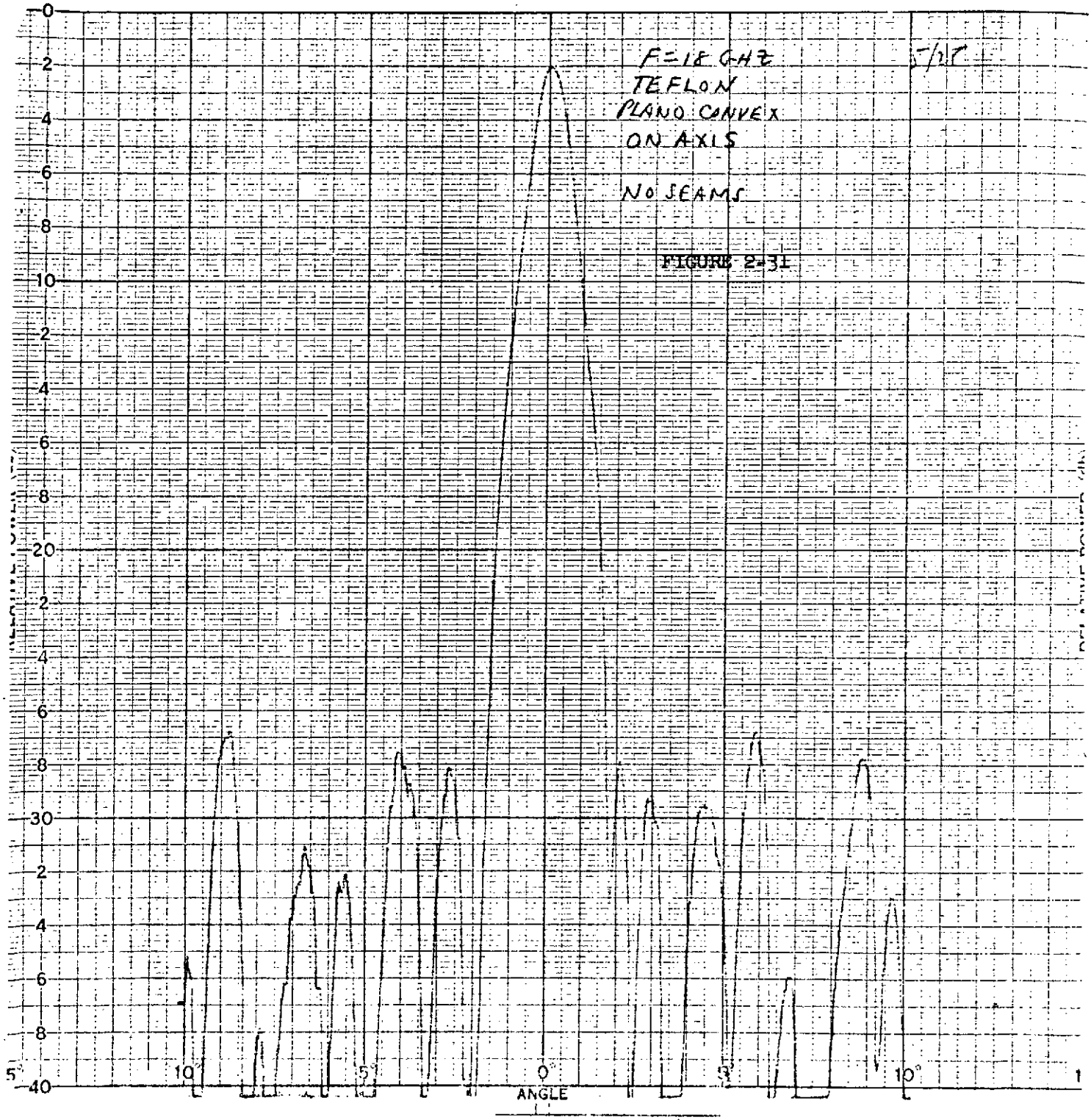

FIGURE 2-31

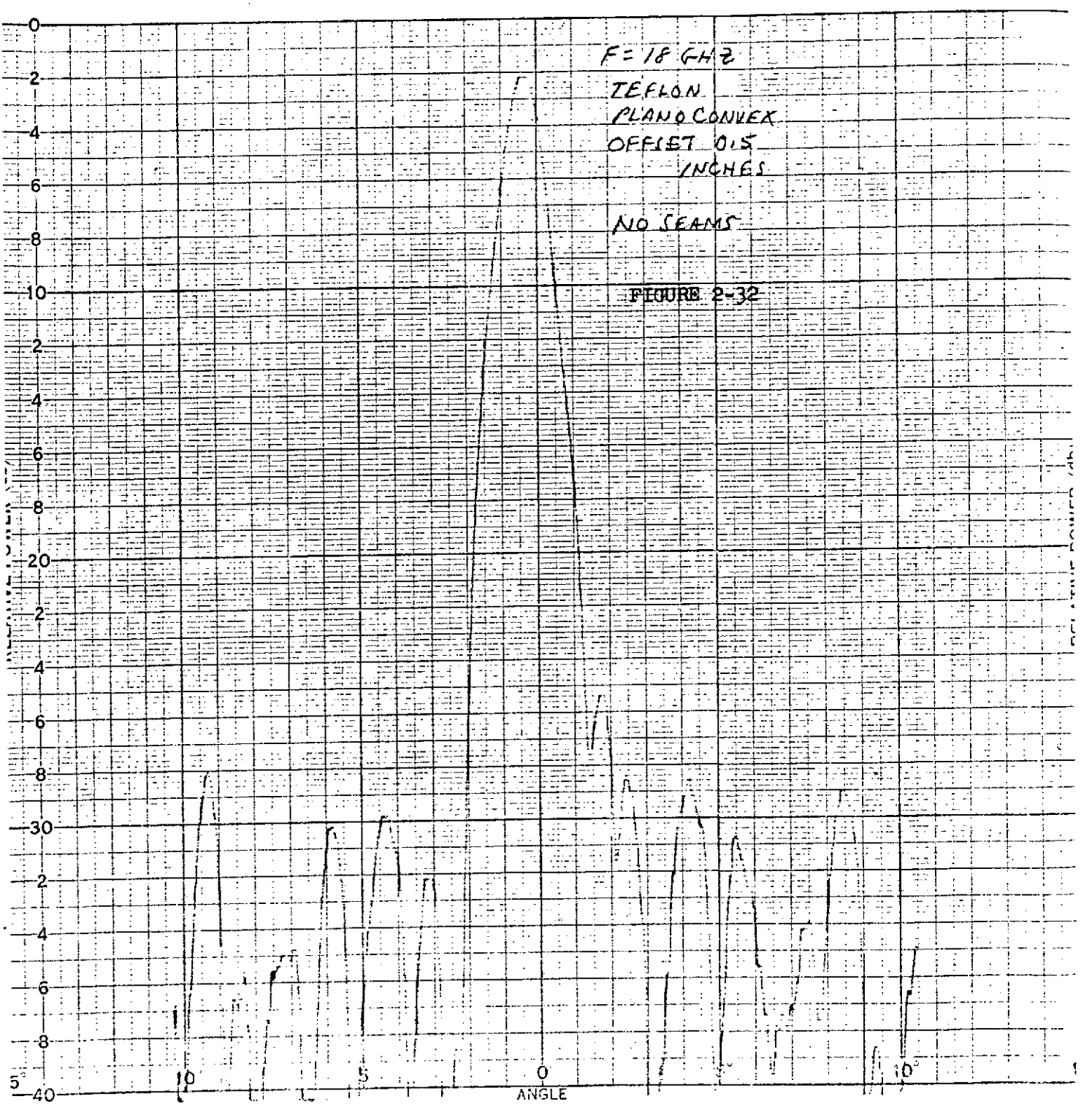
F = 18 GHZ
TEFLON
PLANO CONVEX
OFFSET 0.5
INCHES
NO SEAMS
0
2
4
6
8
10
2
4
6
8
20
2
4
6
8
30
2
4
6
8
40
10°
5°
0
5°
10°
ANGLE

FIGURE 2-32

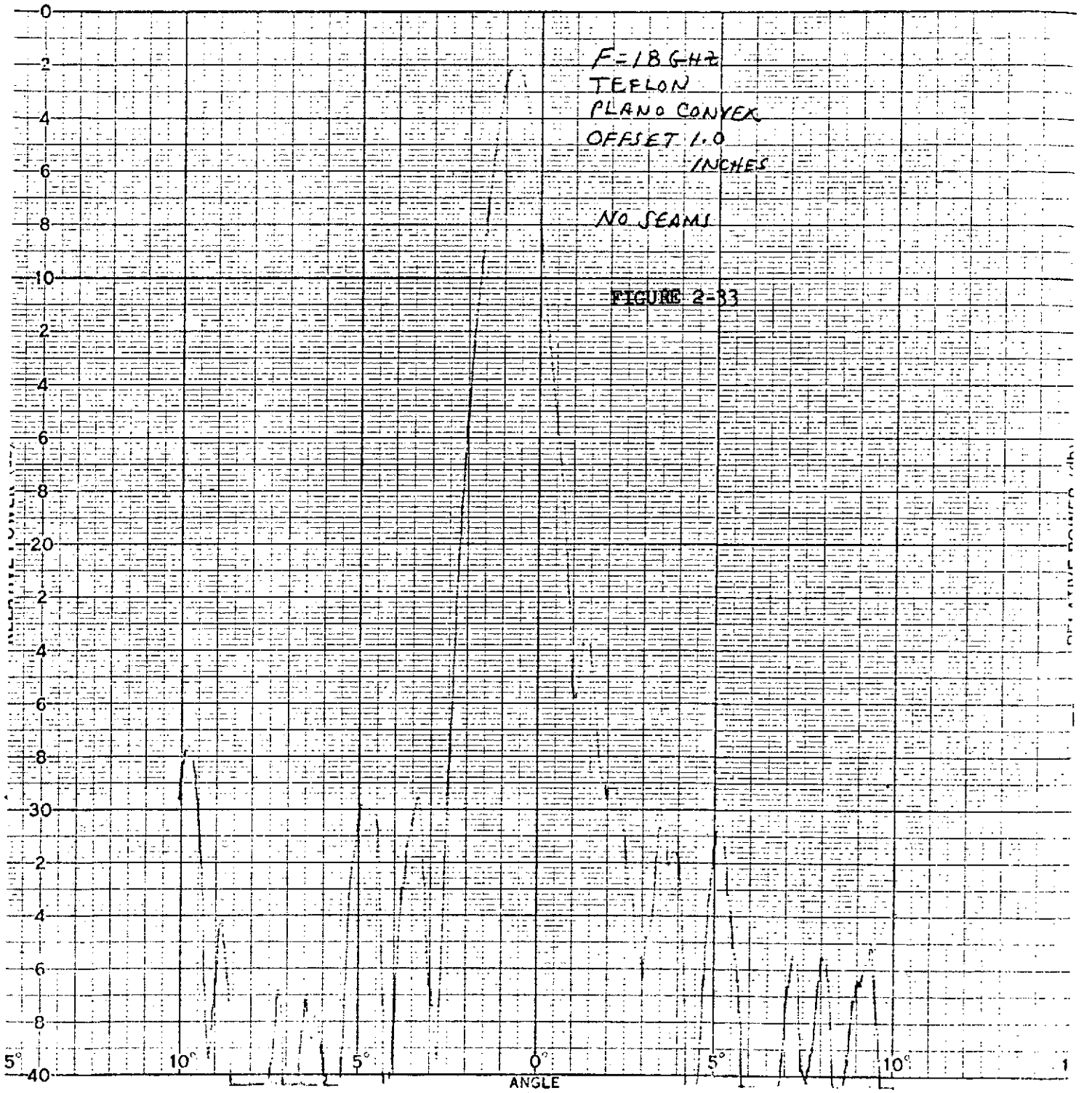
F=18 GHz
TEFLON
PLANO CONVEX
OFFSET 1.0
INCHES
NO SEAMS
0
2
4
6
8
10
2
4
6
8
20
2
4
6
8
30
2
4
6
8
40
5°
10°
5°
0°
5°
10°
ANGLE

FIGURE 2-33

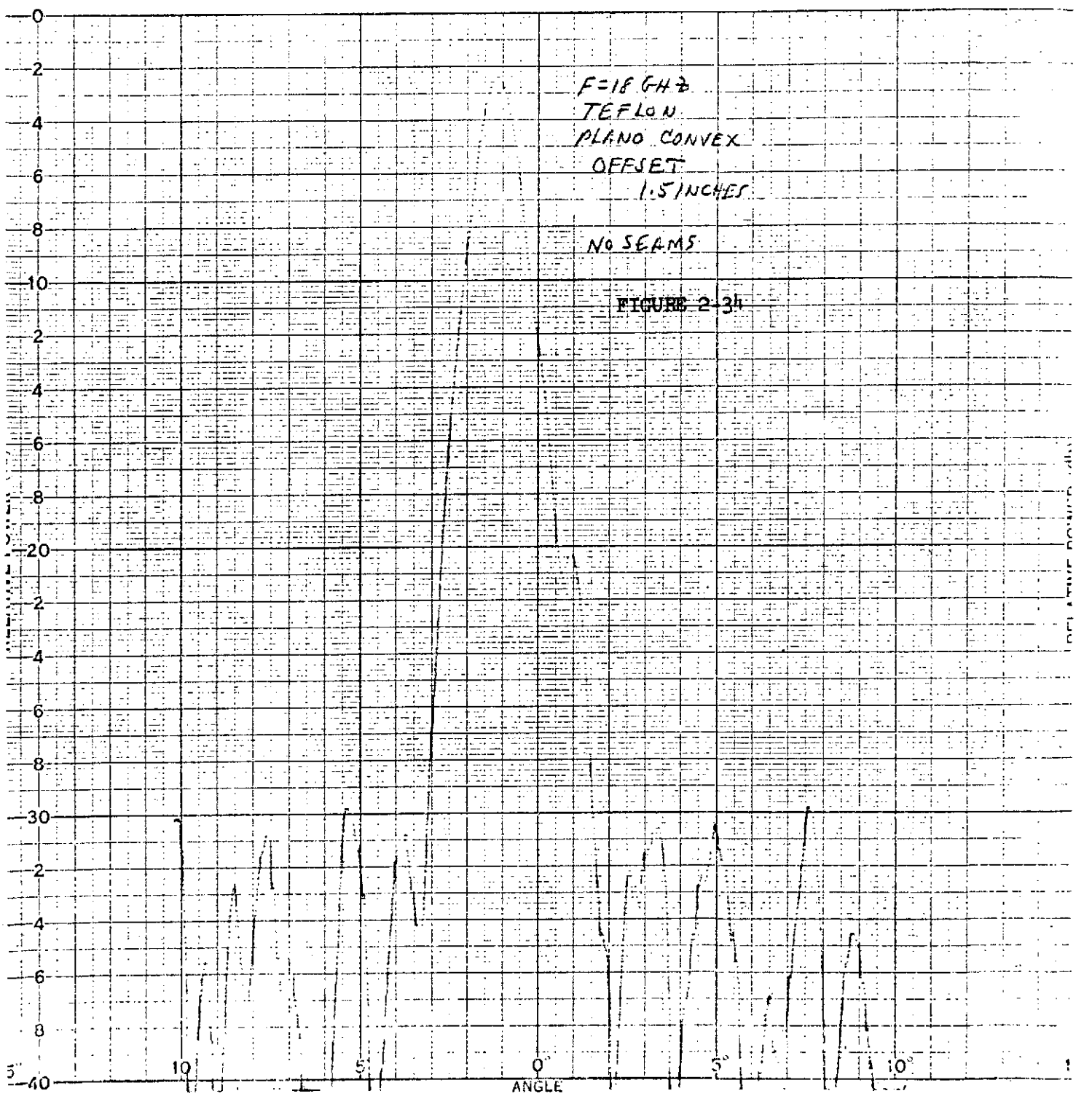
F=18 GHz
TEFLON
PLANO CONVEX
OFFSET
1.5 INCHES
NO SEAMS
0
2
4
6
8
10
2
4
6
8
20
2
4
6
8
30
2
4
6
8
40
10°
5°
0°
5°
10°
ANGLE

FIGURE 2-34

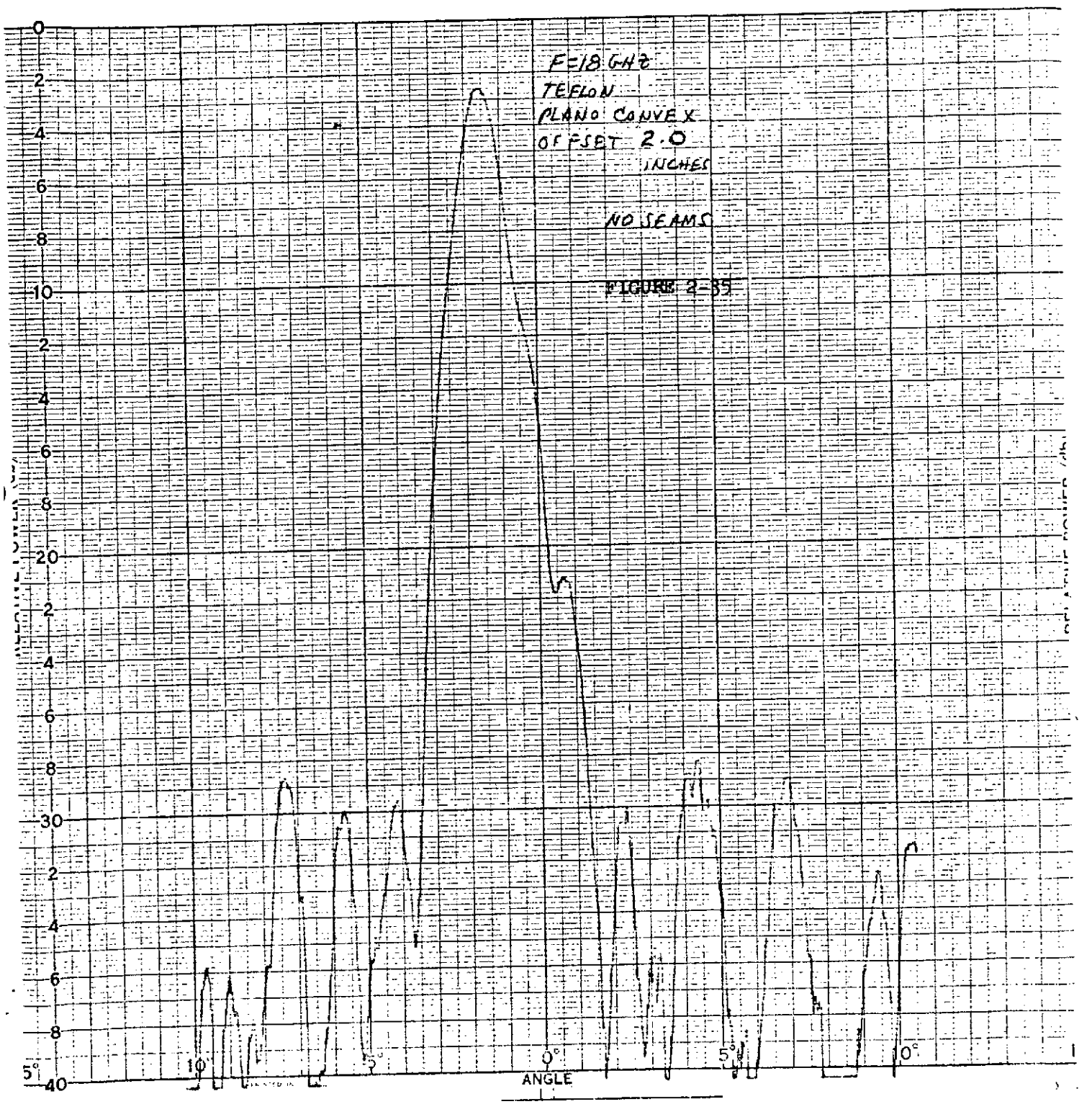
F=18 GHz
TEFLON
PLANO CONVEX
OFFSET 2.0
INCHES
NO SEAMS
FIGURE 2-35
0
2
4
6
8
10
2
4
6
8
20
2
4
6
8
30
2
4
6
8
40
10°
5°
0°
5°
10°
ANGLE

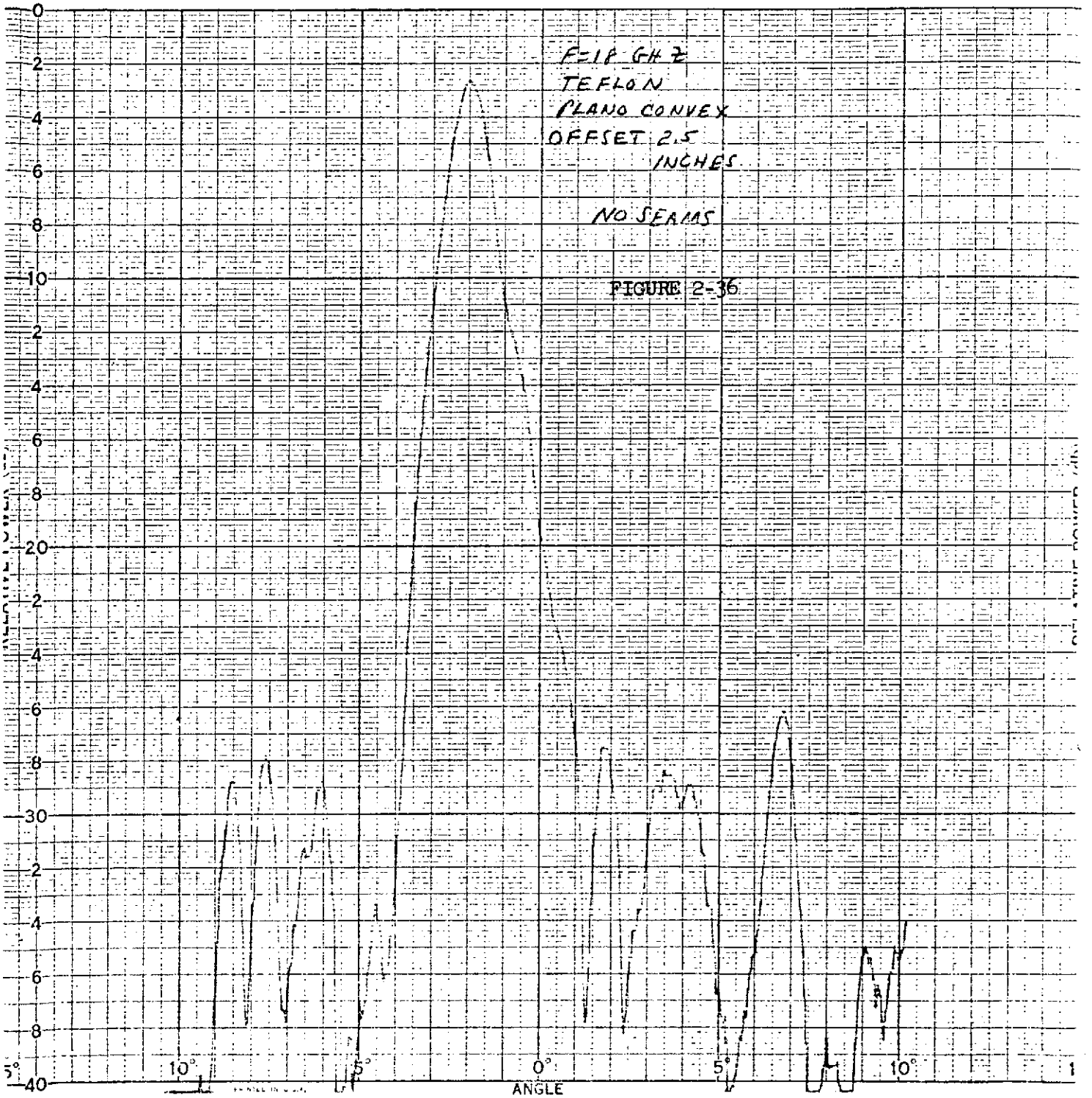
F=18 GHz
TEFLON
PLANO CONVEX
OFFSET 2.5
INCHES
NO SEAMS
0
2
4
6
8
10
2
4
6
8
20
2
4
6
8
30
2
4
6
8
40
10°
5°
0°
5°
10°
ANGLE

FIGURE 2-36

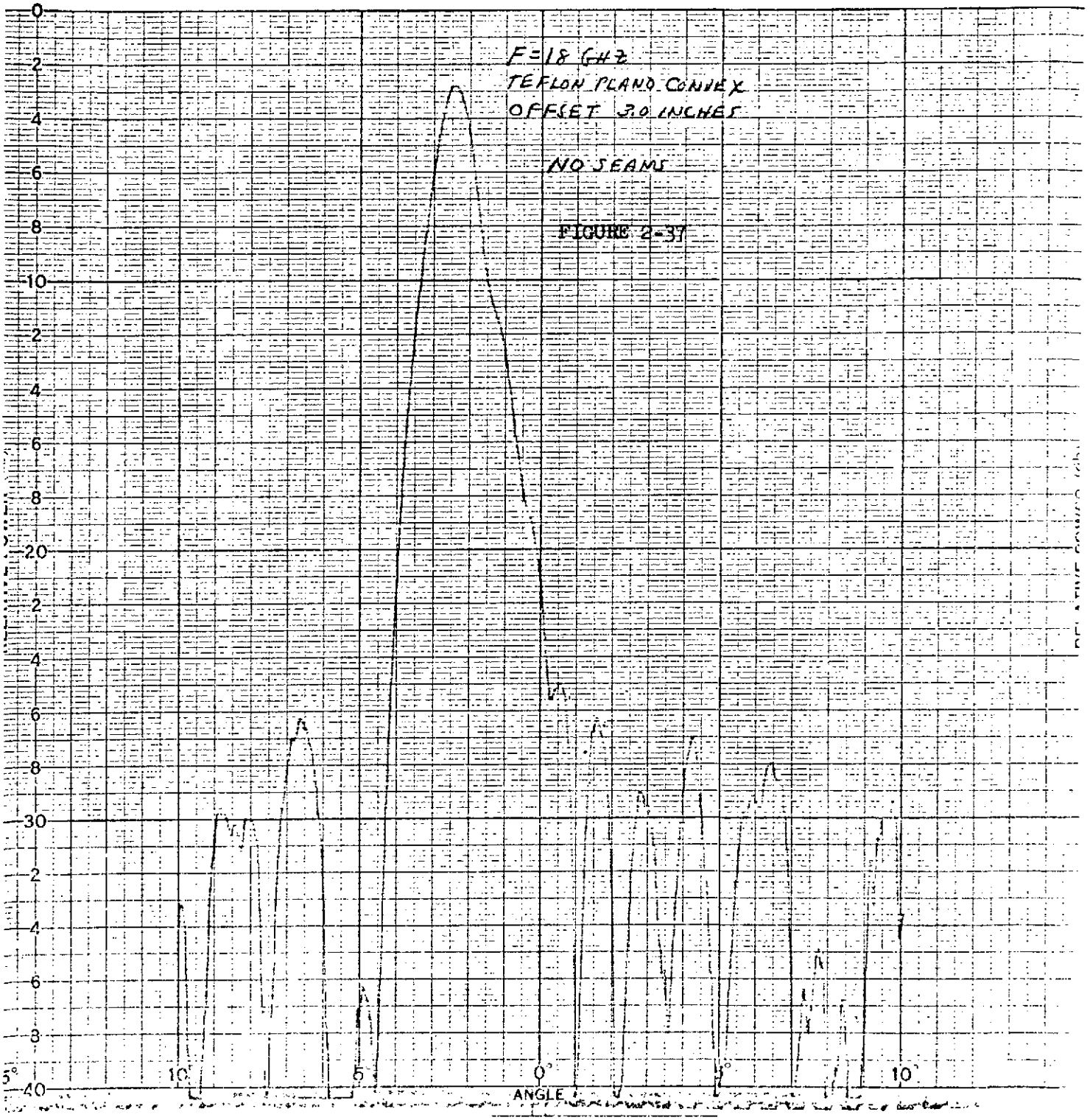
F=18 GHz
TEFLON PLANO CONVEX
OFFSET 3.0 INCHES
NO SEAMS
0
2
4
6
8
10
2
4
6
8
20
2
4
6
8
30
2
4
6
8
40
10°
5°
0°
5°
10°
ANGLE

FIGURE 2-37

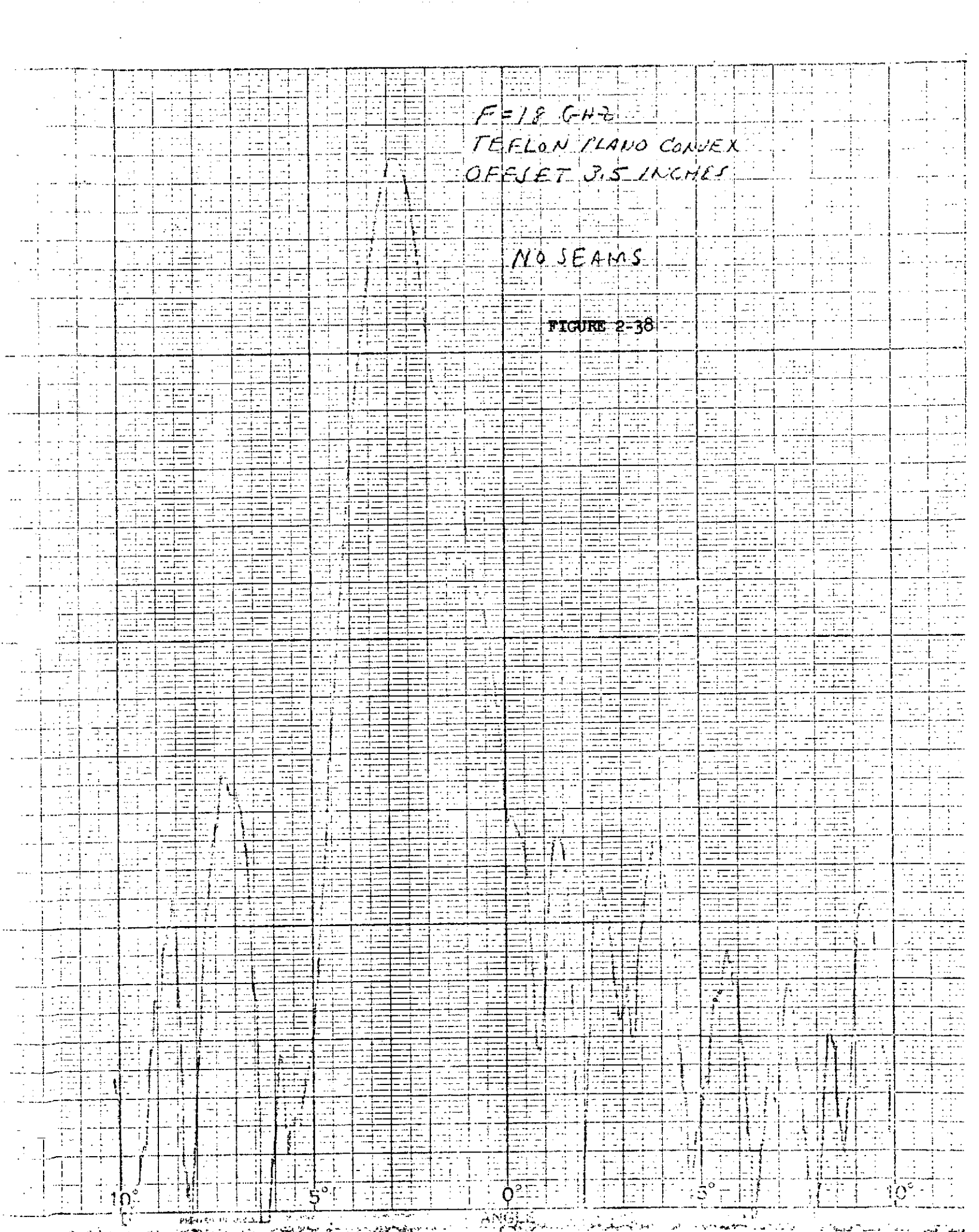
F=18 GHz
TEFLON PLANO CONVEX
OFFSET 3.5 INCHES
NO SEAMS
10°
5°
0°
5°
10°
ANGLE

FIGURE 2-38

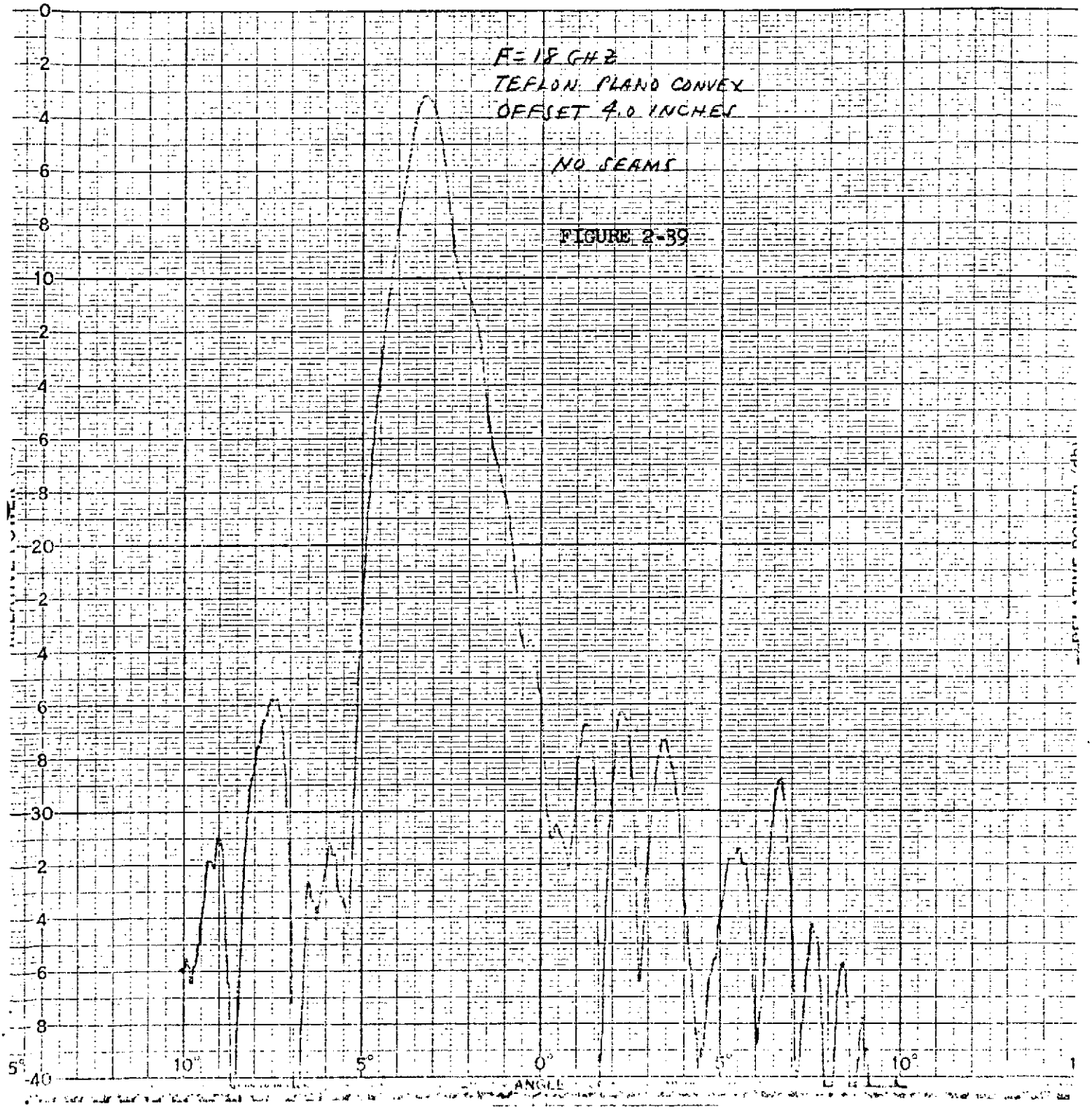
F=18 GHz
TEFLON PLANO CONVEX
OFFSET 4.0 INCHES
NO SEAMS
0
-2
-4
-6
-8
-10
-20
-30
-40
10°
5°
0°
5°
10°
ANGLE

FIGURE 2-39

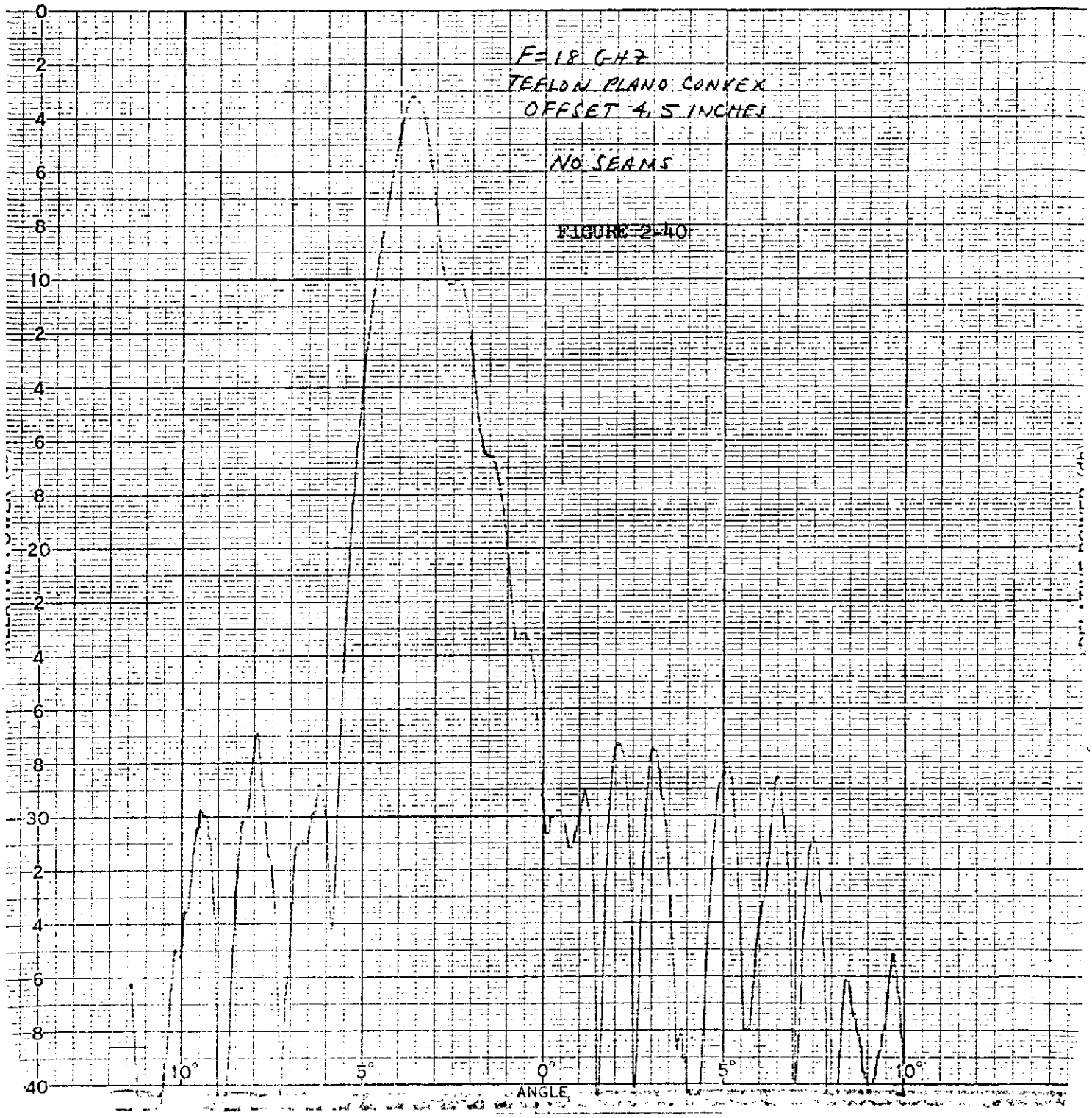
F=18 GHZ
TEFLON PLANO CONVEX
OFFSET 4.5 INCHES
NO SEAMS
FIGURE 2-40
0
2
4
6
8
10
2
4
6
8
20
2
4
6
8
30
2
4
6
8
40
10°
5°
0°
5°
10°
ANGLE

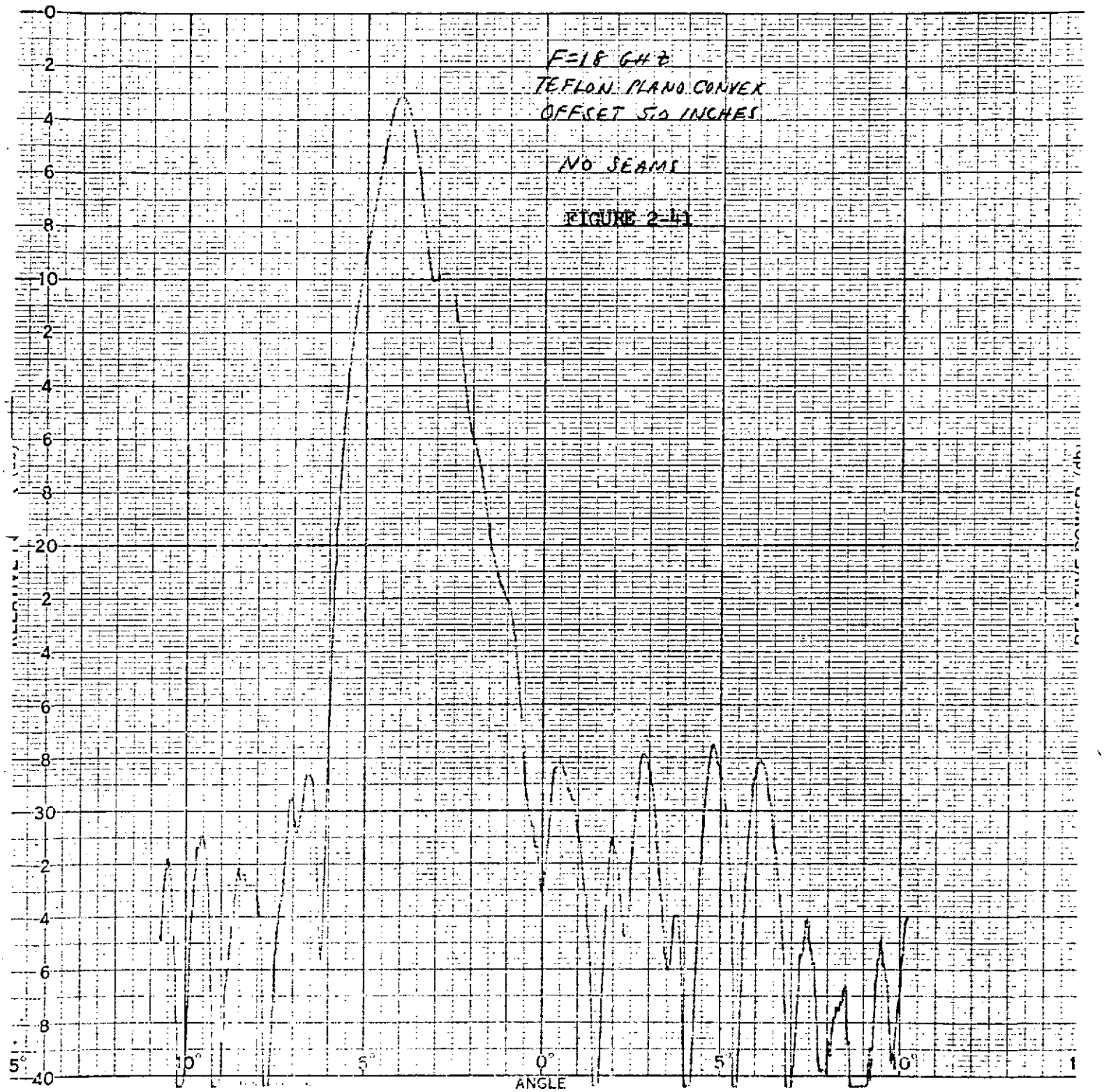
F=18 GHz
TEFLON PLANO CONVEX
OFFSET 5.0 INCHES
NO SEAMS
0
2
4
6
8
10
2
4
6
8
20
2
4
6
8
30
2
4
6
8
40
10°
5°
0°
5°
10°
ANGLE

FIGURE 2-41

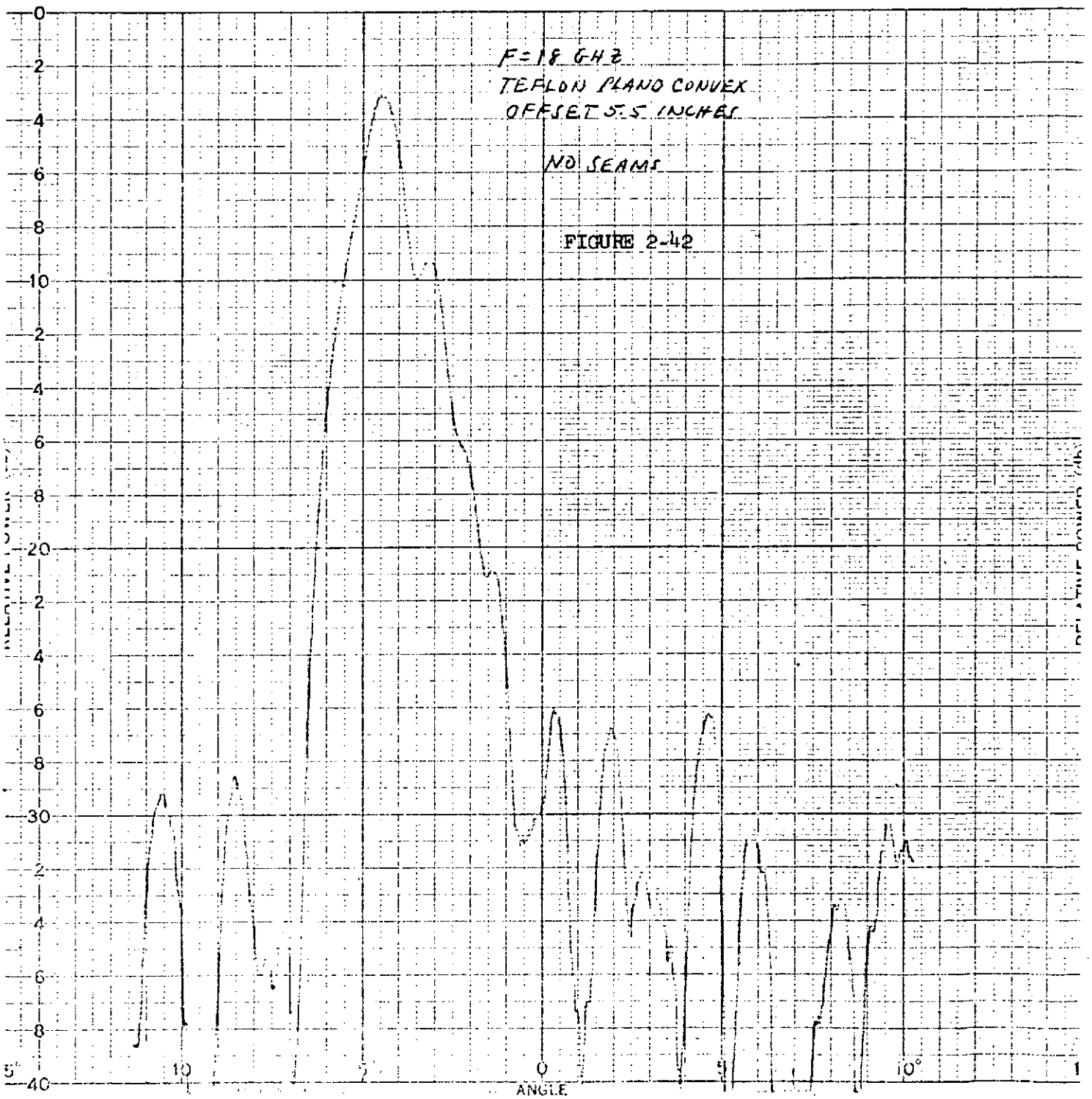
F=1.8 GHZ
TEFLON PLANO CONVEX
OFFSET 5.5 INCHES
NO SEAMS
0
2
4
6
8
10
2
4
6
8
20
2
4
6
8
30
2
4
6
8
40
10°
0
ANGLE

FIGURE 2-42

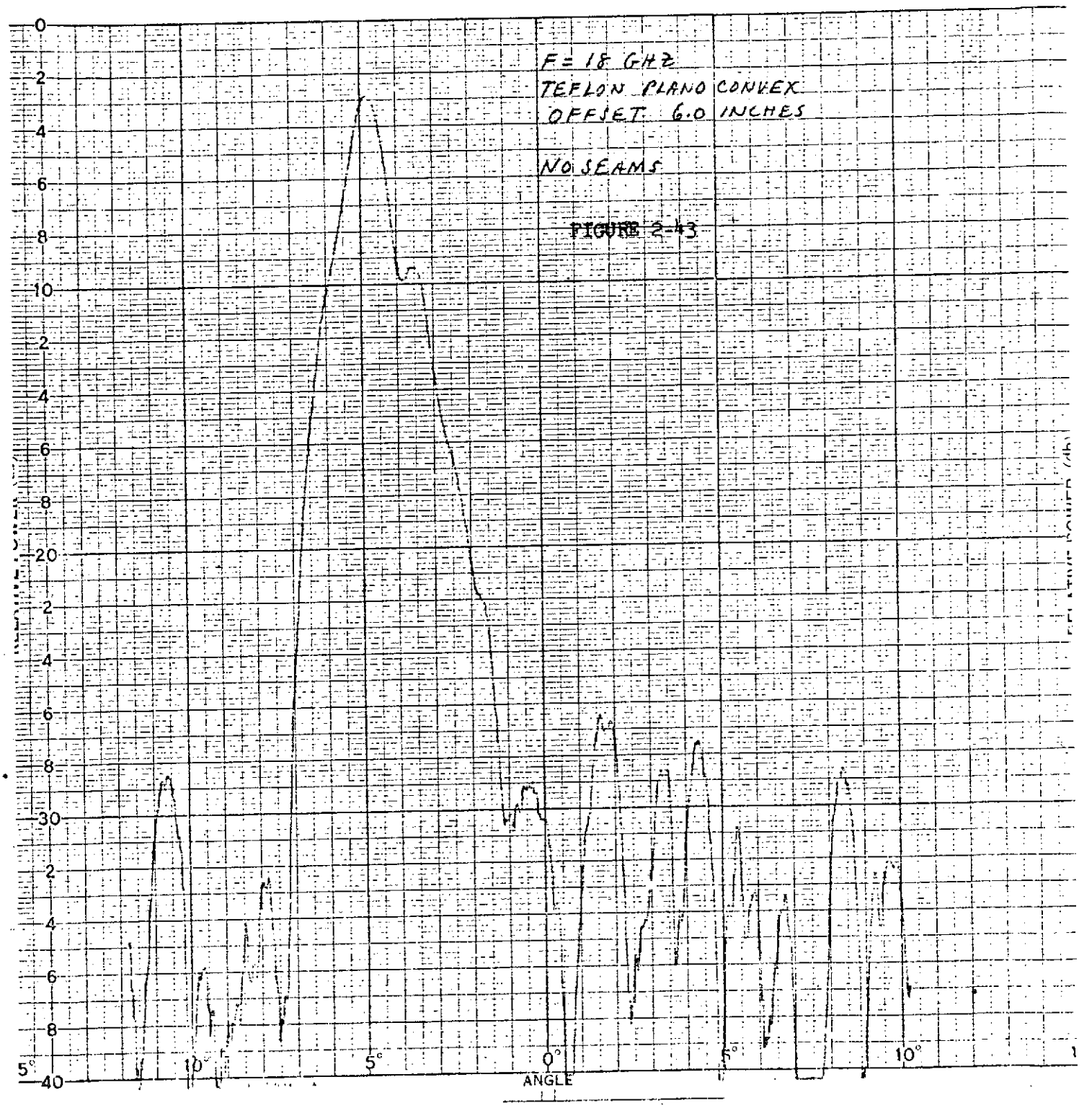
F = 18 GHz
TEFLON PLANO CONVEX
OFFSET 6.0 INCHES
NO SEAMS
0
2
4
6
8
10
2
4
6
8
20
2
4
6
8
30
2
4
6
8
40
5°
10°
5°
0°
5°
10°
ANGLE

FIGURE 2-43

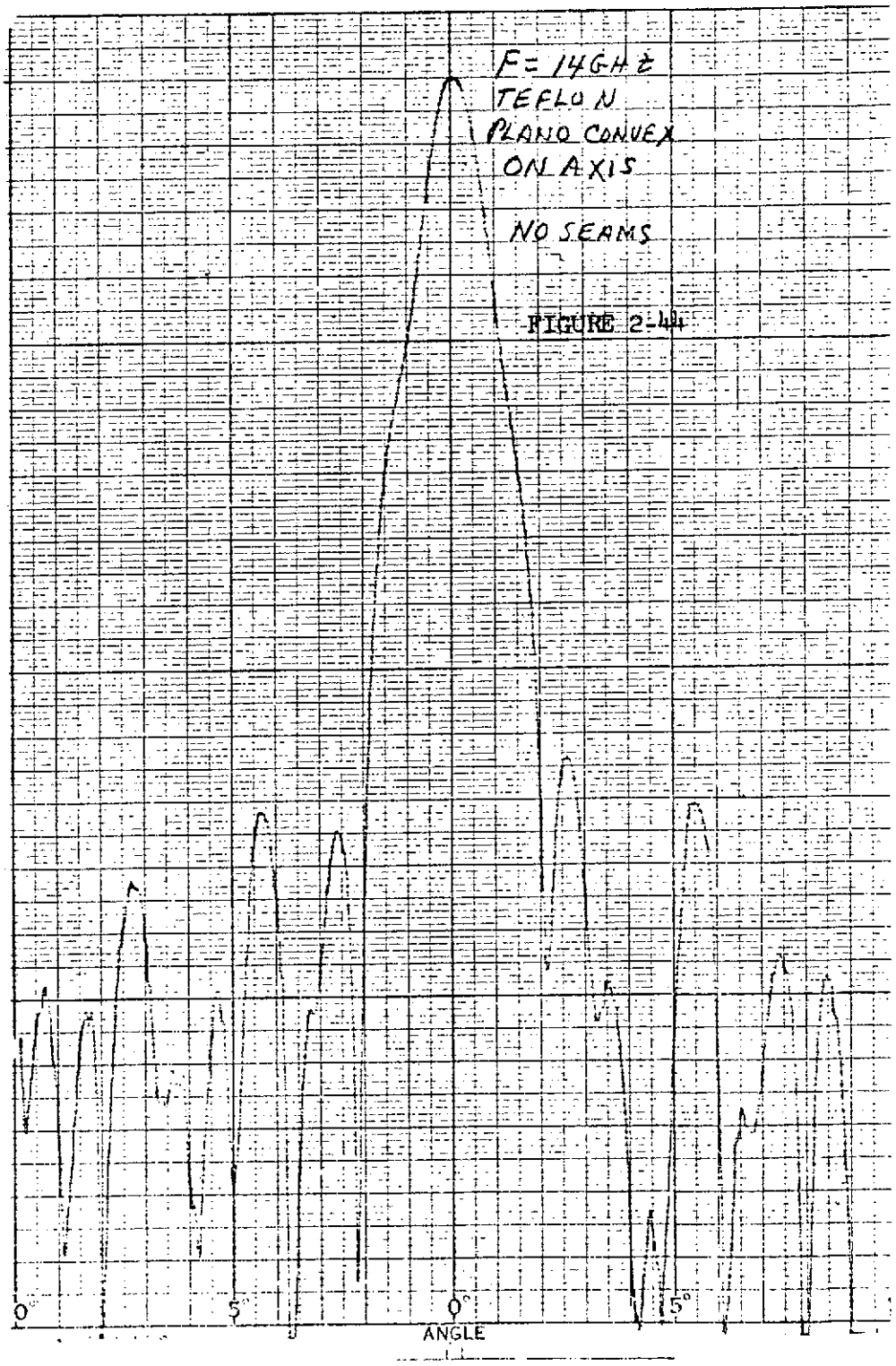

FIGURE 2-44

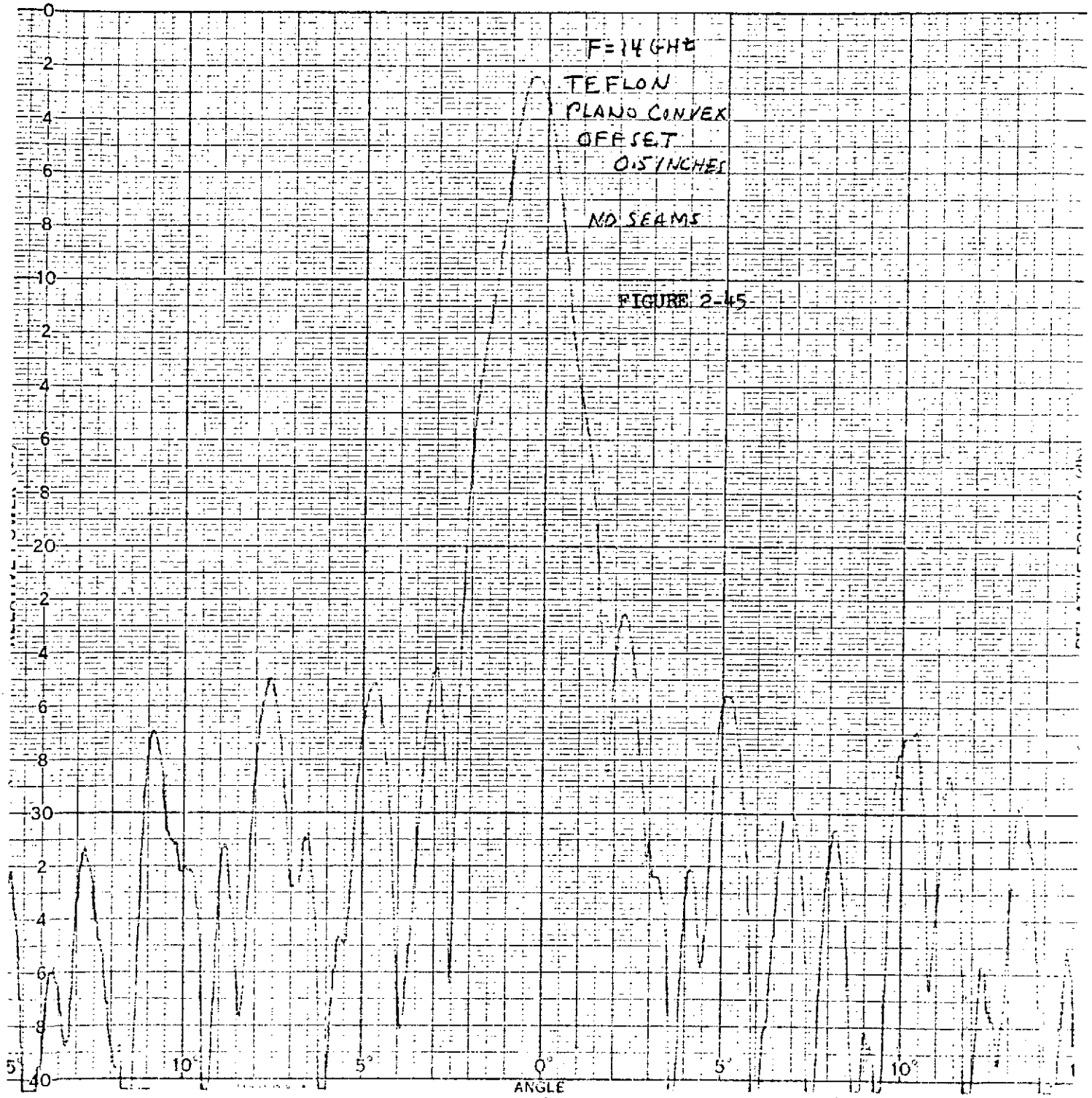
F=14 GHz
TEFLON
PLANO CONVEX
OFFSET
0.5 INCHES
NO SEAMS
0
2
4
6
8
10
2
4
6
8
20
2
4
6
8
30
2
4
6
8
40
10°
5°
0°
5°
10°
ANGLE

FIGURE 2-45

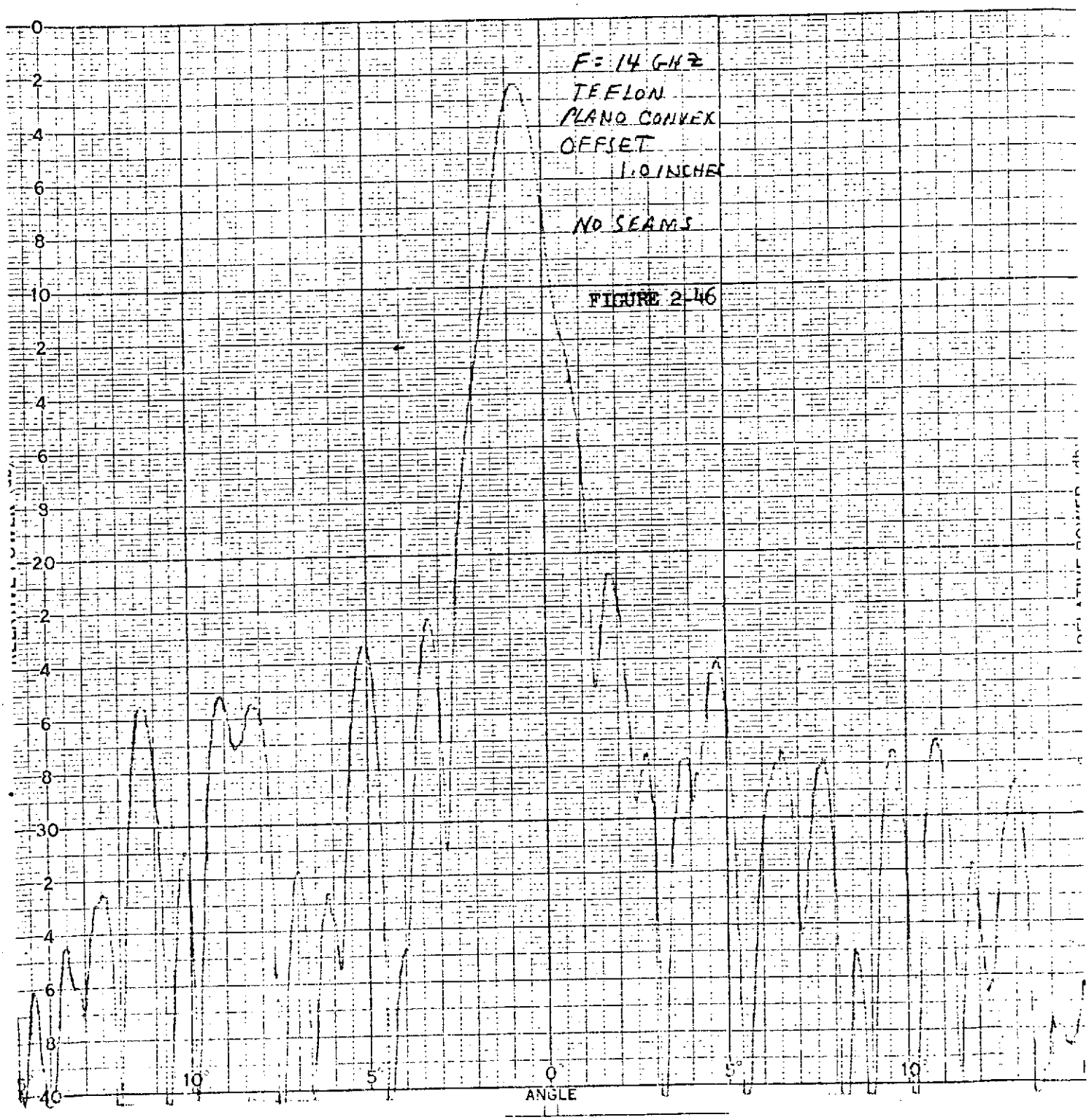
F = 14 GHz
TEFLON
PLANO CONVEX
OFFSET
1.0 INCHES
NO SEAMS
0
2
4
6
8
10
2
4
6
9
20
2
4
6
8
30
2
4
6
8
40
10°
5°
0°
5°
10°
ANGLE

FIGURE 2-46

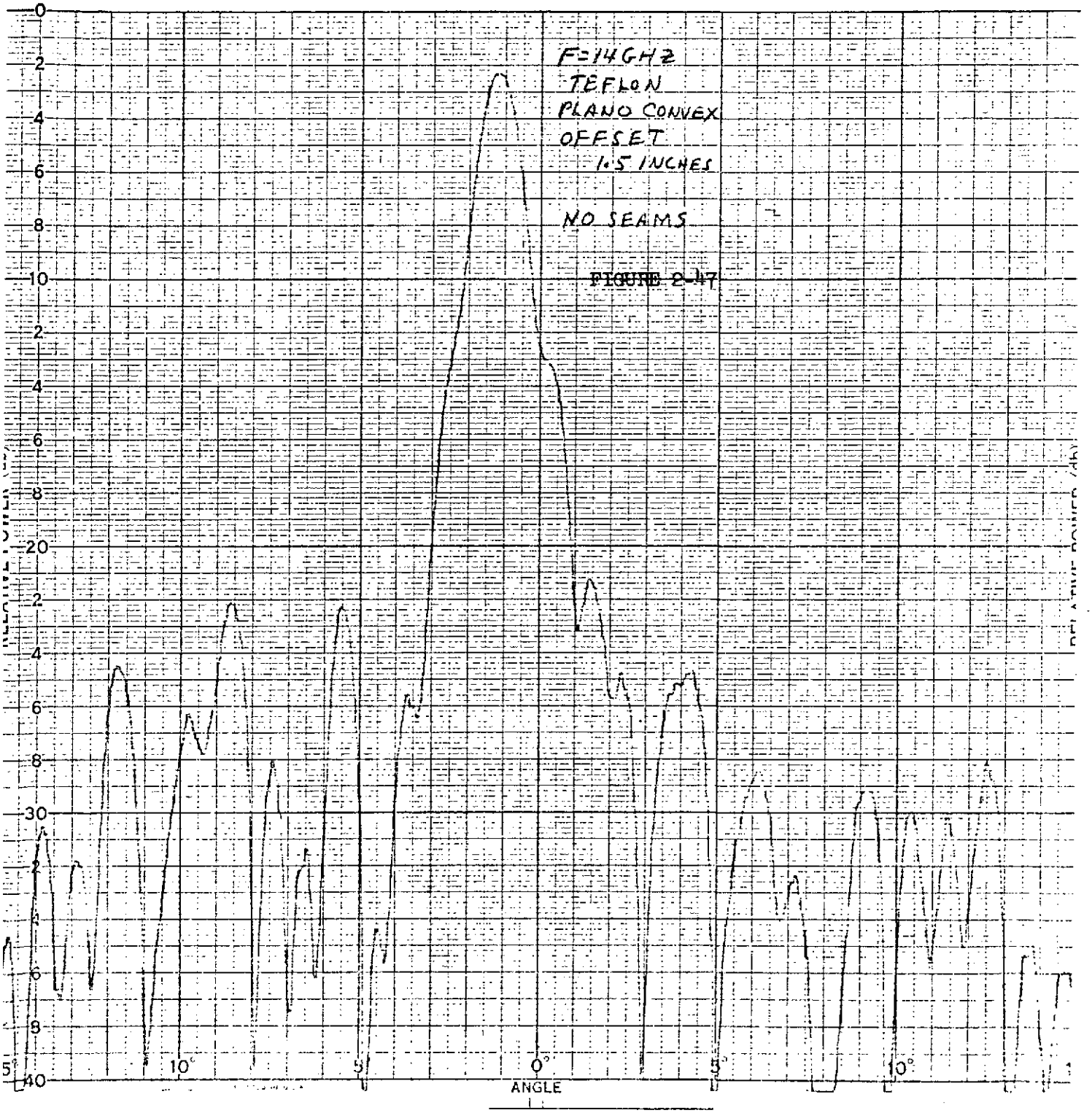
F=14GHz
TEFLON
PLANO CONVEX
OFFSET
1.5 INCHES
NO SEAMS
0
2
4
6
8
10
20
30
40
10°
5°
0°
5°
10°
ANGLE

FIGURE 2-47

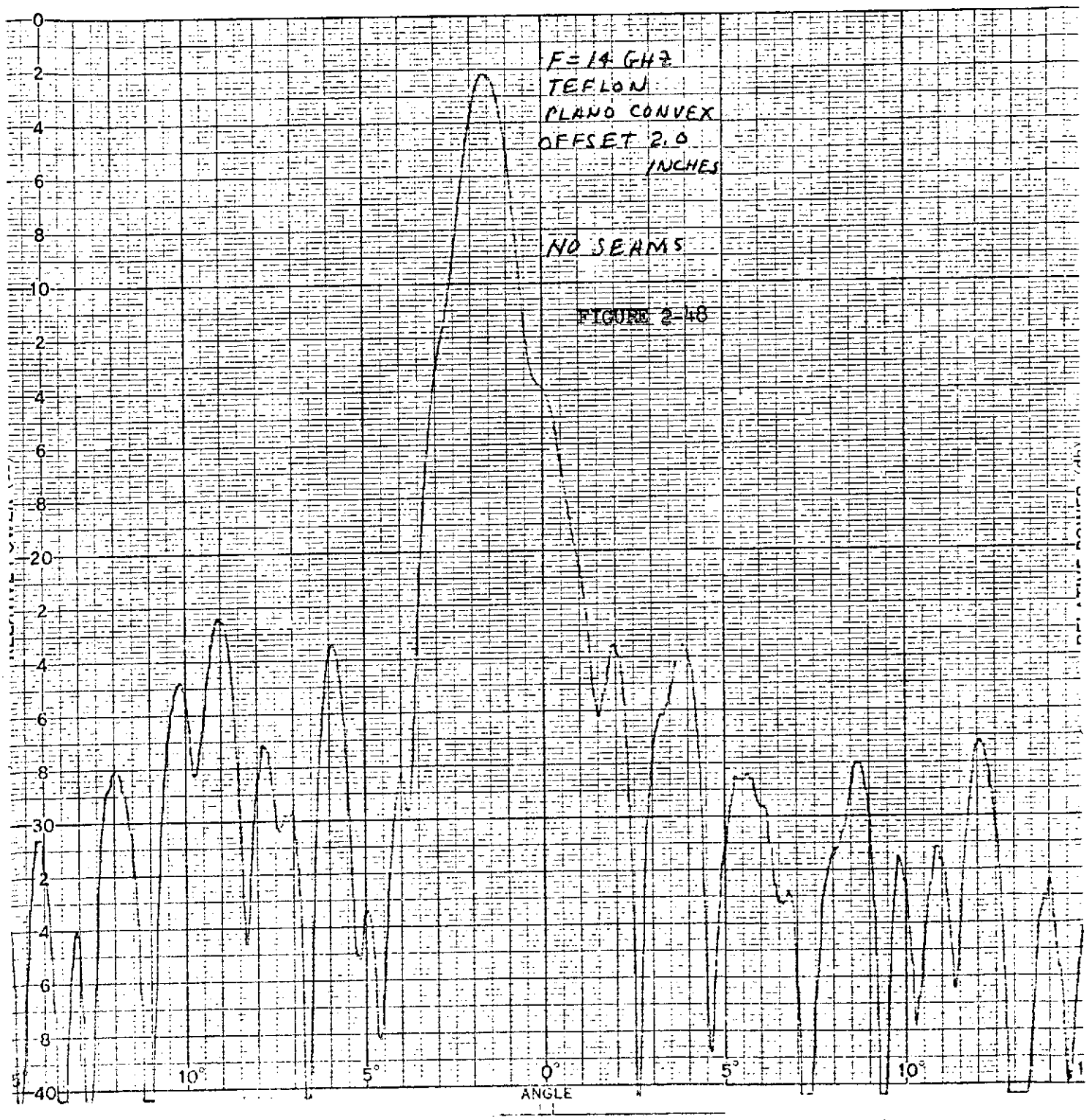
F=14 GHz
TEFLON
PLANO CONVEX
OFFSET 2.0
INCHES
NO SEAMS
0
2
4
6
8
10
2
4
6
8
20
2
4
6
8
30
2
4
6
8
40
10°
5°
0°
5°
10°
ANGLE

FIGURE 2-48

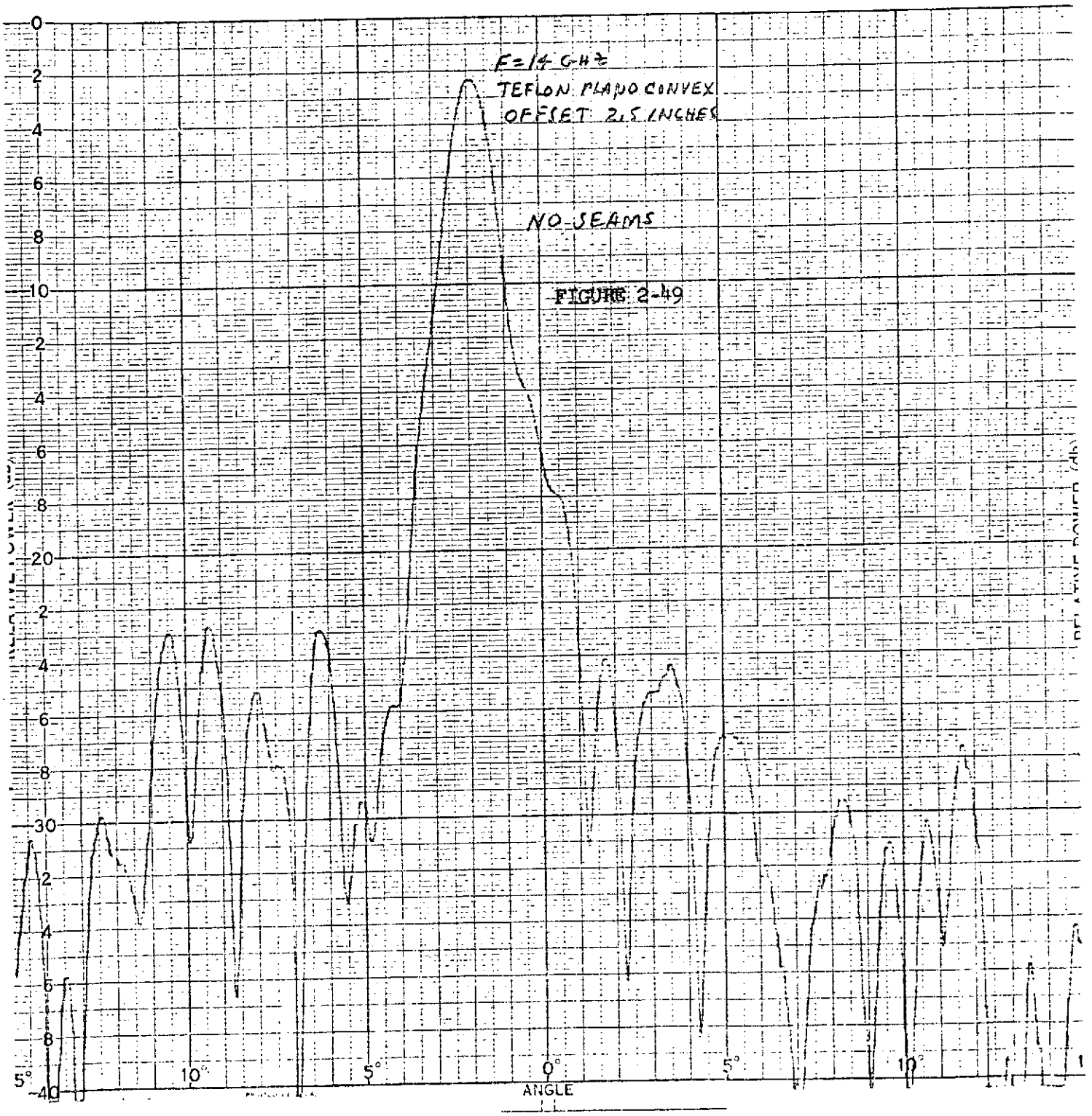
F=14 GHz
TEFLON PLANO CONVEX
OFFSET 2.5 INCHES
NO SEAMS
0
2
4
6
8
10
20
30
40
5°
10°
5°
0°
5°
10°
ANGLE

FIGURE 2-49

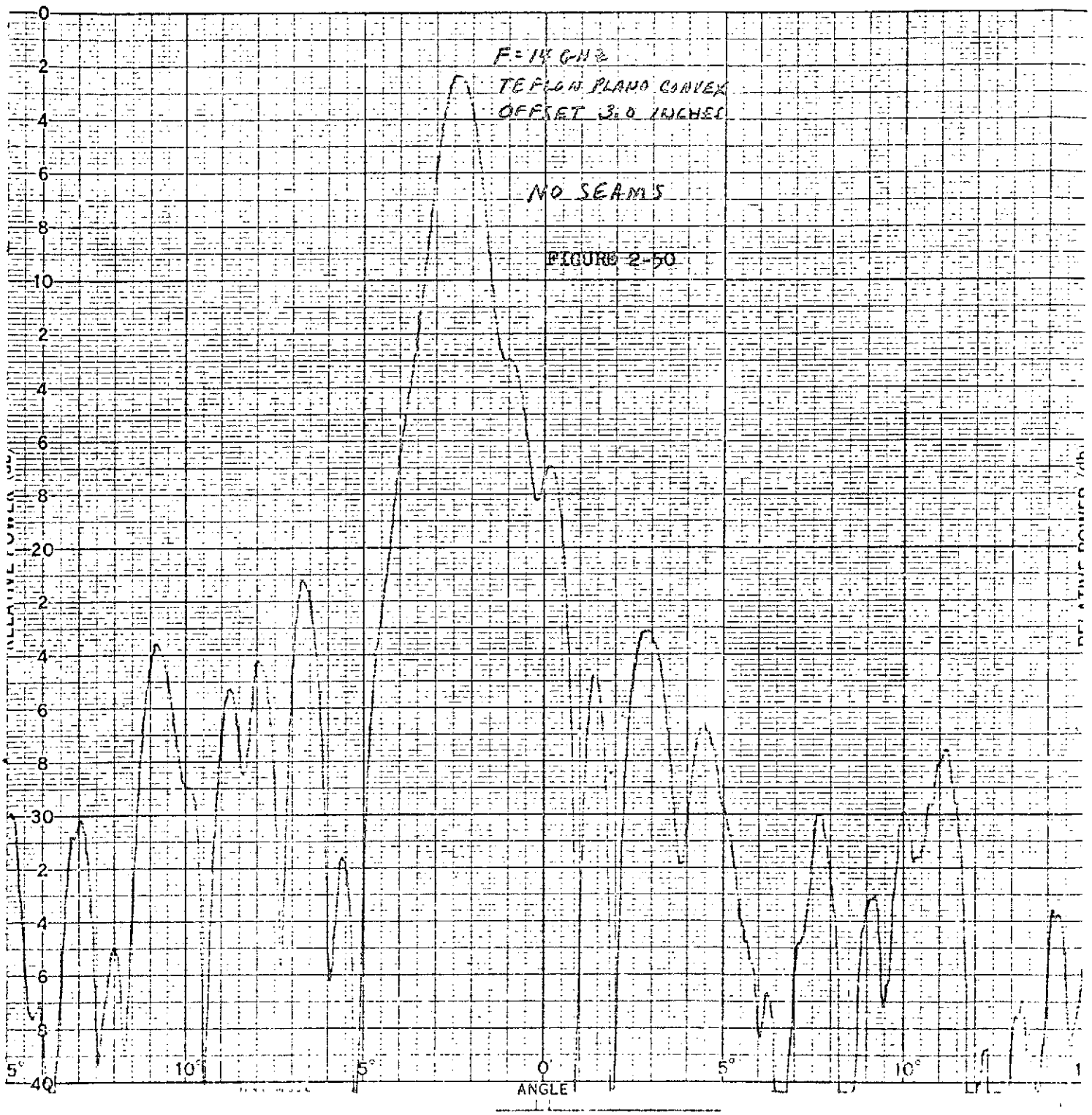
F = 14 GHz
TEFLON PLANO CONVEX
OFFSET 3.0 INCHES
NO SEAMS
0
2
4
6
8
10
2
4
6
8
20
2
4
6
8
30
2
4
6
8
40
5°
10°
5°
0°
5°
10°
ANGLE

FIGURE 2-50

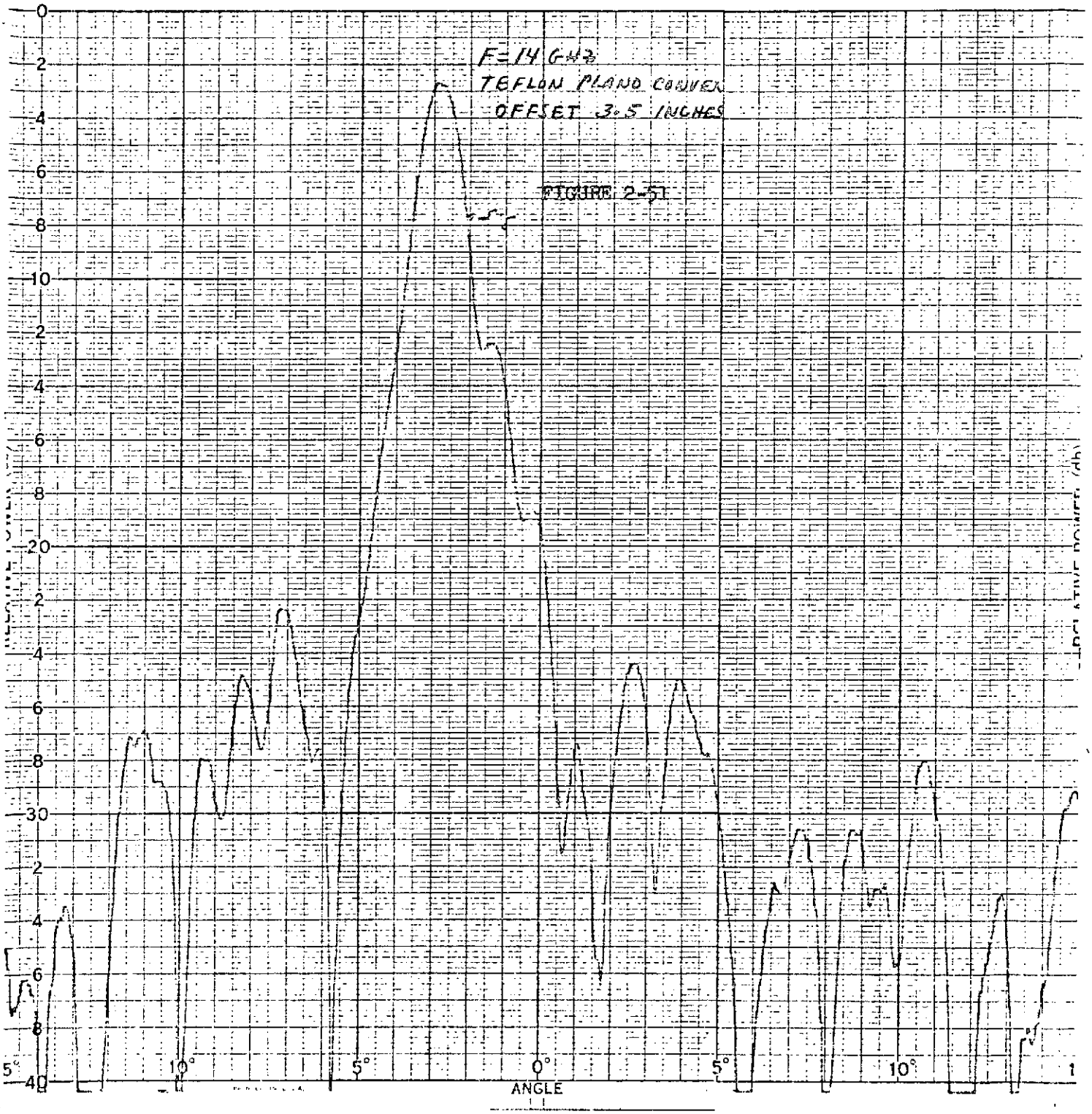
F=14 GHz
TEFLON PLANO CONVEX
OFFSET 3.5 INCHES
FIGURE 2-51
0
2
4
6
8
10
2
4
6
8
20
2
4
6
8
30
2
4
6
8
40
5°
10°
5°
0°
5°
10°
ANGLE

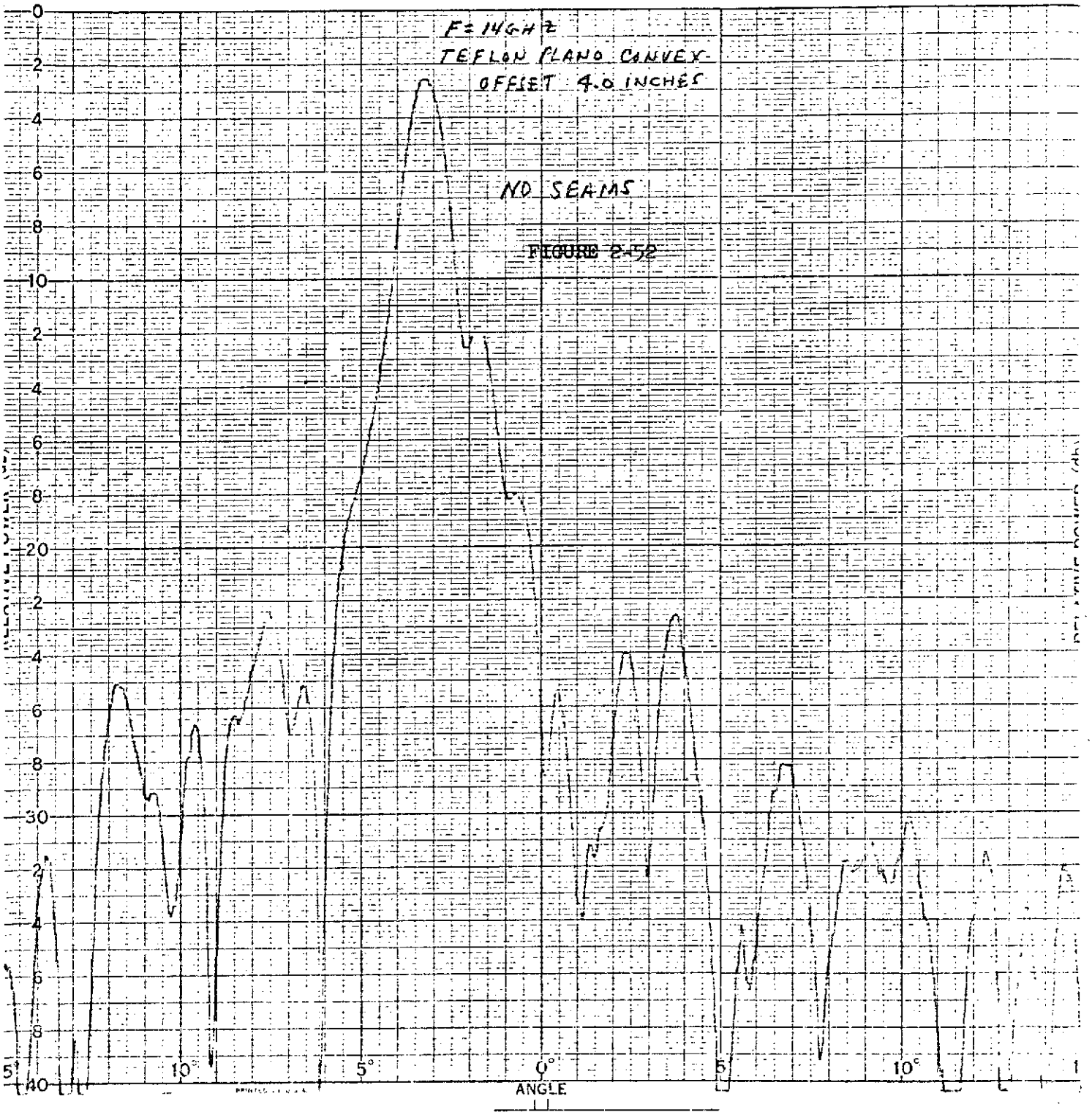
F=14GHz
TEFLON PLANO CONVEX-
OFFSET 4.0 INCHES
NO SEAMS
FIGURE 2-52
0
2
4
6
8
10
2
4
6
8
20
2
4
6
8
30
2
4
6
8
40
10°
5°
0°
5
10°
ANGLE

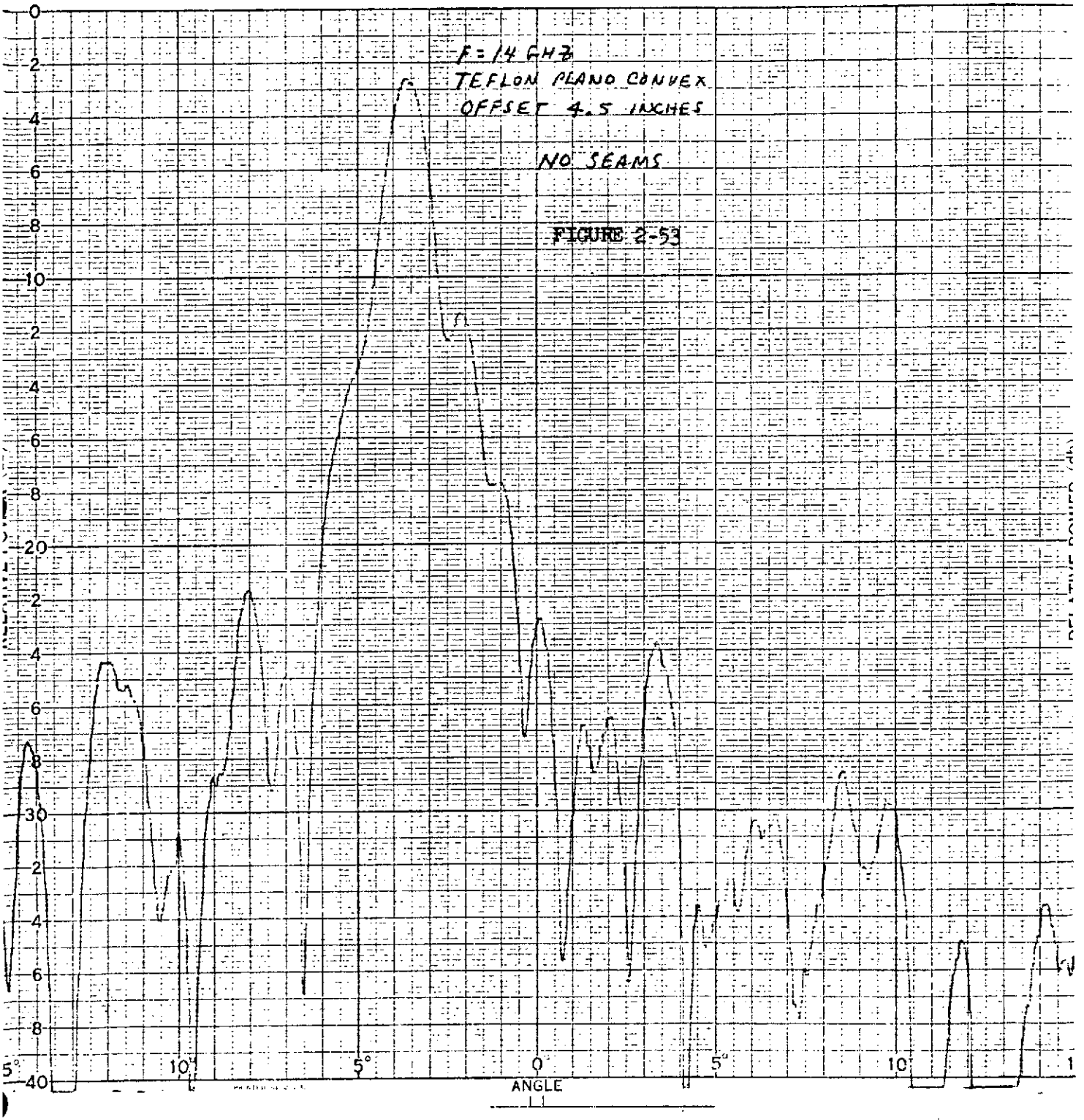
F = 14 GHZ
TEFLON PLANO CONVEX
OFFSET 4.5 INCHES
NO SEAMS
0
2
4
6
8
10
2
4
6
8
20
2
4
6
8
30
2
4
6
8
40
10°
5°
0
5°
10°
ANGLE

FIGURE 2-53

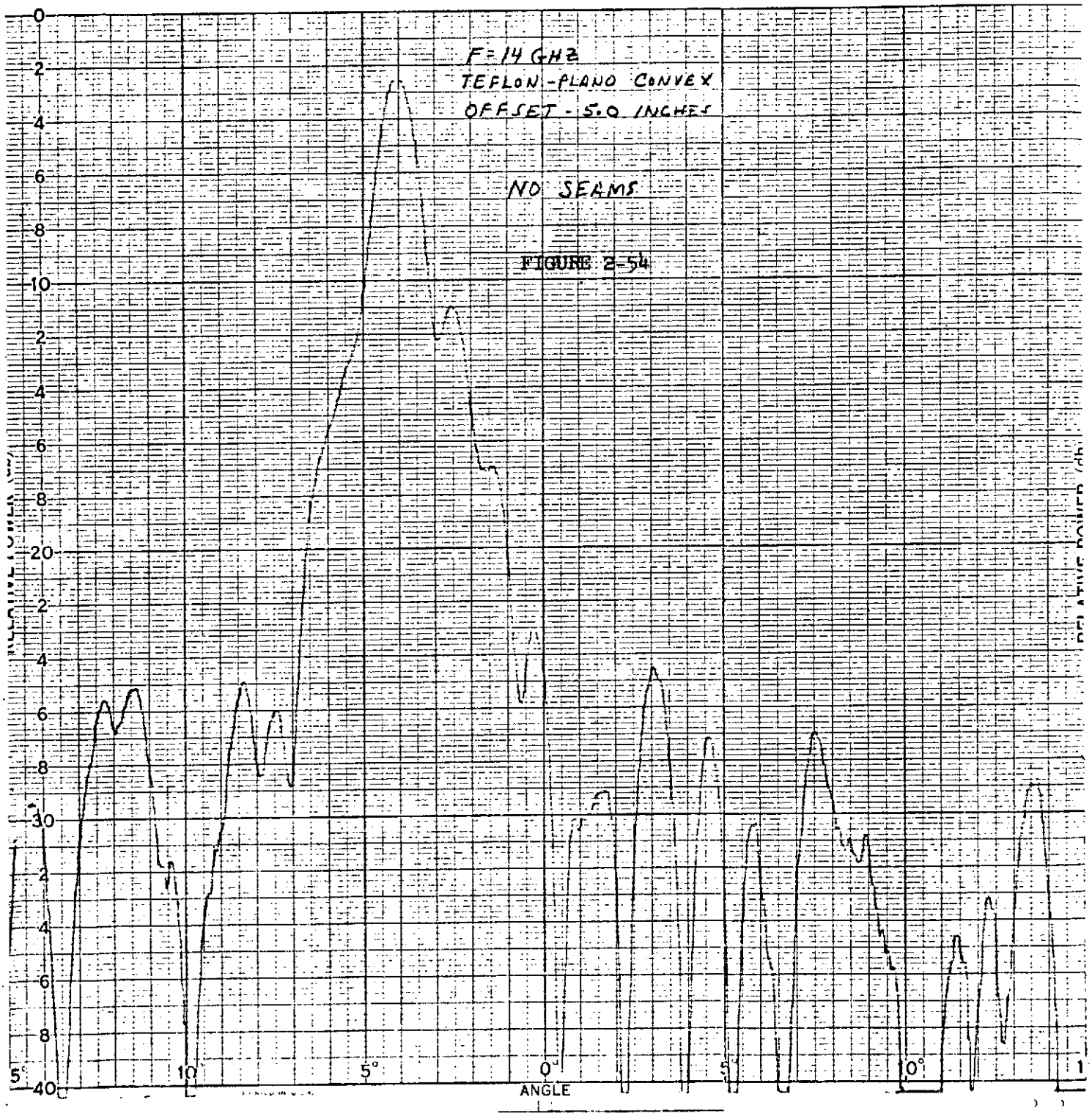
F = 14 GHz
TEFLON - PLANO CONVEX
OFFSET - 5.0 INCHES
NO SEAMS
0
2
4
6
8
10
2
4
6
8
20
2
4
6
8
30
2
4
6
8
40
10°
5°
0°
5°
10°
ANGLE

FIGURE 2-54

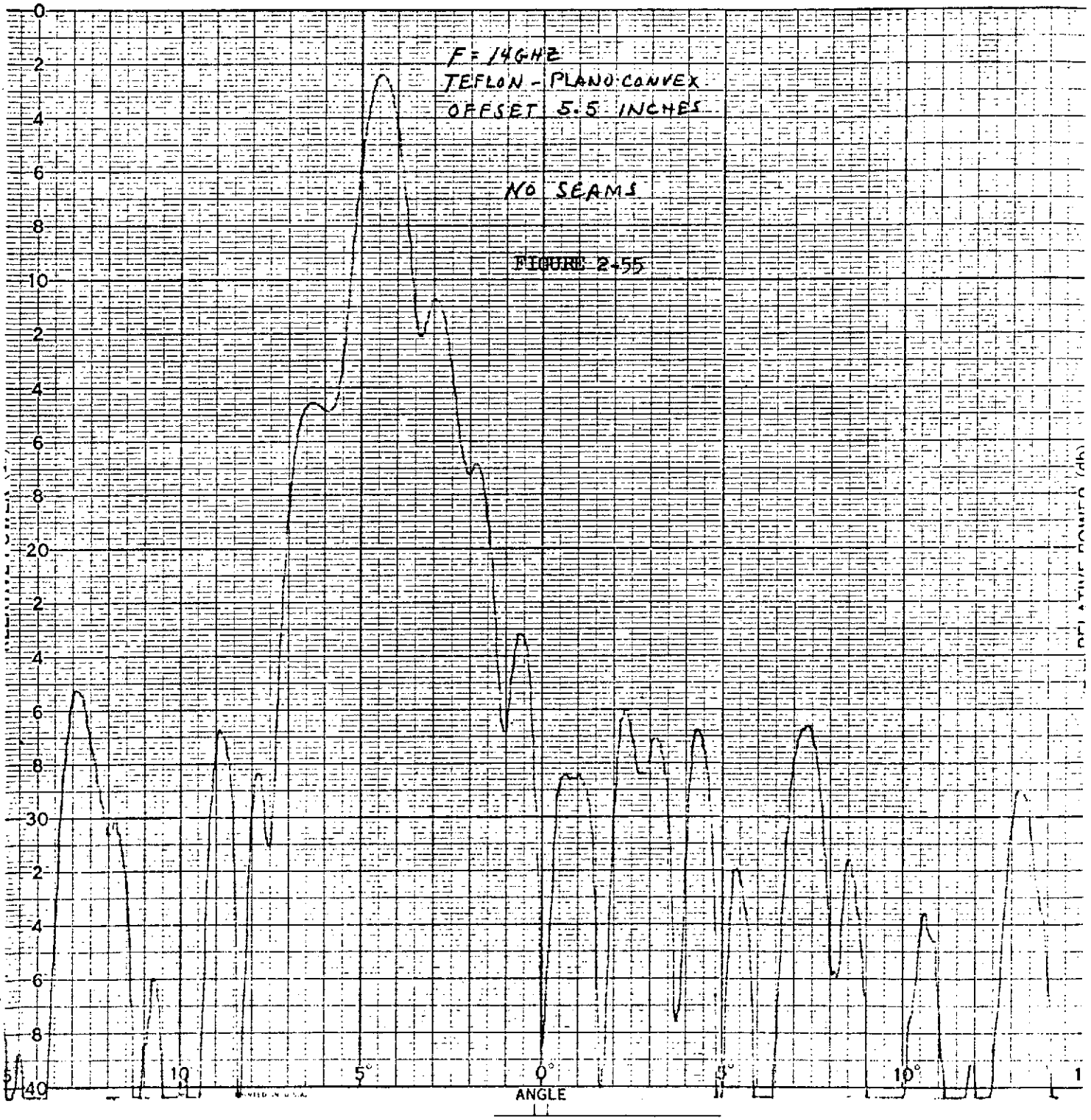
F = 14GHz
TEFLON - PLANO CONVEX
OFFSET 5.5 INCHES
NO SEAMS
0
2
4
6
8
10
20
30
40
5°
0°
ANGLE

FIGURE 2-55

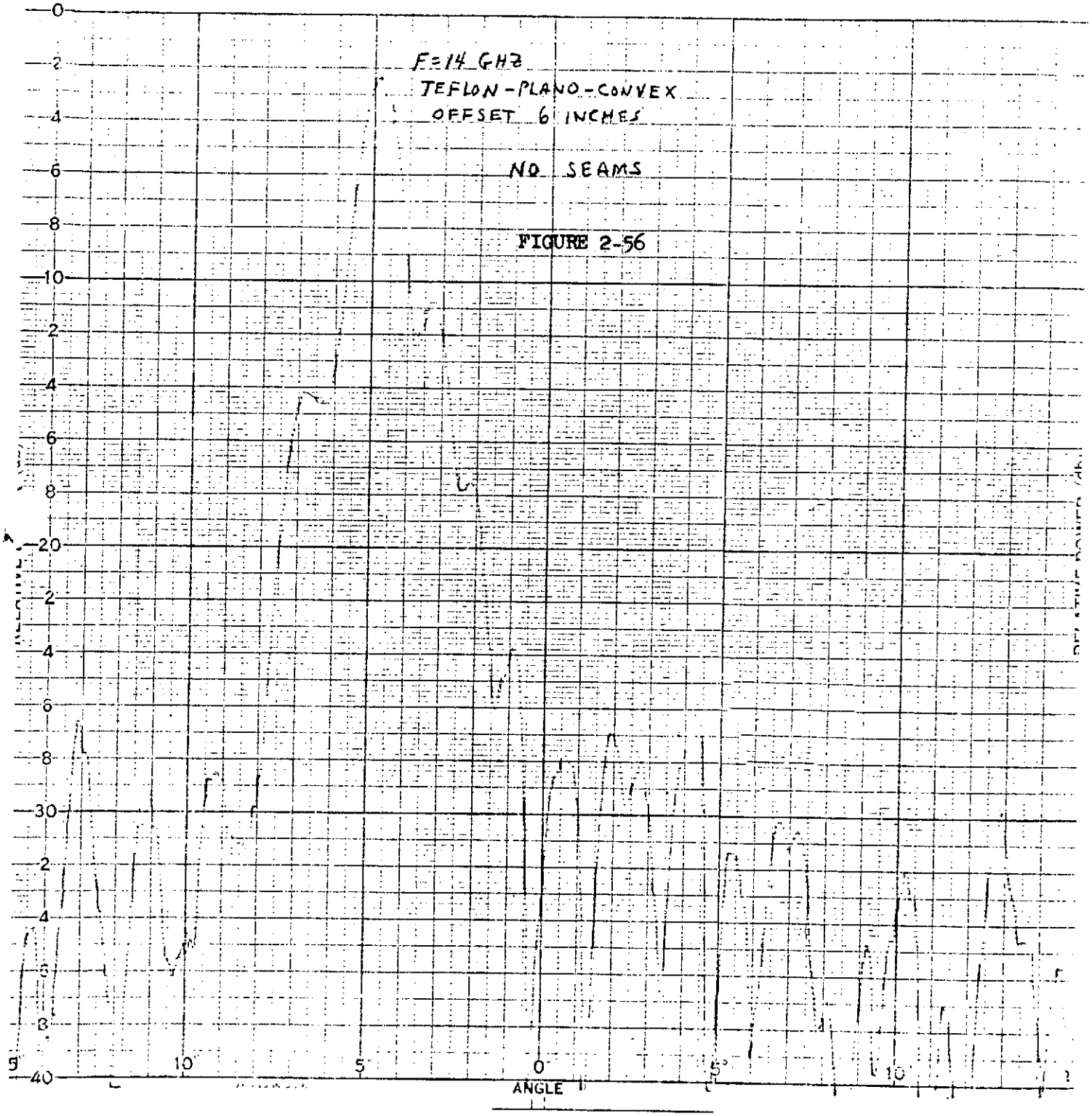
F=14 GHz
TEFLON-PLANO-CONVEX
OFFSET 6 INCHES
NO SEAMS
0
2
4
6
8
10
2
4
6
8
20
2
4
6
8
30
2
4
6
8
40
10
5
0
5
10
ANGLE

FIGURE 2-56

2.6.1 Plano-Convex Teflon Lens - No Seams (continued)

form on the pattern between the lense axis and the beam axis. When the beam is scanned 5 degrees off axis (approximately five beamwidths), the highest coma lobe is only down 7 to 9 dB from the beam peak.

The beam angle as calculated by the computer was predicted to be equal to the feed angle, defined as the angle between the lense axis and the line between the feed phase center and the intersection of the lense axis and the plane (or exit) face of the lense. The comparison between the calculated and measured relationship between feed offset angle and beam offset angle is shown in Fig. 2-57.

2.6.2 Plano-Convex Lens - With Seams

The plano-convex lense was cut into five pieces and then glued back together using Eastman 9-10 adhesive, resulting in four seams or gaps proportionately the same as the seams in the artificial dielectric lense. The seamed Teflon lense was reinstalled in the parallel plates in the same position as before. The VSWR of the feed horn at some selected maximas and minimas are shown in Fig. 2-58. The lense pattern with the feed on-axis at the maximum response position is shown in Fig. 2-59. No lateral offset patterns were measured.

Although the results between the unseamed and seamed Teflon lenses are not identical, they are sufficiently close to conclude that the seams have a minimal affect on the lense performance and may be relegated to second order effects.

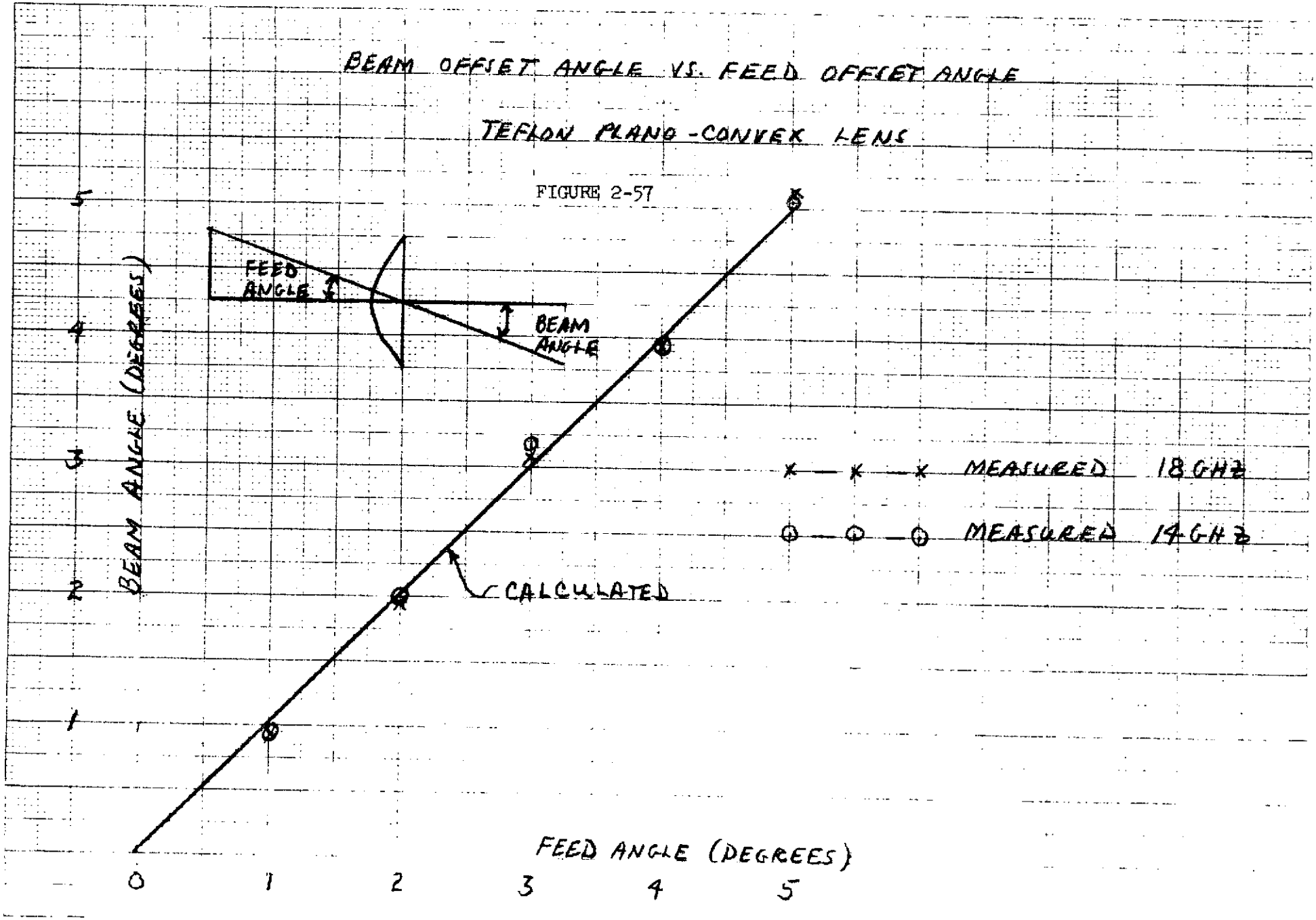
BEAM OFFSET ANGLE VS. FEED OFFSET ANGLE
TEFLON PLANO-CONVEX LENS
FEED ANGLE
BEAM ANGLE
MEASURED 18 GHz
MEASURED 14 GHz
CALCULATED
BEAM ANGLE (DEGREES)
FEED ANGLE (DEGREES)
0
1
2
3
4
5

FIGURE 2-57

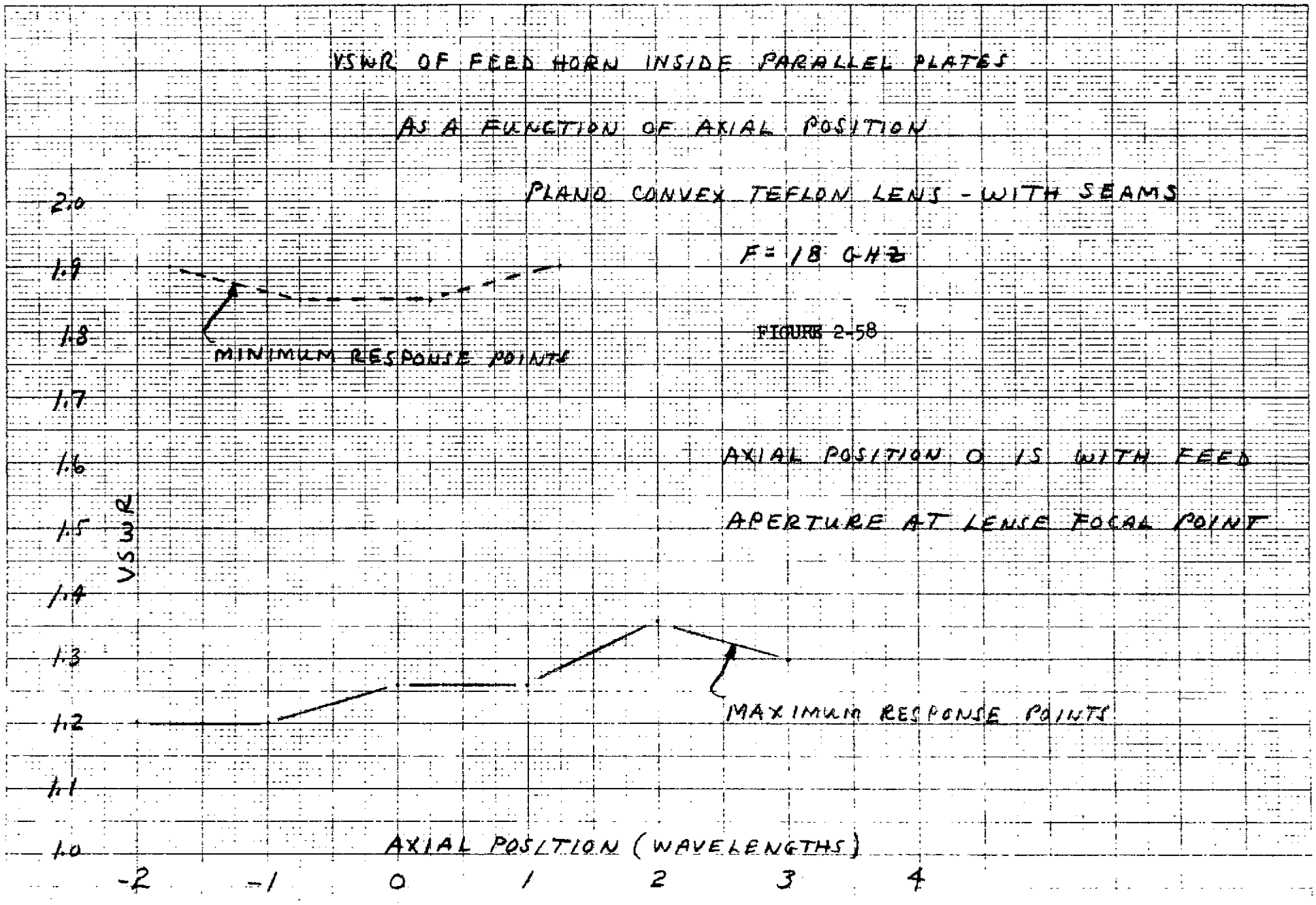
VSWR OF FEED HORN INSIDE PARALLEL PLATES
AS A FUNCTION OF AXIAL POSITION
PLANO CONVEX TEFLON LENS - WITH SEAMS
F = 18 GHz
FIGURE 2-58
MINIMUM RESPONSE POINTS
AXIAL POSITION 0 IS WITH FEED
APERTURE AT LENSE FOCAL POINT
MAXIMUM RESPONSE POINTS
VSWR
2.0
1.9
1.8
1.7
1.6
1.5
1.4
1.3
1.2
1.1
1.0
AXIAL POSITION (WAVELENGTHS)
-2
-1
0
1
2
3
4

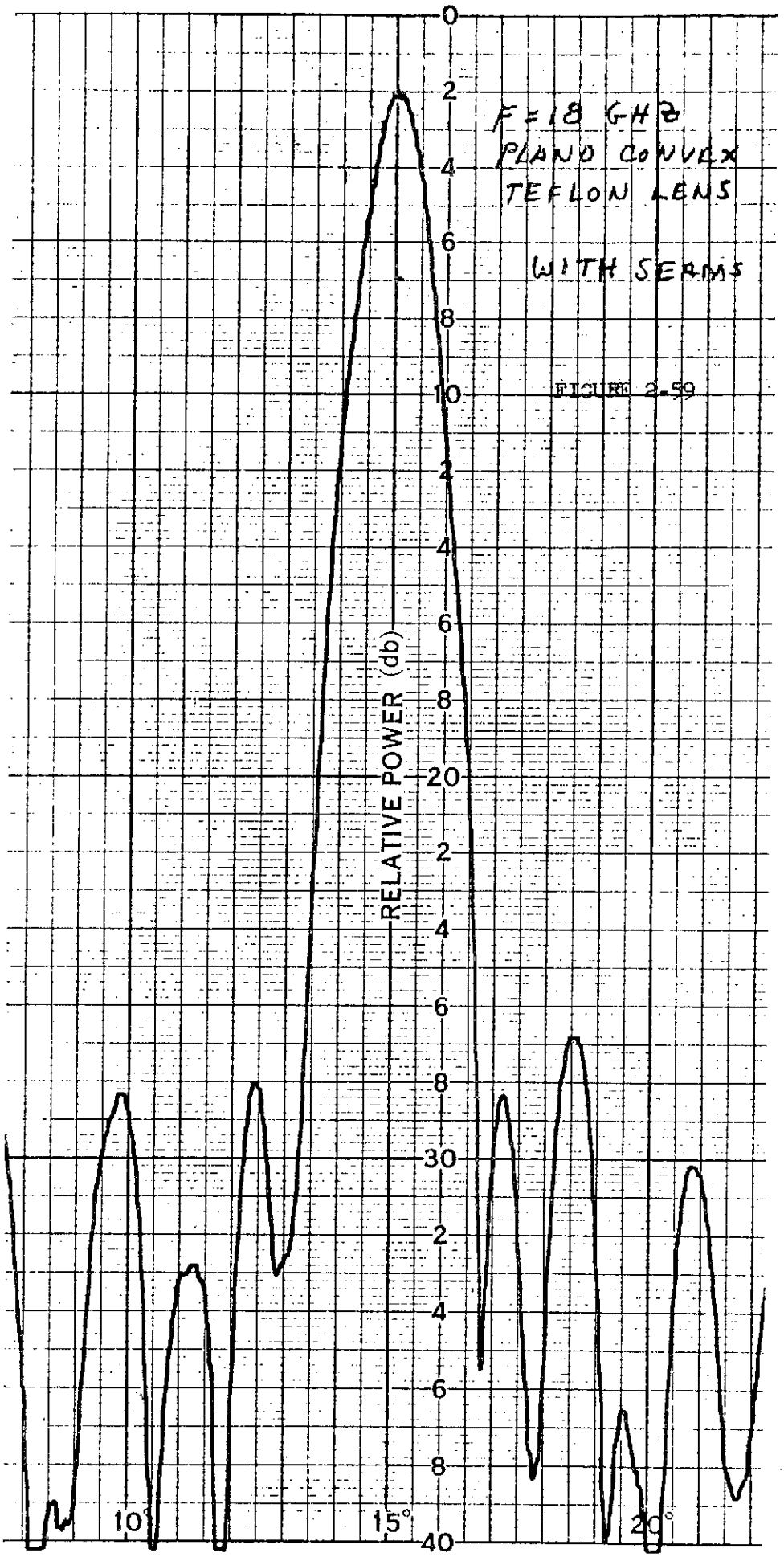
F=18 GHz
PLANO CONVEX
TEFLON LENS
WITH SERRAS
RELATIVE POWER (db)
0
2
4
6
8
10
2
4
6
8
20
2
4
6
8
30
2
4
6
8
40
10°
15°
20°

FIGURE 2-59

2.6.3 Plano-Convex Artificial Dielectric Lens

As described before, the artificial dielectric plano-convex lens is 56 inches in diameter but with the same F/D ratio as the plano convex Teflon lense. The 56 inch diameter parallel plates were installed onto the 3-axis pedestal and the artificial dielectric lense positioned inside the parallel plate. As with the Teflon lense, this lense was covered with conducting tape on the two sides making contact with the plate. A clamping fixture similar to the one used with the Teflon lens was built and positioned on the parallel plates. With no visible air gaps between the plates and the lense, patterns were taken. A typical result is shown in Fig. 2-60 . Many patterns were taken over two days attempting to obtain a good pattern. This was not successful. All of the other patterns were similar to or worse than the pattern shown in Fig. 2-60 .

The pattern is similar to the first patterns obtained with the Teflon lense when there were air gaps between the parallel plates and the Teflon lense. All visual indications were that with the artificial dielectric lense, there was better contact with the plates than when the final patterns were taken with the Teflon lense. All indications are also that the electrical properties of the artificial dielectric are nearly as good as those of Teflon. The pieces used to form the lense were all machined from one 18 inch diameter by 5 inch depth cylinder of material. Measurements on this sample performed by Emerson and Cuming indicated a dielectric constant of 2.00 for either of two orthogonal linear polarizations and a loss tangent of 0.004. No direct measurement was made of the homogeneity across the 18 inch dimension but in this small a sample, the homogeneity should be more than satisfactory.

Although not included here, two patterns were run with this artificial dielectric, one with the clamping fixture in place, and one without any pressure on the plates. The two patterns were essentially identical.

Tests with the Teflon lense have shown that although there may be some small effects on performance due to the seams, they will not cause errors of this gross of magnitude.

All of this information considered together indicate that there is not good contact between the lense and its metal plates and that air gaps do exist. The artificial dielectric material has a consistency similar to polyfoam. The depth of the lense was machined to its 0.22 inch dimension from a 5 inch block. Regardless of how accurately the surfaces were cut, because of the roughness of the material itself, the machined surfaces are just not smooth like the Teflon. Covering the material with conducting tape still leaves

2.6.3 Plano-Convex Artificial Dielectric Lens (continued)

small air gaps in several places between the material and the conductor. The additional pressure exerted by the clamping fixture apparently cannot overcome this.

It is concluded that, because of the relatively irregular consistency of the artificial dielectric material compared to the Teflon, and because extremely good positive contact is required between the parallel plates and the lense, the measured pattern anomalies using the artificial dielectric material are caused, not by the material, but by a lack of contact between the lense and the plates.

It must be noted here that the lack of good patterns with the artificial dielectric lense cannot at this time be directly attributed to the material, but rather its incompatibility with the parallel plate system approach used in these tests. A circularly symmetric, three dimensional lense fabricated from this material still may perform in a similar manner to a lense made from a natural dielectric such as Teflon.

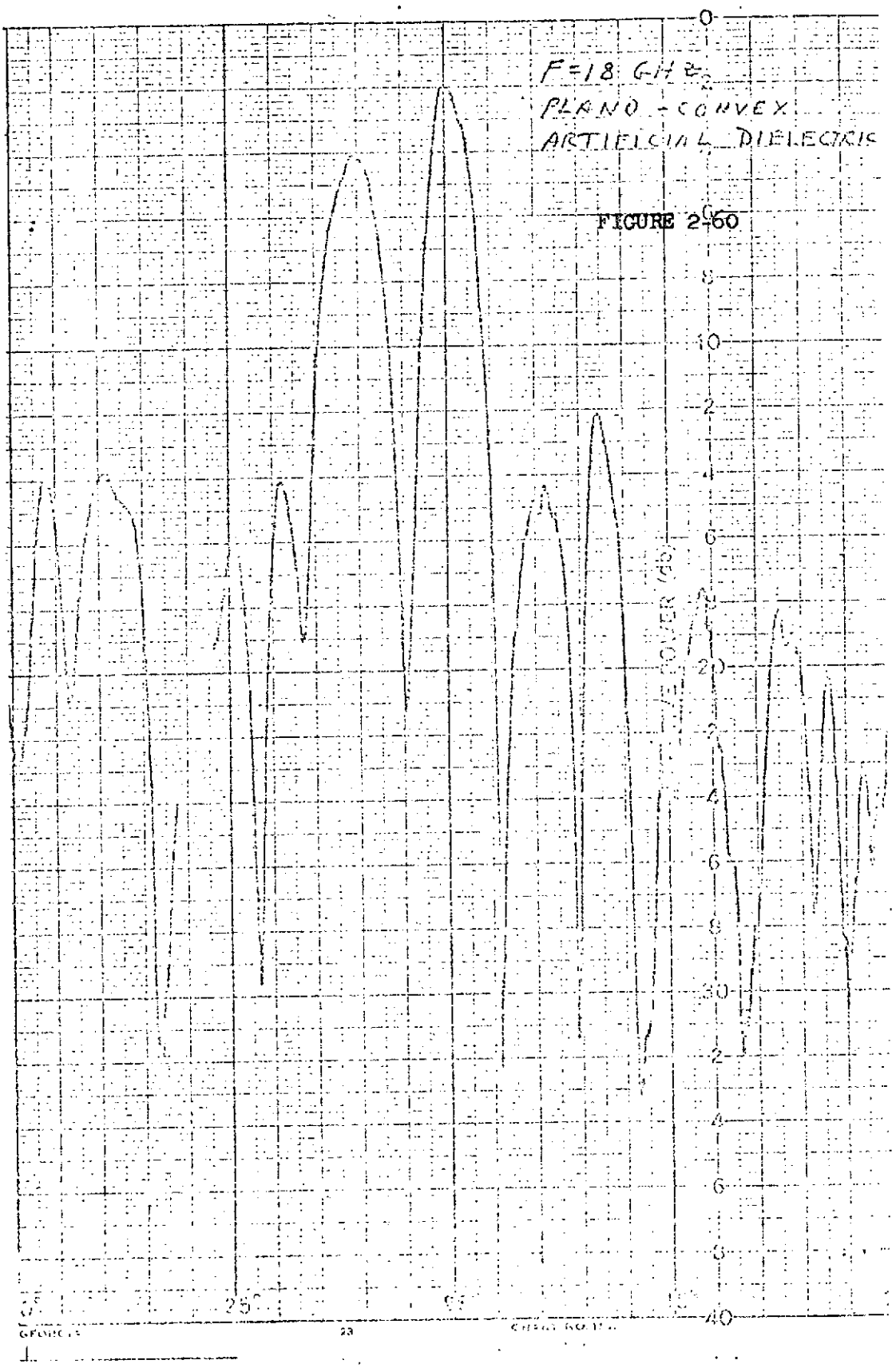

FIGURE 2-60

2.6.4 Two-Point Corrected Teflon Lense - No Seams

The two-point corrected Teflon lens was installed in the parallel plate system. The lense has a diameter of 47.625 inches, a focal length of 61.25 inches (F/D = 1.286), a maximum depth of 11.09 inches and a dielectric constant of 2.09. The lens was covered with conducting tape on the two sides of the lense making contact with the parallel plates. The clamping fixture was installed over the parallel plates at the lense and set to ensure good plate to lens contact. The same feed horn used with the plano-convex lens was installed in the feed positioning structure.

The feed was moved axially (along the lens axis) from a point where the feed aperture to lens vertex distance (FTV) was 62.78 inches to where FTV equaled 57.78 inches.

The variation in signal response at 18 GHz as a function of feed axial position is shown in Figure 2-61.

The VSWR of the feed horn at 18 GHz as a function of axial feed position is shown in Figure 2-62.

The lens patterns at 18 GHz as a function of axial feed position for the first three maximum response positions is shown in Figure 2-63.

With the feed set to the axial position for maximum response, the feed was moved laterally off axis in 0.5 inch steps and to a maximum offset of 6 inches. The lens patterns at 18 GHz as a function of lateral feed position are shown in Figures 2-64 thru 2-76.

The peak gain at maximum response is 22.9 dBi. The frequency was then changed to 14 GHz. The variation in signal response at 14 GHz as a function of axial position is shown in Figure 2-77.

The VSWR of the feed horn at 14 GHz as a function of axial feed position is shown in Figure 2-78.

The lense patterns at 14 GHz as a function of axial feed position are shown in Figures 2-79 through 2-82.

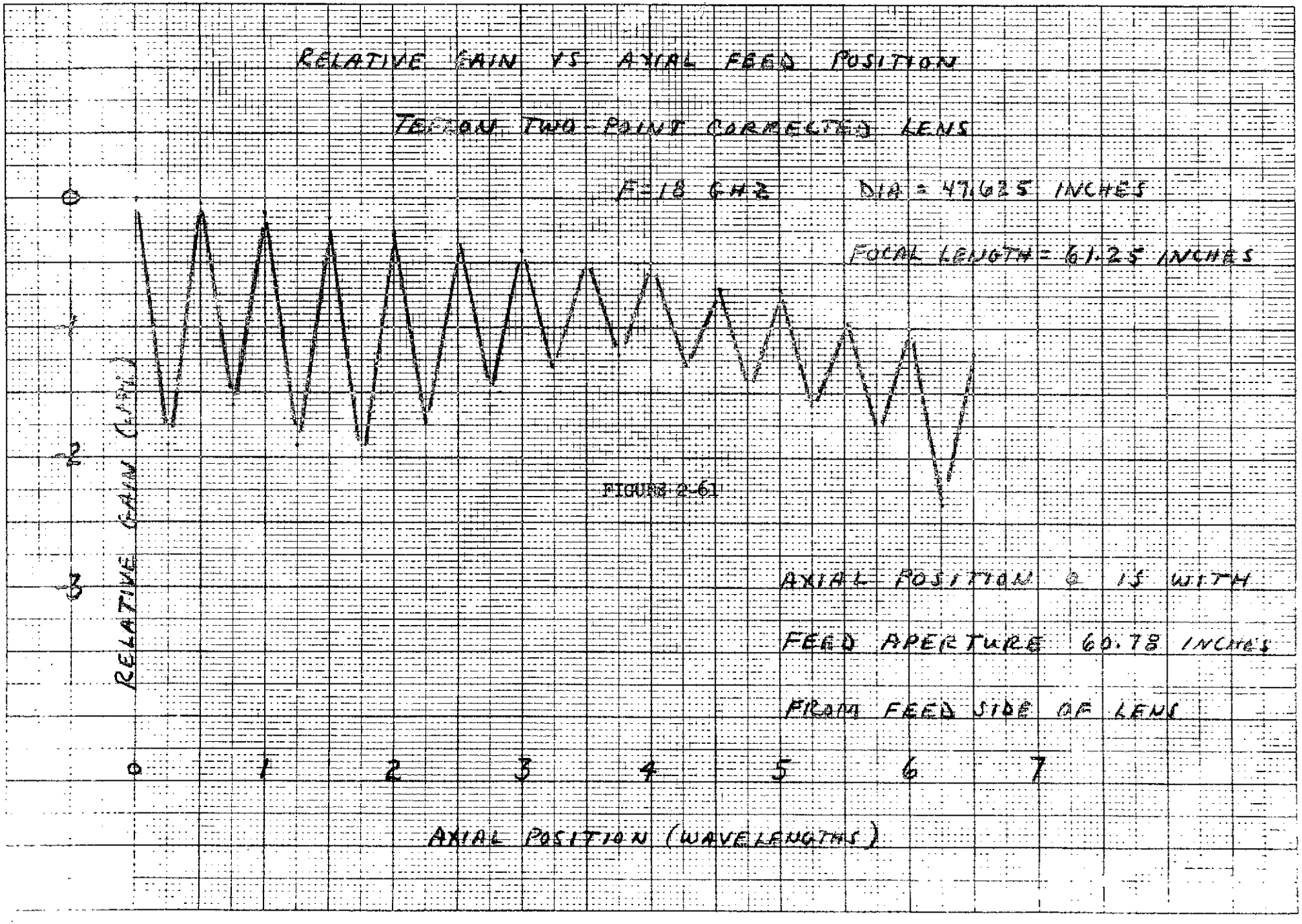
RELATIVE GAIN VS AXIAL FEED POSITION
TEFLON TWO-POINT CORRECTED LENS
F=18 GHz
DIA = 47.625 INCHES
FOCAL LENGTH = 61.25 INCHES
RELATIVE GAIN (dB)
0
1
2
3
0
1
2
3
4
5
6
7
AXIAL POSITION (WAVELENGTHS)
AXIAL POSITION @ 15 WITH
FEED APERTURE 60.78 INCHES
FROM FEED SIDE OF LENS

FIGURE 2-61

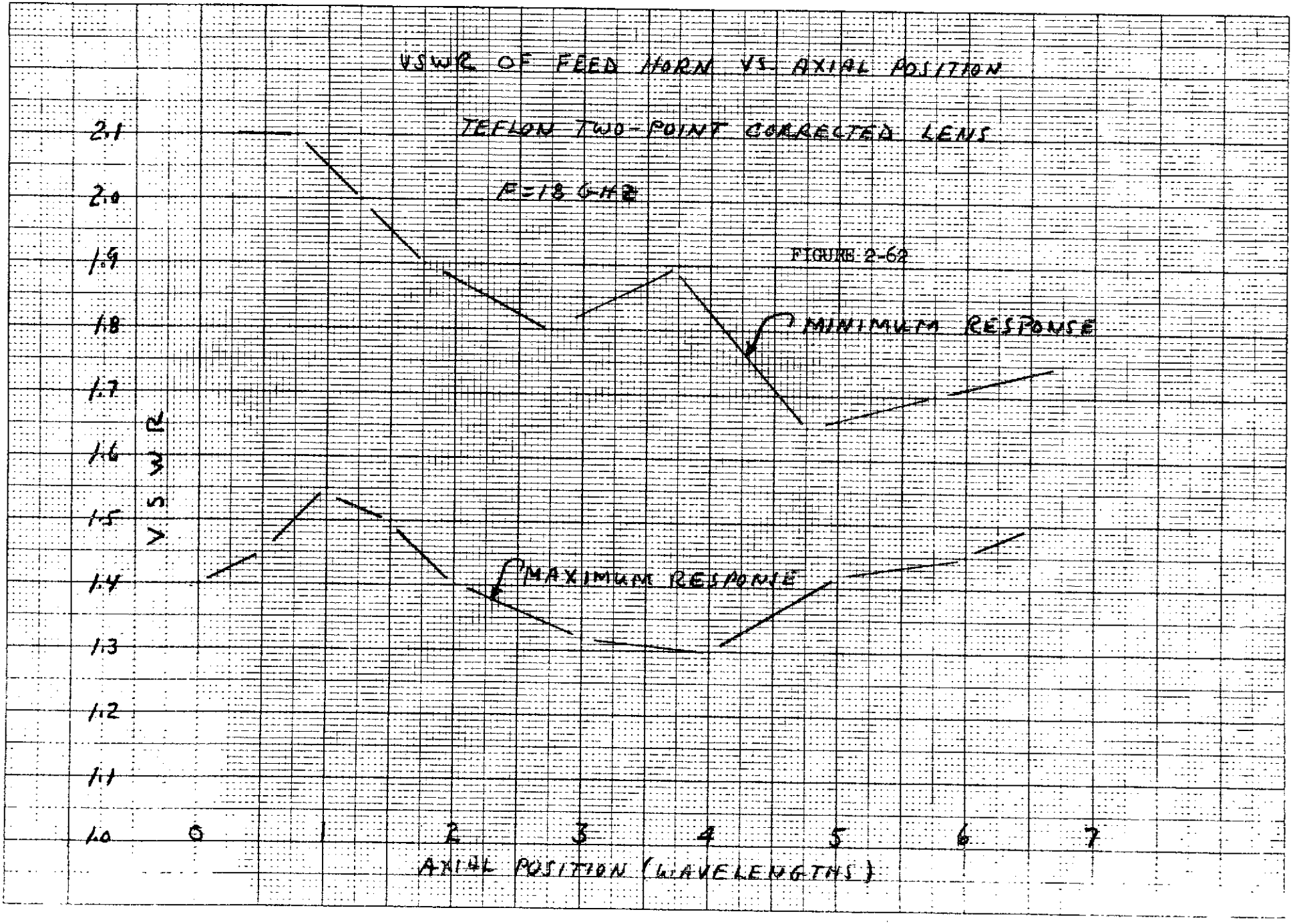
VSWR OF FEED HORN VS. AXIAL POSITION
TEFLON TWO-POINT CORRECTED LENS
F=18 GHz
MINIMUM RESPONSE
MAXIMUM RESPONSE
VSWR
2.1
2.0
1.9
1.8
1.7
1.6
1.5
1.4
1.3
1.2
1.1
1.0
0
1
2
3
4
5
6
7
AXIAL POSITION (WAVELENGTHS)

FIGURE 2-62

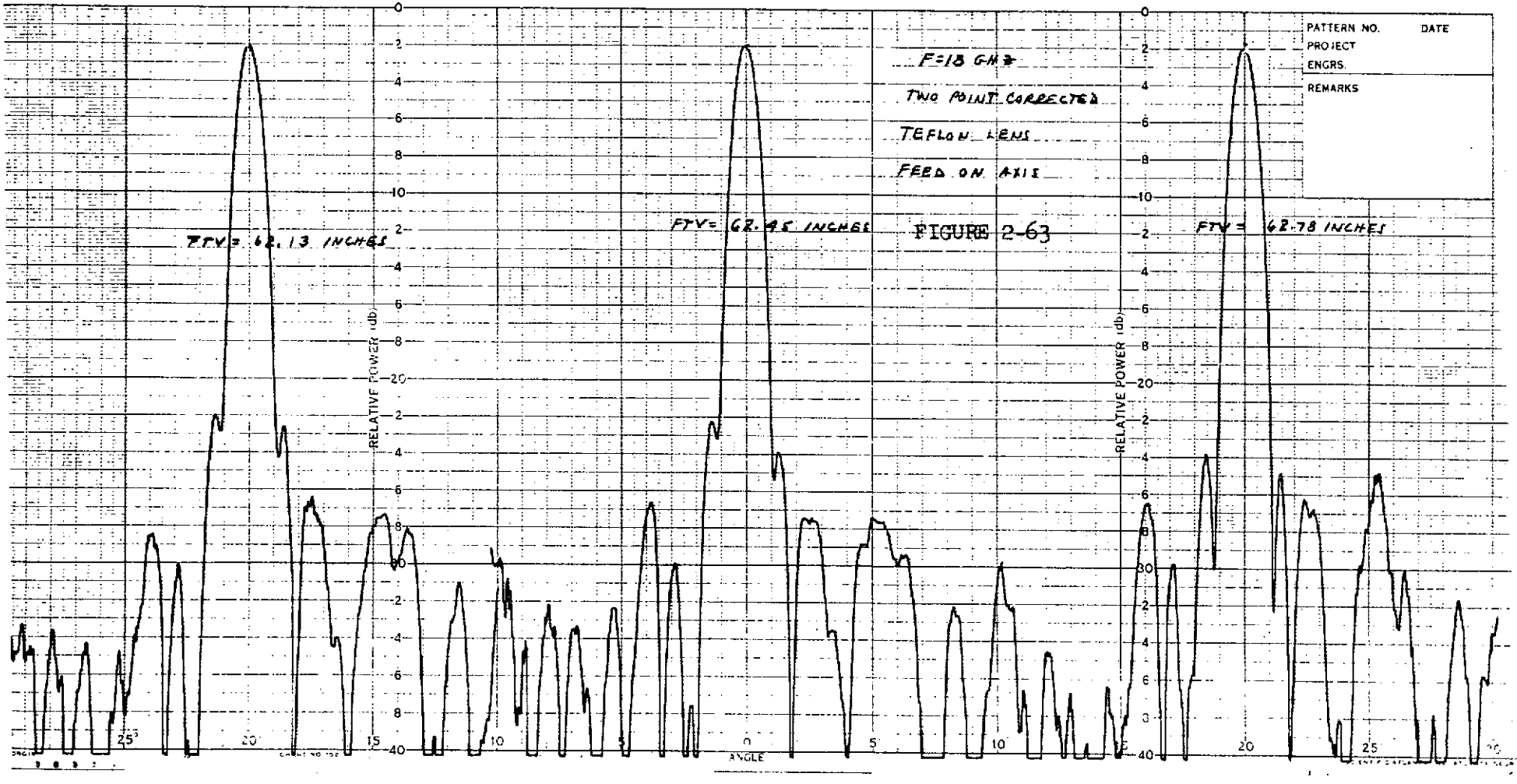
F=18 GHz
TWO POINT CORRECTED
TEFLON LENS
FEED ON AXIS
FTV= 62.13 INCHES
FTV= 62.45 INCHES
FTV= 62.78 INCHES
PATTERN NO.
DATE
PROJECT
ENGRS.
REMARKS
RELATIVE POWER (db)
ANGLE

FIGURE 2-63

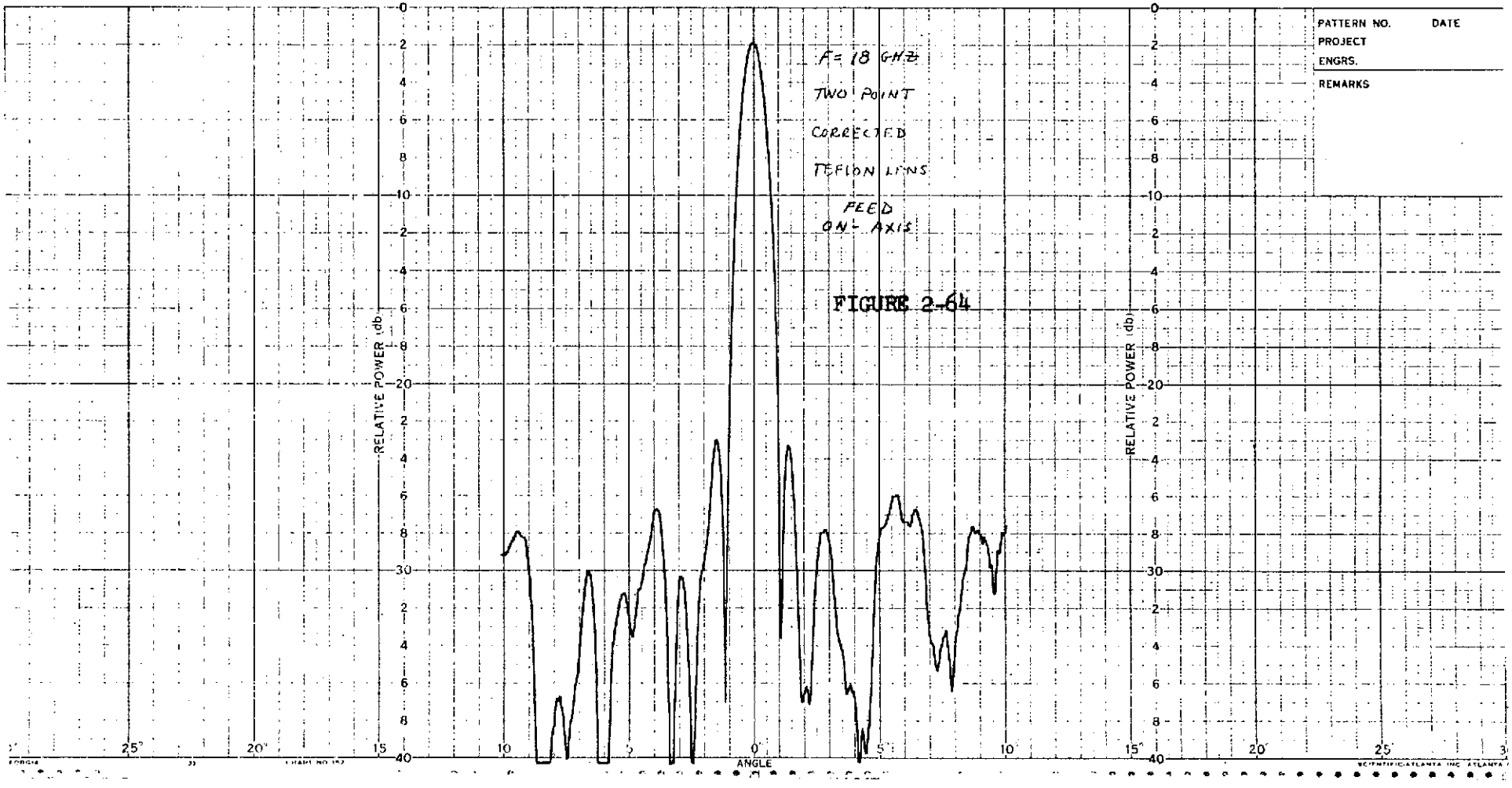
F = 18 GHZ
TWO POINT
CORRECTED
TEFLON LENS
FEED
ON-AXIS
PATTERN NO.
DATE
PROJECT
ENGRS.
REMARKS
RELATIVE POWER (db)
ANGLE
0
2
4
6
8
10
20
30
40
25°
20°
15
10
5
0
5
10
15
20
25

FIGURE 2-64

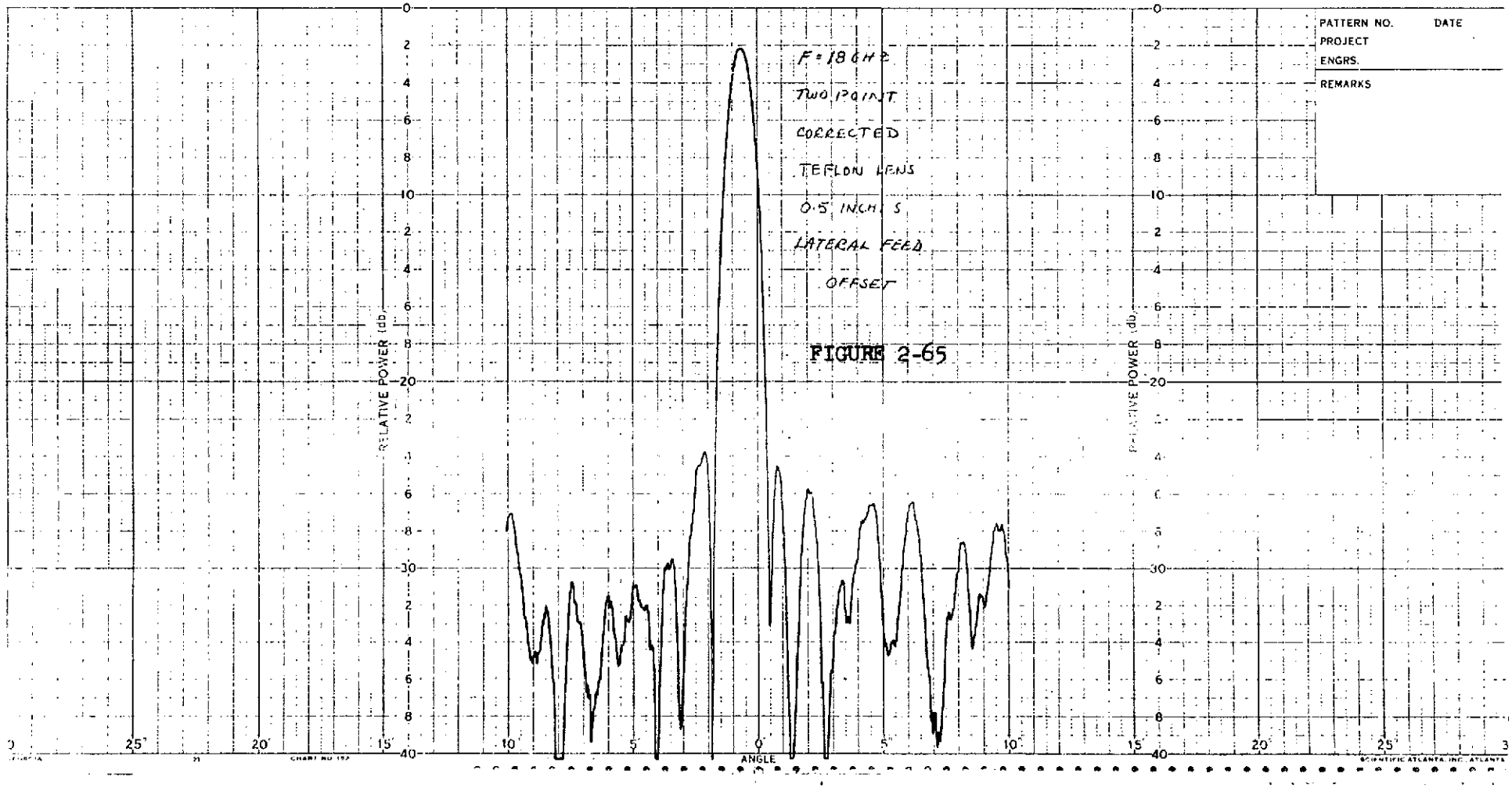
F = 18 GHz
TWO POINT
CORRECTED
TEFLON LENS
0.5 INCH S
LATERAL FEED
OFFSET
PATTERN NO.
DATE
PROJECT
ENGRS.
REMARKS
RELATIVE POWER (db)
ANGLE
SCIENTIFIC ATLANTA, INC. ATLANTA

FIGURE 2-65

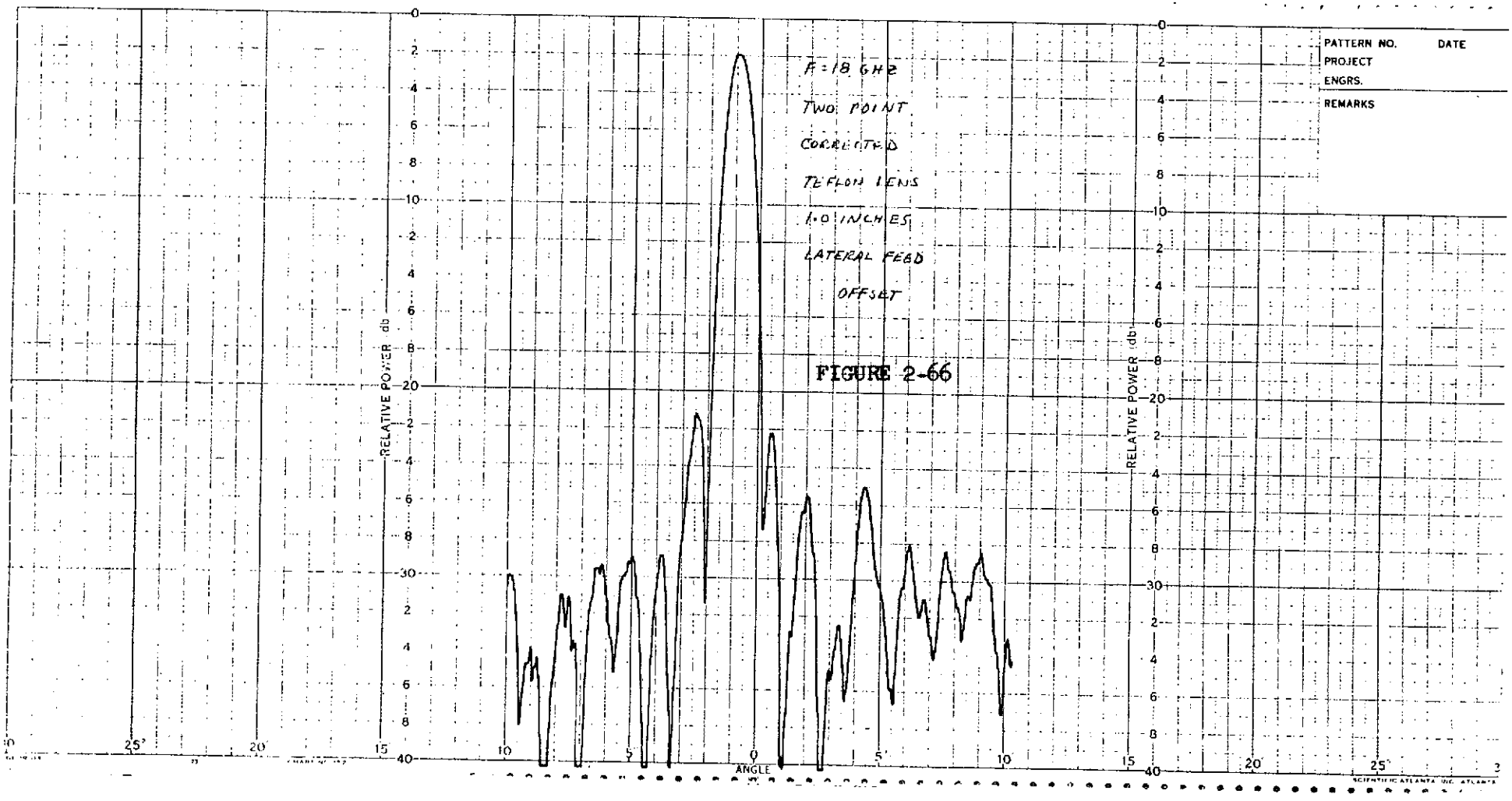
F = 18 GHz
TWO POINT
CORRECTED
TEFLON LENS
1.0 INCHES
LATERAL FEED
OFFSET
PATTERN NO.
DATE
PROJECT
ENGRS.
REMARKS
RELATIVE POWER db
ANGLE

FIGURE 2-66

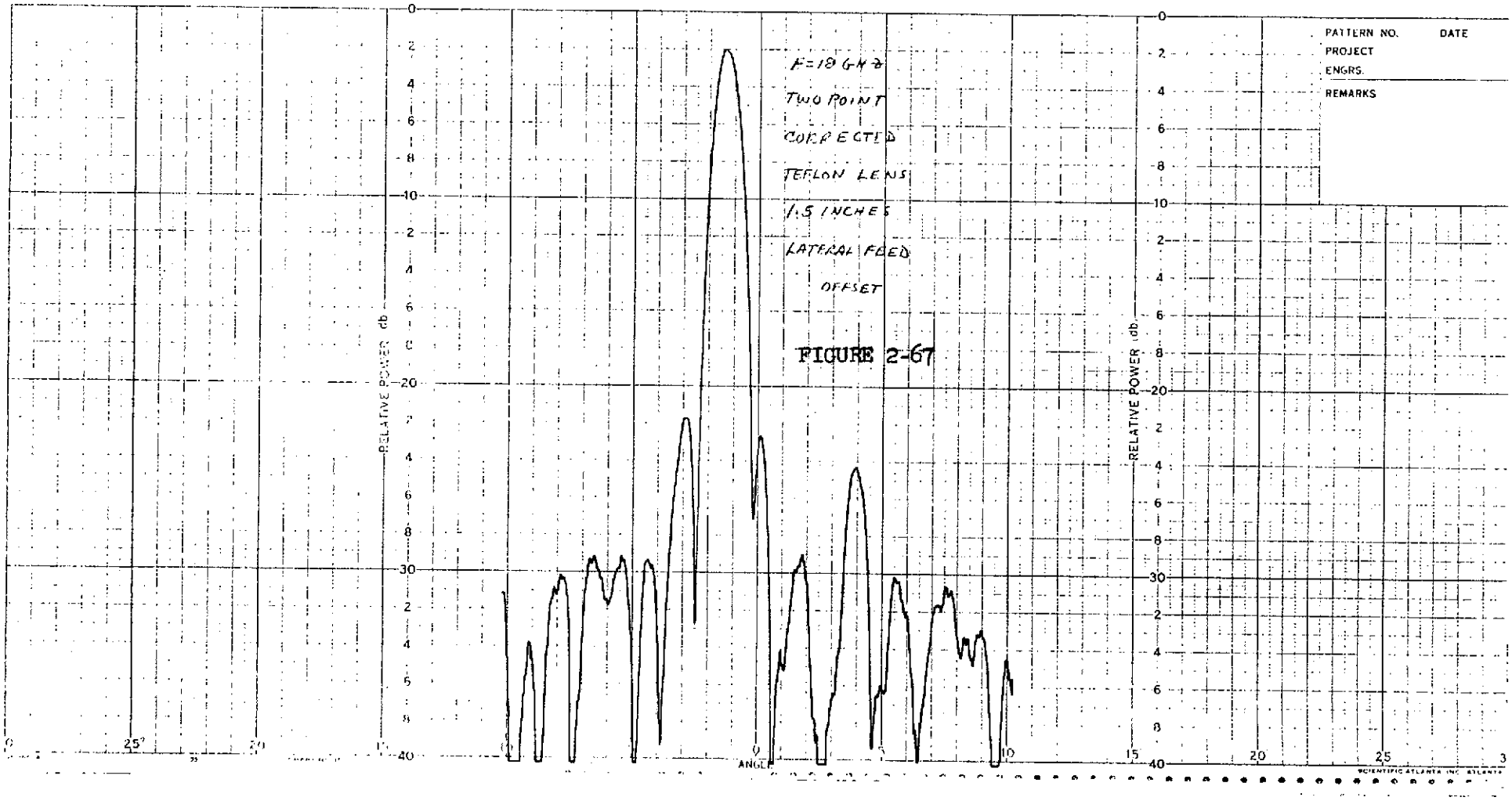
F=18 GHz
TWO POINT
CORRECTED
TEFLON LENS
1.5 INCHES
LATERAL FEED
OFFSET
PATTERN NO.
DATE
PROJECT
ENGRS.
REMARKS
RELATIVE POWER db
ANGLE
SCIENTIFIC ATLANTA INC ATLANTA

FIGURE 2-67

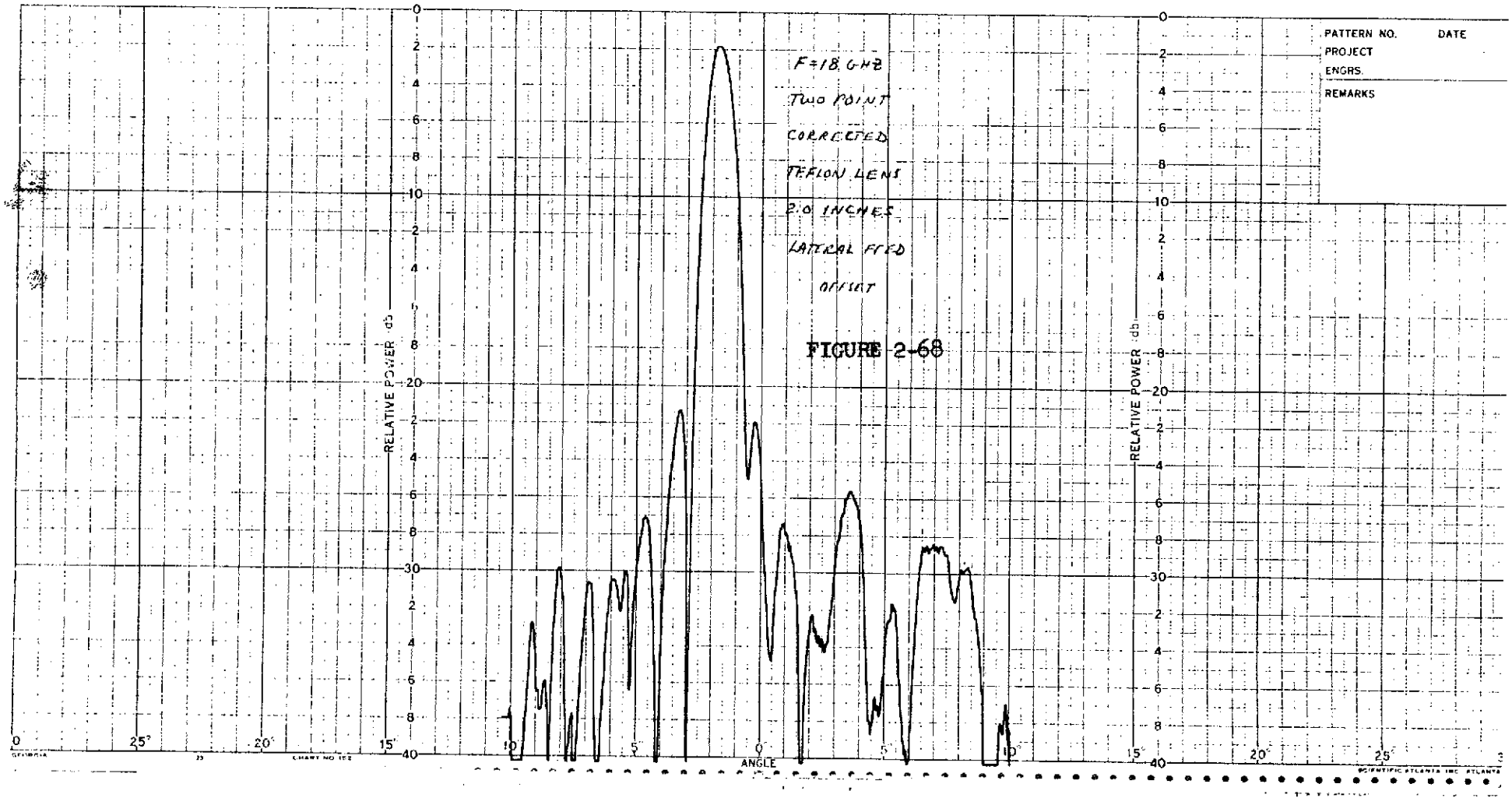
F=18 GHz
TWO POINT
CORRECTED
TEFLON LENS
2.0 INCHES
LATERAL FEED
OFFSET
PATTERN NO.
DATE
PROJECT
ENGRS.
REMARKS
RELATIVE POWER db
ANGLE
SCIENTIFIC ATLANTA INC. ATLANTA

FIGURE 2-68

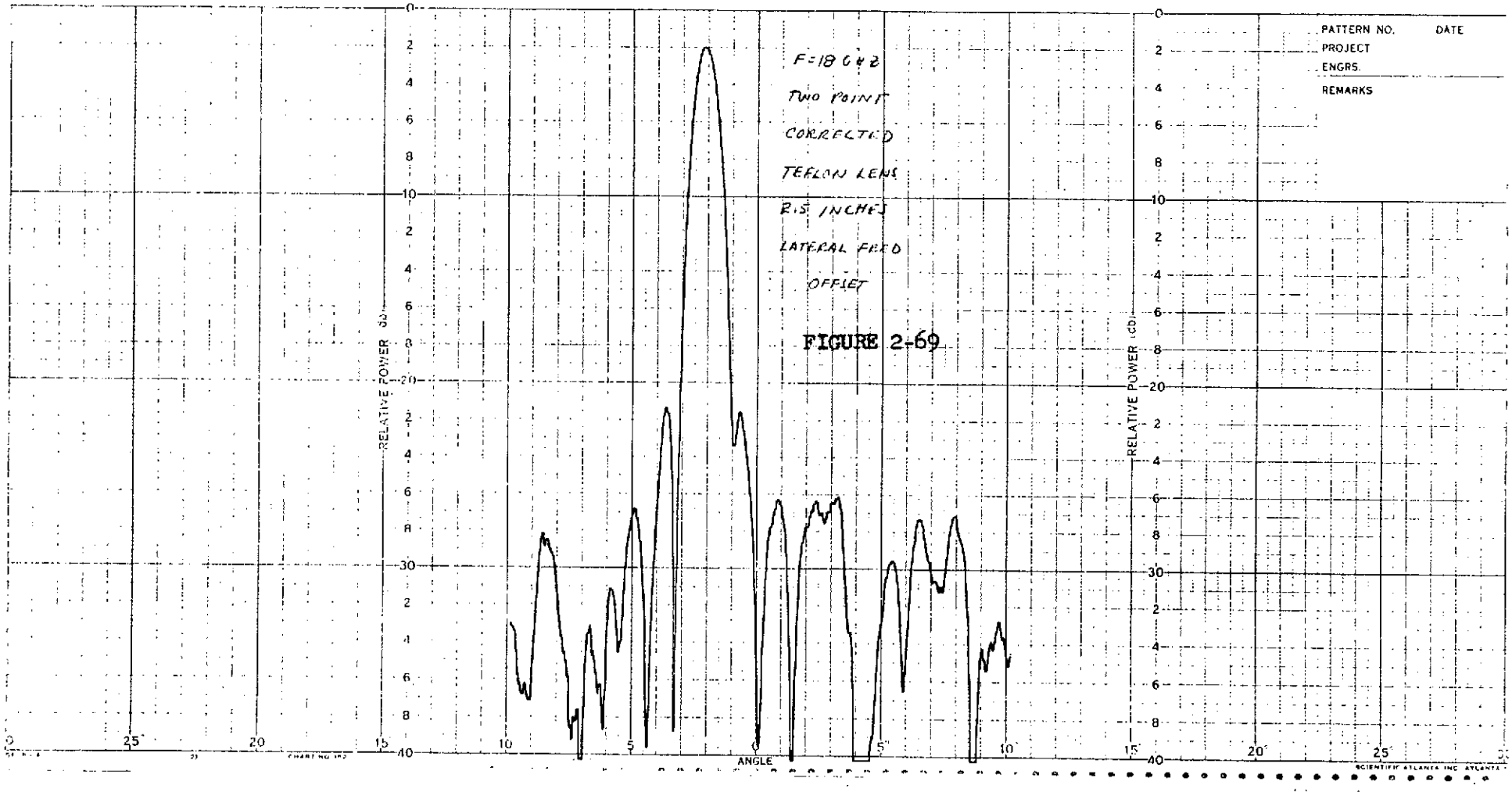
F=18 GHz
TWO POINT
CORRECTED
TEFLON LENS
2.5 INCHES
LATERAL FEED
OFFSET
PATTERN NO.
DATE
PROJECT
ENGRS.
REMARKS
RELATIVE POWER (dB)
ANGLE
SCIENTIFIC ATLANTA INC ATLANTA

FIGURE 2-69

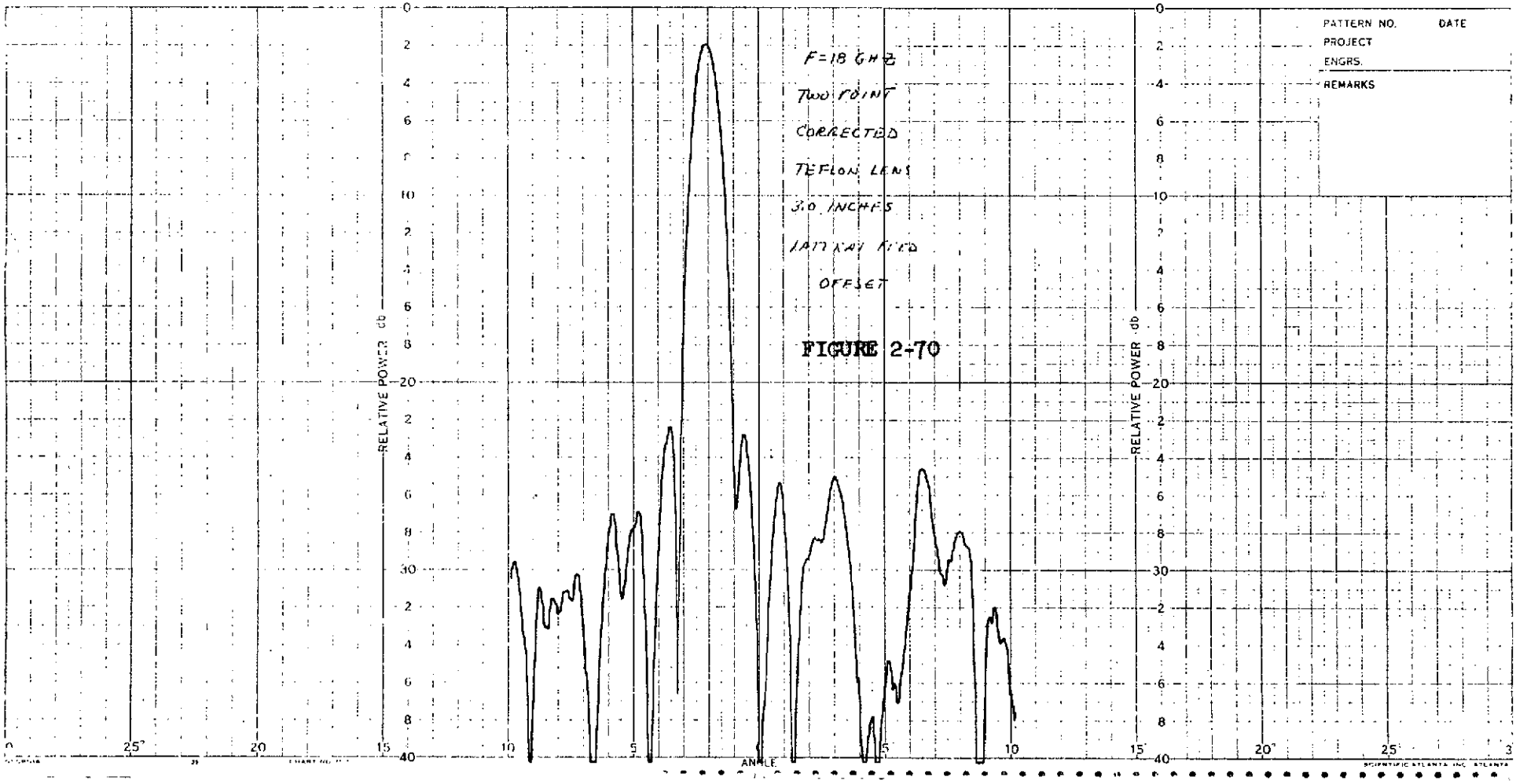
F=18 GHz
TWO POINT
CORRECTED
TEFLON LENS
3.0 INCHES
LAMINATED
OFFSET
PATTERN NO.
DATE
PROJECT
ENGRS.
REMARKS
RELATIVE POWER db
ANGLE
SCIENTIFIC ATLANTA INC. ATLANTA

FIGURE 2-70

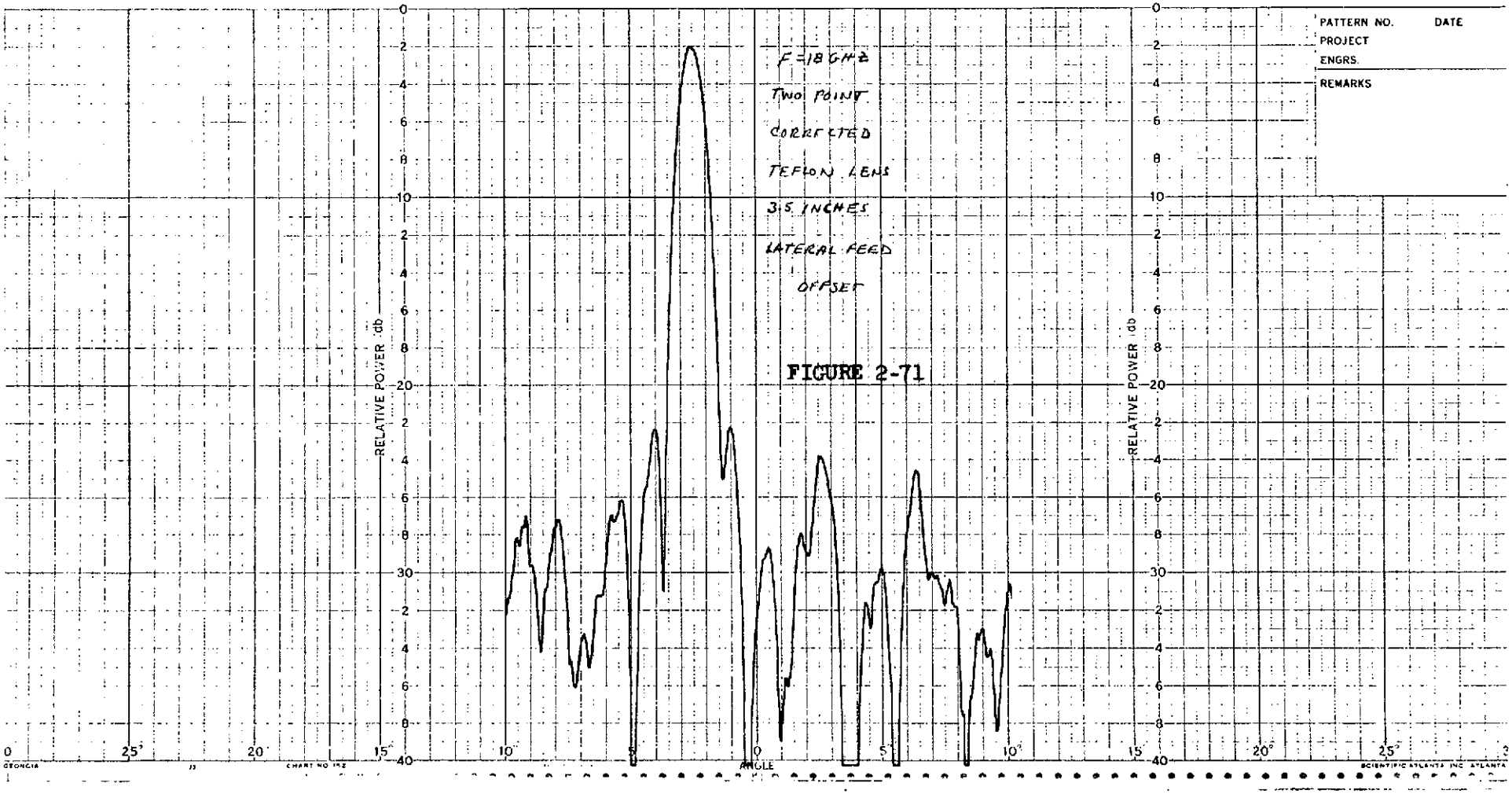
F=18 GHz
TWO POINT
CORRECTED
TEFLON LENS
3.5 INCHES
LATERAL FEED
OFFSET
PATTERN NO.
DATE
PROJECT
ENGRS.
REMARKS
RELATIVE POWER db
ANGLE
GEORGIA
CHART NO. 1K2
SCIENTIFIC ATLANTA INC ATLANTA

FIGURE 2-71

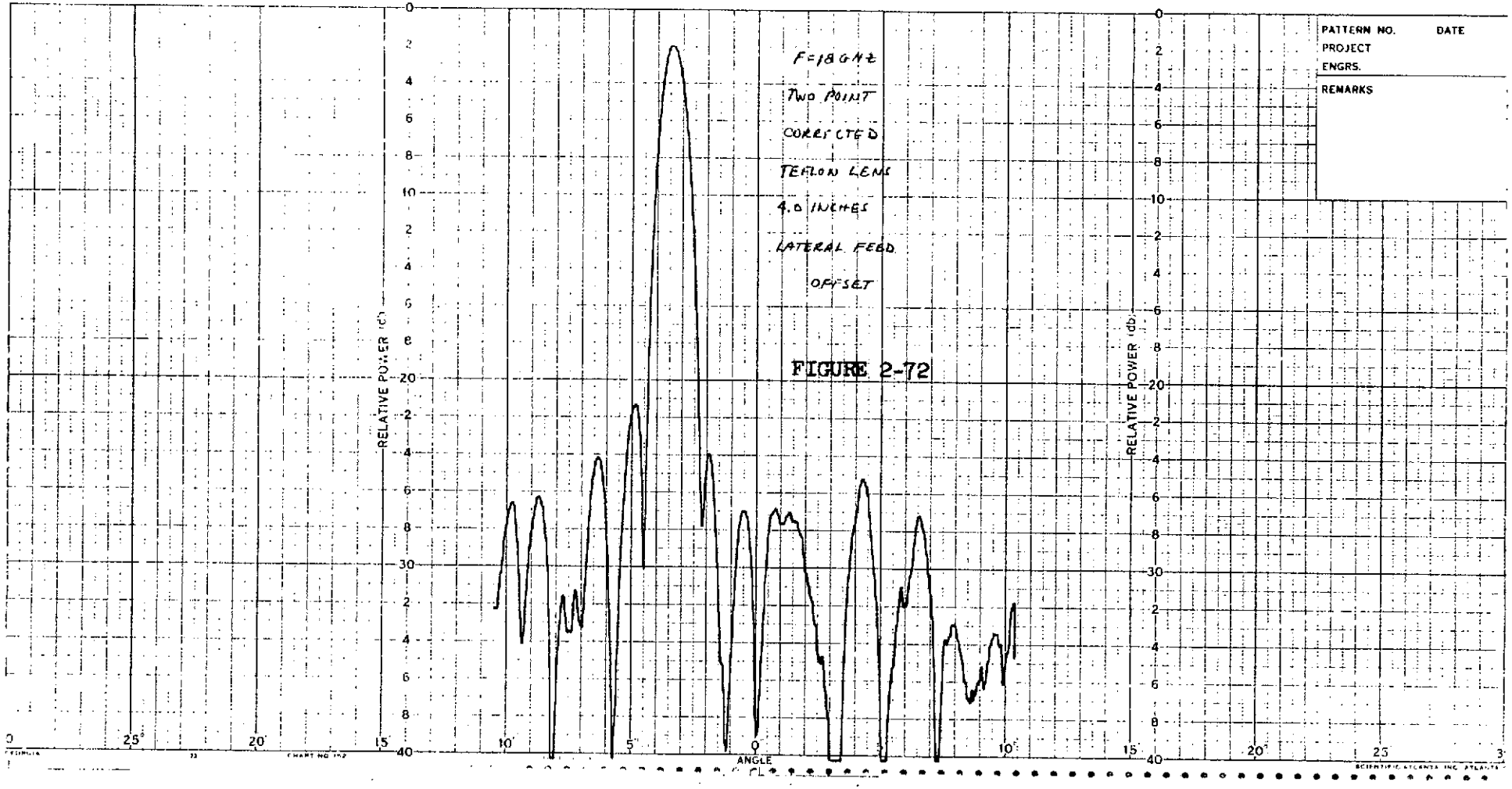
F=18 GHz
TWO POINT
CORRECTED
TEFLON LENS
4.0 INCHES
LATERAL FEED
OFFSET
PATTERN NO.
DATE
PROJECT
ENGRS.
REMARKS
RELATIVE POWER (db)
ANGLE
SCIENTIFIC-ATLANTA INC. ATLANTA

FIGURE 2-72

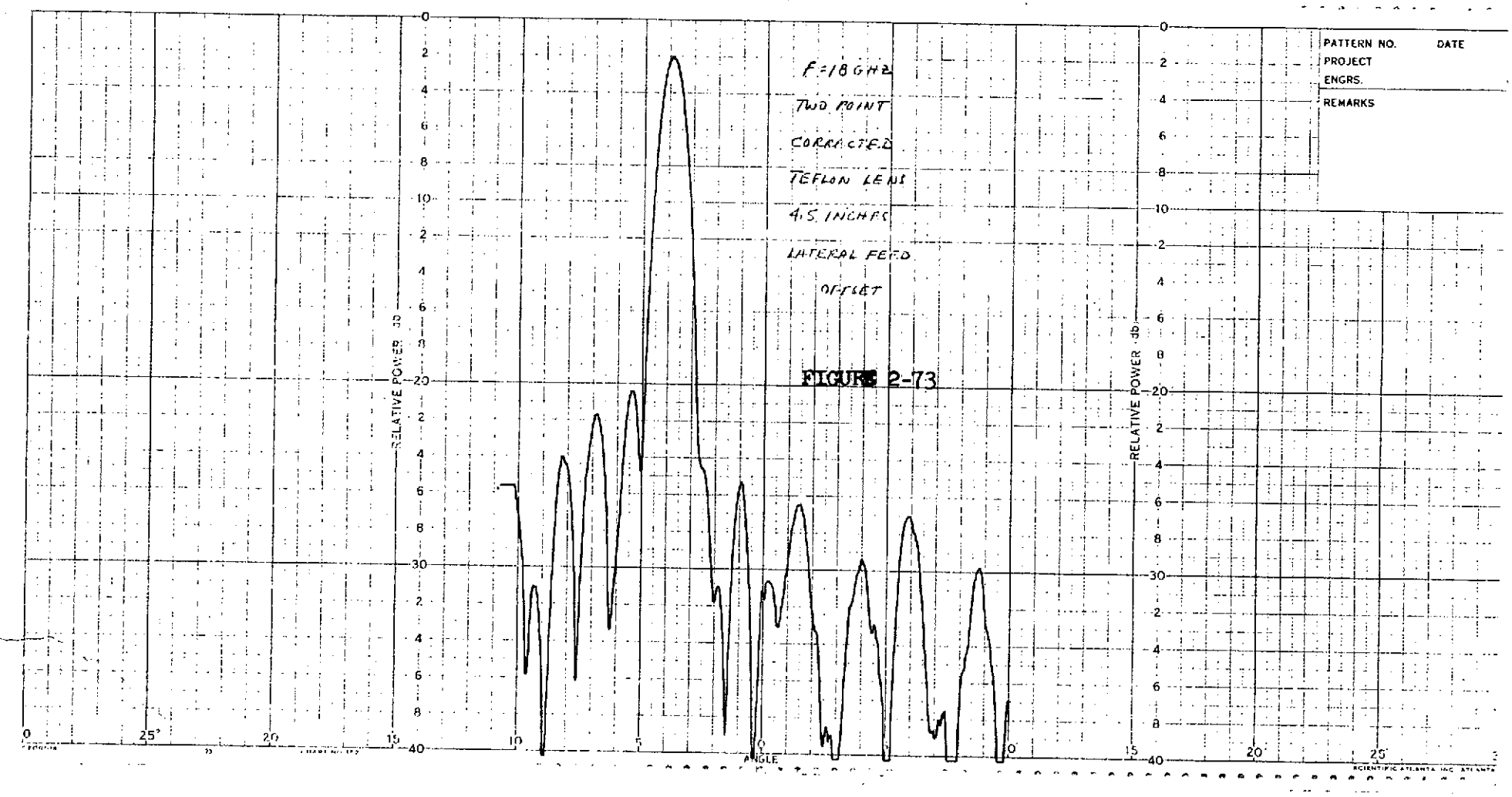
F=18 GHz
TWO POINT
CORRECTED
TEFLON LENS
4.5 INCHES
LATERAL FEED
OFFSET
PATTERN NO.
DATE
PROJECT
ENGRS.
REMARKS
RELATIVE POWER - db
ANGLE
SCIENTIFIC ATLANTA INC. ATLANTA

FIGURE 2-73

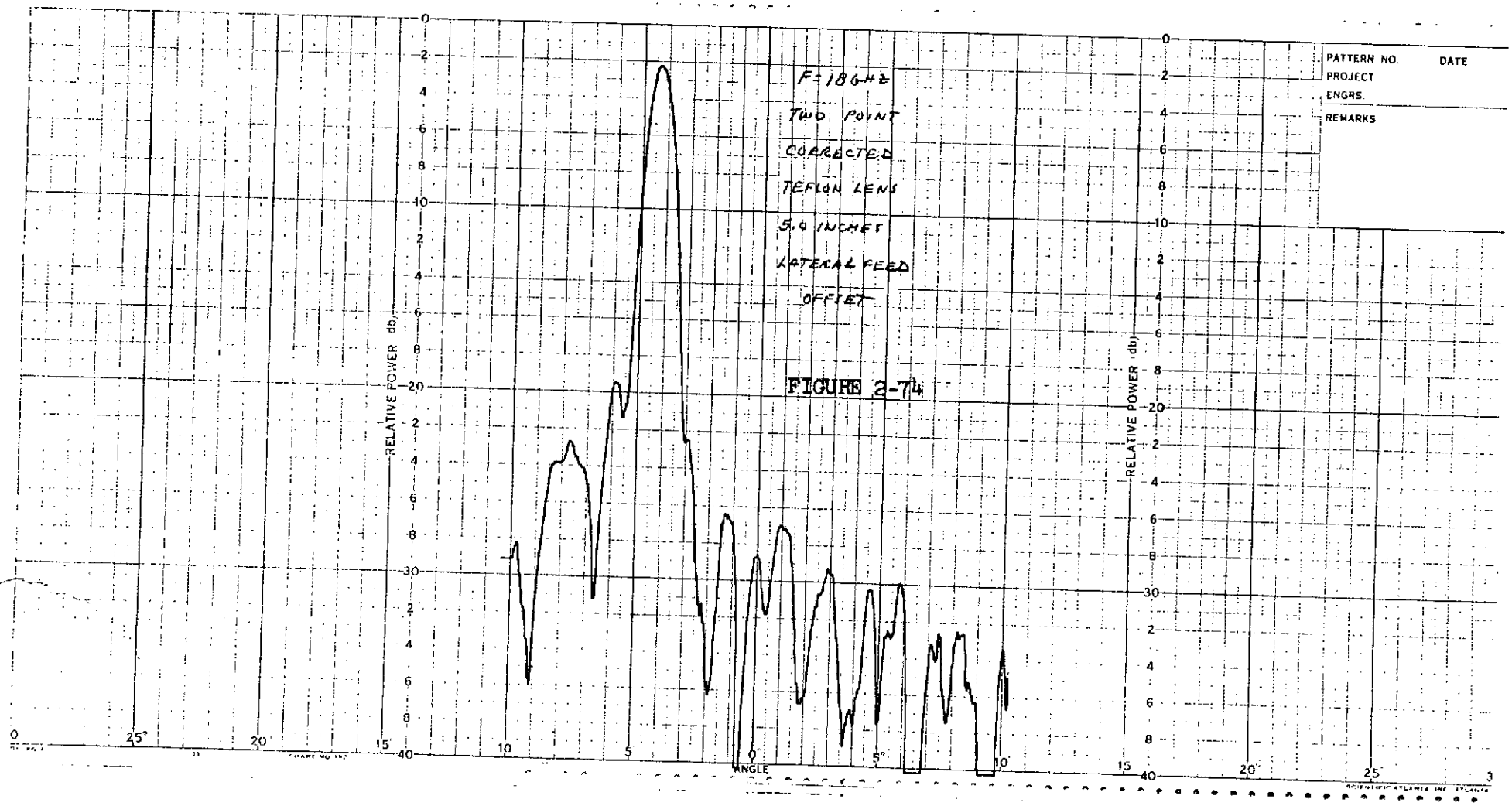
F=18GHz
TWO POINT
CORRECTED
TEFLON LENS
5.4 INCHES
LATERAL FEED
OFFSET
PATTERN NO.
DATE
PROJECT
ENGRS.
REMARKS
RELATIVE POWER db
ANGLE
SCIENTIFIC ATLANTA INC. ATLANTA

FIGURE 2-74

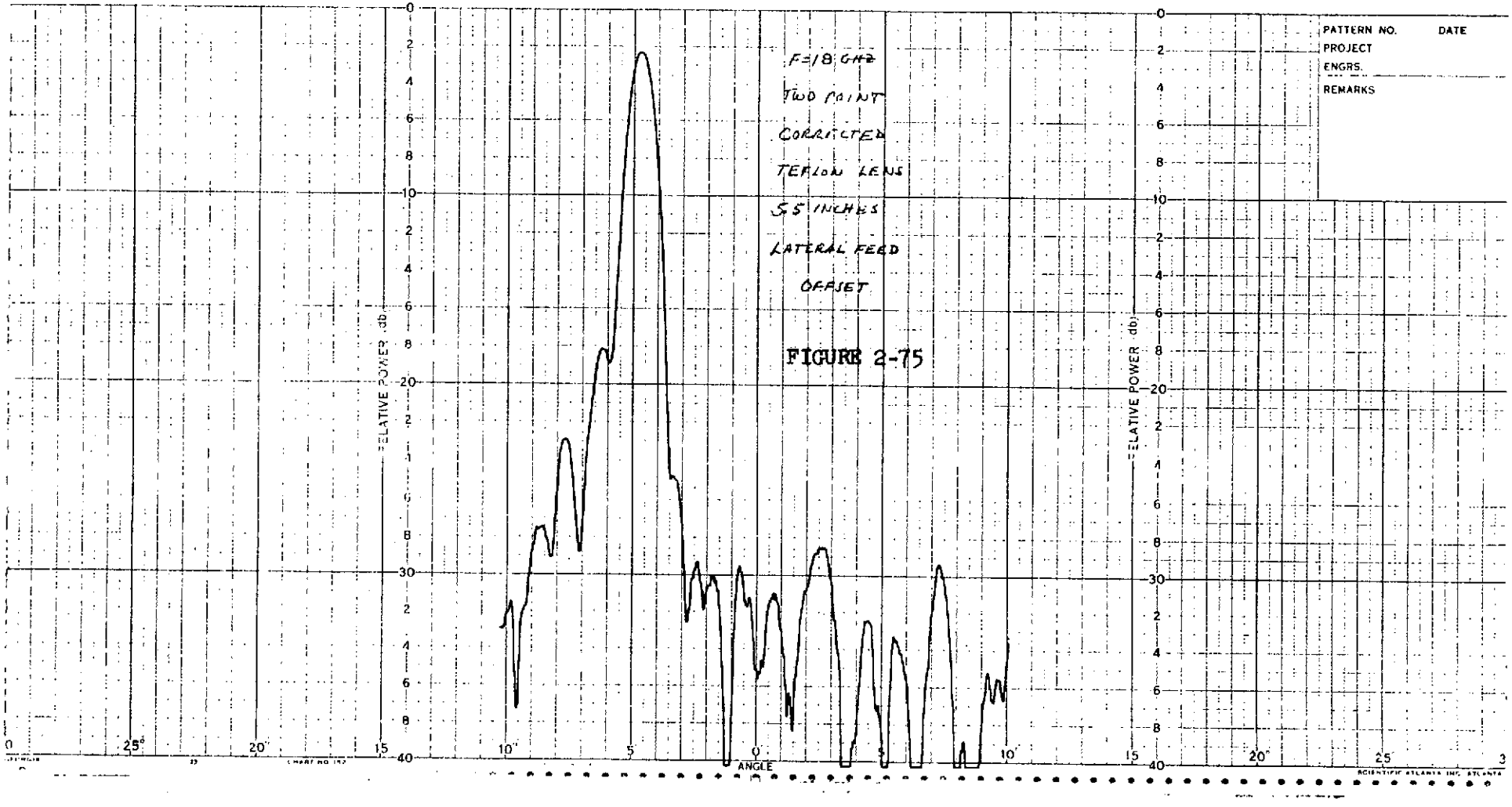
F=18 GHz
TWO POINT
CORRECTED
TEFLON LENS
55 INCHES
LATERAL FEED
OFFSET
PATTERN NO.
DATE
PROJECT
ENGRS.
REMARKS
RELATIVE POWER db
ANGLE
SCIENTIFIC ATLANTA INC. ATLANTA

FIGURE 2-75

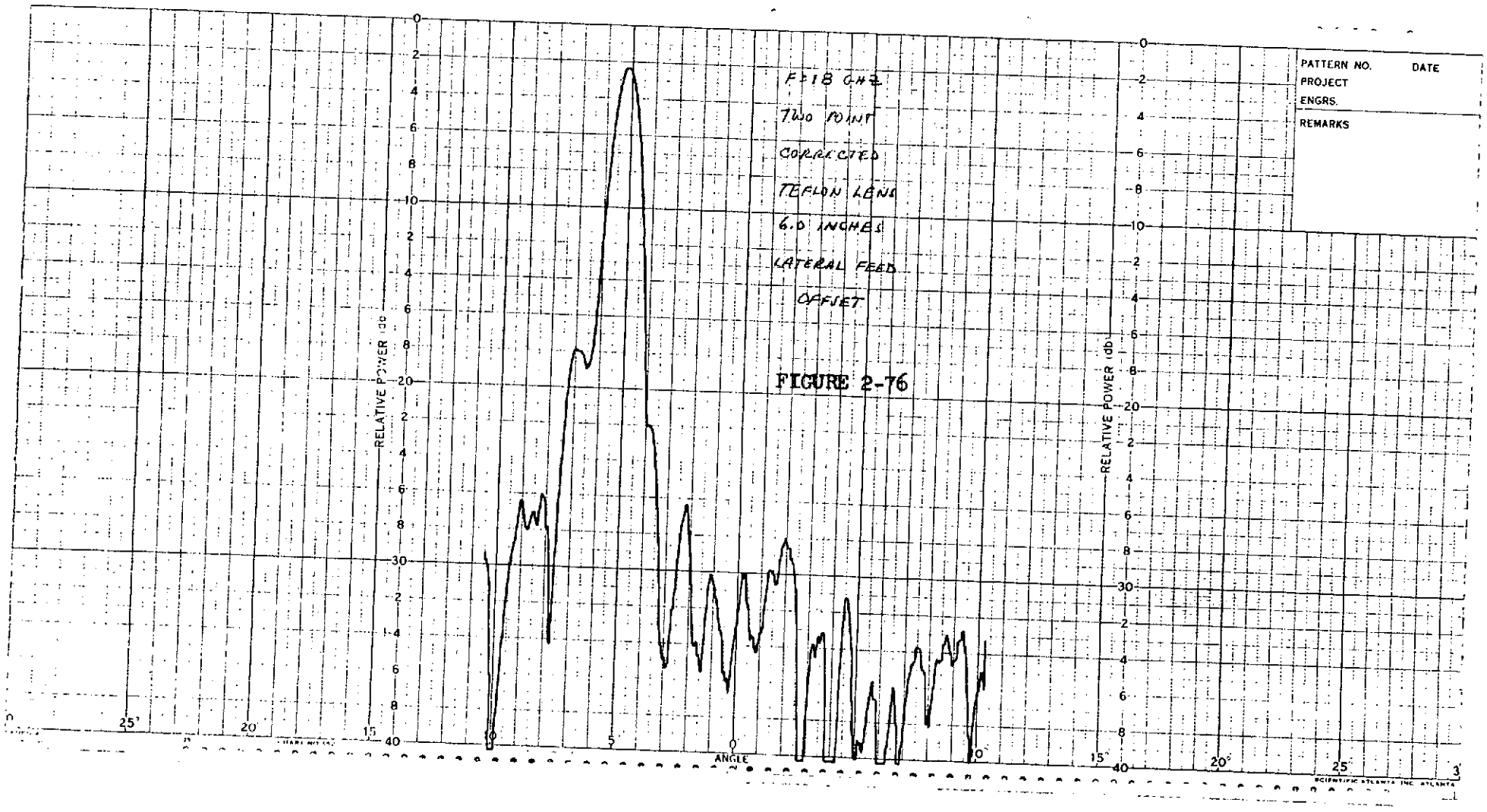
F-18 GHz
TWO POINT
CORRECTED
TEFLON LENS
6.0 INCHES
LATERAL FEED
OFFSET
PATTERN NO.
DATE
PROJECT
ENGRS.
REMARKS
RELATIVE POWER (db)
ANGLE
SCIENTIFIC ATLANTA INC. ATLANTA

FIGURE 2-76

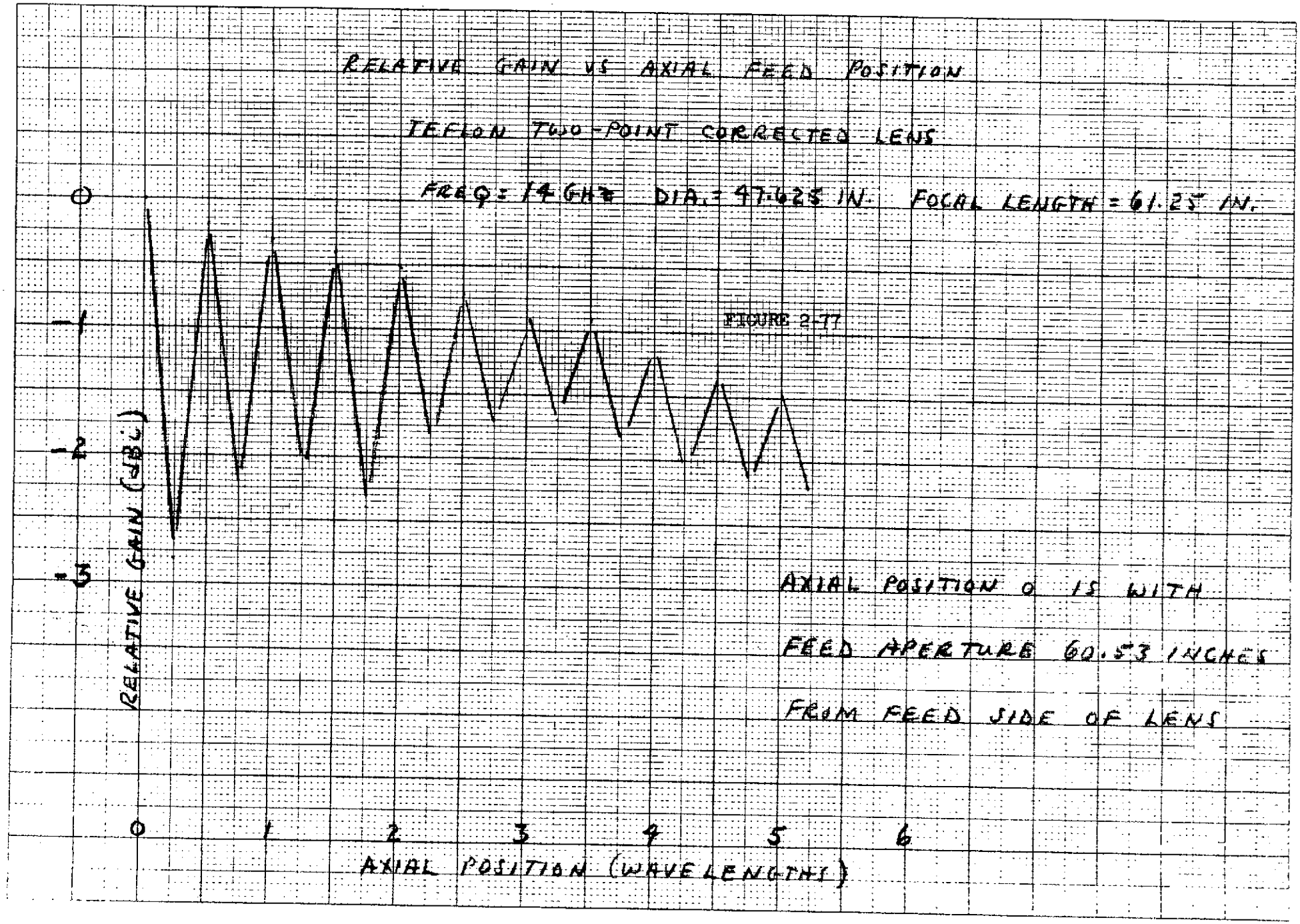
RELATIVE GAIN VS AXIAL FEED POSITION
TEFLON TWO-POINT CORRECTED LENS
FREQ = 14 GHz DIA. = 47.625 IN. FOCAL LENGTH = 61.25 IN.
FIGURE 2-17
AXIAL POSITION 0 IS WITH
FEED APERTURE 60.53 INCHES
FROM FEED SIDE OF LENS
RELATIVE GAIN (DB)
0
-1
-2
-3
0
1
2
3
4
5
6
AXIAL POSITION (WAVELENGTHS)

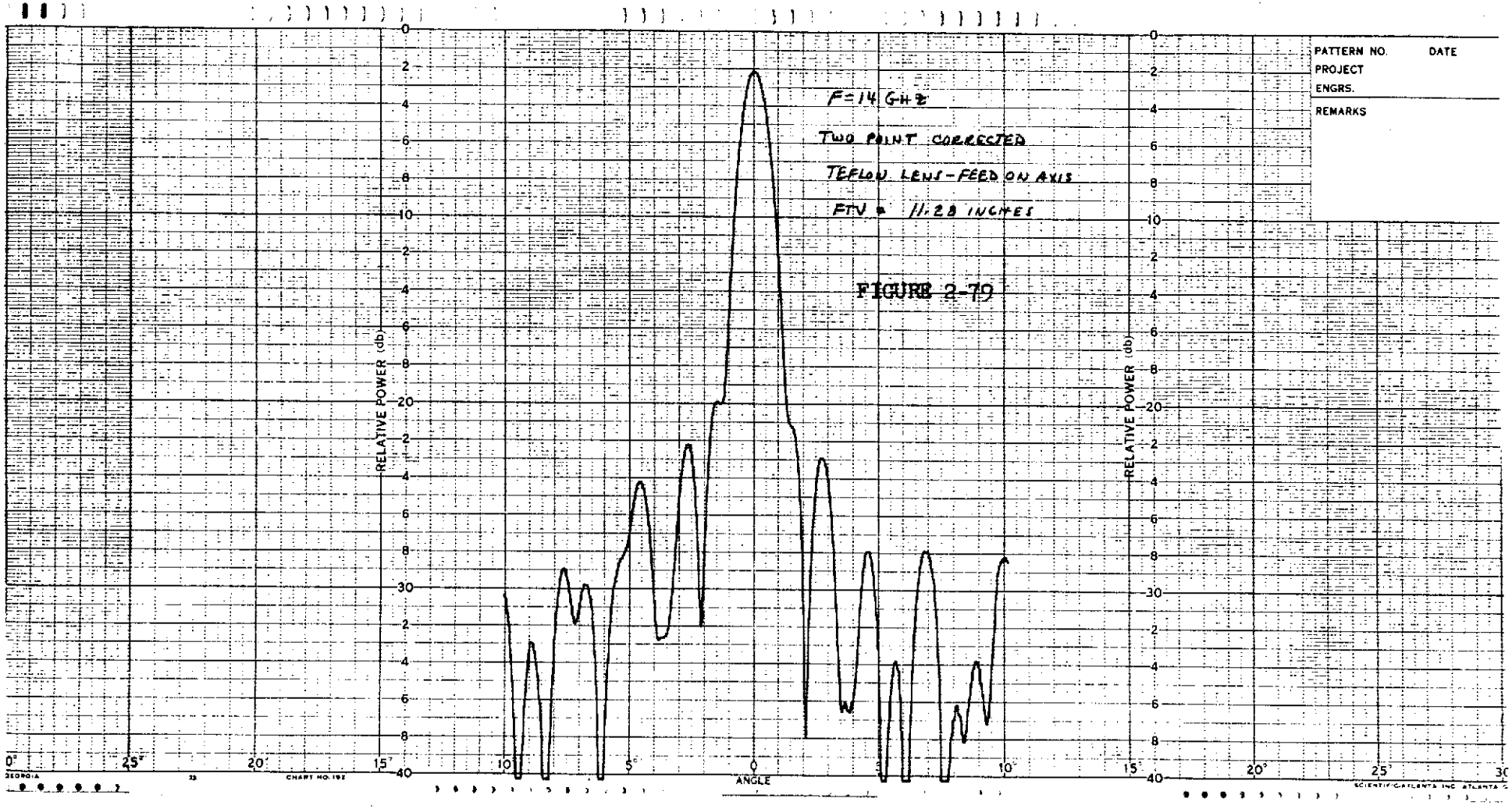
F=14 GHz
TWO POINT CORRECTED
TEFLON LENS-FEED ON AXIS
FTV = 11.28 INCHES
PATTERN NO.
DATE
PROJECT
ENGRS.
REMARKS
RELATIVE POWER (db)
ANGLE
0
2
4
6
8
10
20
30
40
0°
5°
10°
15°
20°
25°

FIGURE 2-79

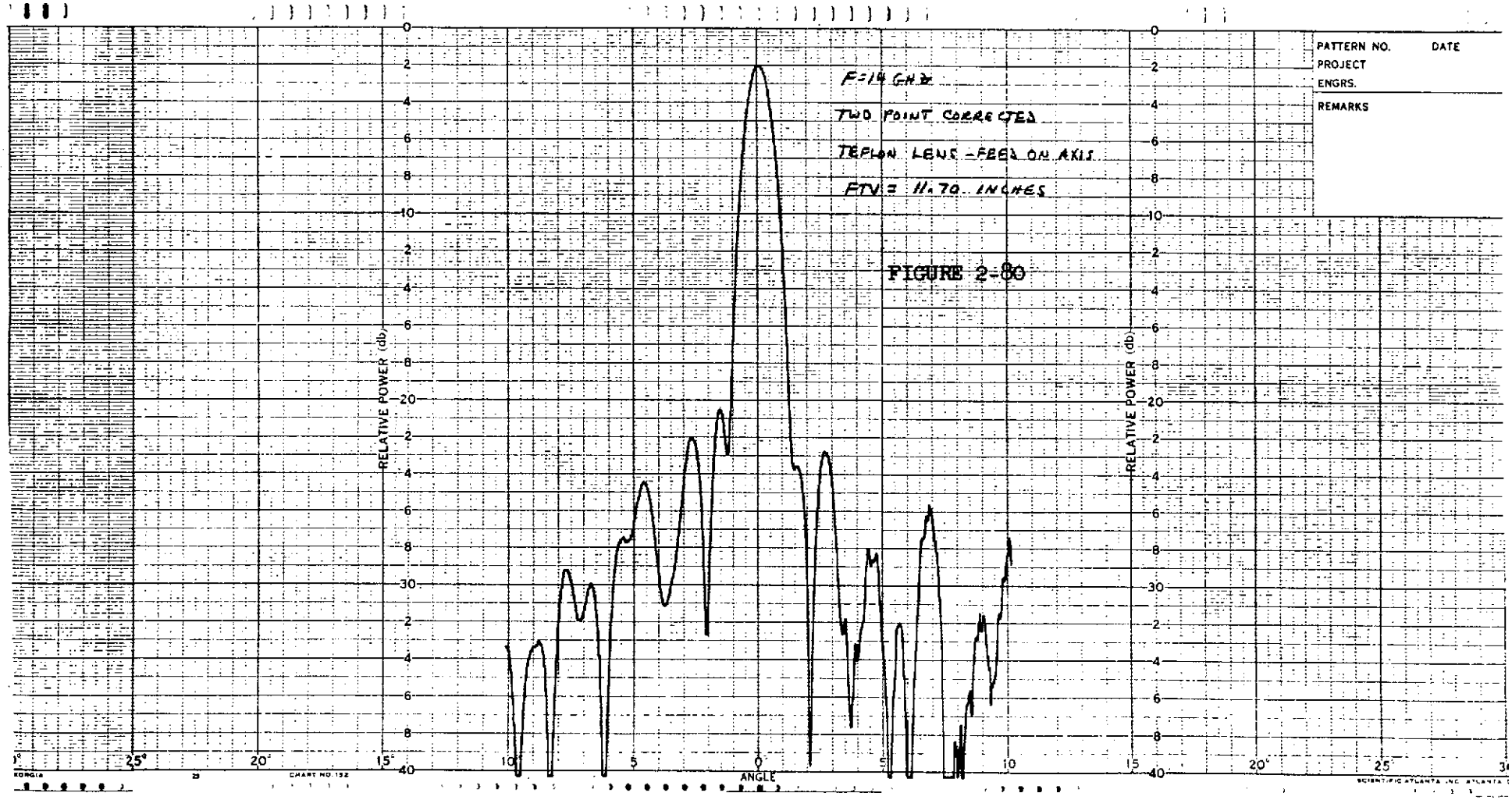
F=14 GHz
TWO POINT CORRECTED
TEFLON LENS - FEED ON AXIS
FTV = 11.70 INCHES
PATTERN NO.
DATE
PROJECT
ENGRS.
REMARKS
RELATIVE POWER (db)
ANGLE
CHART NO. 132
SCIENTIFIC ATLANTA, INC. ATLANTA

FIGURE 2-80

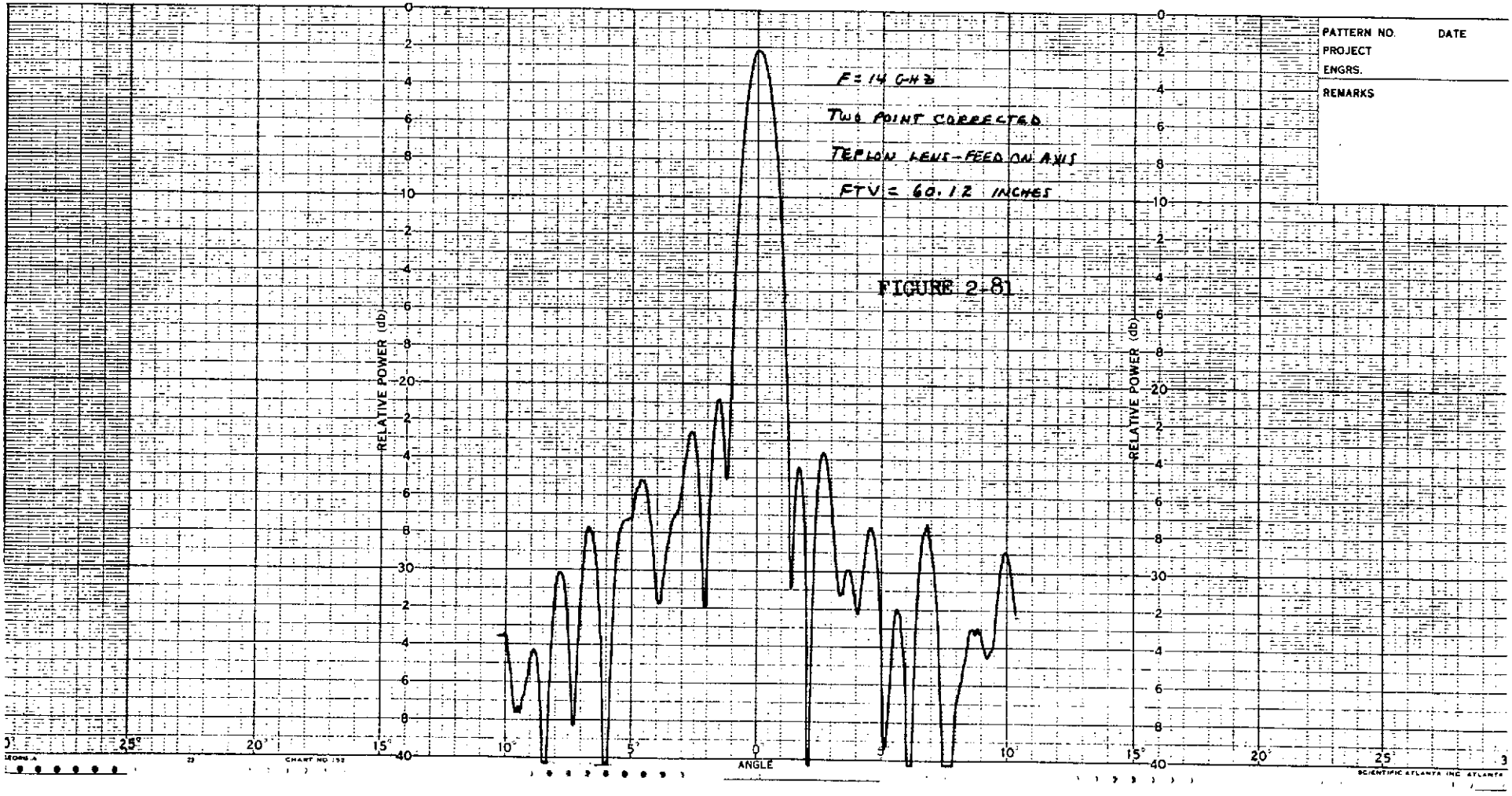
F = 14 GHz
TWO POINT CORRECTED
TEFLON LENS-FEED ON AXIS
FTV = 60.12 INCHES
PATTERN NO.
DATE
PROJECT
ENGRS.
REMARKS
RELATIVE POWER (db)
ANGLE
SCIENTIFIC ATLANTA INC. ATLANTA

FIGURE 2-81

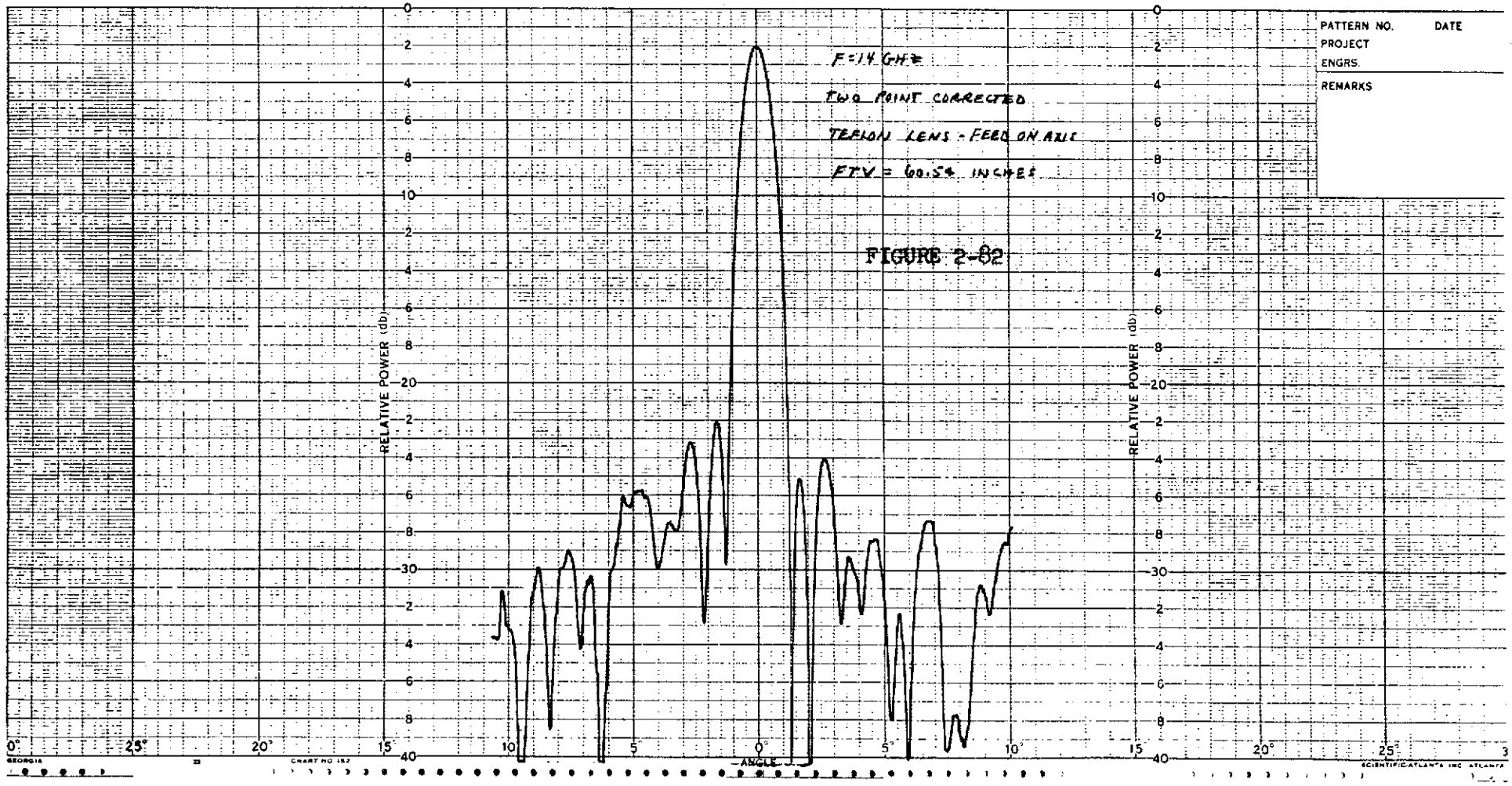
F=1.4 GHz
TWO POINT CORRECTED
TEFLON LENS - FEED ON AXIS
FTV = 60.54 INCHES
PATTERN NO.
DATE
PROJECT
ENGRS.
REMARKS
RELATIVE POWER (db)
ANGLE
0°
5°
10°
15°
20°
25°
0
2
4
6
8
10
20
30
40
GEORGIA
CHART NO 182
SCIENTIFIC-ATLANTA INC ATLANTA

FIGURE 2-82

2.6.4 Two-Point Corrected Teflon Lense - No Seams (continued)

With the feed set to the axial position for maximum response the feed was moved laterally off axis in one inch steps to a maximum offset of 6 inches. The lense patterns at 14 GHz as a function of lateral offset feed position are shown in Figures 2-83 through 2-89 .

The peak gain at maximum response is 21.9 dBi.

2.6.5 Two Point Corrected Artificial Dielectric Lens

A 47.625 inch diameter two point corrected dielectric lens was designed and fabricated with four seams similar to the artificial dielectric plano-convex lens. However, when the pieces were glued together using the same adhesive as was used in assembling the plano-convex lense, the adhesive ate away the artificial dielectric material, rendering the lense unsuitable for testing. Even if the fabrication had been successful, it is doubtful that this lense would have been tested, as there was insufficient time and money remaining. No tests of any kind were performed on the two point corrected artificial dielectric lense.

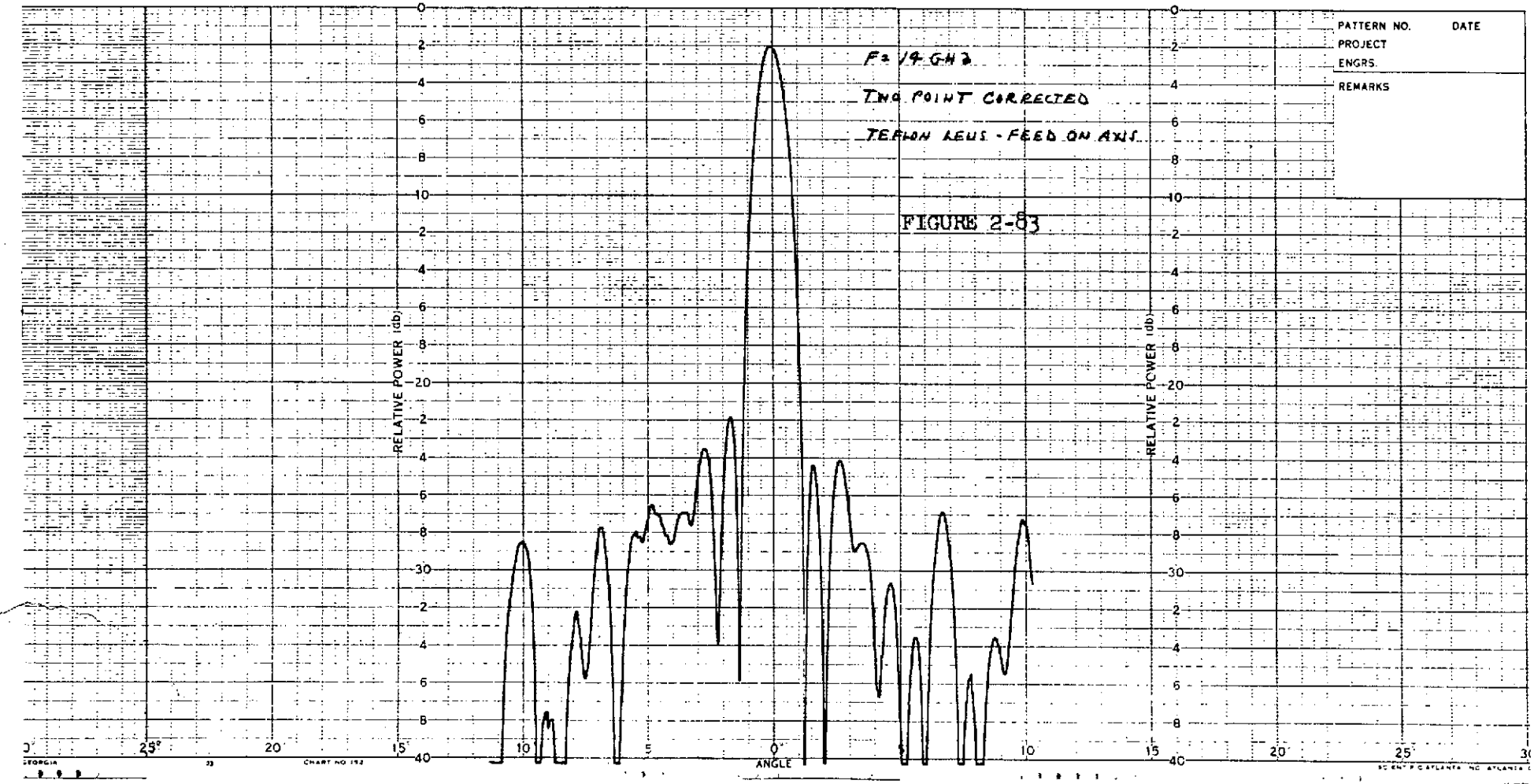
F = 1.9 GHz
TWO POINT CORRECTED
TEFLON LENS - FEED ON AXIS
PATTERN NO.
DATE
PROJECT
ENGRS.
REMARKS
RELATIVE POWER (db)
ANGLE
CHART NO 152

FIGURE 2-83

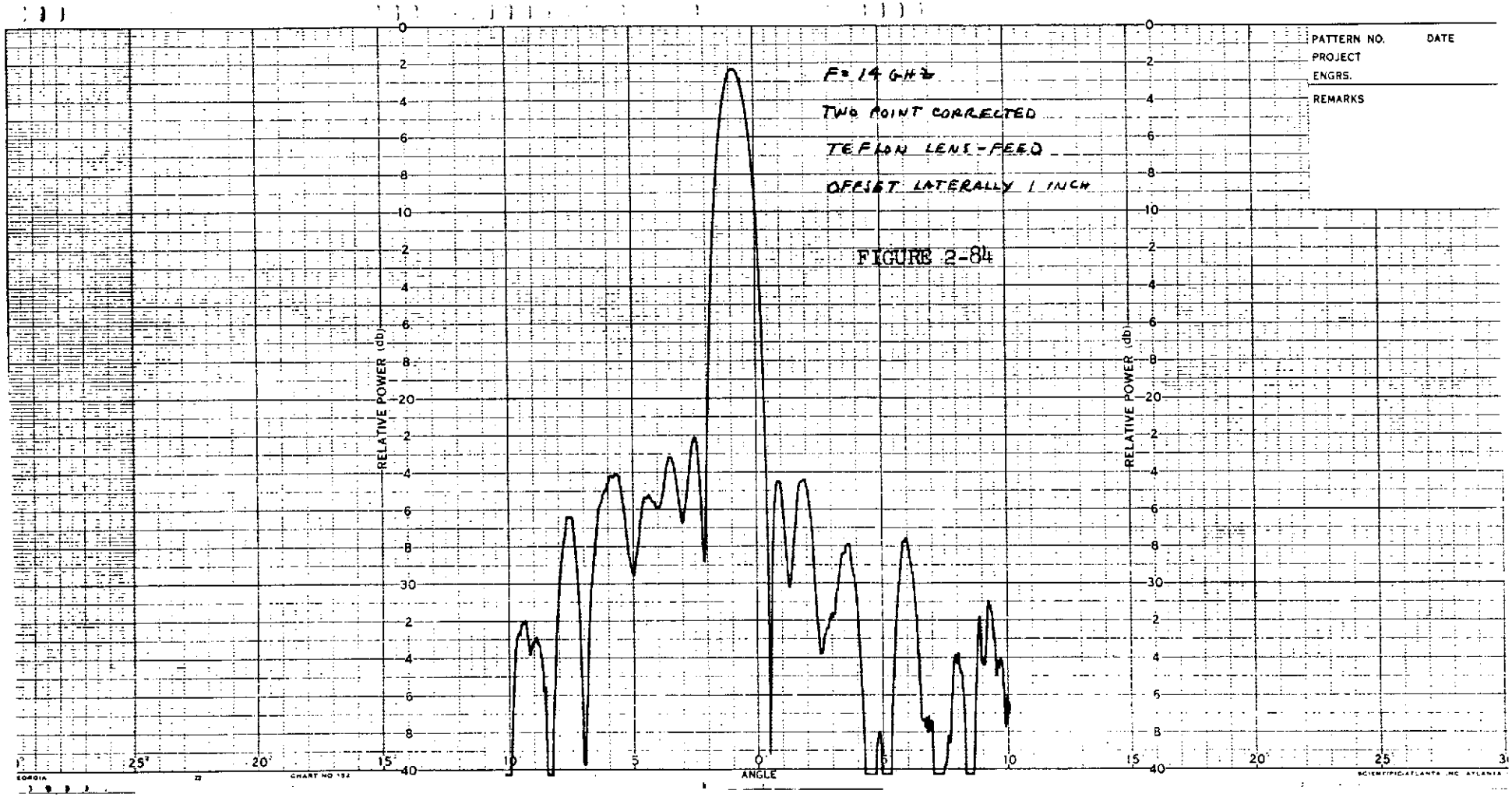
F= 14 GHz
TWO POINT CORRECTED
TEFLON LENS-FEED
OFFSET LATERALLY 1 INCH
PATTERN NO.
DATE
PROJECT
ENGRS.
REMARKS
RELATIVE POWER (dB)
ANGLE
CHART NO 132

FIGURE 2-84

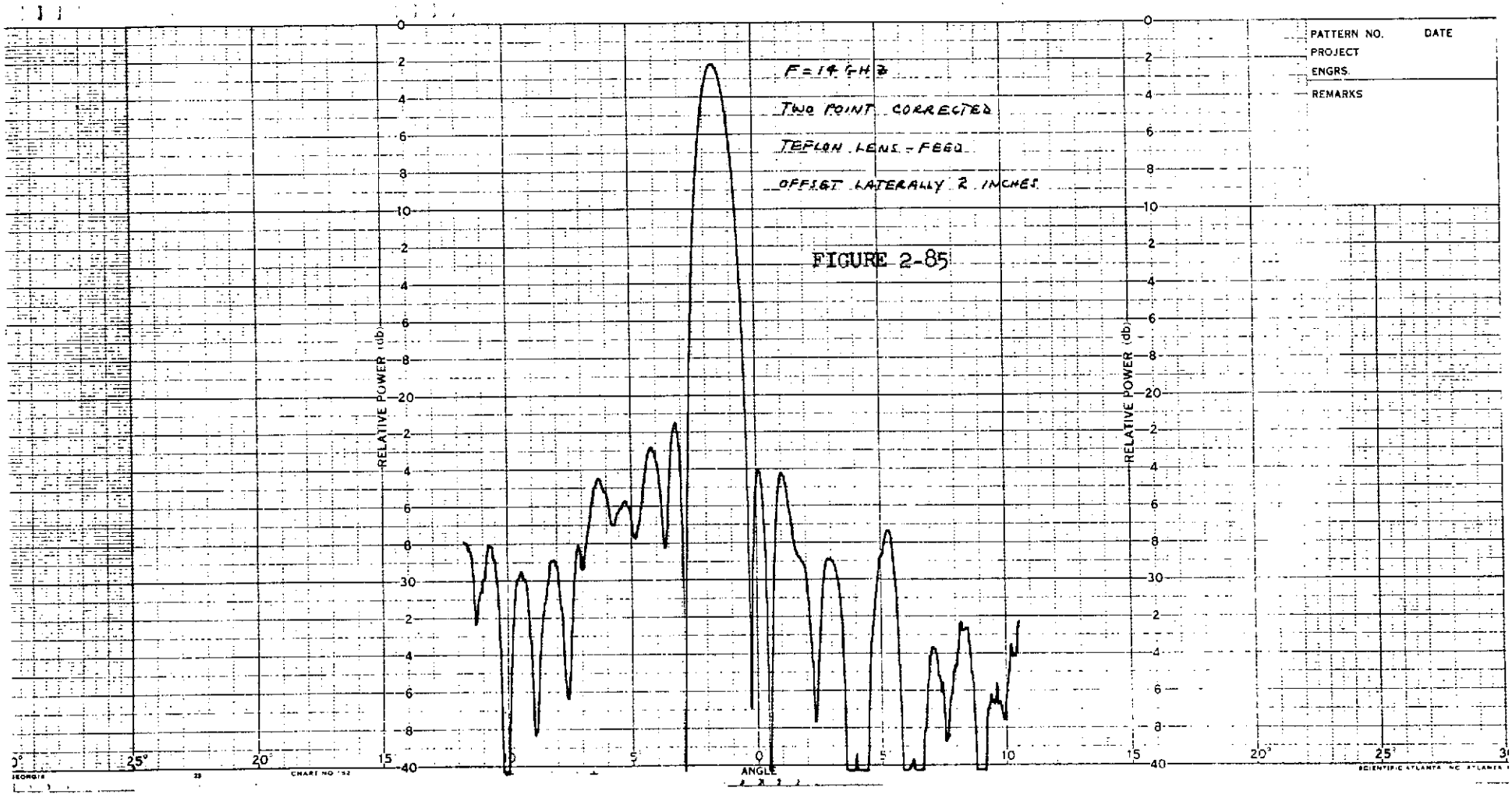
F = 14 GHz
TWO POINT CORRECTED
TEFLON LENS - FEED
OFFSET LATERALLY 2 INCHES
PATTERN NO.
DATE
PROJECT
ENGRS.
REMARKS
RELATIVE POWER (db)
ANGLE
CHART NO. 132
SCIENTIFIC ATLANTA INC ATLANTA

FIGURE 2-85

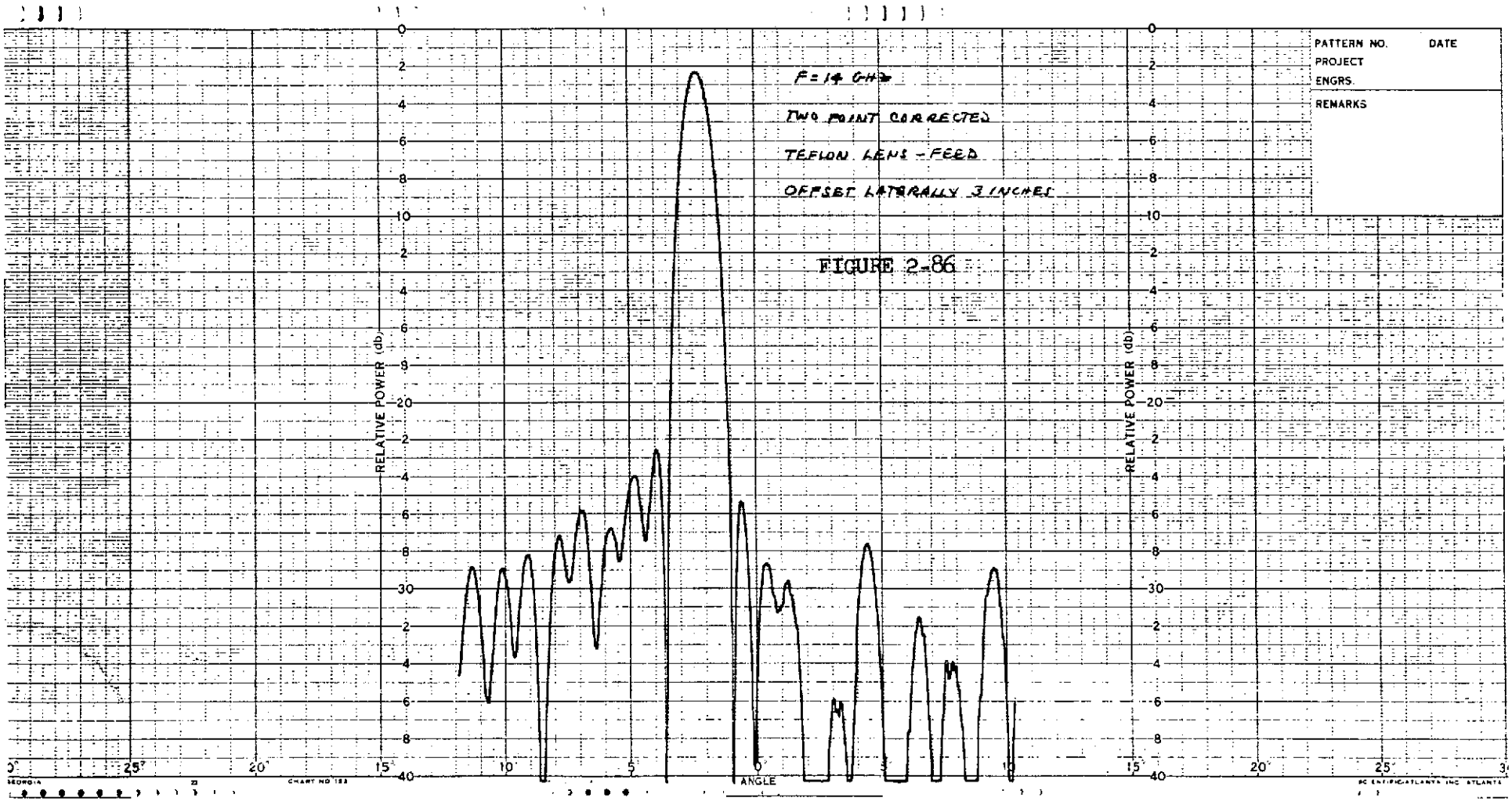
F = 14 GHz
TWO POINT CORRECTED
TEFLON LENS - FEED
OFFSET LATERALLY 3 INCHES
PATTERN NO.
DATE
PROJECT
ENGRS.
REMARKS
RELATIVE POWER (db)
ANGLE

FIGURE 2-86

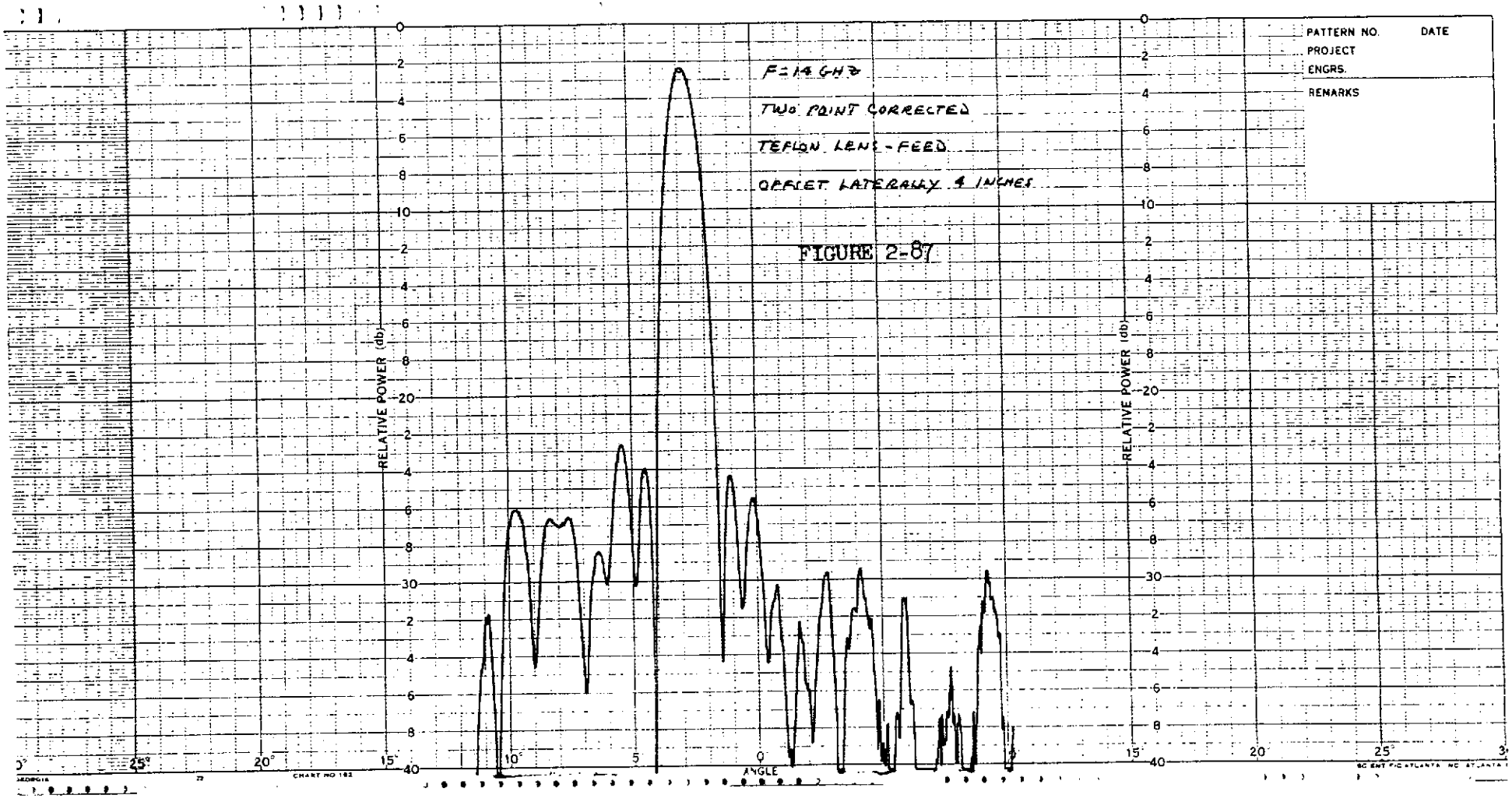
F=14 GHz
TWO POINT CORRECTED
TEFLON LENS-FEED
OFFSET LATERALLY 4 INCHES
PATTERN NO.
DATE
PROJECT
ENGRS.
REMARKS
RELATIVE POWER (db)
ANGLE

FIGURE 2-87

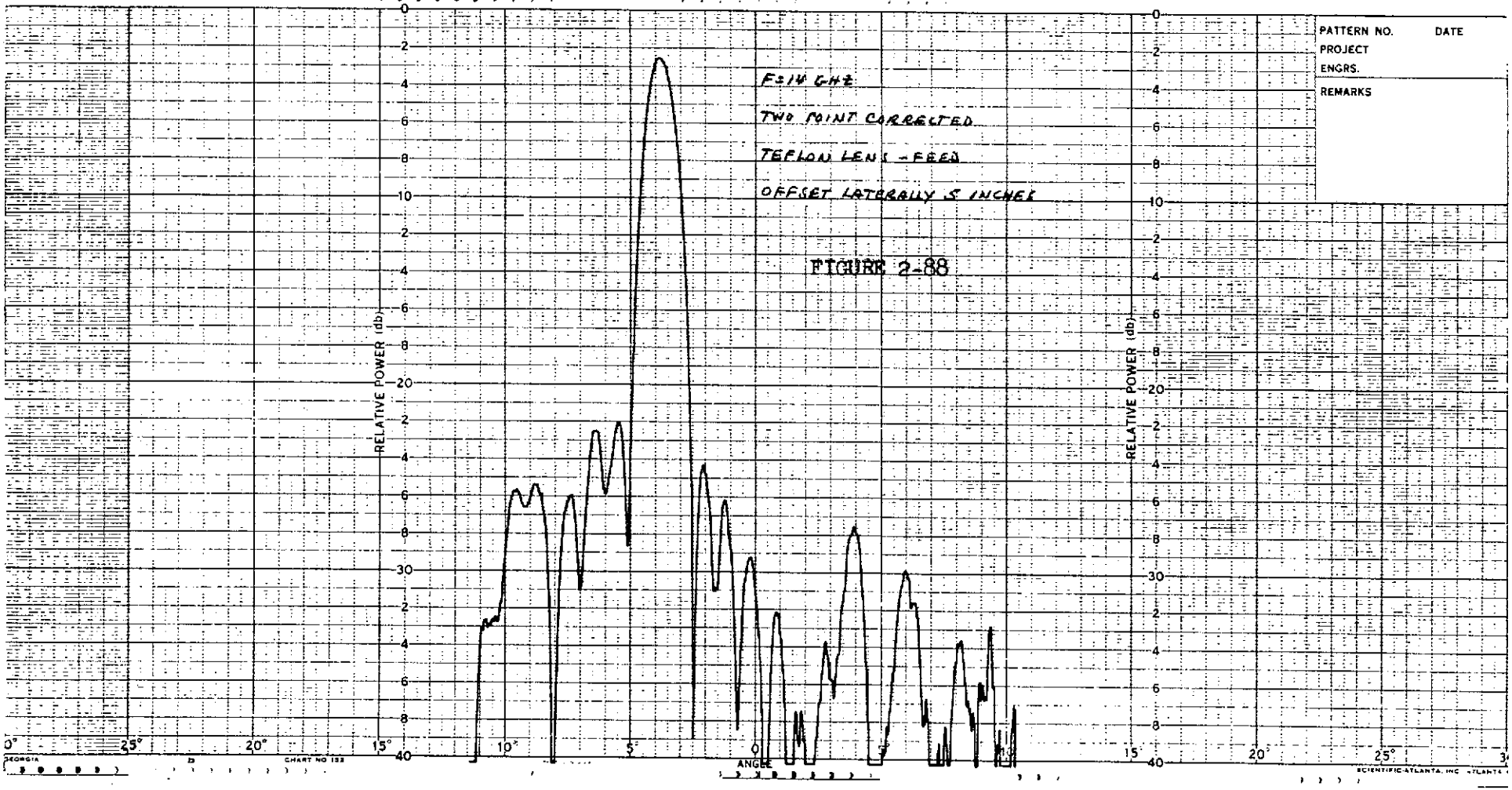
F=14 GHz
TWO POINT CORRECTED
TEFLON LENS - FEED
OFFSET LATERALLY 5 INCHES
PATTERN NO.
DATE
PROJECT
ENGRS.
REMARKS
RELATIVE POWER (db)
ANGLE
CHART NO 133
SCIENTIFIC-ATLANTA, INC

FIGURE 2-88

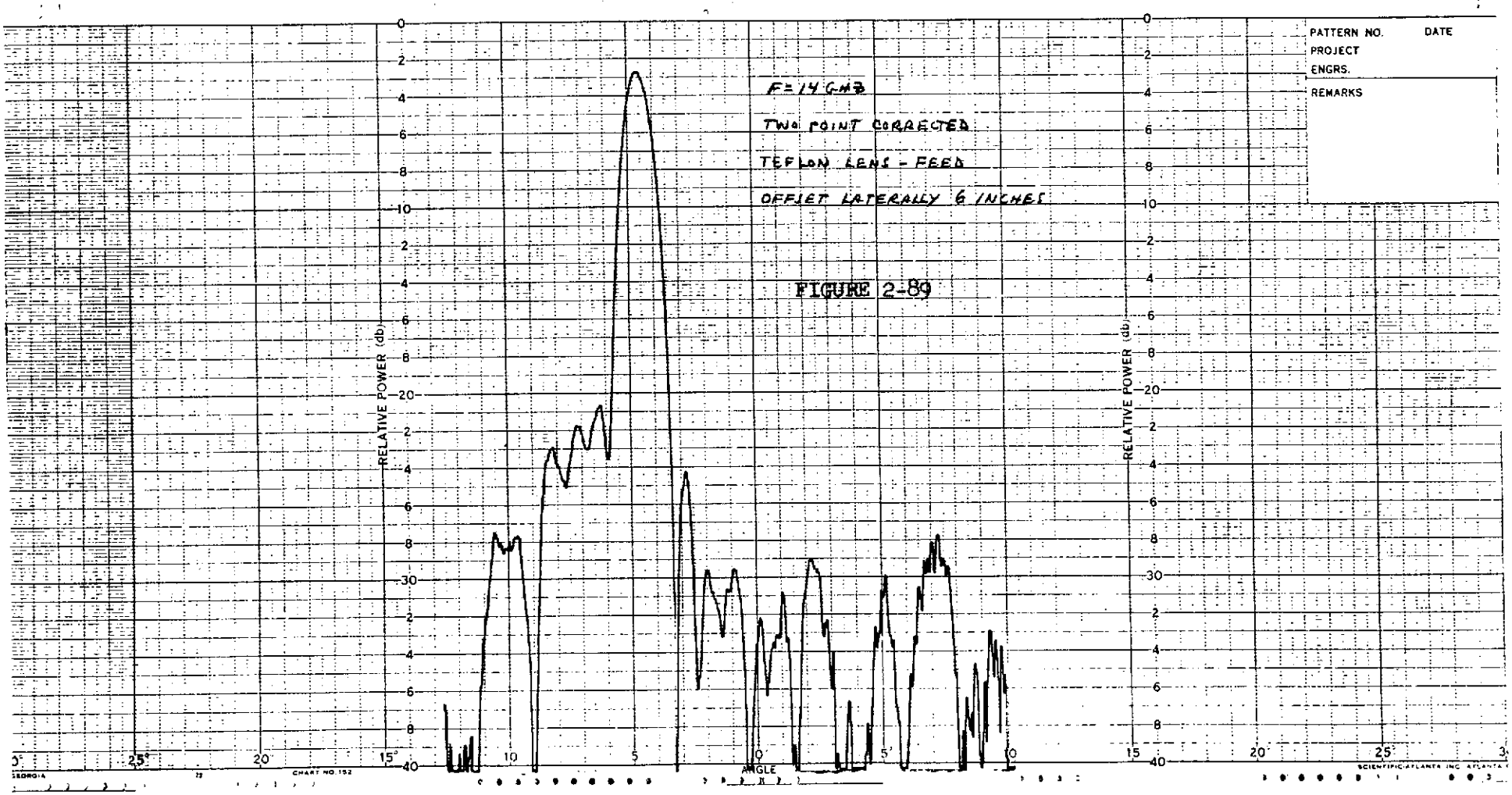
F=14 GHz
TWO POINT CORRECTED
TEFLON LENS - FEED
OFFSET LATERALLY 6 INCHES
PATTERN NO.
DATE
PROJECT
ENGRS.
REMARKS
RELATIVE POWER (db)
ANGLE
CHART NO. 152

FIGURE 2-89

3.0 INTERPRETATION OF EXPERIMENTAL RESULTS

3.1 Response vs Axial Feed Position

For both the plano-convex lense and the two point corrected lense, the maximum response and best pattern occurs when the feed is the maximum distance away from the lense and yet still within the parallel plate system.

The parallel plate system was designed so that the geometric focus of the plano-convex lense was two inches inside the feed end of the parallel plates. The axial movement of the feed was designed to allow five inches of axial movement from a position where the geometric focus was 2 inches in front of the feed aperture to a position where the focus was 3 inches inside the feed aperture. It was anticipated that this range of movement would be sufficient to determine an optimum axial position. When this system was designed, the shape and maximum depth of the two point corrected lens was not yet determined.

When the two point corrected Teflon lens was designed, the maximum thickness turned out to be 2.26 inches thicker than the plano-convex Teflon lens. Thus, when this lens was positioned inside the parallel plates, the geometric focus was 0.26 inches beyond the feed end of the plates. Therefore, the five inch axial movement of the feed horn using the two point corrected Teflon lense was such that the geometric focus was always inside of the feed horn aperture.

In comparing the results of the relative response vs axial feed position for the two types of lenses, it is interesting to note that the two maximum response feed positions which are nearly the same relative to the parallel plates are significantly different relative to the geometric focus of the particular lens.

When the feed position for the plano-convex lens and the two point corrected lens are the same relative to the foci of the two lenses, the results are not the same. This leads one to believe that the optimum position of the feed is not only influenced by the location of lense focus but is also affected by the parallel plate system itself, and specifically how well the energy is coupled from the feed into the parallel plate region.

3.1 Response vs Axial Feed Position (continued)

This phenomena is somewhat substantiated by tests which LMSC has performed in the new LMSC large anechoic chamber. The anechoic chamber is designed in the shape of an electromagnetic horn, flaring up from a conical shaped feed end to a rectangular testing area. The variation in amplitude across the test area has been measured as a function of the feed position in the conical chamber throat. Although the results depend somewhat on the type of antenna used as a feed (i.e., dipole, horn, conical spiral, etc.), in general, the best results occur when the feed is located as far back in the chamber throat as possible. As the feed is moved toward the test end of the chamber, larger amplitude variations are measured across the rectangular test area.

It is possible that a similar effect is produced in the parallel plate system used here (which is also flared out from the feed end to the lense end), which would explain why the feed position for best pattern performance is with the feed as far back as possible in the plates for either lense, but not in the same position relative to the focii of the two lenses.

Therefore, the results of these tests regarding feed position relative to the lens focus should not be used when a three dimensional lens is designed. The best feed position will have to be determined by experimental diagnostic measurement.

3.2 VSWR vs Axial Feed Position

The plots of VSWR vs axial feed position show a sinusoidal variation with successive maxima and minima occurring every one-half wavelength. The points of maximum VSWR correspond to points of minimum signal response and the points of minimum VSWR correspond to points of maximum signal response. This type of VSWR variation is the result of several reflections combining in- and out- of phase as the feed horn position is varied.

The VSWR of the feed horn itself in air is 1.65 to 1. The reflections produced by the parallel plate to air interface resulted in the horn VSWR having a nominal value of 1.45 to 1 when the feed horn was positioned on the axis of the parallel plates (which coincides with the lense axis when it is installed in the lense). There are addition reflections at the lense to air interface, the magnitude of which were not determined.

3.2 VSWR vs Axial Feed Position (continued)

The plano-convex Teflon lens has designed into the plane face a matching surface. No measurements were made without this matching surface on the lense. After viewing the results of the plano-convex lense, it was decided that initially no matching surface would be incorporated into the two point corrected lense. If time were available, a matching surface would be added, and the results compared. It turned out that there was not sufficient time for this additional test.

3.3 Plano-Convex Lens Patterns

All of the patterns were measured using the same feed horn. It was originally intended to use more than one feed horn during these tests to evaluate the affects of different edge illuminations, but because of the difficulties encountered and the time spent in arriving at a point where believable patterns could be obtained, there was not time available for using additional feed horns.

The feed horn used had an edge directed illumination of 14 dB at 18 GHz and 9 dB at 14 GHz. These values vary slightly for the two types of lenses as the half angle from the geometric focus to the edge of the lense is 18.3 degrees for the plano-convex lense and 19.5 degrees for the two point corrected lense. The value is also different depending on the axial feed position.

For each lense, patterns were recorded as a function of axial feed position. In each case, the position of maximum response also was the position of best pattern.

For each lens, patterns were recorded as a function of lateral feed position with the axial feed position set to the maximum response position. At 18 GHz, with the feed on axis, the plano-convex hyperbolic lense produced a beam with a 3 dB beamwidth of 1.05 degrees, 1st side lobes 26 dB below the beam peak, highest side lobes 25 dB below the beam peak, and nulls 30 to 40 dB deep. The on-axis gain was 22.8 dBi. As the feed was moved laterally off axis, the side lobe on the side of the beam between the beam peak and the mechanical axis of the lense increased rapidly. This is the well known coma lobe normally associated with off-axis feeds in a parabolic reflector. At one beamwidth off axis, the coma lobe is down 18 dB from the beam peak, an increase of 8 dB. At two beamwidths off axis, this coma lobe has become a shoulder to the main beam 17 dB below the beam peak, and another

3.3 Plano-Conves Lens Patterns (continued)

coma lobe has formed 10 dB below beam peak. At 3.3 beamwidths off axis (3.5 degrees), three coma lobes are visible, 7 dB, 13 dB, and 20 dB below the beam peak. The main beam is broadened considerably and the peak gain is 1 dB below the on-axis gain.

At 14 GHz, the results were very similar. With the feed on axis the 1st side lobes were 21 and 23 dB below the beam peak. At 3.0 beamwidths off axis (3.5 degrees), there are two coma lobes visible, 9 dB and 16 dB below the beam peak. The main beam has broadened considerably and the peak gain has decreased 0.6 dB.

This pattern performance is what was predicted with an uncorrected plano-convex hyperbolic lens. It is very similar as to the off-axis performance of a reflector with similar F/D ratio.

One peculiarity to the patterns with the feed on-axis is the slight broadening of the main beam beginning 10 dB below the beam peak. The effect is more noticeable at 14 GHz than at 18 GHz. Many things were tried, some scientific, and some "grasping at straws", to eliminate this beam spreading, but nothing was successful. Going ahead for a moment, the patterns with the two point corrected lense do not have this main beam spreading. There are three things different between the two lenses: (1) The surfaces were determined from different analyses and are, of course, different in shape; (2) The hyperbolic lense has a matching surface on the plane surface while the two point corrected lense has no matching surface, and (3) The feed position is different relative to the geometric focus of the lense. The equations of the surface and the templates made from these equations were double checked and no errors could be found in either one. The calculations for the matching surface were checked and found to be correct. When the feed horn had the same relative position to the hyperbolic lens focus as to the two point corrected lens focus, the beam spreading was still present. Based only on an engineering guess, the most likely cause in the matching surface, not because the equations or calculations are incorrect but because the techniques may not be directly applicable to our particular case.

3.4 Two Point Corrected Lense Patterns

The same feed horn used with the hyperbolic lens was used for the two point corrected lense. The best pattern obtained at 18 GHz with this system is shown in Figure 2- 90 . This is considered the best pattern in that it has deep nulls and equal 1st side lobes 25 dB below the beam peak. The pattern is shown to

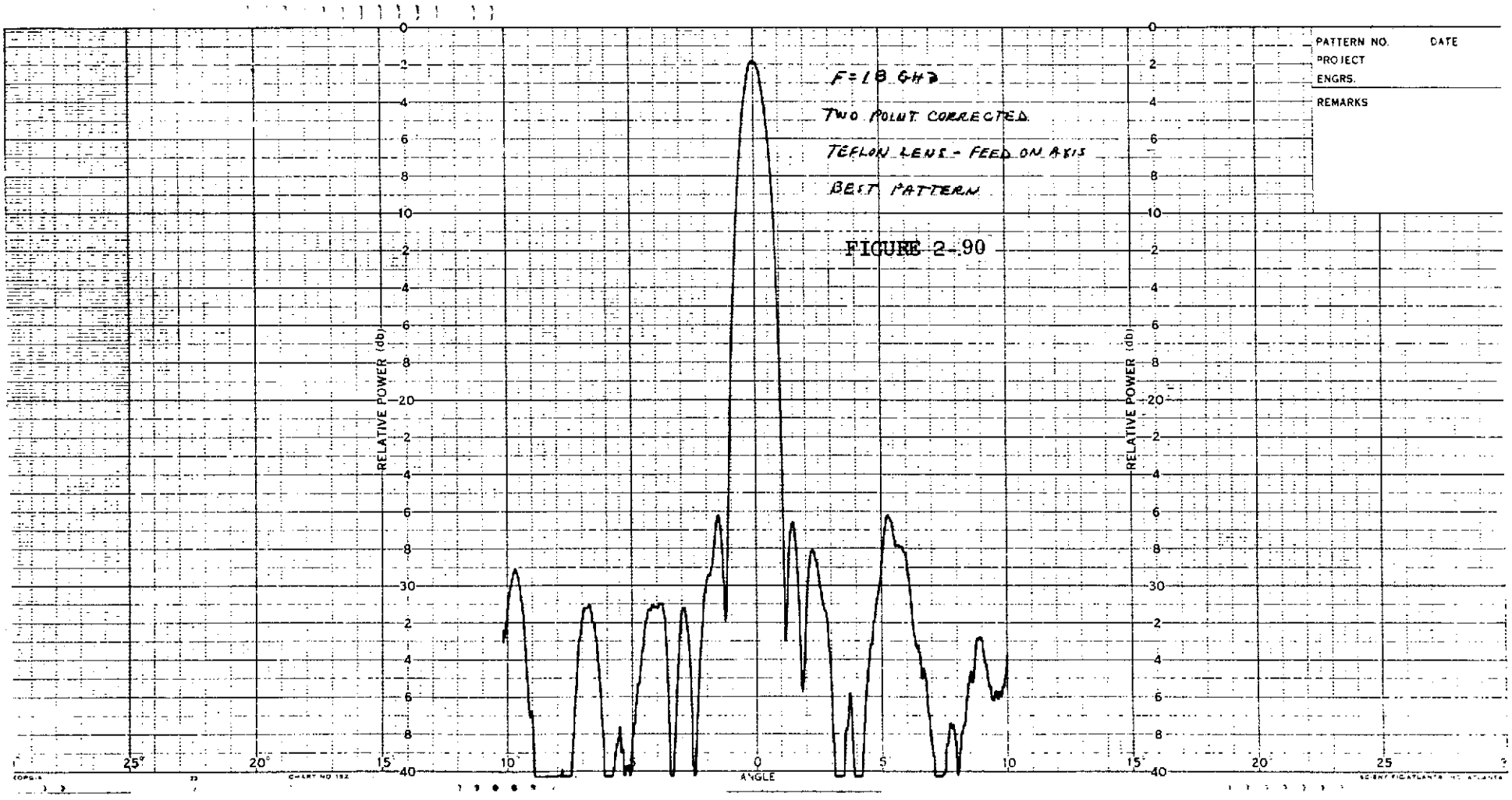
F = 18 GHz
TWO POINT CORRECTED
TEFLON LENS - FEED ON AXIS
BEST PATTERN
PATTERN NO.
DATE
PROJECT
ENGRS.
REMARKS
RELATIVE POWER (db)
ANGLE

FIGURE 2-90

3.4 Two Point Corrected Lense Patterns (continued)

demonstrate that side lobe performance similar to the hyperbolic lense with the feed on-axis is also obtained with the two point corrected lense, using the same feed. After the pattern was recorded, several other measurements were made, and several changes made to the clamping fixture to attempt to improve on this pattern. Needless to say, Murphy's Law came into play, and this pattern was never able to be repeated. In fact, the on-axis pattern used for the lateral feed offsets has 21 dB 1st side lobes. It was decided not to make any more changes to the system to improve the pattern as we may have ended up with 10 dB side lobes.

At 18 GHz, the two point corrected lens produced a pattern with a 3 dB beamwidth of 1.05 degrees, 1st side lobes 21 dB below the beam peak, which were the highest side lobes and nulls 30 to 40 dB deep. The main beam has no spreading but is nicely shaped from the beam peak to the deep 1st nulls. The on-axis gain is 23.0 dBi.

The two point corrected lense was designed for the focii to be 3.5° from the exit face of the base. At 18 GHz, as the feed is moved laterally off-axis out to 3.5 degrees, there is very little change in the pattern performance. The 1st side lobes vary from 19 to 23 dB below the beam peak. The highest side lobes other than the 1st side lobes, vary from 24 dB with the feed on-axis to 22 dB with the feed off-axis. Considering the ground reflection errors possible with this set-up, it is reasonable to say that the side lobe variation from on-axis to 3.5 degrees off axis is at most 1 dB. The peak gain and the main beam shape remained constant over this angular range.

Once the beam offset went beyond 3.5 degrees, the pattern deteriorated. The 1st null on the side of the beam between the beam axis and the lense axis filled in while the 1st side lobe on the opposite side increased by 5 dB to 16 dB below the beam peak. The side lobe levels are shown in Figure 3-1.

At 14 GHz, the effects of lateral feed movement was very similar. The 1st side lobes with the feed on-axis were unequal, 20 and 22 dB below the beam peak, but again varied only slightly as the beam was scanned off axis 3.5 degrees. The peak gain and the main beam shape remained constant over this angular range. Again, once the beam went beyond the design angle of 3.5 degrees, the pattern deteriorated.

SIDE LOBE LEVEL VS. BEAM OFFSET ANGLE

PLANO CONVEX AND TWO POINT CORRECTED

TEFLON LENSES

FIGURE 3-1

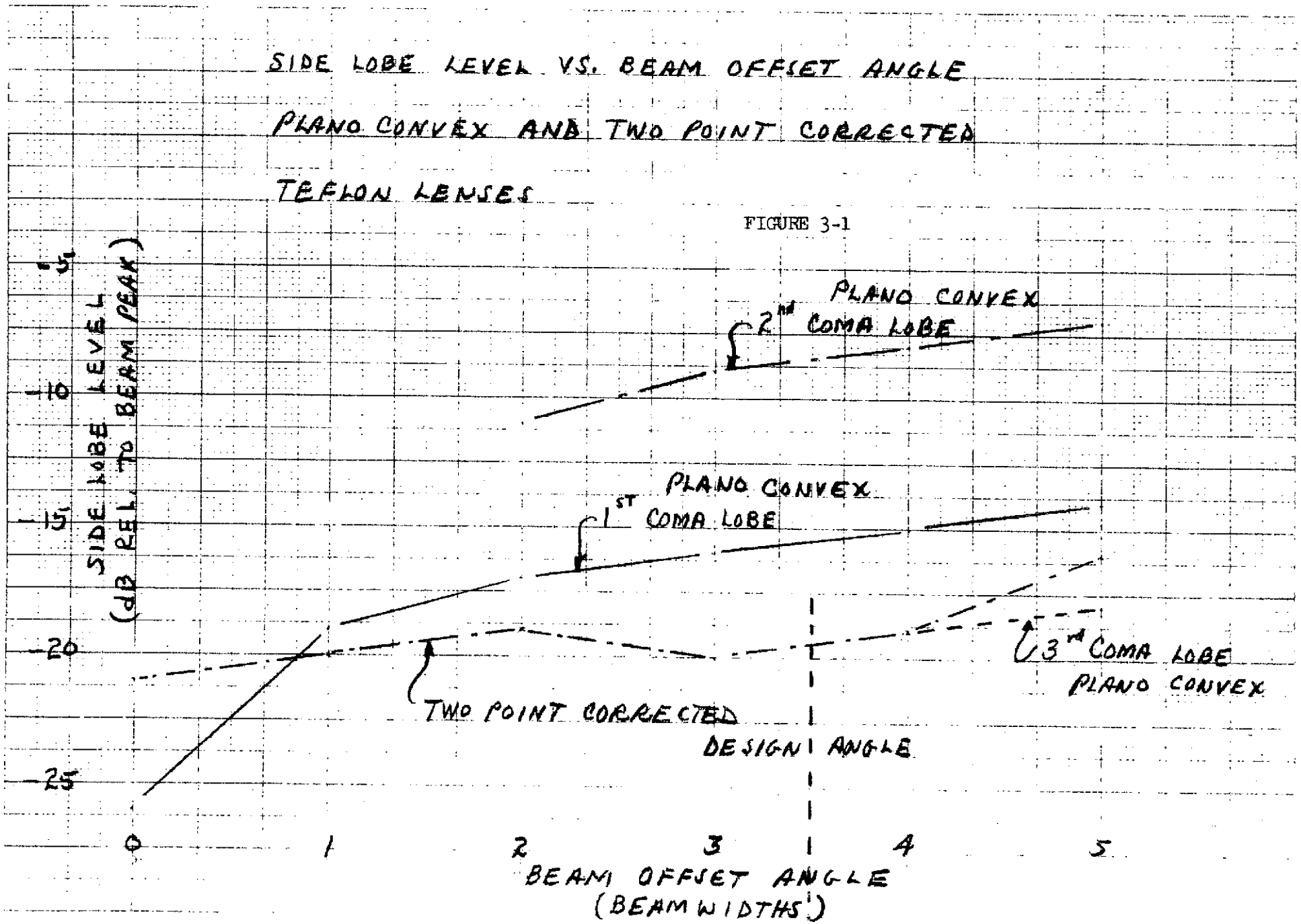

4.0 COMPUTER DESIGN

In addition to the experimental test program described above, an operational system design would be conducted, using an LMSC Computer aided analysis developed on an LMSC Independent Development Program during the first quarter of 1973. The analysis developed equations which allow the calculation of secondary patterns from dielectric lenses (natural or artificial) using a current integration method. These calculated patterns will be overlayed onto the applicable earth areas (in our case, the Continental United States) when the lense is located on a synchronous orbit satellite positioned above any fixed earth longitude.

4.1 Lens Pattern Calculations

The theoretical lens patterns were calculated using an analysis and computer program developed during the first quarter of 1973 on an LMSC-sponsored research project. This analysis has not been published, but we shall outline here the general analytical approach used.

The analytical method involves three basic phases in the computation of the lens pattern. These phases are ray tracing, interpolation, and integration. First, rays from a point source feed are traced through the lens to determine the point of emergance, the relative phase, the relative amplitude, and the direction of the emerging ray. Then, since regular sampling of the feed pattern does not produce a uniformly or regularly distributed set of aperture sampling points, the sampling points at the radiating aperture are converted to a regularly distributed set by interpolation. The resulting point set can then be used directly to find the lens pattern by integration using the aperture field method.

4.2 Ray Tracing

The ray tracing program will trace rays from a point source feed through any type of rotationally symmetric lens to the radiating aperture. Input options include:

1. Lens contour
2. Refractive Index
3. Lens Diameter
4. Lens Focal Length
5. Feed Pattern Sampling Interval (in θ and ϕ)

4.2 Ray Tracing (continued)

6. Feed Position
7. Feed Orientation
8. Feed Pattern Shape
9. Choice of Polarization

The ray tracing program will handle any type of rotationally symmetric lens contours. Each lens surface is represented by an equation of the form:

$$Az^2 + B(x^2+y^2) + Cz + D = 0$$

This is the general surface equation speciallized to the case of surface contours which are symmetrical around the z axis. Two equations are required, one for the first surface (the surface toward the feed) and one for the second surface. In some cases an equation of the above form can be used to represent either or both surfaces of the lens exactly. With the proper choice of A, B, C, and D, the above equation represents planes, spheres, ellipsoids, paraboloids, and hyperboloids. The program contains built-in options which allow the user to select the two conventional lenses which can be represented by the above equation. These are the hyperbolic lens and the elliptic lens. Both these lenses have a single surface of refraction and are not capable of wide-angle scanning. The hyperbolic lens shown in Fig. 4-1 has a hyperboloidal contour for the first surface which is the surface of refraction. The second or exit surface of the lens is a plane and does nothing to focus the radiating energy. The elliptic lens shown in Figure 4-2 has a spherical first

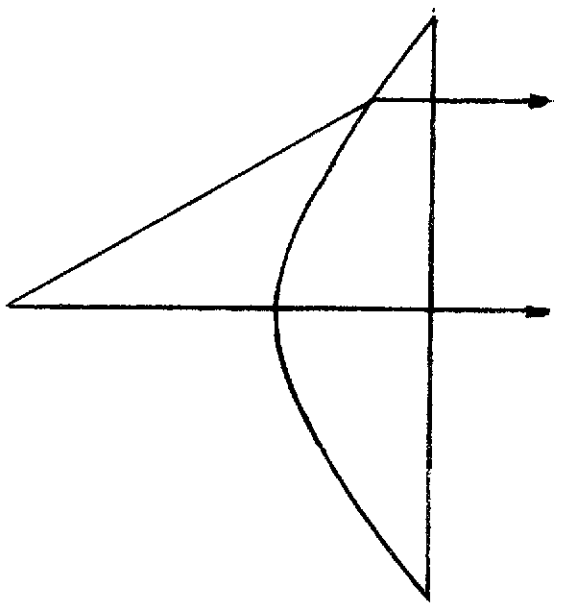

HYPERBOLIC LENS

FIG. 4-1

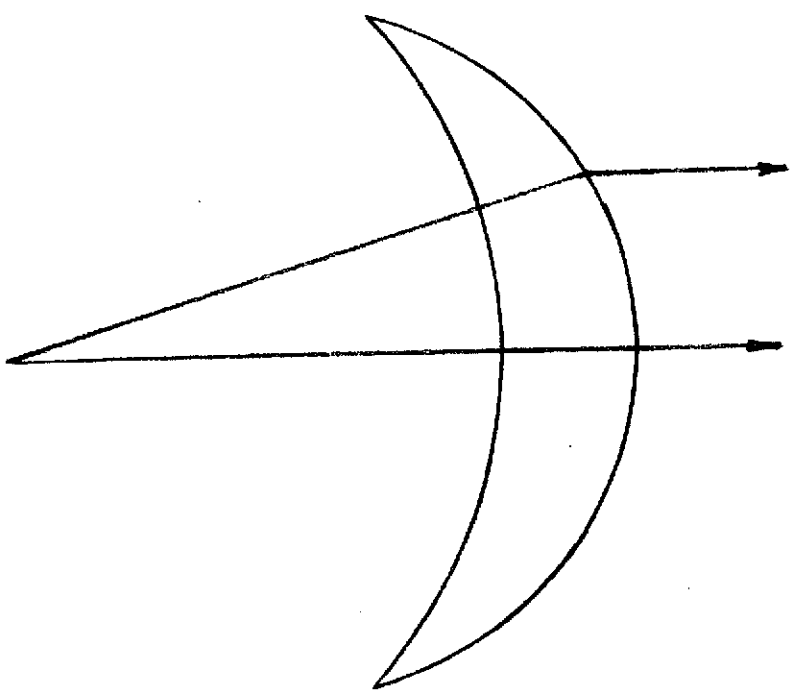

ELLIPTICAL LENS

FIG. 4-2

4.2 Ray Tracing (continued)

surface. The second surface, which is the surface of refraction for this lens, is an ellipsoid.

Generally, at least one, sometimes both, of the lens surfaces cannot be exactly represented by the above equation. For example, the wide angle aplanatic lens is a plano-convex surface (the plane side is toward the feed) when the refractive index is 1.61803399. While the plane side can, of course, be represented by the above functional form, the convex side is only approximated by it. The convex side is calculated using parametric equations which, so far, we have not been able to reduce to the form $f(x, y, z)=0$. Another example is the two-point corrected lens which has a pair of surfaces determined by successive ray tracing. If there is an exact representation of either of the two surfaces of the two-point corrected lens, it has not been found.

When this situation occurs, the procedure is to calculate the lens surface point-by-point by whatever means is available. From a tabular representation of the lens surface, an appropriate set of constants A, B, C, and D can be found which will represent the first-order approximation to the surface. These constants are used to calculate the approximate location of the intersection point where a ray strikes the surface. Then using nearby points from the tabular representation of the surface, the constants are re-determined and a more accurate location is determined for the intersection point.

Various design parameters are entered as input to the program. Focal length is measured along the lens axis from the (on-axis) feed poisition to the first surface, and we shall use this definition throughout this discussion. The feed position is specified in terms of rectangular coordinates with the center of the first surface as the origin. The feed may be aimed at the center of either surface of the lens. The feed may be rotated to any angle around its own axis. The user may select either dipole or slot modes of polarization; circular polarization is obtained by calculating both linears and superposing the radiated fields.

The feed pattern is assumed to be of the form

$$G(\theta, \phi) = 2(m+1) \cos^{m} \theta \qquad 0 \leq \theta \leq \pi/2$$

$$G(\theta, \phi) = 0 \qquad \theta > \pi/2$$

How well this function represents typical feed patterns for the lens case is not known. When this feed pattern is used for reflector patterns calculations, the resultant gain for the reflector is about 1.5 to 1.7 dB too high, due primarily to the unrealistic spillover

4.2 Ray Tracing (continued)

radiation properties associated with the above functional form. For reflector feeds m would be of the order of 1 to 10. For lenses m is much higher, of the order of 20 to 60. While we do not have much experience as yet in correlating theoretical calculations with this type of feed pattern for the lens, our limited experience does indicate that the resulting gain is about 1.5 to 1.7 dB higher than we would expect from the aperture size.

The feed pattern is sampled in equal increments in θ and ϕ, θ being the polar angle measured from the feed axis and ϕ being the azimuthal angle around the feed axis. This sampling is the same as is used for digital pattern records taken with Scientific-Atlanta digital pattern recording equipment. This was done purposely so that experimental patterns can be easily used instead of the theoretical feed pattern when it is desired to add this refinement. It may be mentioned in passing that in our reflector calculations we have obtained agreement between the theoretical and experimental gain figures to within 0.1 dB (and usually no worse than 0.3 dB) when experimental feed patterns are used in the gain calculations. We should ultimately expect to do as well for the lens case.

In tracing a ray through the lens, the first step is to determine the amplitude of the field, the rectangular components of the polarization vector, and the direction (direction cosines) of the ray path as the ray leaves the feed (point A in Fig. 4-3). The intersection of the ray with the first surface (point B) is determined and the phase and amplitude of the field is corrected for the path AB. This is the field incident on the first surface. Next, the changes occurring at the interface are determined by resolving the incident wave into components parallel and perpendicular to the plane of incidence and applying boundary conditions. This results in a change in polarization, amplitude, and direction of the wave as it passes into the lens. The new ray direction is then used to determine the intersection of the ray with the second surface (point C). The field is corrected for amplitude and phase changes occurring while passing through the lens. Boundary conditions are again applied as the ray passes through the second surface. The ray is then traced to the radiating aperture (the z=0 plane) at point D. (For a planar second surface, points C and D are coincident).

The resulting output is a set of points $(x_{ij}, y_{ij}, 0)$ with the associated direction cosines of the emerging rays, the rectangular components of the unit polarization vector, and the amplitude and relative phase of the aperture field.

The ray tracing takes into account any power lost by reflections at either surface. It is assumed, however, that power reflected from the second surface is completely

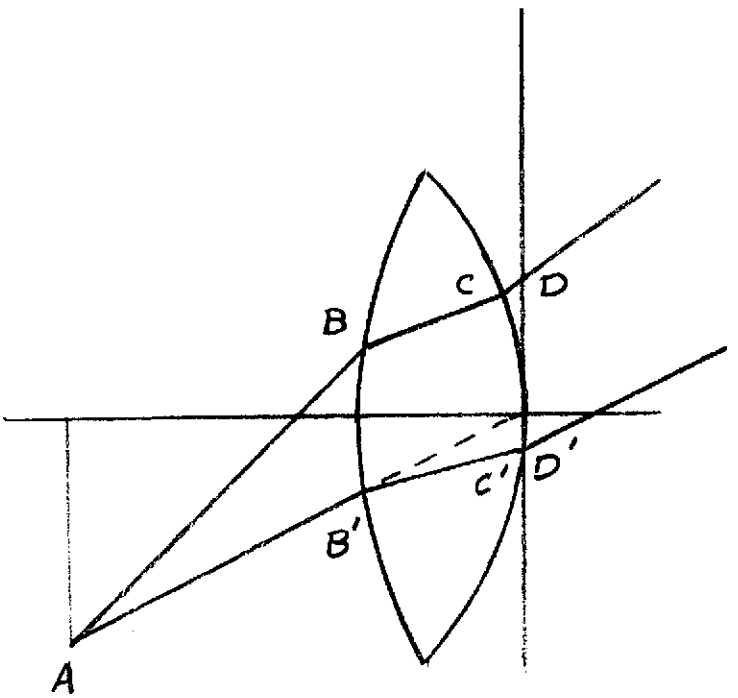

FIG. 4-3 RAY PATHS

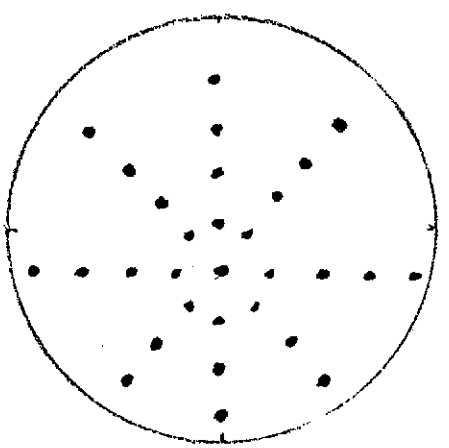

FIG. 4-4 POINT SET RESULTING FROM RAY TRACING

4.2 Ray Tracing (continued)

lost -- that is, multiple internal reflections do not occur to cause reflected power to contribute to the far field pattern. The ray tracing program does not take into account the dissipative losses within the lens. A first approximation can readily be applied for the ray path length in the lens material, but actually the situation in a rigorous sense is more complicated than that. When a dielectric material has a non-zero loss tangent, the boundary conditions at the surfaces are modified resulting in a change in transmission coefficient. It was decided not to include the effect of dissipative losses in the calculation until we had time to examine the problem thoroughly and attack it on a rigorous basis.

The modification of the wave amplitude as it passes through one of the regions is due to spreading of the rays. Between the feed and the first surface the wave power decreases in proportion to the inverse square of the path length, as it does in a reflector system between the feed and the reflector. In going from the first surface to the second surface the wave amplitude changes if the rays are not parallel. The principle of conservation of energy was applied (total power transmitted through the first surface must equal total power incident upon the second surface) to determine the change in wave amplitude. (The modification of the wave amplitude given by Silver[1] is incorrect since it assumes that reflections do not occur, a condition which cannot exist).

4.3 Interpolation

The point set which results from the ray tracing program is appropriate for direct use in integrating to find the far-zone pattern. For one thing, though we may aim the feed at the center of the radiating aperture, the exit point corresponding to the axial direction from the feed is displaced from the center of the radiating aperture unless the feed is on the lens axis. This can be seen by considering the ray path AB'C'D' in Fig.4-3. This exit point (for the axial feed ray) becomes the center of the aperture point set. Other points in the radiating aperture are distributed approximately along radial lines from the displaced center as illustrated in Fig. 4-4. Secondly, while the feed pattern is incremented equally in θ and ϕ, the aperture point set is not incremented equally in the radial aperture coordinate, even though it is very nearly correctly incremented in the (displaced) ϕ coordinate. Therefore, before the pattern can be found by integration in polar coordinates of the aperture, the ray tracing point set is converted to an integration point set in equal increments of the integration variables. The procedure is simply to find the three closest points (of the ray tracing point set) and use planar (linear) interpolation to find values of the direction cosines of the ray, the field polarization vector components,

4.3 Interpolation (continued)

and the wave amplitude and phase at any particular integration point. The ray tracing point set is converted to an integration point set before integration is attempted and the integration point set can be retained for other pattern points and/or frequencies, if desired.

4.4 Pattern Integration

For any frequency and for a set of far-field point coordinates the aperture field is integrated to determine the gain value in each desired direction. The ray tracing procedure is independent of frequency (so long as phase is expressed in terms of relative path length in physical coordinates such as inches) and thus the same ray tracing point set or integration point set can be used over again for a different frequency. The position of the far-field observation point may be expressed in terms of antenna coordinates to produce antenna patterns or antenna contours in the conventional sense. For application to satellite missions, the far field observation points can be expressed in earth coordinates and together with the knowledge of satellite position and satellite antenna orientation, the appropriate antenna coordinates can be calculated. In this case the antenna pattern is plotted in the form of earth pattern contour maps.

The far-zone pattern is determined by integrating the aperture field distribution. The usual aperture field method integrates the amplitude and phase distribution over the aperture without regard to the direction of the rays passing through the aperture. In effect this is equivalent to assuming that the aperture distribution represents the power flow normal to the aperture plane. The aperture field is taken as being polarized parallel to the aperture plane. In the method used here the actual ray direction and the actual polarization orientation (not necessarily parallel to the aperture plane) are both used in the integration process.

4.5 Two-Point Corrected Lens Calculations

During the study a computer program was developed to compute the surface contours of a two-point-corrected lens. The method of Holt and Mayer[1] was used for calculating the surfaces.

The analytical procedure involves the tracing of rays from an offset feed position through the lens to a wave front oriented at a prescribed angle after the ray emerges from the lens. Conditions applied are constant phase along the wavefront and symmetry of the lens contour, the latter condition a consequence of the desire to have two foci symmetrically located with respect to the lens axis.

The input parameters for the program are the focal length Fo shown in Fig. 4-5 the lens diameter D, the offset angle of the beam θ and the refractive index n. An additional input parameter is C, the distance from the focal plane to the first surface of the lens measured along the lens axis.

The required feed offset is calculated from the equation

$$y_f = -\sqrt{f_o^2 \tan^2\theta + a_o^2 \sin^2\theta}$$

where $a_o = D/2$

The phase constant is

$$d_o = -y_f \cos\theta + (C - f_o)\cos\theta$$

Using the coordinate system shown in the figure, the feed is located at the point $x = x_f = -C$, $y = y_f$. Outgoing rays are calculated from the following formulas:

---

1 Holt, F. S. and Mayer, A, "A Design Procedure for Dielectric Microwave Lenses of Large Aperture Ratio and Large Scanning Angle", IRE Transactions, Antennas and Propagation, Jan. 1957, pp 25-30.

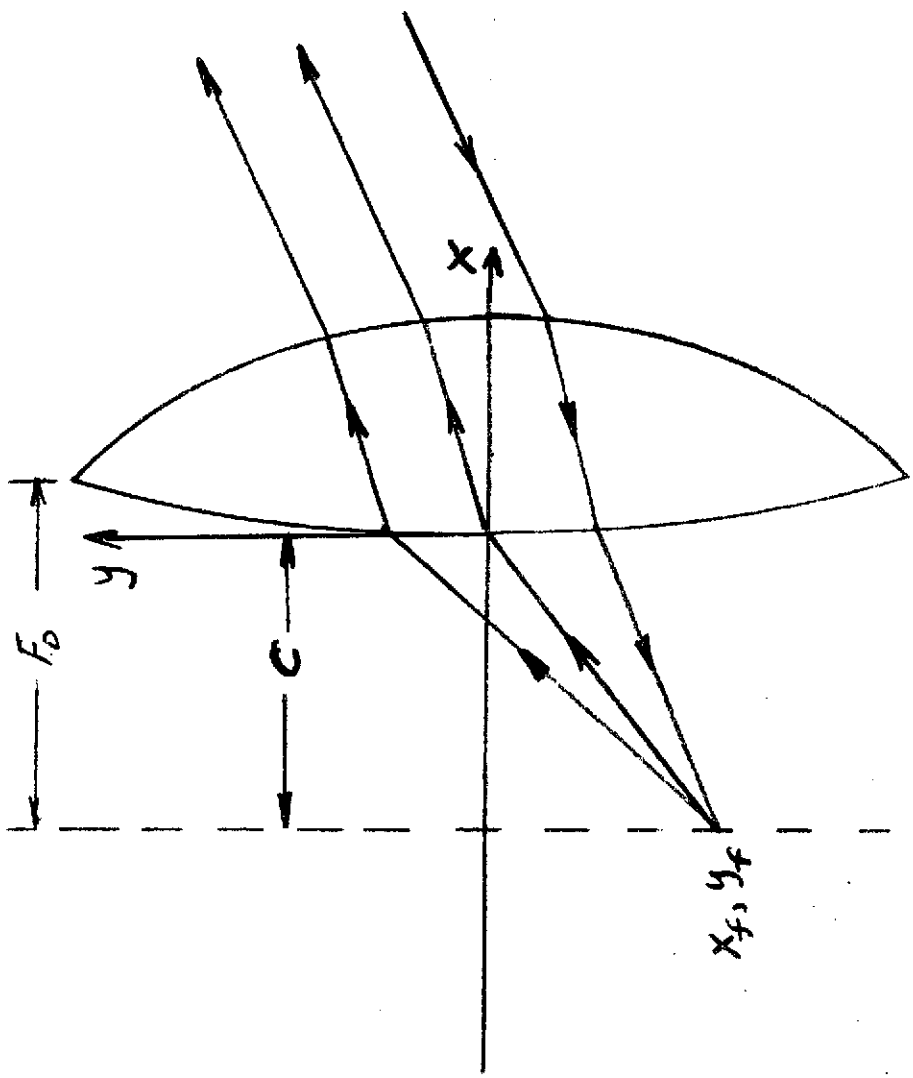

FIGURE 4-5

$$\alpha = \tan^{-1}\left(\frac{Y(I) - Y_f}{X(I) + C}\right)$$

$$\phi(I) = \sin^{-1}\left(\frac{\sin(\alpha - \psi(I))}{n}\right)$$

$$X(I+1) = X(I) + \frac{d_0 + X(I)\cos\theta + Y(I)\sin\theta - \sqrt{(X(I)-X_f)^2 + (Y(I)-Y_f)^2}}{n\sec(\psi(I)+\phi(I)) - \cos\theta - \sin\theta\tan(\psi(I)+\phi(I))}$$

$$Y(I+1) = Y(I) + (X(I+1) - X(I))\tan(\psi(I)+\phi(I))$$

$$\psi(I+1) = \tan^{-1}\frac{n\sin(\psi(I)+\phi(I)) - \sin\theta}{n\cos(\psi(I)+\phi(I)) - \cos\theta}$$

where α is the angle the ray from the feed makes with the positive x axis, $\phi(I)$ is the angle between the ray inside the lens and the normal to the first surface, X(I) and Y(I) are the coordinates of the intersection of the ray and the first surface, X(I+1) and Y(I+1) are the coordinates of the intersection of the ray with the second surface, and ψ (I+1) is the angle the normal to the second surface makes with the x axis.

The first ray is from the feed to the origin where it is known that the surface is normal to the x axis (due to symmetry). The initial point is X(1)=Y(1)= ψ(1)=0; using these values in the above equations allows us to calculate the exit point of the ray at the second surface.

By applying symmetry, we find another point below the x axis. Thus

$$\overline{X}(I+1) = X(I+1)$$
$$\overline{Y}(I+1) = -Y(I+1)$$
$$\overline{\psi}(I+1) = \psi(I+1)$$

Then a ray is traced backward through the lens to the feed using the formulas

$$\bar{\phi}(I+1) = \sin^{-1}\left(\frac{\sin(\theta - \bar{\psi}(I+1))}{\eta}\right)$$

$$\bar{X}(I+2) = \bar{X}(I+1) + \frac{-B + \sqrt{B^2 - AC}}{A}$$

$$\bar{Y}(I+2) = \bar{Y}(I+1) + (\bar{X}(I+2) - \bar{X}(I+1)) \tan(\bar{\psi}(I+1) + \bar{\phi}(I+1))$$

$$\bar{\psi}(I+2) = \tan^{-1}\left(\frac{n \sin(\bar{\psi}(I+1) + \bar{\phi}(I+1)) \sqrt{(\bar{X}(I+2) - X_f)^2 + (\bar{Y}(I+2) - Y_f)^2} - (\bar{Y}(I+2) - Y_f)}{n \cos(\bar{\psi}(I+1) + \bar{\phi}(I+1)) \sqrt{(\bar{X}(I+2) - X_f)^2 + (\bar{Y}(I+2) - Y_f)^2} - (\bar{X}(I+2) - X_f)}\right)$$

where

$$A = (n^2 - 1) \sec^2(\bar{\psi}(I+1) + \bar{\phi}(I+1))$$

$$B = n(d_o + \bar{X}(I+1)\cos\theta + \bar{Y}(I+1)\sin\theta) \sec(\bar{\psi}(I+1) + \bar{\phi}(I+1))$$
$$- (\bar{X}(I+1) - X_f)$$
$$- (\bar{Y}(I+1) - Y_f) \tan(\bar{\psi}(I+1) + \bar{\phi}(I+1))$$

$$C = (d_o + \bar{X}(I+1)\cos\theta + \bar{Y}(I+1)\sin\theta)^2$$
$$- (\bar{X}(I+1) - X_f)^2 - (\bar{Y}(I+1) - Y_f)^2$$

and where $\bar{\phi}(I+1)$ is the angle between the ray inside the lens and the normal to the second surface, $\bar{X}(I+1)$ and $\bar{Y}(I+1)$ are the coordinates of the entry point of the (incoming) ray at the second surface and $\bar{X}(I+2)$ and $\bar{Y}(I+2)$ are the coordinates of the exit point at the first surface. The angle $\bar{\psi}$ (I+2) is the angle the normal to the first surface (at the exit point) makes with the x axis.

Conditions of symmetry are applied once again to convert the resulting exit point for an incoming ray on the first surface of the lens below the axis to an entry point for the next outgoing ray about the axis. Thus

$$X(I+2) = \bar{X}(I+2)$$
$$Y(I+2) = -\bar{Y}(I+2)$$
$$\psi(I+2) = -\bar{\psi}(I+2)$$

The process of tracing rays continues, conditions of symmetry being applied each time to start the next ray.

Except for the indexing nomenclature and for the correction of several errors, the above equations are the ones derived by Holt and Mayer.

The input parameters lead to an infinite set of lens contours, each one identified with a particular value of C (with all other input parameters held constant). If the value of C chosen is too small, both surfaces of the lens bend toward the feed and presumably never meet. If the value of C chosen is too large, both lens surfaces bend away from the feed and presumably never meet. If the value of C is exactly right, the two lens surfaces meet at the point $x=F_o-C$, $y=\pm S_o$.

The program will terminate and print the last ray data calculated if, in calculating the surface in the positive y region, one of the following situations occurs:

(1) The y coordinate of ray exceeds the desired radius

(2) The outward normal of the second surface makes an angle of 90 degrees or more with respect to the positive y axis

(3) The y coordinate of the second surface becomes negative.

Condition (1) rarely, if ever, occurs. Presumably it would occur if exactly the correct C value were used. Condition (2) occurs when the C value is too large and condition (3) occurs when the C value is too small.

The parameter C is very critical as is indicated by the run sequence shown in Appendix A. After each calculation the program prints either "increase C" or "decrease C" as appropriate followed by the last valid ray calculated. Although not labelled, the data printed is the point number, x and y coordinates of first surface, ψ and ϕ at first surface followed by point number, x y and ψ of the second surface. Each line of data represents one ray.

The first run shown used a value of 62 inches for C. This resulted in 34 points (17 rays) being calculated with the lens reaching a diameter of almost 27 inches. As the C value used gets closer and closer to the correct value the first and second surface points on the last valid ray approach each other and approach the desired intersection point ($X = F_o - C$, $Y = D/2$). Also the number of rays increases although there tends to be fewer rays when C is greater than the correct value.

The critical nature of C is indicated by the fact that six significant figures are required to bring the lens within 0.1 inch of the desired radius (C=59.4943). The lens is also about .090 inch thick at the edge. Actually this is a fairly good stopping point since the lens is a valid wide angle lens out to 23.71 inches and the calculated surface can be extrapolated the remaining 0.1 inch without introducing too much error. However, we continued the calculation to determine C to 10 or eleven significant figures (C=59.494268254) to show how the C value controls the size and number of points. There is absolutely no physical significance to having a C value accurate to 10 digits and in some respects it is questionable that C has been determined to that accuracy, since the numerical accuracy of the machine is of the same order. But, since the final ray is the culmination of a long series of successive calculations, only a very particular value of C will allow these calculations to proceed to the desired result.

In adapting this program to some other type of computer, one should be aware of possible complications relating to the numerical accuracy of the machine being used. Also, one should make certain of the way that the arctangent result is expressed so that related IF statements will work properly. The arctangent function used in our runs places the arctangent result in the proper quadrant but in the range from $-\pi$ to $+\pi$.

4.6 Computer Patterns

To simulate an operational system, a two-point corrected circularly symmetric dielectric (natural or artificial) lense was designed using the analysis described above and in Appendix A. The lense has a diameter of 85 feet, an F/D ratio of 1.286, and an index of refraction of 1.414. The lense has 24 feeds, located in the focal plane of the lense such that when the lense is positioned on a synchronous orbit satellite, the resultant 23 beams cover the Continental United States, as shown in Figure 4-6. The operating frequency is 11.8 GHz.

For the calculations, the satellite is positioned at 102.5 degrees W. Longitude, and the antenna is fixed in position with its mechanical boresight aimed at 40 degrees N. Latitude and 102.5° W. Longitude. The 23 individual beams are shown in Figures 4-7 through 4-29 . For each beam, the -27 dB and -30 dB contours (relative to the beam peak) have been identified. The area within these contours represents those areas where frequency re-use within co-polarized beams would not be possible depending upon whether the required beam-to-beam isolation is 27 dB or 30 dB.

The value of this computer simulation is that it will allow the complete system to be theoretically designed prior to the initiation of hardware fabrication. By varying satellite position, antenna aim point, and individual beam aim points, a system which allows the maximum amount of co-polarized beam-to-beam isolation, and therefore to optimize the re-use of frequency, can be designed to reduce the risks in building and flying an operational system.

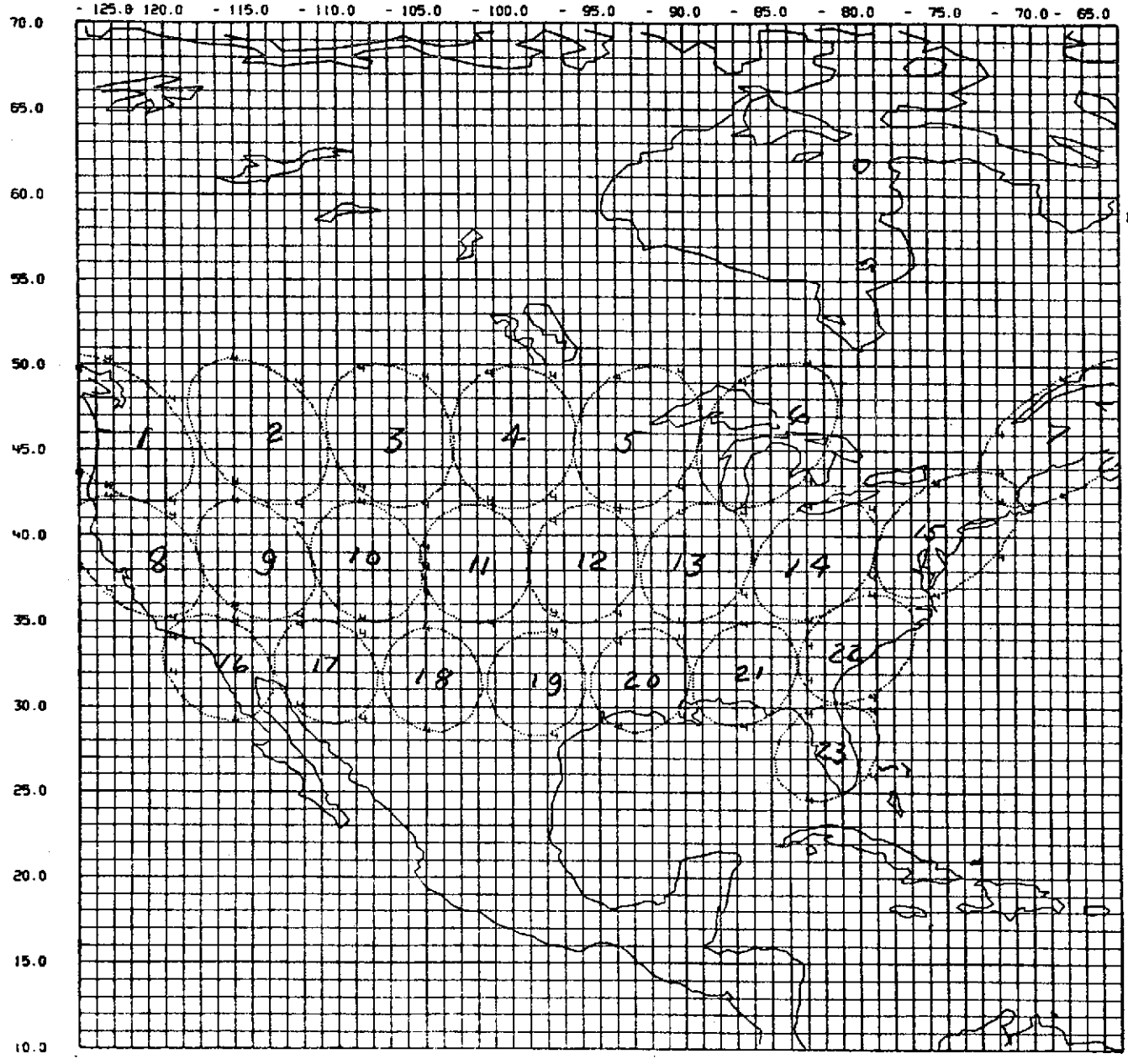

XMIN	XMAX	YMIN	YMAX
-125.0000	-65.0000	10.0000	70.0000
XBIGD	SLAMB	SDEL	SIGMA
~~85.0000~~ 96.00	1.0000	.0000	.0000
XPHI	AMU	BDNS	BDEW
-100.0000	.0000	.0000	.0000
ALTS	A3		
19323.0000	.0000		
CONTOUR VALUES			
-4.0000			
BLONG	BLAT		
-122.8000	46.0000		
-114.5000	45.8000		
-107.0000	45.6000		
-100.0000	45.5000		
-92.9000	45.5000		
-85.5000	45.7000		
-68.0000	46.0000		
-121.5000	38.6000		
-114.8000	38.4000		
-108.4000	38.3000		
-102.2000	38.2000		
-96.0000	38.2000		
-89.5000	38.3000		
-82.7000	38.5000		
-75.3000	40.0000		
-117.0000	32.2000		
-110.8000	32.0000		
-104.7000	31.5000		
-98.7000	31.3000		
-92.7000	31.5000		
-86.7000	31.9000		
-80.3000	33.4000		
-82.0000	27.4000		

D/λ corrected
= 1.13 × 85 = 96

FIG.4-6 -4 dB CONTOURS, 23 BEAM CASE

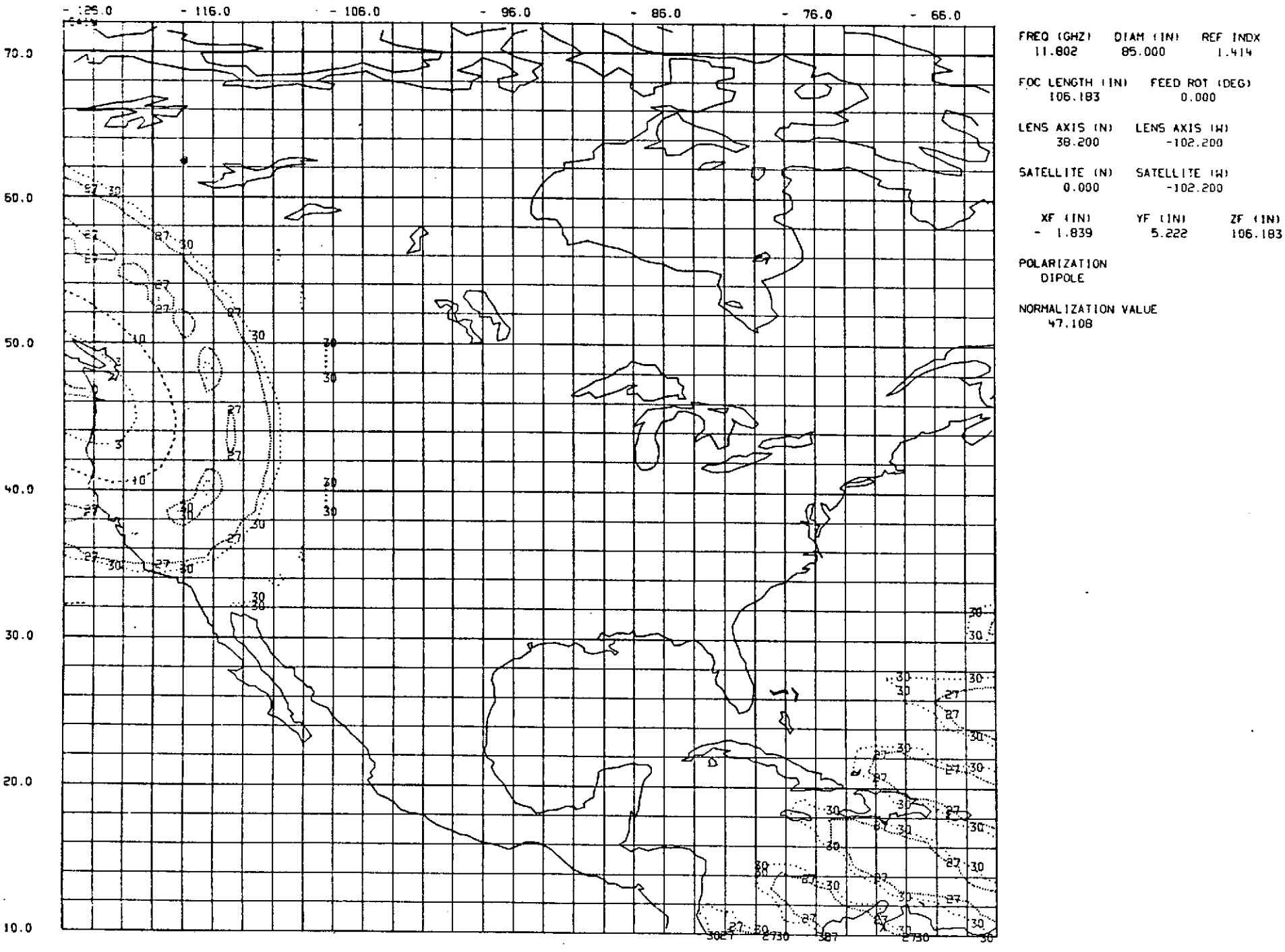
- 126.0
- 116.0
- 106.0
- 96.0
- 86.0
- 76.0
- 66.0
70.0
60.0
50.0
40.0
30.0
20.0
10.0
FREQ (GHZ)
11.802
DIAM (IN)
85.000
REF INDX
1.414
FOC LENGTH (IN)
106.183
FEED ROT (DEG)
0.000
LENS AXIS (N)
38.200
LENS AXIS (W)
-102.200
SATELLITE (N)
0.000
SATELLITE (W)
-102.200
XF (IN)
- 1.839
YF (IN)
5.222
ZF (IN)
106.183
POLARIZATION
DIPOLE
NORMALIZATION VALUE
47.108

Figure 4-7

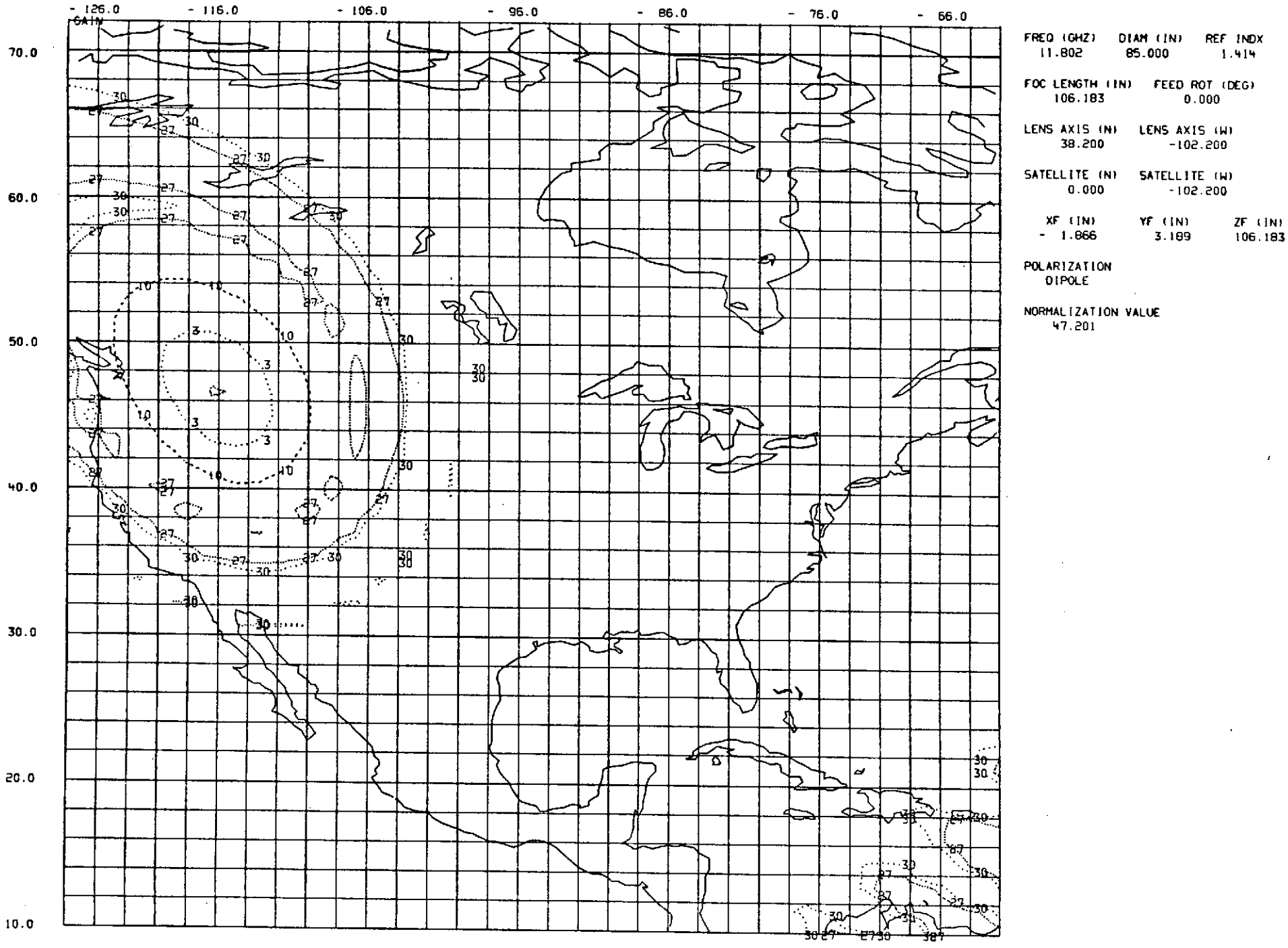
- 126.0
- 116.0
- 106.0
- 96.0
- 86.0
- 76.0
- 66.0
GAIN
70.0
60.0
50.0
40.0
30.0
20.0
10.0
FREQ (GHZ) 11.802
DIAM (IN) 85.000
REF INDX 1.414
FOC LENGTH (IN) 106.183
FEED ROT (DEG) 0.000
LENS AXIS (N) 38.200
LENS AXIS (W) -102.200
SATELLITE (N) 0.000
SATELLITE (W) -102.200
XF (IN) - 1.866
YF (IN) 3.189
ZF (IN) 106.183
POLARIZATION
DIPOLE
NORMALIZATION VALUE
47.201

Figure 4-8

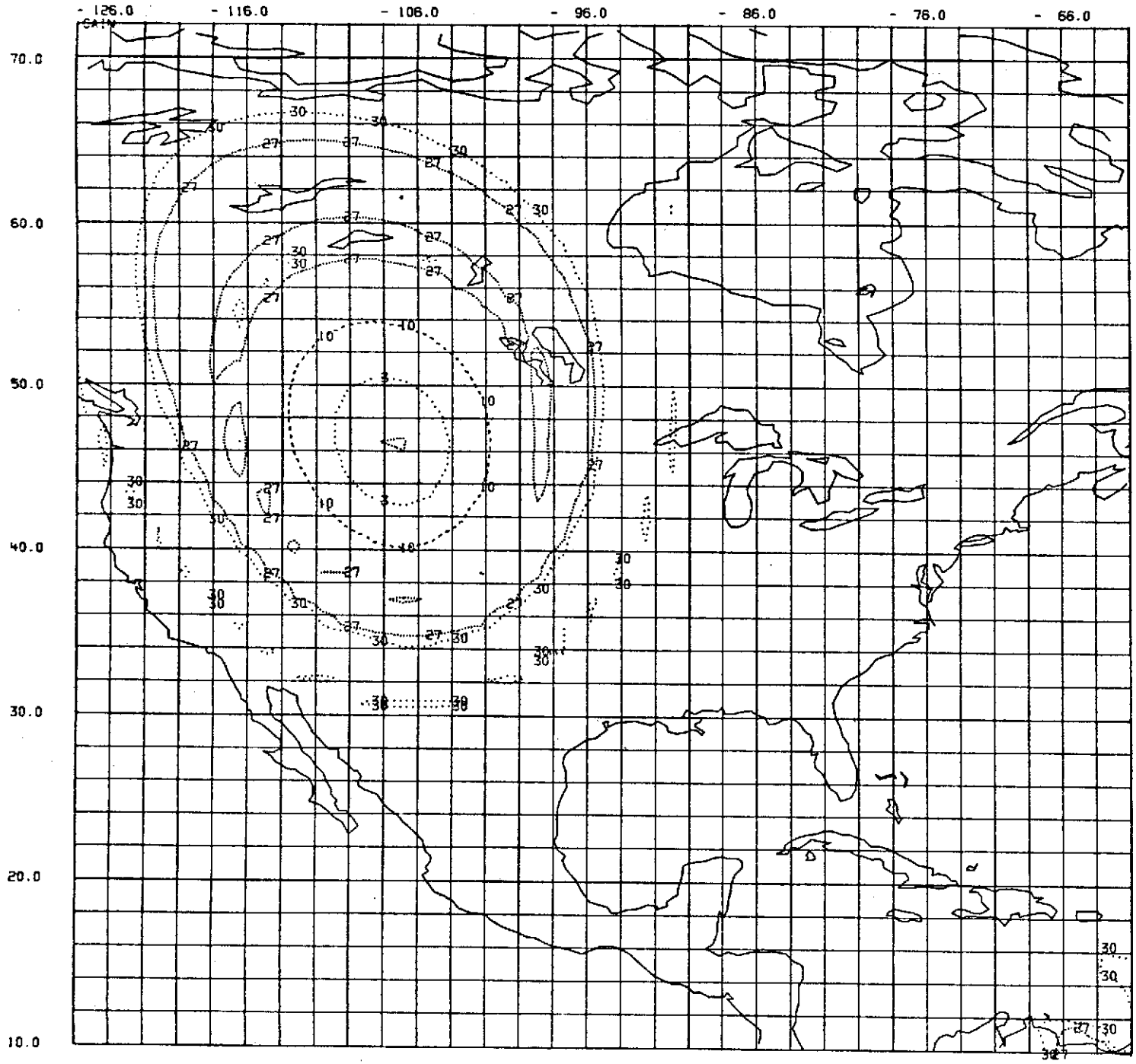

FREQ (GHZ)	DIAM (IN)	REF INDX
11.802	85.000	1.414

FOC LENGTH (IN)	FEED ROT (DEG)
106.183	0.000

LENS AXIS (N)	LENS AXIS (W)
38.200	-102.200

SATELLITE (N)	SATELLITE (W)
0.000	-102.200

XF (IN)	YF (IN)	ZF (IN)
- 1.856	1.260	106.183

POLARIZATION
DIPOLE

NORMALIZATION VALUE
47.198

Figure 4-9

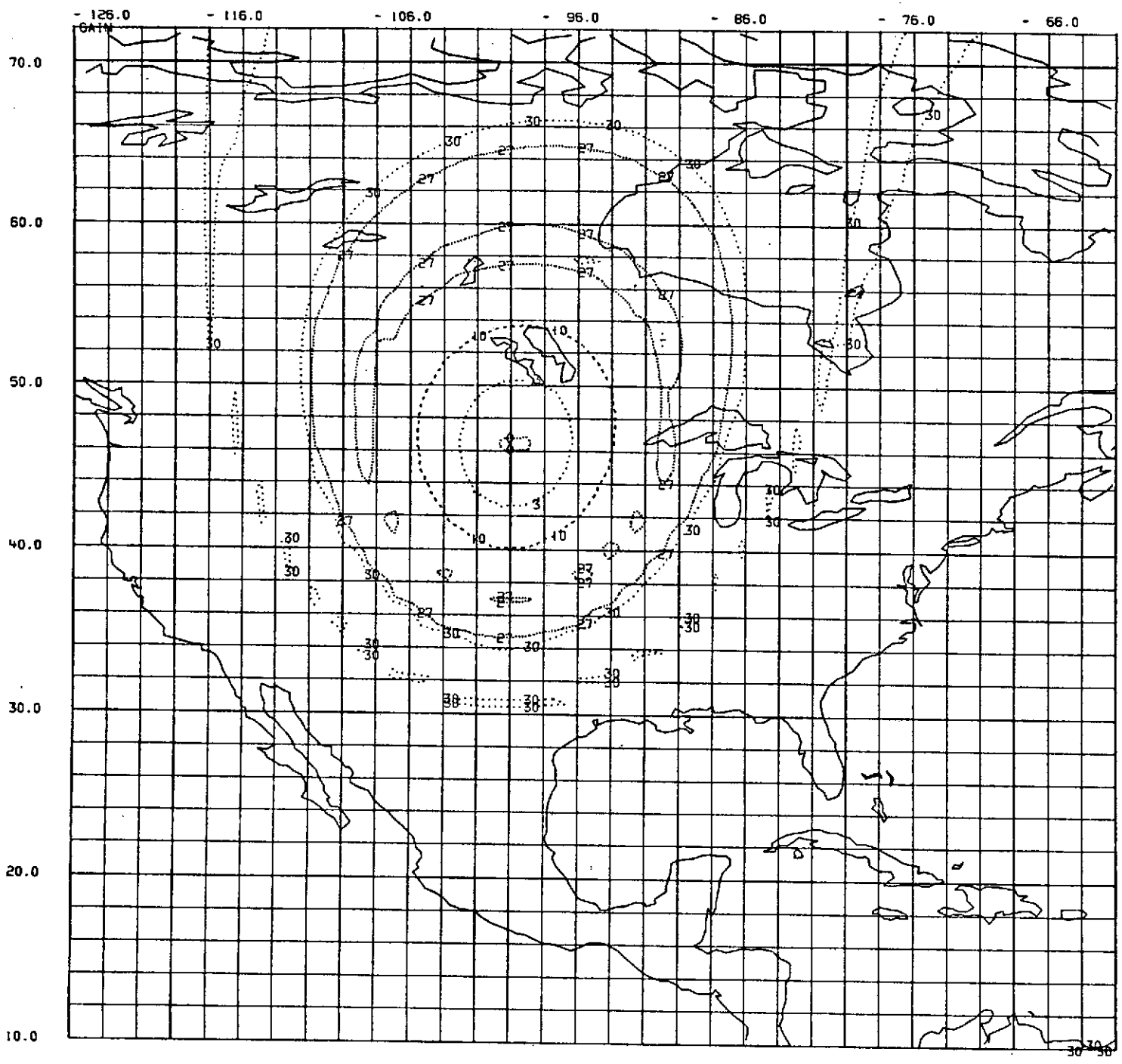

FREQ (GHZ)	DIAM (IN)	REF INDX
11.802	85.000	1.414

FOC LENGTH (IN)	FEED ROT (DEG)
106.183	0.000

LENS AXIS (N)	LENS AXIS (W)
38.200	-102.200

SATELLITE (N)	SATELLITE (W)
0.000	-102.200

XF (IN)	YF (IN)	ZF (IN)
- 1.838	- 0.579	106.183

POLARIZATION
DIPOLE

NORMALIZATION VALUE
47.147

Figure 4-10

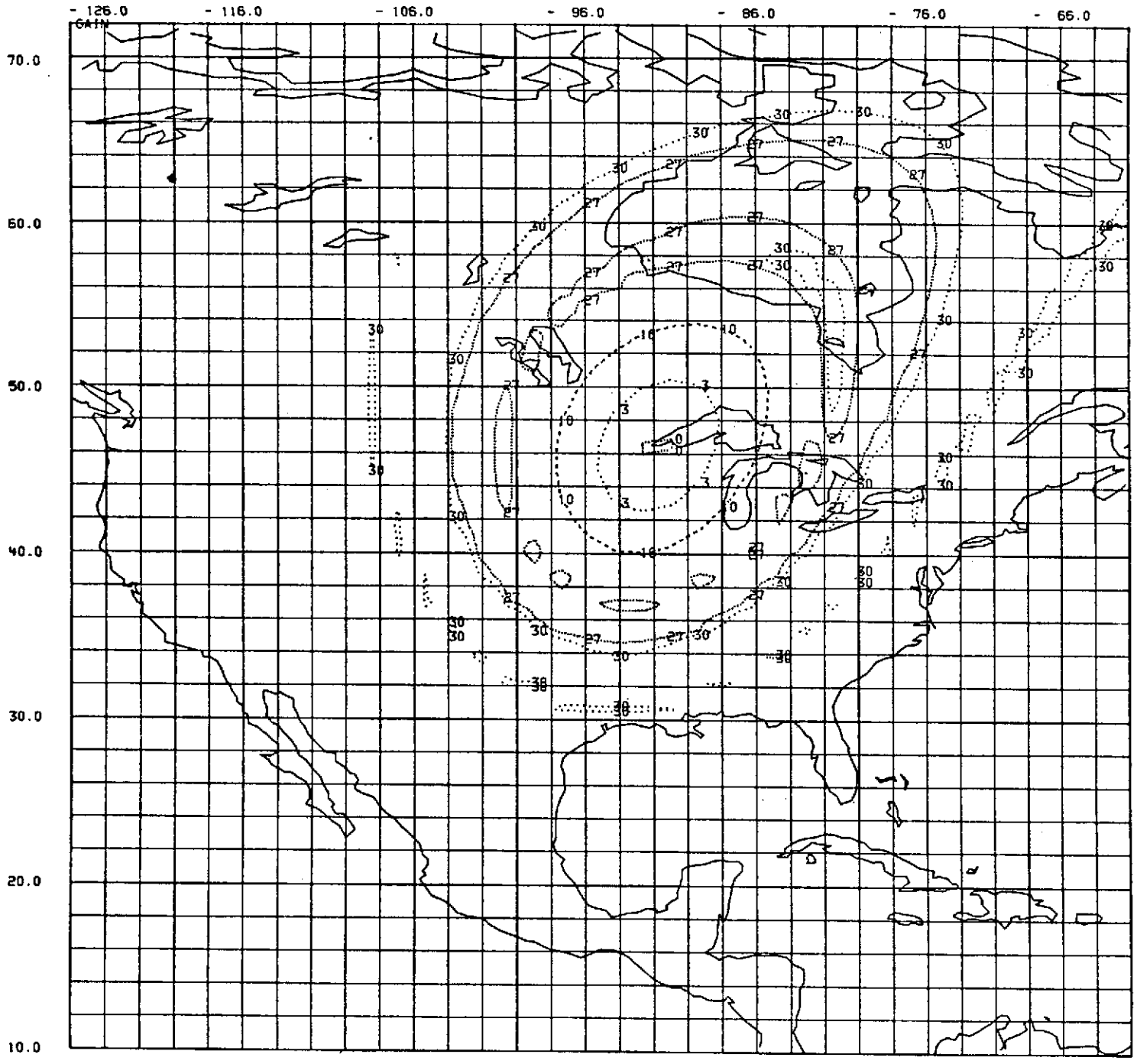

FREQ (GHZ) 11.802 | DIAM (IN) 85.000 | REF INDX 1.414

FOC LENGTH (IN) 106.183 | FEED ROT (DEG) 0.000

LENS AXIS (N) 38.200 | LENS AXIS (W) -102.200

SATELLITE (N) 0.000 | SATELLITE (W) -102.200

XF (IN) - 1.815 | YF (IN) - 2.437 | ZF (IN) 106.183

POLARIZATION
DIPOLE

NORMALIZATION VALUE
47.138

Figure 4-11

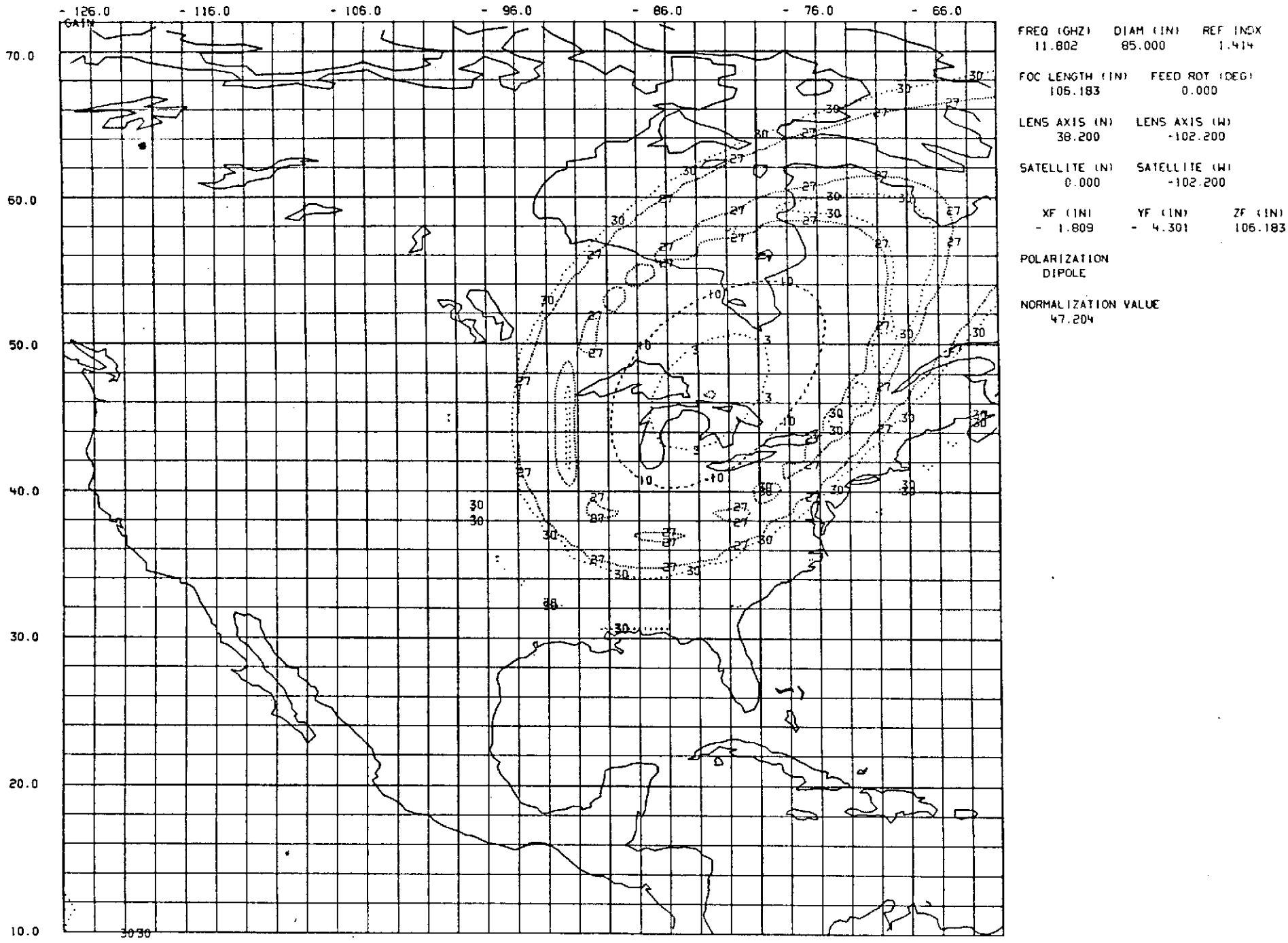
- 126.0
- 116.0
- 106.0
- 96.0
- 86.0
- 76.0
- 66.0
GAIN
70.0
60.0
50.0
40.0
30.0
20.0
10.0
FREQ (GHZ)
11.802
DIAM (IN)
85.000
REF INDX
1.414
FOC LENGTH (IN)
106.183
FEED ROT (DEG)
0.000
LENS AXIS (N)
38.200
LENS AXIS (W)
-102.200
SATELLITE (N)
0.000
SATELLITE (W)
-102.200
XF (IN)
- 1.809
YF (IN)
- 4.301
ZF (IN)
106.183
POLARIZATION
DIPOLE
NORMALIZATION VALUE
47.204

Figure 4-12

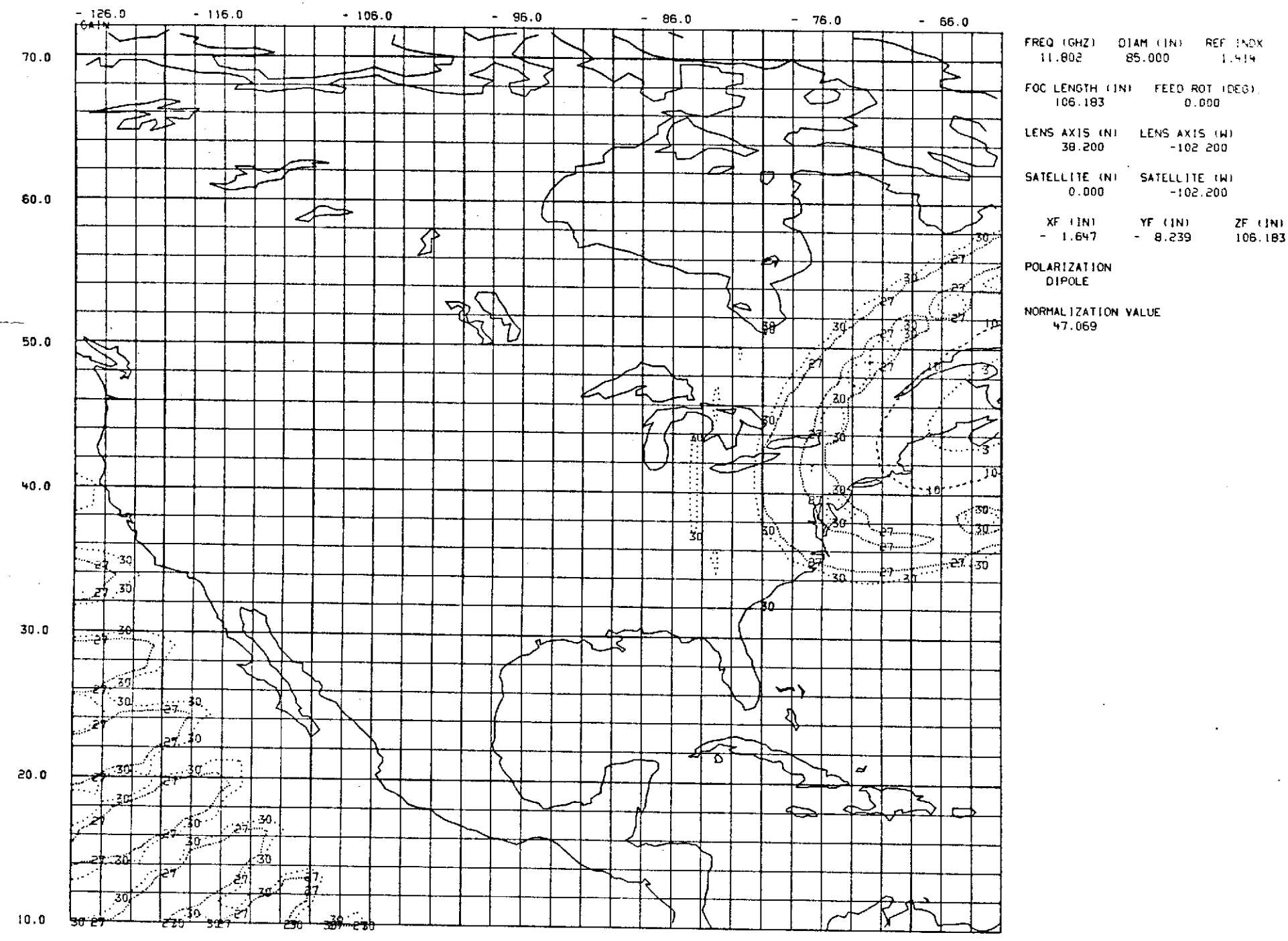
- 126.0
- 116.0
- 106.0
- 96.0
- 86.0
- 76.0
- 66.0
GAIN
70.0
60.0
50.0
40.0
30.0
20.0
10.0
FREQ (GHZ) 11.802
DIAM (IN) 85.000
REF INDX 1.414
FOC LENGTH (IN) 106.183
FEED ROT (DEG) 0.000
LENS AXIS (N) 38.200
LENS AXIS (W) -102.200
SATELLITE (N) 0.000
SATELLITE (W) -102.200
XF (IN) - 1.647
YF (IN) - 8.239
ZF (IN) 106.183
POLARIZATION
DIPOLE
NORMALIZATION VALUE
47.069

Figure 4-13

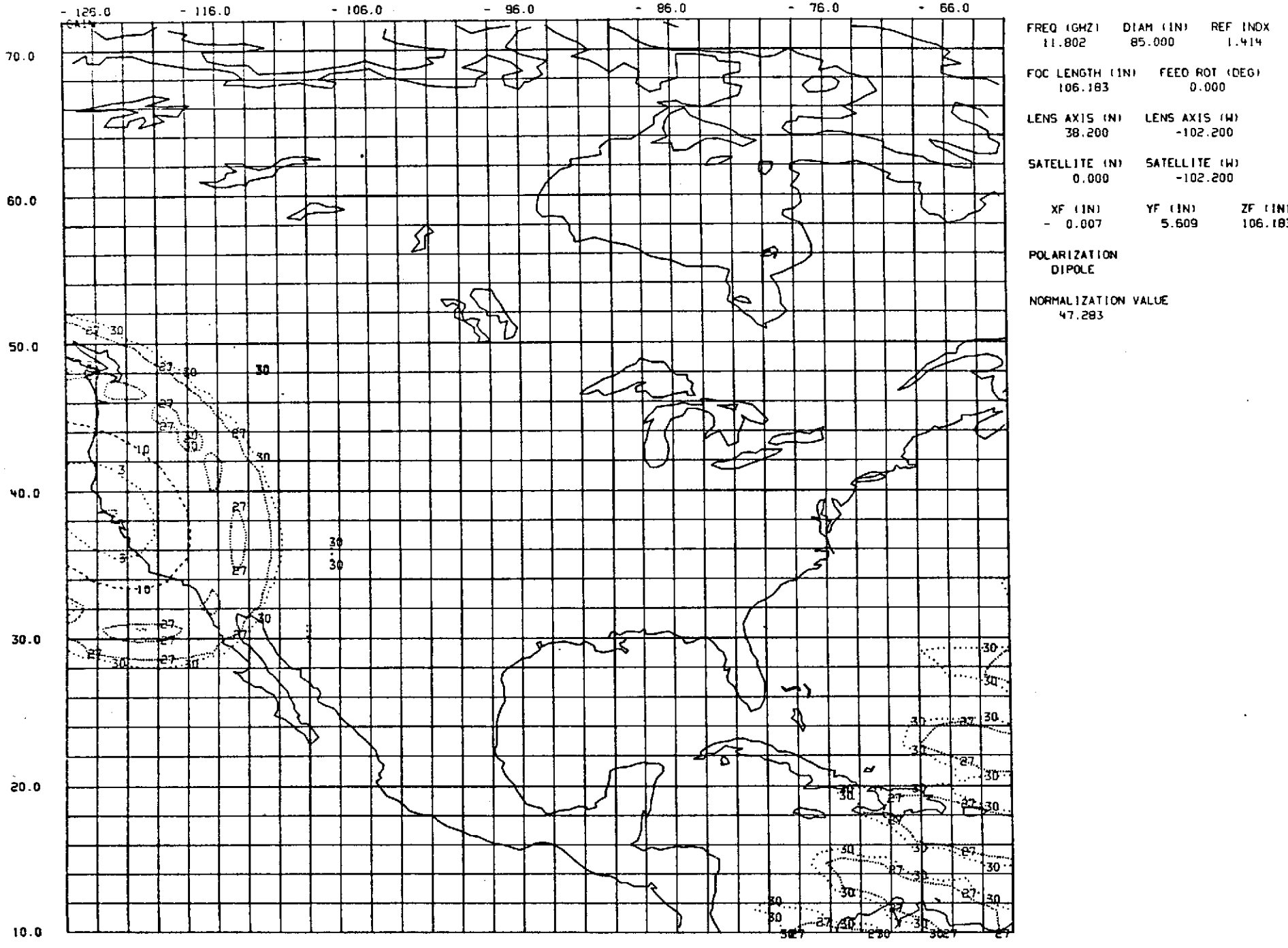
- 126.0
- 116.0
- 106.0
- 96.0
- 86.0
- 76.0
- 66.0
70.0
60.0
50.0
40.0
30.0
20.0
10.0
FREQ (GHZ) 11.802
DIAM (IN) 85.000
REF INDX 1.414
FOC LENGTH (IN) 106.183
FEED ROT (DEG) 0.000
LENS AXIS (N) 38.200
LENS AXIS (W) -102.200
SATELLITE (N) 0.000
SATELLITE (W) -102.200
XF (IN) - 0.007
YF (IN) 5.609
ZF (IN) 106.183
POLARIZATION
DIPOLE
NORMALIZATION VALUE
47.283

Figure 4-14

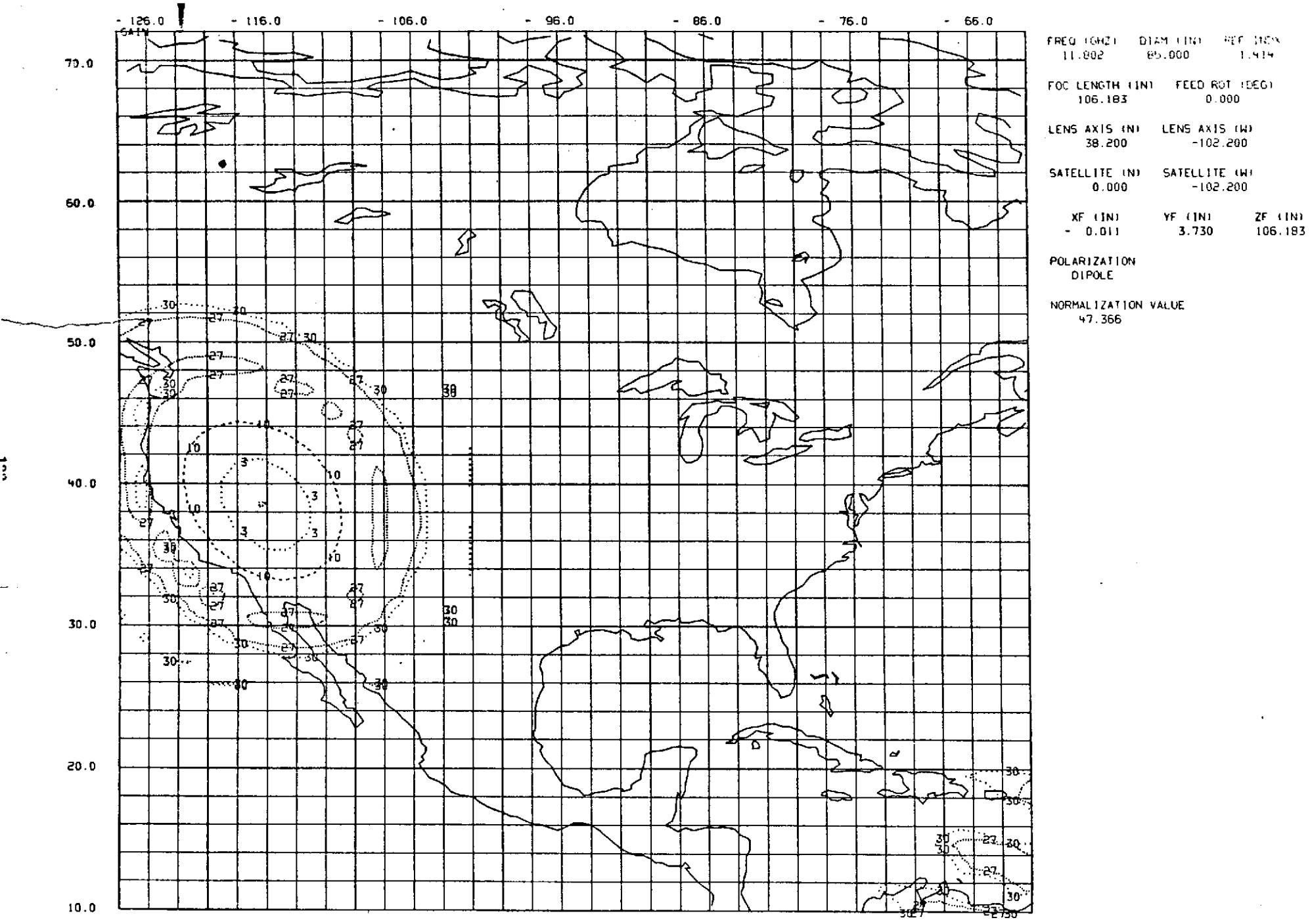
- 126.0
- 116.0
- 106.0
- 96.0
- 86.0
- 76.0
- 66.0
70.0
60.0
50.0
40.0
30.0
20.0
10.0
FREQ (GHZ)
11.802
DIAM (IN)
85.000
REF INDX
1.414
FOC LENGTH (IN)
106.183
FEED ROT (DEG)
0.000
LENS AXIS (N)
38.200
LENS AXIS (W)
-102.200
SATELLITE (N)
0.000
SATELLITE (W)
-102.200
XF (IN)
- 0.011
YF (IN)
3.730
ZF (IN)
106.183
POLARIZATION
DIPOLE
NORMALIZATION VALUE
47.366

Figure 4-15

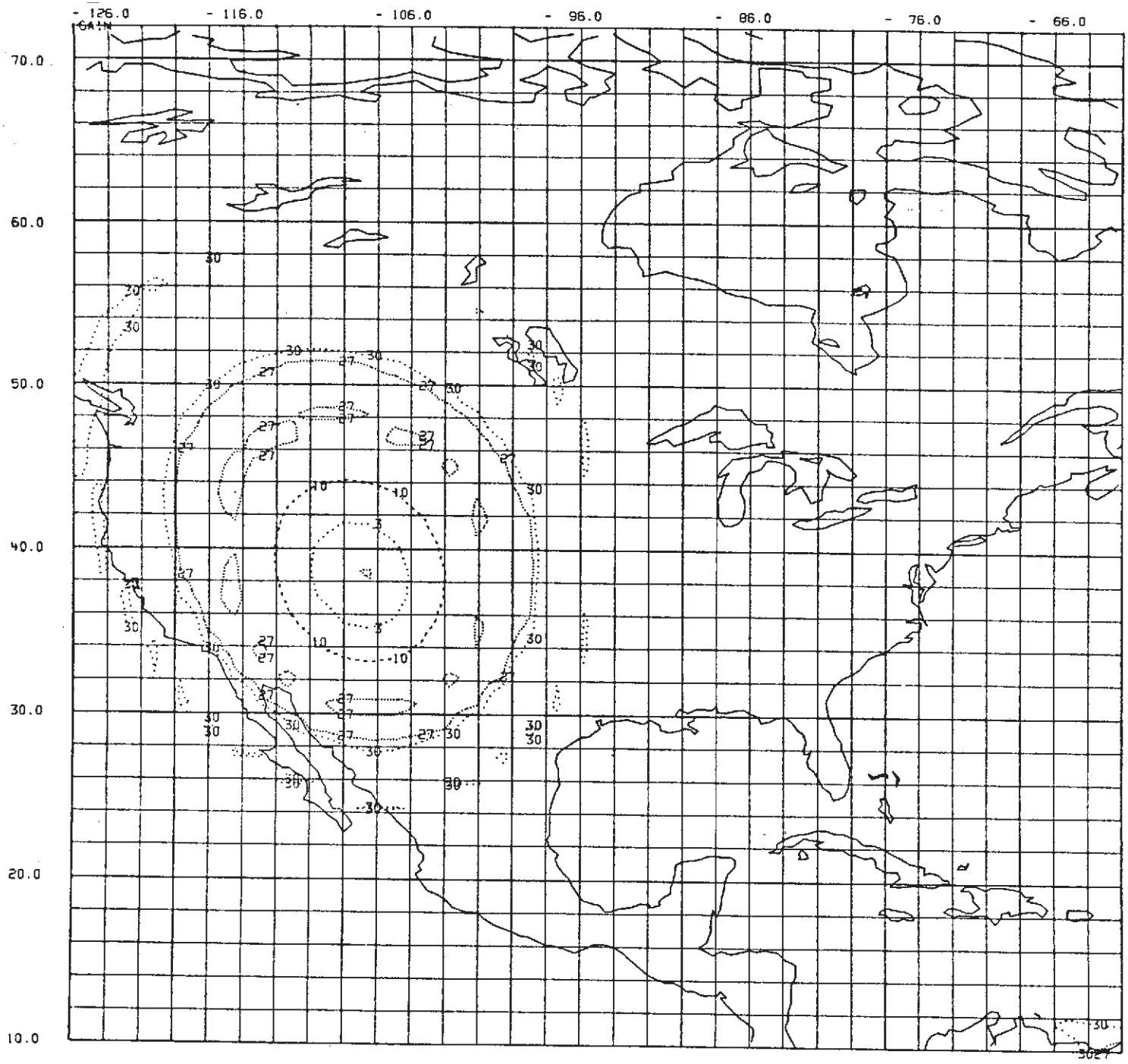

FREQ (GHZ) 11.802
DIAM (IN) 85.000
REF INDX 1.414

FOC LENGTH (IN) 106.183
FEED ROT (DEG) 0.000

LENS AXIS (N) 38.200
LENS AXIS (W) -102.200

SATELLITE (N) 0.000
SATELLITE (W) -102.200

XF (IN) - 0.016
YF (IN) 1.854
ZF (IN) 106.183

POLARIZATION
DIPOLE

NORMALIZATION VALUE
47.343

Figure 4-16

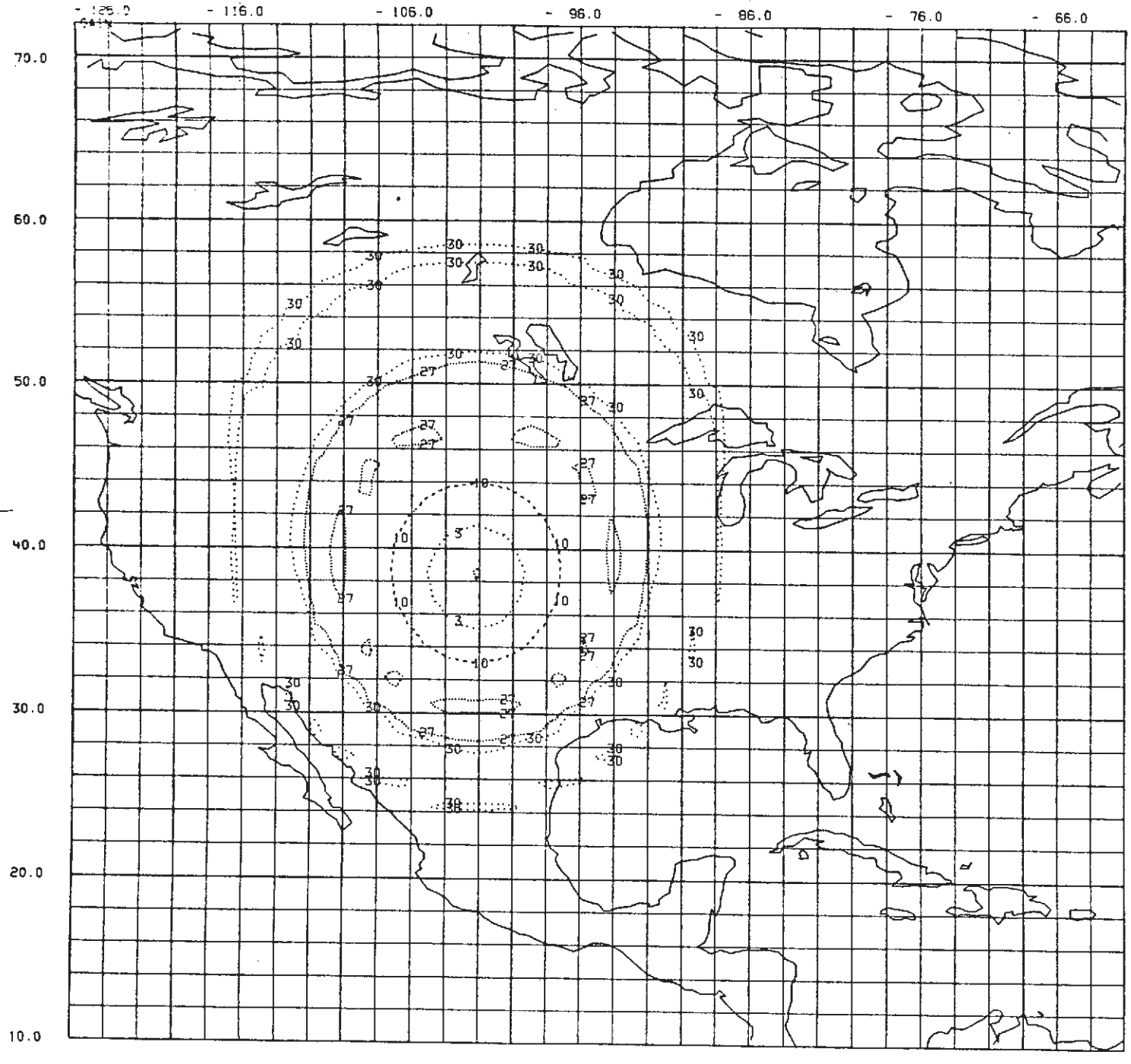
- 126.0
- 116.0
- 106.0
- 96.0
- 86.0
- 76.0
- 66.0
70.0
60.0
50.0
40.0
30.0
20.0
10.0
FREQ (GHZ) 11.802
DIAM (IN) 85.000
REF INDX 1.414
FOC LENGTH (IN) 106.183
FEED ROT (DEG) 0.000
LENS AXIS (N) 38.200
LENS AXIS (W) -102.200
SATELLITE (N) 0.000
SATELLITE (W) -102.200
XF (IN) 0.000
YF (IN) 0.000
ZF (IN) 106.183
POLARIZATION
DIPOLE
NORMALIZATION VALUE
47.598

Figure 4-17

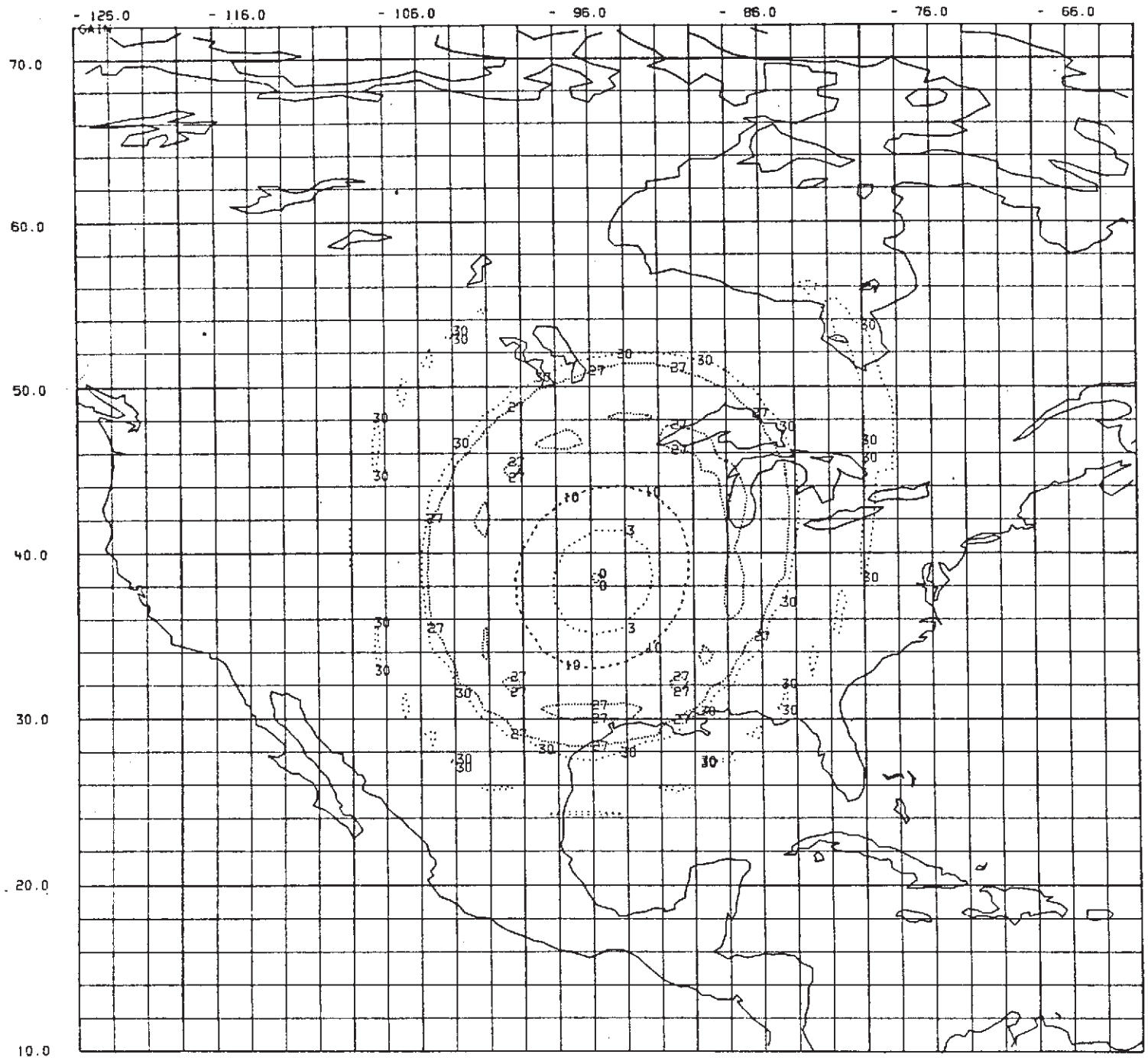

FREQ (GHZ)	DIAM (IN)	REF INDX
11.802	85.000	1.414

FOC LENGTH (IN)	FEED ROT (DEG)
106.183	0.000

LENS AXIS (N)	LENS AXIS (W)
38.200	-102.200

SATELLITE (N)	SATELLITE (W)
0.000	-102.200

XF (IN)	YF (IN)	ZF (IN)
0.010	- 1.857	106.183

POLARIZATION
DIPOLE

NORMALIZATION VALUE
47.346

Figur 4-19

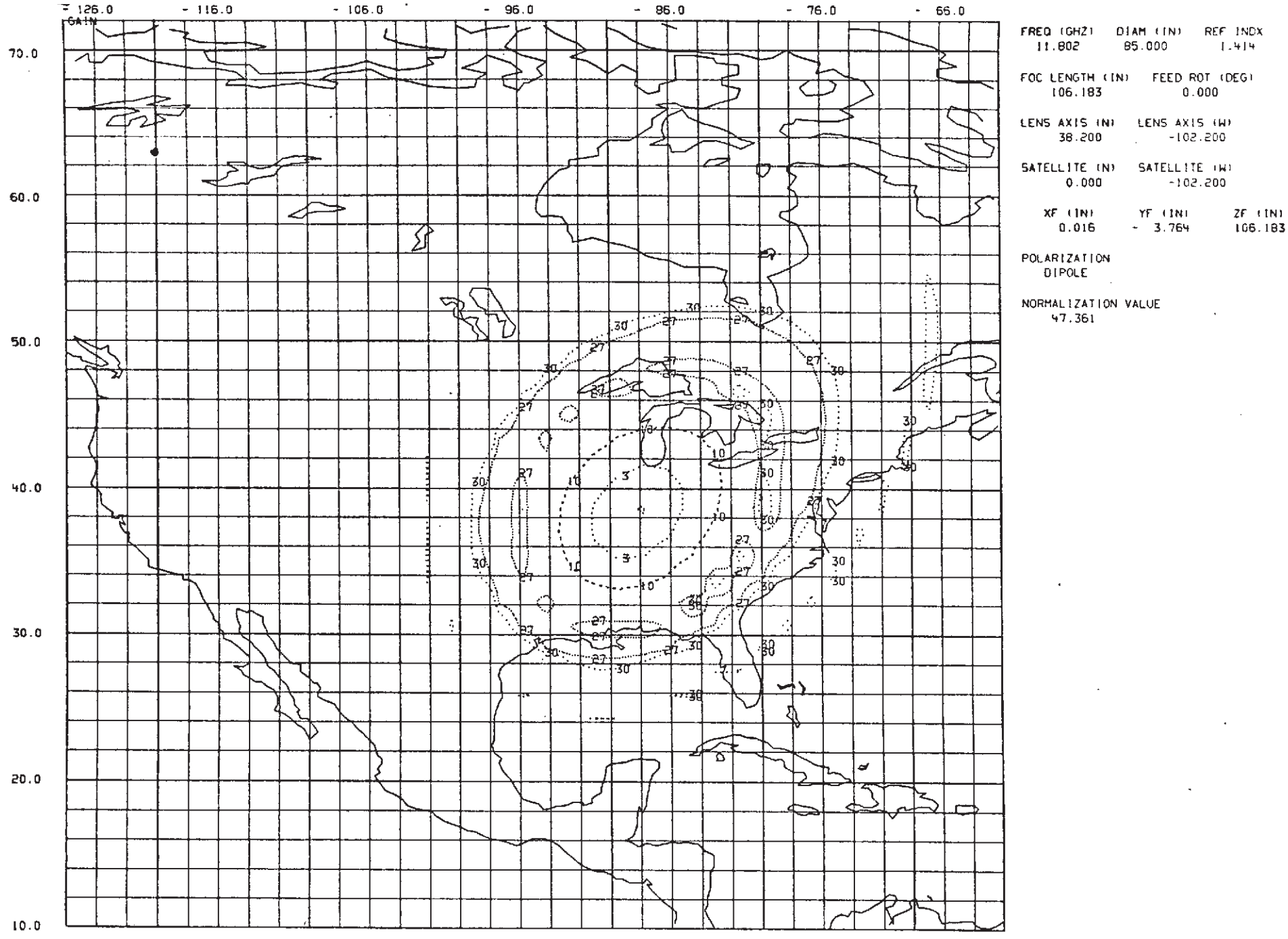
- 126.0
- 116.0
- 106.0
- 96.0
- 86.0
- 76.0
- 66.0
GAIN
70.0
60.0
50.0
40.0
30.0
20.0
10.0
FREQ (GHZ) 11.802
DIAM (IN) 85.000
REF INDX 1.414
FOC LENGTH (IN) 106.183
FEED ROT (DEG) 0.000
LENS AXIS (N) 38.200
LENS AXIS (W) -102.200
SATELLITE (N) 0.000
SATELLITE (W) -102.200
XF (IN) 0.016
YF (IN) - 3.764
ZF (IN) 106.183
POLARIZATION
DIPOLE
NORMALIZATION VALUE
47.361

Figure 4-19

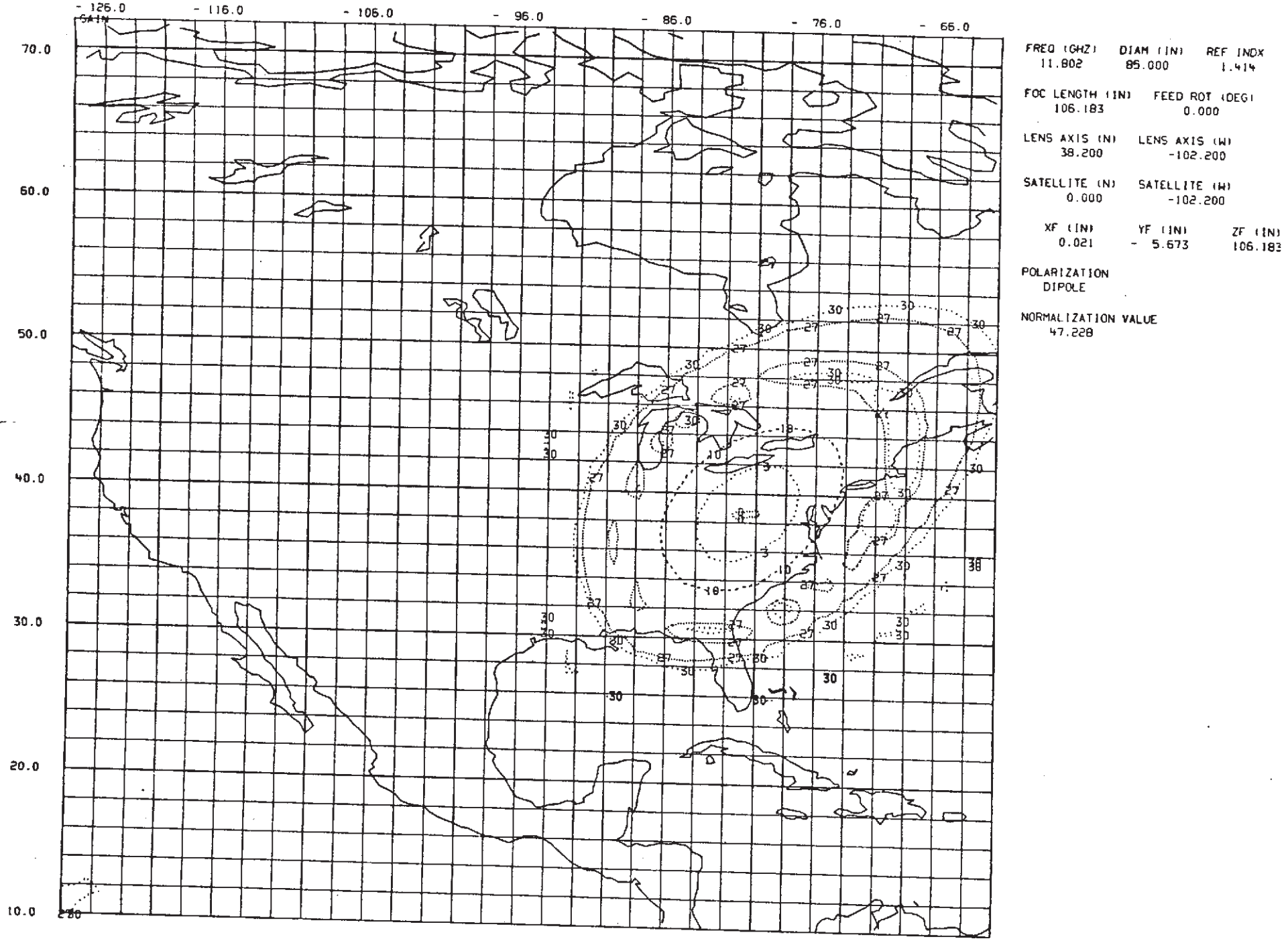
- 126.0
- 116.0
- 106.0
- 96.0
- 86.0
- 76.0
- 66.0
70.0
60.0
50.0
40.0
30.0
20.0
10.0
FREQ (GHZ)
11.802
DIAM (IN)
85.000
REF INDX
1.414
FOC LENGTH (IN)
106.183
FEED ROT (DEG)
0.000
LENS AXIS (N)
38.200
LENS AXIS (W)
-102.200
SATELLITE (N)
0.000
SATELLITE (W)
-102.200
XF (IN)
0.021
YF (IN)
- 5.673
ZF (IN)
106.183
POLARIZATION
DIPOLE
NORMALIZATION VALUE
47.228

Figure 4-20

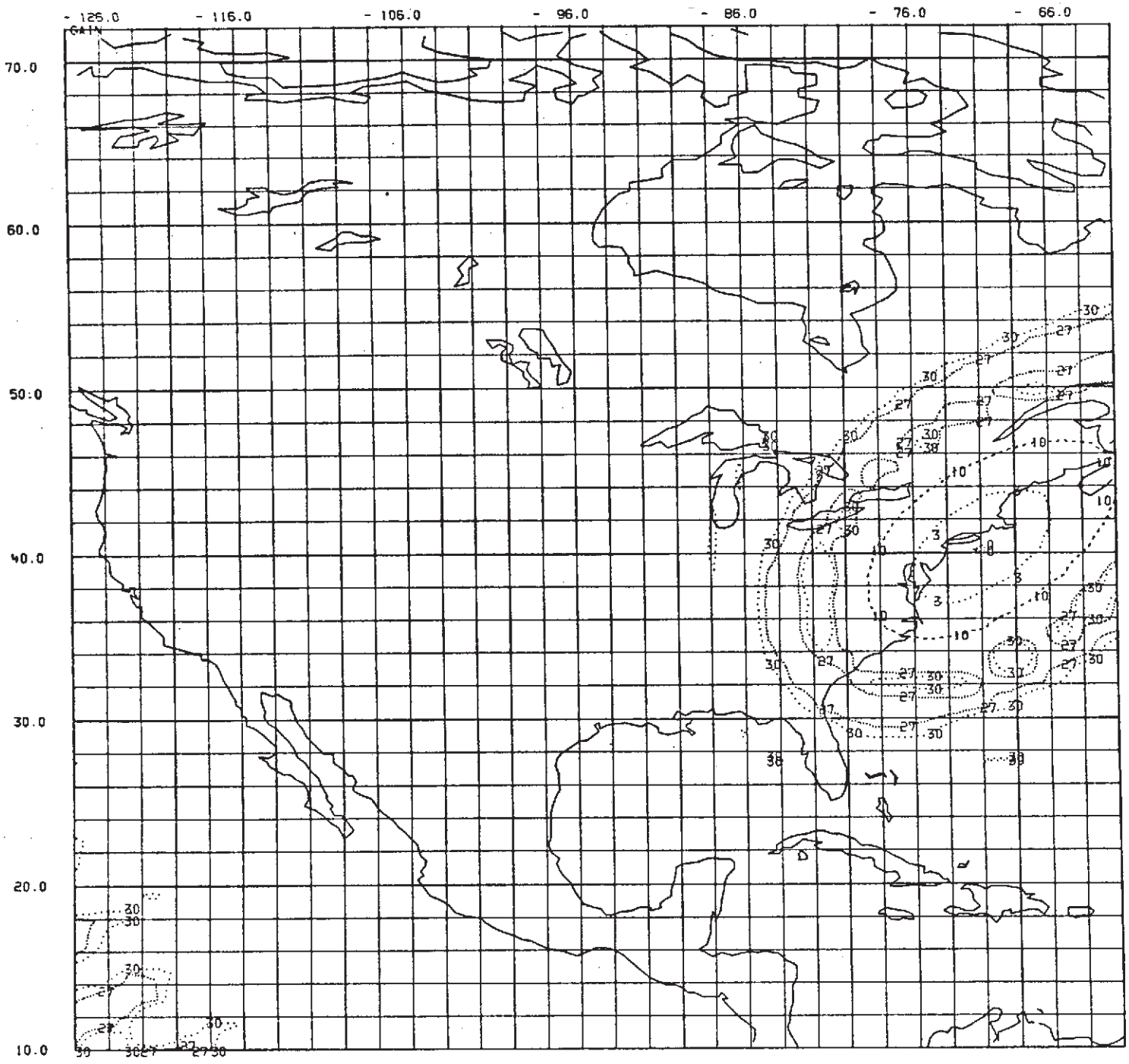

FREQ (GHZ) 11.802
DIAM (IN) 85.000
REF INDX 1.414

FOC LENGTH (IN) 106.183
FEED ROT (DEG) 0.000

LENS AXIS (N) 38.200
LENS AXIS (W) -102.200

SATELLITE (N) 0.000
SATELLITE (W) -102.200

XF (IN) - 0.288
YF (IN) - 7.456
ZF (IN) 106.183

POLARIZATION
DIPOLE

NORMALIZATION VALUE
47.372

Figure 4-21

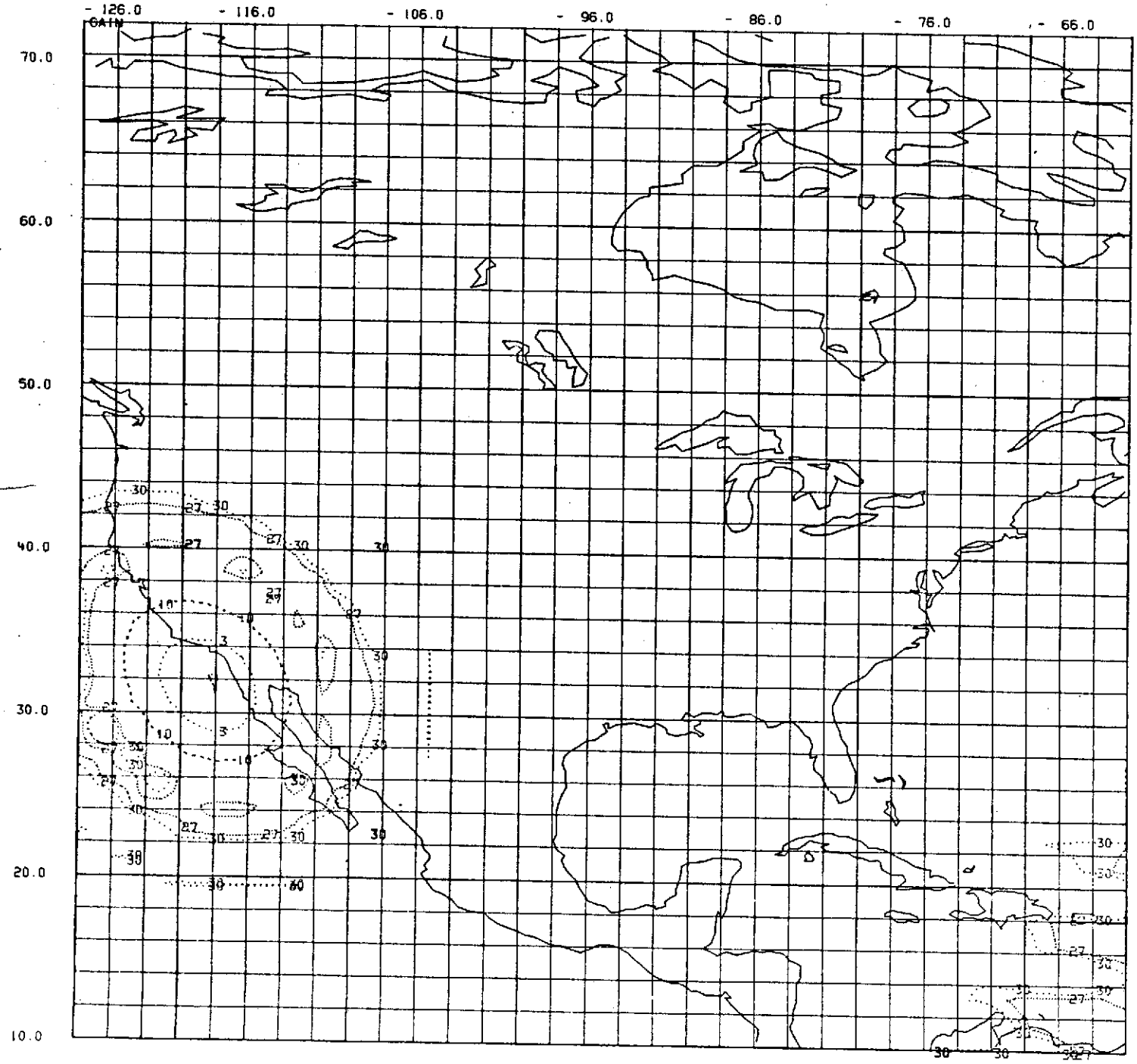

FREQ (GHZ) 11.802
DIAM (IN) 85.000
REF INDX 1.414

FOC LENGTH (IN) 106.183
FEED ROT (DEG) 0.000

LENS AXIS (N) 38.200
LENS AXIS (W) -102.200

SATELLITE (N) 0.000
SATELLITE (W) -102.200

XF (IN) 1.800
YF (IN) 4.766
ZF (IN) 106.183

POLARIZATION
DIPOLE

NORMALIZATION VALUE
47.327

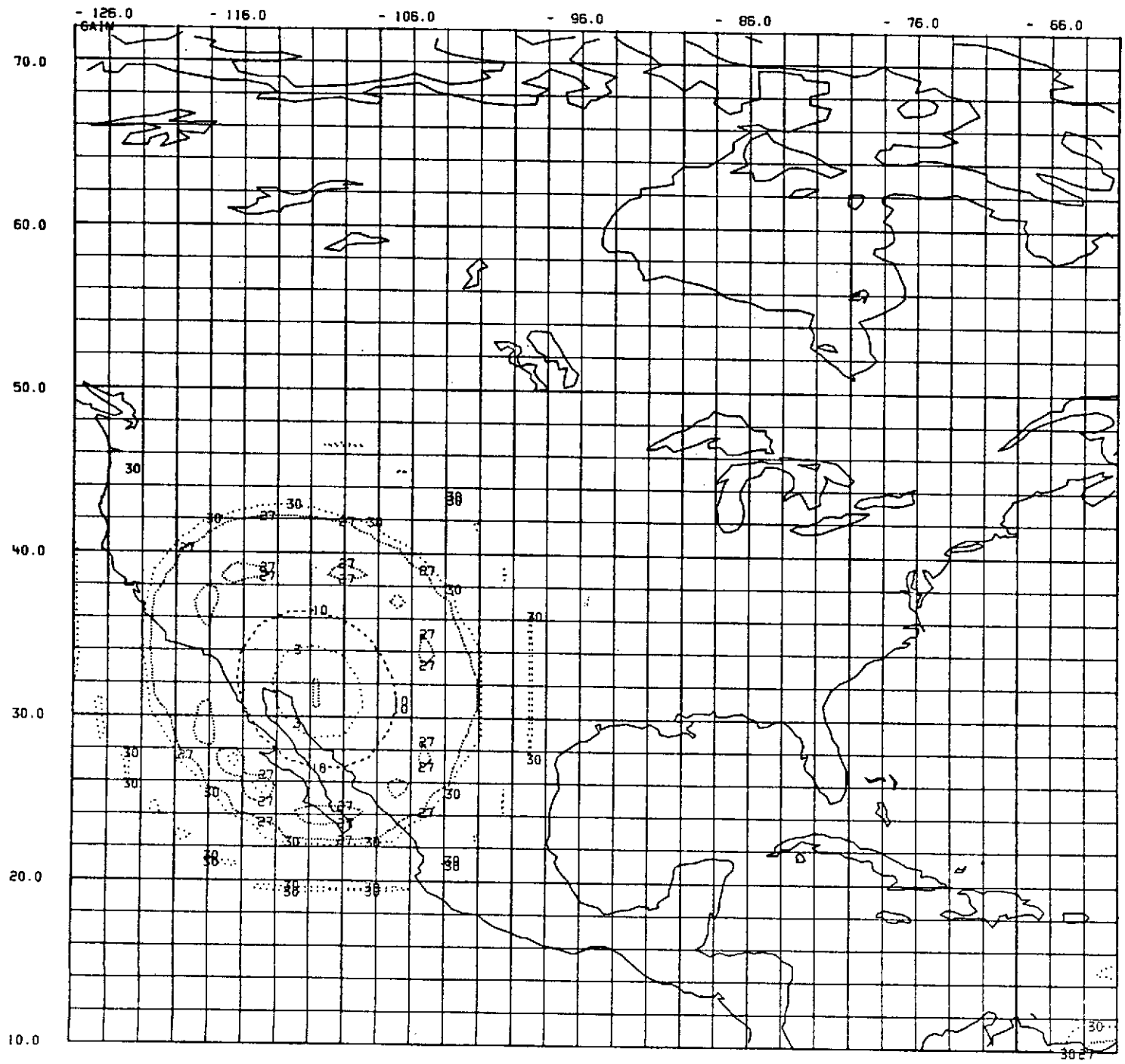

FREQ (GHZ)	DIAM (IN)	REF INDX
11.802	85.000	1.414

FOC LENGTH (IN)	FEED ROT (DEG)
106.183	0.000

LENS AXIS (N)	LENS AXIS (W)
38.200	-102.200

SATELLITE (N)	SATELLITE (W)
0.000	-102.200

XF (IN)	YF (IN)	ZF (IN)
1.824	2.806	106.183

POLARIZATION
DIPOLE

NORMALIZATION VALUE
47.327

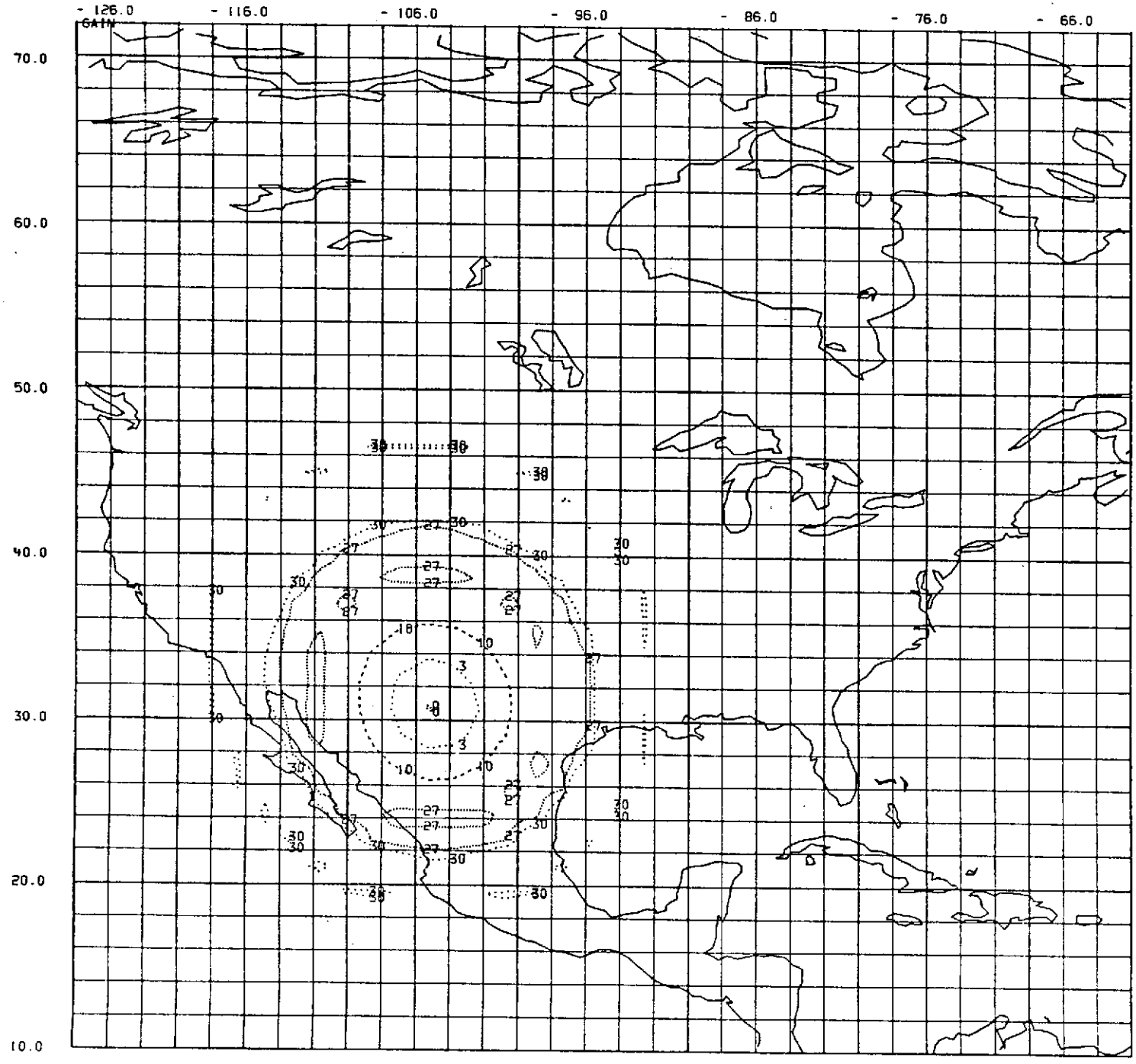

FREQ (GHZ)	DIAM (IN)	REF INDX
11.802	85.000	1.414

FOC LENGTH (IN)	FEED ROT (DEG)
106.183	0.000

LENS AXIS (N)	LENS AXIS (W)
38.200	-102.200

SATELLITE (N)	SATELLITE (W)
0.000	-102.200

XF (IN)	YF (IN)	ZF (IN)
1.961	0.825	106.183

POLARIZATION
DIPOLE

NORMALIZATION VALUE
47.498

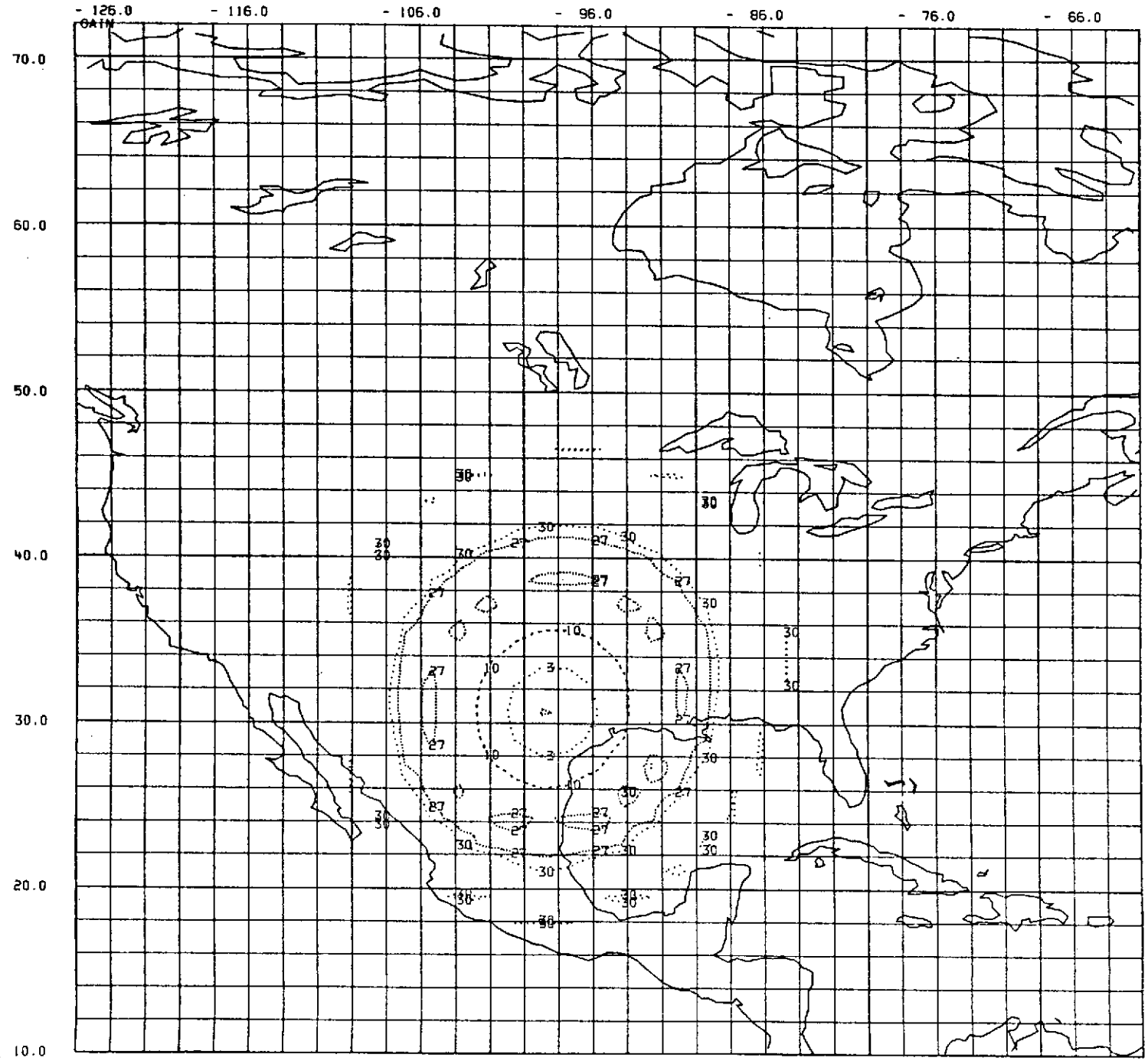

FREQ (GHZ)	DIAM (IN)	REF INDX
11.802	85.000	1.414

FOC LENGTH (IN)	FEED ROT (DEG)
106.183	0.000

LENS AXIS (N)	LENS AXIS (W)
38.200	-102.200

SATELLITE (N)	SATELLITE (W)
0.000	-102.200

XF (IN)	YF (IN)	ZF (IN)
2.025	- 1.157	106.183

POLARIZATION
DIPOLE

NORMALIZATION VALUE
47.456

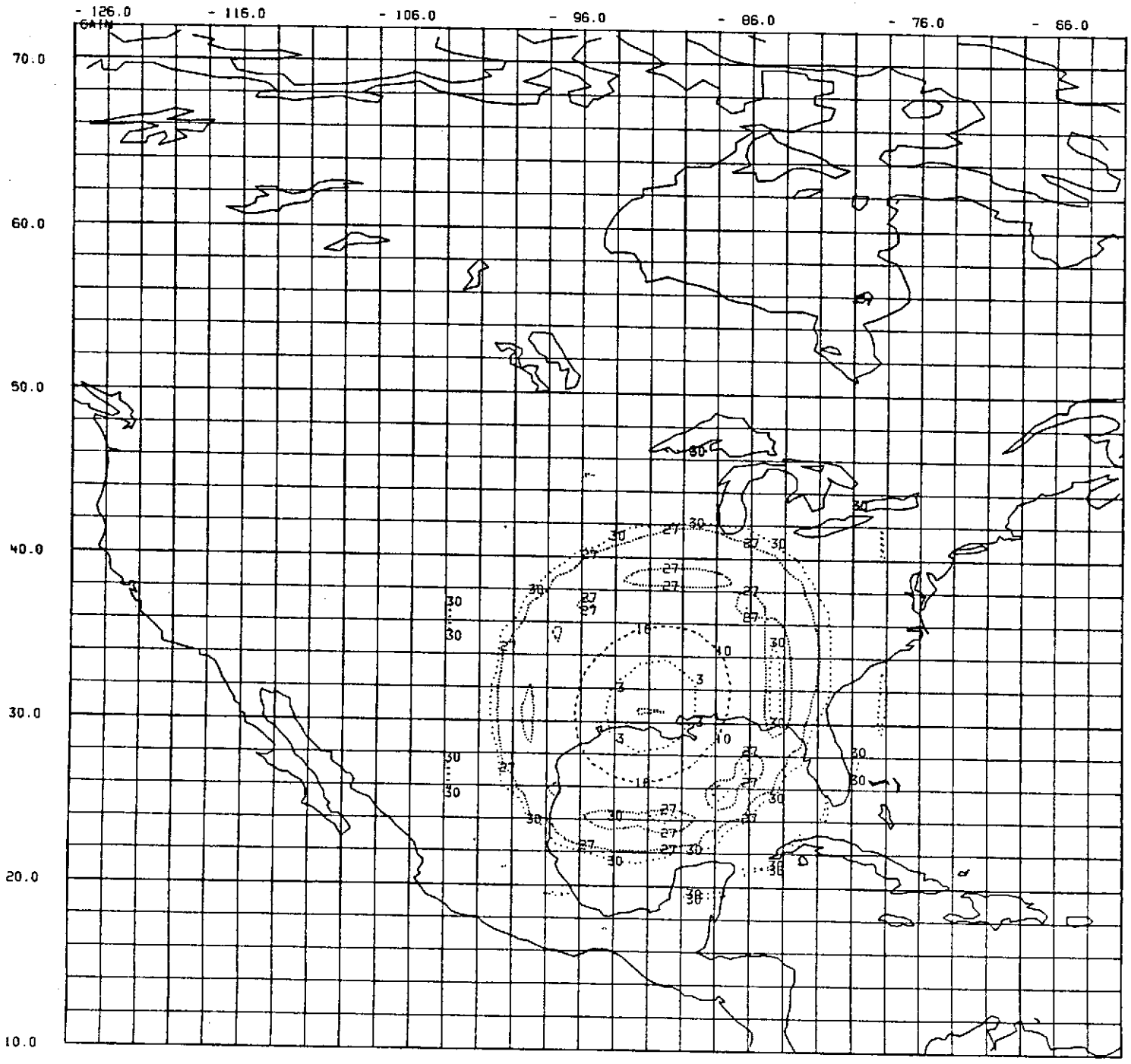

FREQ (GHZ)	DIAM (IN)	REF INDX
11.802	85.000	1.414

FOC LENGTH (IN)	FEED ROT (DEG)
106.183	0.000

LENS AXIS (N)	LENS AXIS (W)
38.200	-102.200

SATELLITE (N)	SATELLITE (W)
0.000	-102.200

XF (IN)	YF (IN)	ZF (IN)
1.983	- 3.116	106.183

POLARIZATION
DIPOLE

NORMALIZATION VALUE
47.344

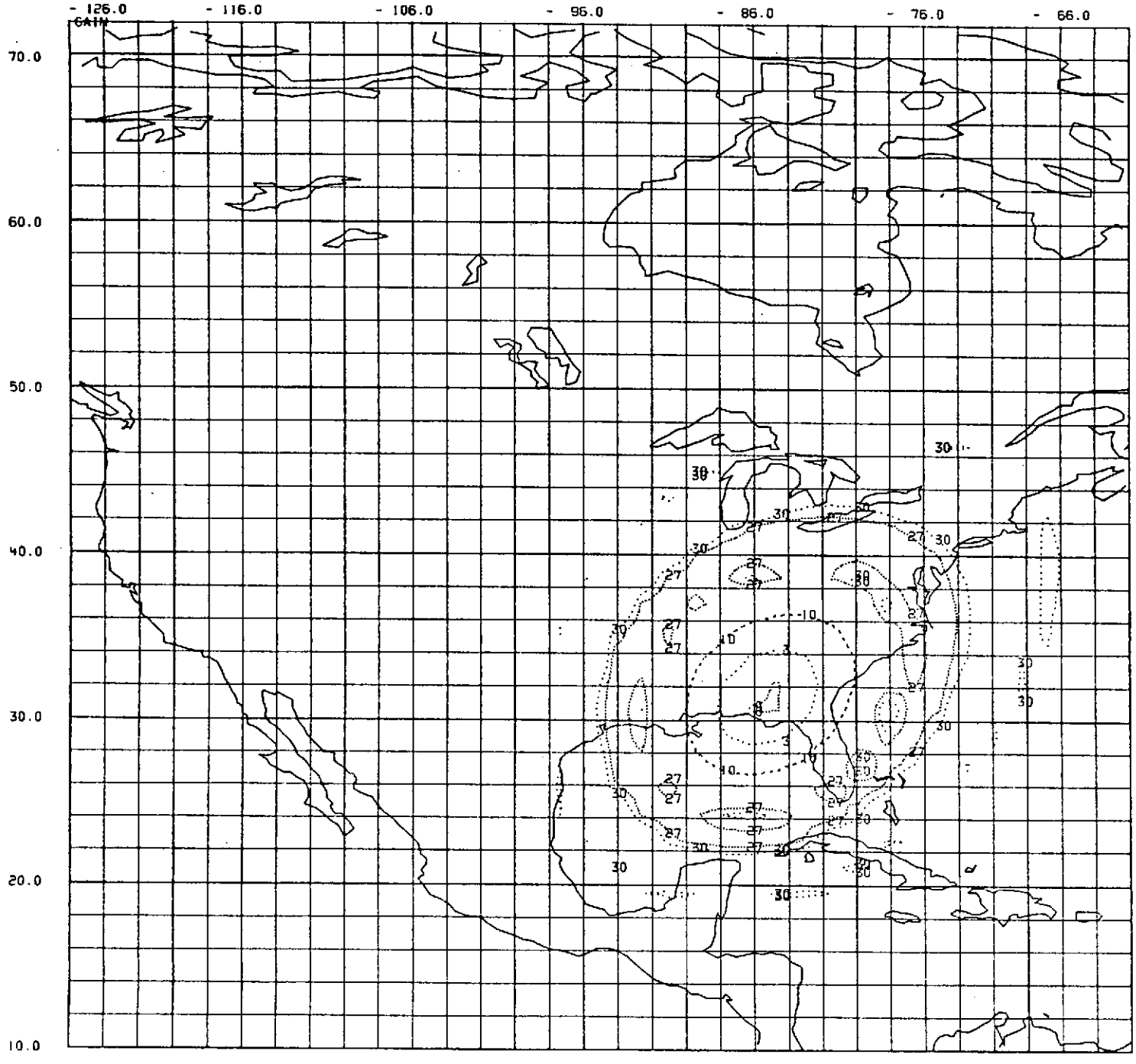

FREQ (GHZ)	DIAM (IN)	REF INDX
11.802	85.000	1.414

FOC LENGTH (IN)	FEED ROT (DEG)
106.183	0.000

LENS AXIS (N)	LENS AXIS (W)
38.200	-102.200

SATELLITE (N)	SATELLITE (W)
0.000	-102.200

XF (IN)	YF (IN)	ZF (IN)
1.898	- 5.003	106.183

POLARIZATION
DIPOLE

NORMALIZATION VALUE
47.185

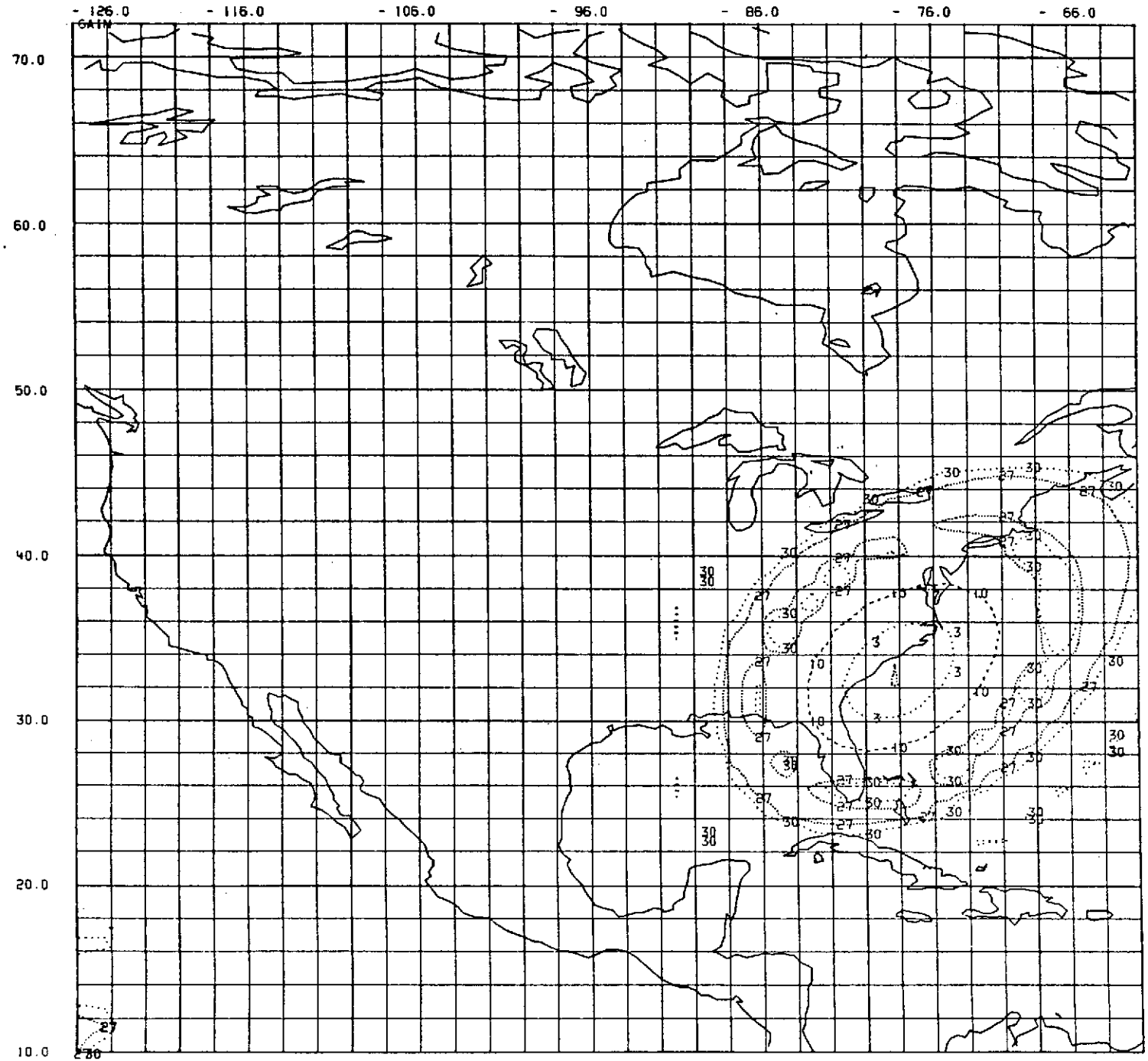

FREQ (GHZ)	DIAM (IN)	REF INDX
11.802	85.000	1.414

FOC LENGTH (IN)	FEED ROT (DEG)
106.183	0.000

LENS AXIS (N)	LENS AXIS (W)
38.200	-102.200

SATELLITE (N)	SATELLITE (W)
0.000	-102.200

XF (IN)	YF (IN)	ZF (IN)
1.504	- 6.813	106.183

POLARIZATION
DIPOLE

NORMALIZATION VALUE
47.371

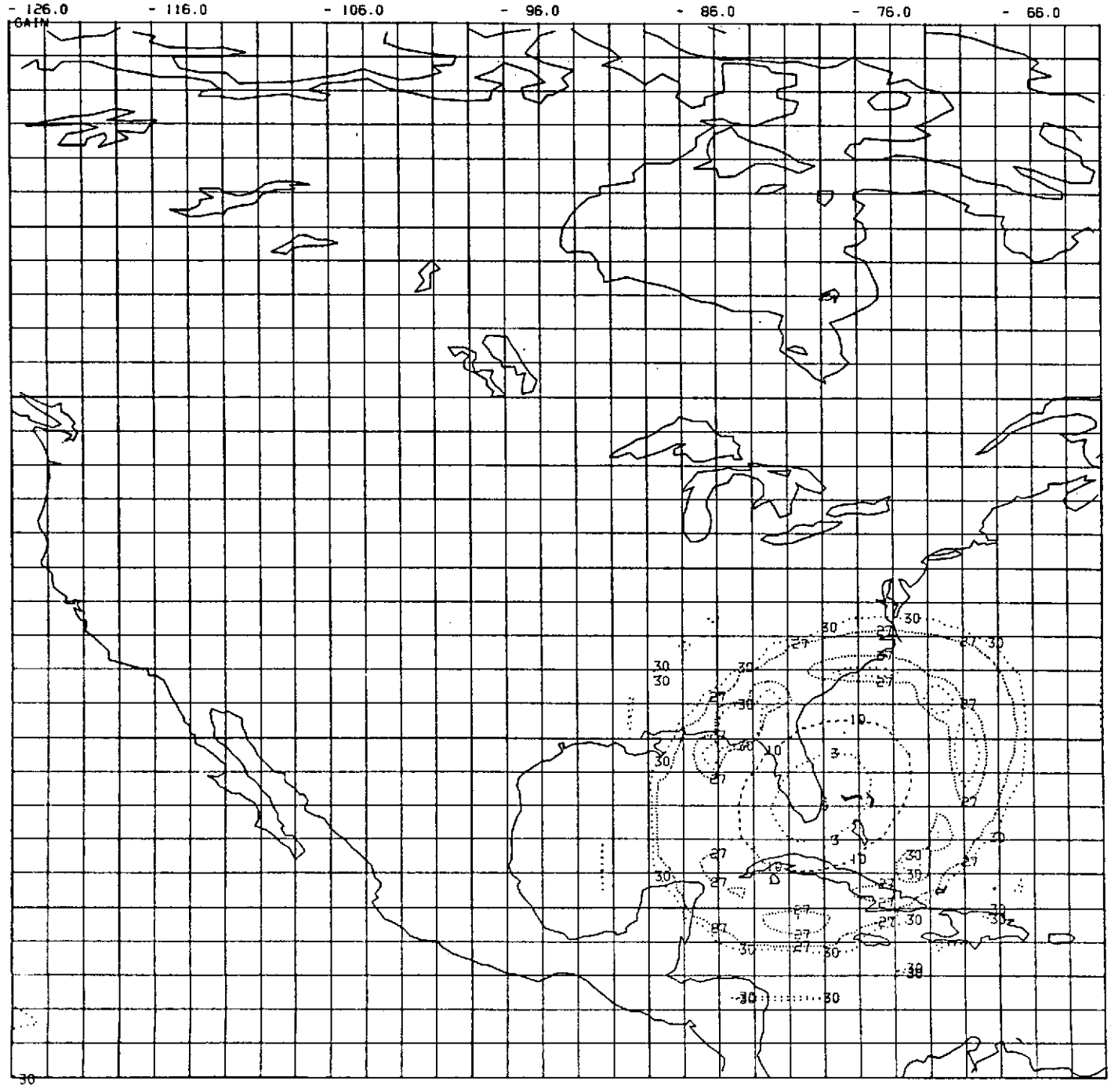

FREQ (GHZ)	DIAM (IN)	REF INDX
11.802	85.000	1.414

FOC LENGTH (IN)	FEED ROT (DEG)
106.183	0.000

LENS AXIS (N)	LENS AXIS (W)
38.200	-102.200

SATELLITE (N)	SATELLITE (W)
0.000	-102.200

XF (IN)	YF (IN)	ZF (IN)
3.372	- 6.786	106.183

POLARIZATION
DIPOLE

NORMALIZATION VALUE
47.475

5.0 CONCLUSIONS AND RECOMMENDATIONS

5.1 Conclusions

The following conclusions are made regarding the Phase II effort of this study:

(1) The capability of using a computer aided analysis to design a multibeam lense antenna having no deterioration in performance with off-axis feeds has been demonstrated experimentally. Thus, a multibeam antenna system for a synchronous orbit satellite can be designed using a single lens aperture with multiple feeds to provide high beam-to-beam isolation and permit the re-use of frequency.

(2) Using a computer aided analysis developed under an LMSC Independent Development Study, a two-dimensional two-point corrected dielectric lense was designed, fabricated, and tested.

(3) Measurements on the two-point corrected lense demonstrated that the side lobes and gain remain essentially constant as a feed is moved laterally off-axis out to the design angle of the lense. This is what had been predicted from the analysis.

(4) A plano-convex hyperbolic lens was designed, fabricated, and tested. The pattern tests on this lens showed the off-axis performance to be essentially the same as that of a parabolic reflector. As the feed is moved off-axis, coma lobes form on the side of the beam between the beam peak and the axis of the antenna.

(5) The two-dimensional lenses were tested in a parallel plate system. The axial feed position for best pattern performance was more influenced by the parallel plates than its location relative to the geometric focus of the lenses.

5.2 Recommendations

The following recommendations are made based upon the results of this study:

(1) A three dimensional circularly symmetric dielectric lense should be designed, fabricated, and tested with multiple feeds to measure the beam-to-beam isolation for a complete operational system.

(2) A developmental program should be initiated to obtain a low density artificial dielectric material compatible for use as a lens antenna in a space environment.

6.0 ACKNOWLEDGEMENTS

The success of this study is due to a concerted effort by several members of LMSC's Antenna Systems organization. To John B. Damonte, Manager of Antenna Systems, for his continuing advice and technical aid over the sixteen months of this study. To Jack Bellamy, Bill Carr, and Will Chang, for their contribution during the Phase I analysis, in reducing 48 candidate antennas to one single preferred concept. Again, to Jack Bellamy for the dielectric lense analysis which allowed us to design and fabricate a coma-corrected lense that worked; and also to Phil Jacques for assisting Jack in this analysis, and for helping to program the analysis into the computer. To Glen Fisher for the mechanical design of the Parallel Plate System, and to Paul Horinek for helping to make the measurements a success.

APPENDIX A

```
      DIMENSION X(1000),Y(1000),PSI(1000),PHI(1000)
      WRITE 1,500
  500 FORMAT($FOCAL LENGTH(IN)? $)
      READ 0,501,FO
  501 FORMAT(F13.7/)
      WRITE 1,502
  502 FORMAT($DIAMETER(IN)? $)
      READ 0,501,D
      SO =0.5*D
      WRITE 1,503
      READ 0,501,THD
  503 FORMAT($OFFSET ANGLE(DEG)? $)
      WRITE 1,506
  506 FORMAT($N? $)
      READ 0,501,AN
      DTR=3.1415927/180.
      THR=THD*DTR
      ST=SIN(THR)
      CT=COS(THR)
      YF=-SQRT((FO*FO/(CT*CT)+SO*SO)*ST*ST)
      WRITE 1,507,YF
  507 FORMAT($YF= $,F12.4/)
      WO=-YF/ST
   10 CONTINUE
      WRITE 1,504
  504 FORMAT($C VALUE(IN)? $)
      READ 0,501,C
      DSO=WO+(C-FO)*CT
      XF=-C
      X(1)=0.
      Y(1)=0.
      PSI(1)=0.
      I=1
   20 CONTINUE
      ALP=ATAN((Y(I)-YF),(X(I)+C))
      SPHI=SIN(ALP-PSI(I))/AN
      PHI(I)=ATAN(SPHI,SQRT(1.-SPHI*SPHI))
      SB=SIN(PSI(I)+PHI(I))
      CB=COS(PSI(I)+PHI(I))
      X(I+1)=X(I)+(DSO+X(I)*CT+Y(I)*ST-SQRT((X(I)-XF)**2+(Y(I)
     1 -YF)**2))/(AN/CB-CT-ST*SB/CB)
      Y(I+1)=Y(I)+(X(I+1)-X(I))*SB/CB
      PSI(I+1)=ATAN((AN*SB-ST),(AN*CB-CT))
      K=I+1
      IF(PSI(K))30,30,31
  530 FORMAT(I3,4F7.3,I5,3F7.3/)
   30 WRITE(1,510)
  510 FORMAT($DECREASE C$/)
      GO TO 21
   31 IF(Y(K))32,32,50
   32 WRITE(1,511)
  511 FORMAT($INCREASE C$/)
      I=I-2
      K=I+1
```

```
      GO TO 21
   50 CONTINUE
      XBA=X(I+1)
      YBA=-Y(I+1)
      PSIBA=-PSI(I+1)
      SPHIB=SIN(THR-PSIBA)/AN
      PHIBA=ATAN(SPHIB,SQRT(1.-SPHIB*SPHIB))
      CB=COS(PSIBA+PHIBA)
      SB=SIN(PSIBA+PHIBA)
      AA=(AN*AN-1)/CB/CB
      DD=DSO+XBA*CT+YBA*ST
      BB=AN*DD/CB-(XBA-XF)-(YBA-YF)*SB/CB
      CC=DD*DD-(XBA-XF)**2-(YBA-YF)**2
      XBB=XBA+(-BB+SQRT(BB*BB-AA*CC))/AA
      YBB=YBA+(XBB-XBA)*SB/CB
      QQ=SQRT((XBB-XF)**2+(YBB-YF)**2)
      PSIBB=ATAN((AN*SB*QQ-(YBB-YF)),(AN*CB*QQ-(XBB-XF)))
      X(I+2)=XBB
      Y(I+2)=-YBB
      PSI(I+2)=-PSIBB
      IF(Y(I+2)-SO)19,19,21
   19 CONTINUE
      I=I+2
      GO TO 20
   21 CONTINUE
      WRITE 1,530,I,X(I),Y(I),PSI(I),PHI(I),K,X(K),Y(K),PSI(K)
      WRITE 1,531
  531 FORMAT($PRINT? $)
      READ 0,521,NSIR
      IF(NSIR-1HN)90,91,90
   90 DO 92 J=1,I,2
      L=J+1
      WRITE 1,530,J,X(J),Y(J),PSI(J),PHI(J),L,X(L),Y(L),PSI(L)
   92 CONTINUE
   91 CONTINUE
      WRITE 1,520
  520 FORMAT($CHANGE C(Y OR N)? $)
      READ 0,521,NSIR
  521 FORMAT(A1/)
      IF(NSIR-1HN)10,22,10
   22 STOP
      END
```

```
-GO /WALENS-G4/

FOCAL LENGTH(IN)? 61.246
DIAMETER(IN)? 47.625
OFFSET ANGLE(DEG)? 3.5
N? 1.414213562
YF=       -4.0182
C VALUE(IN)? 62.
DECREASE C
 33  2.228 13.182  -.422    .463    34  9.723 13.491  -.007
PRINT? N
CHANGE C(Y OR N)? Y
C VALUE(IN)? 61.
DECREASE C
 43  2.819 16.036  -.509    .540    44  8.774 16.217  -.043
PRINT? N
CHANGE C(Y OR N)? Y
C VALUE(IN)? 60.
DECREASE C
 59  2.895 19.191  -.574    .601    60  6.741 19.296  -.054
PRINT? N
CHANGE C(Y OR N)? Y
C VALUE(IN)? 59.
INCREASE C
135   .464 19.470  2.263  -.737   136   .507 20.458  2.176
PRINT? N
CHANGE C(Y OR N)? Y
C VALUE(IN)? 59.5
DECREASE C
117  2.038 23.110  -.656    .670   118  2.686 23.119  -.100
PRINT? N
CHANGE C(Y OR N)? Y
C VALUE(IN)? 59.4
INCREASE C
149   .969 21.462  2.270  -.742   150   .993 22.017  2.177
PRINT? N
CHANGE C(Y OR N)? Y
C VALUE(IN)? 59.45
INCREASE C
157  1.158 22.050  2.273  -.743   158  1.175 22.470  2.179
PRINT? N
CHANGE C(Y OR N)? Y
C VALUE(IN)? 59.46
INCREASE C
159  1.203 22.206  2.268  -.745   160  1.222 22.592  2.174
PRINT? N
CHANGE C(Y OR N)? Y
C VALUE(IN)? 59.47
INCREASE C
163  1.272 22.407  2.271  -.745   164  1.288 22.745  2.176
PRINT? N
CHANGE C(Y OR N)? Y
C VALUE(IN)? 59.48
INCREASE C
```

```
169  1.361 22.666  2.272  -.745  170  1.373 22.943  2.177
PRINT? N
CHANGE C(Y OR N)? Y
C VALUE(IN)? 59.49
INCREASE C
183  1.507 23.092  2.276  -.745  184  1.514 23.267  2.179
PRINT? N
CHANGE C(Y OR N)? Y
C VALUE(IN)? 59.495
DECREASE C
141  1.869 23.483  -.620   .657  142  2.172 23.494  -.023
PRINT? N
CHANGE C(Y OR N)? Y
C VALUE(IN)? 59.494
INCREASE C
215  1.667 23.564  2.270  -.748  216  1.670 23.625  2.173
PRINT? N
CHANGE C(Y OR N)? Y
C VALUE(IN)? 59.4945
DECREASE C
155  1.827 23.602  -.619   .657  156  2.021 23.609  -.019
PRINT? N
CHANGE C(Y OR N)? Y
C VALUE(IN)? 59.4944
DECREASE C
163  1.817 23.651  -.653   .672  164  1.968 23.653  -.083
PRINT? N
CHANGE C(Y OR N)? Y
C VALUE(IN)? 59.4943
DECREASE C
179  1.786 23.714  -.612   .654  180  1.876 23.718  -.002
PRINT? N
CHANGE C(Y OR N)? Y
C VALUE(IN)? 59.4942
INCREASE C
231  1.701 23.666  2.266  -.750  232  1.703 23.702  2.169
PRINT? N
CHANGE C(Y OR N)? Y
C VALUE(IN)? 59.49425
INCREASE C
247  1.722 23.724  2.267  -.750  248  1.723 23.746  2.170
PRINT? N
CHANGE C(Y OR N)? Y
C VALUE(IN)? 59.49426
INCREASE C
257  1.730 23.748  2.270  -.749  258  1.731 23.764  2.173
PRINT? N
CHANGE C(Y OR N)? Y
C VALUE(IN)? 59.49427
DECREASE C
215  1.763 23.781  -.632   .664  216  1.792 23.782  -.039
PRINT? N
CHANGE C(Y OR N)? Y
C VALUE(IN)? 59.494265
```

```
INCREASE C
269  1.737 23.768  2.277  -.747  270  1.737 23.779  2.179
PRINT? N
CHANGE C(Y OR N)? Y
C VALUE(IN)? 59.494266
INCREASE C
273  1.739 23.773  2.273  -.748  274  1.739 23.783  2.175
PRINT? N
CHANGE C(Y OR N)? Y
C VALUE(IN)? 59.494267
INCREASE C
279  1.741 23.781  2.262  -.751  280  1.741 23.789  2.166
PRINT? N
CHANGE C(Y OR N)? Y
C VALUE(IN)? 59.494268
INCREASE C
299  1.746 23.796  2.267  -.750  300  1.746 23.800  2.170
PRINT? N
CHANGE C(Y OR N)? Y
C VALUE(IN)? 59.494269
DECREASE C
225  1.760 23.790  -.619   .658  226  1.781 23.791  -.014
PRINT? N
CHANGE C(Y OR N)? Y
C VALUE(IN)? 59.4942685
DECREASE C
239  1.757 23.798  -.636   .666  240  1.771 23.798  -.045
PRINT? N
CHANGE C(Y OR N)? Y
C VALUE(IN)? 59.4942684
DECREASE C
245  1.756 23.800  -.621   .659  246  1.767 23.801  -.017
PRINT? N
CHANGE C(Y OR N)? Y
C VALUE(IN)? 59.4942683
DECREASE C
259  1.754 23.805  -.628   .662  260  1.762 23.805  -.031
PRINT? N
CHANGE C(Y OR N)? Y
C VALUE(IN)? 59.4942682
INCREASE C
317  1.748 23.802  2.265  -.750  318  1.748 23.805  2.168
PRINT? N
CHANGE C(Y OR N)? Y
C VALUE(IN)? 59.49426825
INCREASE C
347  1.748 23.806  2.274  -.748  348  1.748 23.808  2.176
PRINT? N
CHANGE C(Y OR N)? Y
C VALUE(IN)? 59.49426826
DECREASE C
289  1.752 23.809  -.616   .657  290  1.755 23.810  -.009
PRINT? N
CHANGE C(Y OR N)? Y
```

```
C VALUE(IN)? 59.494268255
DECREASE C
293  1.752 23.810  -.630   .663  294  1.754 23.810  -.035
PRINT? N
CHANGE C(Y OR N)? Y
C VALUE(IN)? 59.494268254
DECREASE C
307  1.752 23.811  -.647   .670  308  1.753 23.811  -.066
PRINT? N
CHANGE C(Y OR N)? Y
C VALUE(IN)? 59.494268253
INCREASE C
355  1.748 23.806  2.269  -.749  356  1.748 23.808  2.171
PRINT? N
CHANGE C(Y OR N)? N

*STOP*

-
```